EVALUATING CONCRETE BRIDGE DECK PERFORMANCE

FHWA/MT-06-006/8156-002

Final Report

prepared for
THE STATE OF MONTANA
DEPARTMENT OF TRANSPORTATION

in cooperation with
THE U.S. DEPARTMENT OF TRANSPORTATION
FEDERAL HIGHWAY ADMINISTRATION

July 2006

prepared by
Eli Cuelho
Jerry Stephens
Peter Smolenski
Jeff Johnson

Western Transportation Institute
College of Engineering
Montana State University - Bozeman

RESEARCH PROGRAMS

Montana Department of Transportation
MDT
serving you with pride

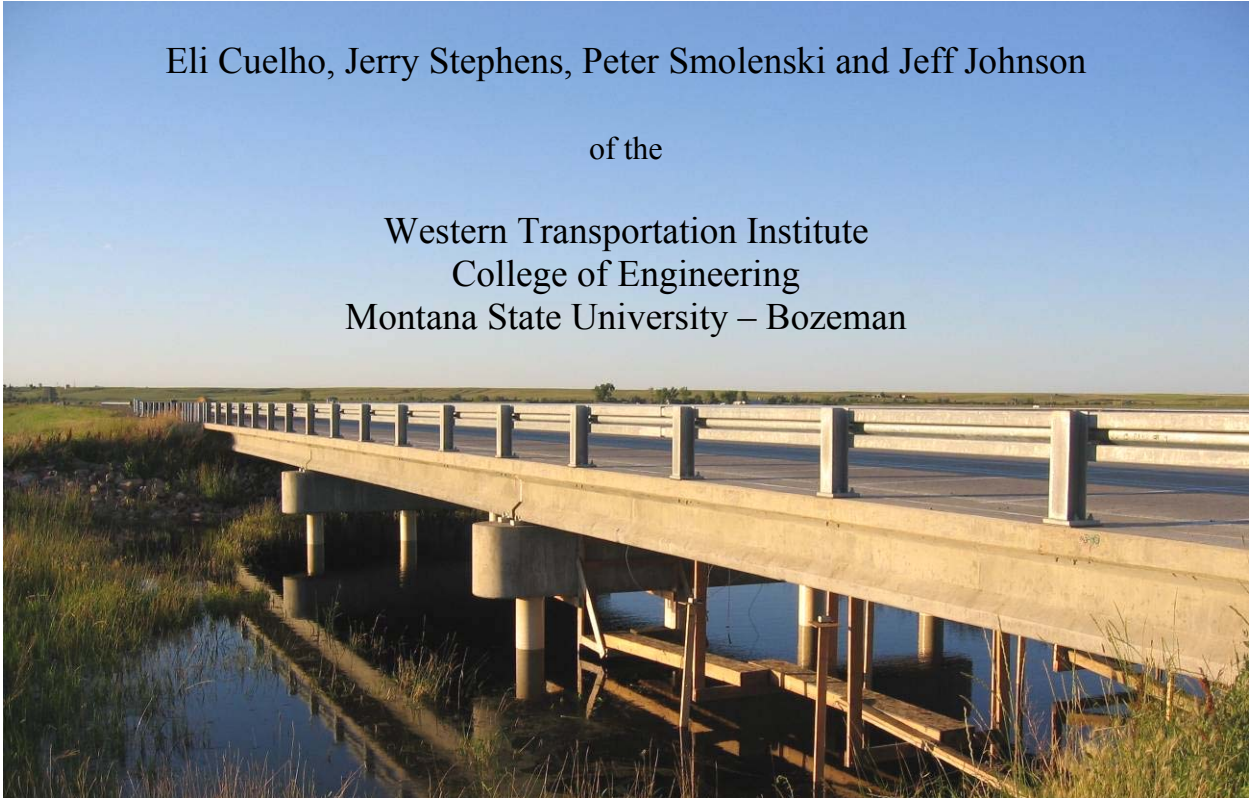# EVALUATING CONCRETE BRIDGE DECK PERFORMANCE

Final Project Report

by

Eli Cuelho, Jerry Stephens, Peter Smolenski and Jeff Johnson

of the

Western Transportation Institute
College of Engineering
Montana State University – Bozeman

prepared for the

State of Montana
Department of Transportation
Research Programs

in cooperation with the

U.S. Department of Transportation
Federal Highway Administration

June 2006

TECHNICAL REPORT DOCUMENTATION PAGE

1. Report No. FHWA/MT-06-006/8156-002	2. Government Access No.	3. Recipient's Catalog No.
4. Title and Subtitle Evaluating Concrete Bridge Deck Performance		5. Report Date June 2006
		6. Performing Organization Code
7. Author(s) Eli Cuelho, Jerry Stephens, Peter Smolenski & Jeff Johnson		8. Performing Organization Report Code
9. Performing Organization Name and Address Western Transportation Institute PO Box 174250 Montana State University – Bozeman Bozeman, Montana 59717-4250		10. Work Unit No. (TRAIS)
		11. Contract or Grant No. MSU G&C #426380 MDT Project #8156
12. Sponsoring Agency Name and Address Research Programs Montana Department of Transportation 2701 Prospect Avenue Helena, Montana 59620-1001		13. Type of Report and Period Covered Final Report February 2002 – May 2006
		14. Sponsoring Agency Code 5401

15. Supplementary Notes

Research performed in cooperation with the Montana Department of Transportation and the U.S. Department of Transportation, Federal Highway Administration. This report can be found at http://www.mdt.mt.gov/research/projects/mat/high_concrete.shtml.

16. Abstract

Since the service life of concrete bridge decks designed by traditional procedures is often shorter than desired, their ability to withstand constant and heavy use in a variety of operating environments is of major concern. In this project, the relative performance of three bridge decks constructed with different concretes and reinforcing steel configurations was studied to help determine which deck offers the best performance over time. To achieve this objective, an array of strain and temperature instrumentation was embedded in each of the bridge decks prior to placing the deck concrete. The decks were tested under controlled live loads to characterize their structural behavior. The first set of such tests was performed immediately after the bridge decks were completed, and the second was conducted two years later. The long term performance of the three decks under environmental loads (notably, changes in temperature) was studied by continuously monitoring selected strain gages in each bridge, and by conducting periodic visual distress surveys and corrosion tests. In the data collected and analyzed from the live load tests and environmental response monitoring of the three decks, only subtle behavioral differences have been observed. While some aspects of the response have been found to statistically differ between bridges and over time, the significance of these differences remains uncertain, as the bridges are relatively young, and they only exhibit nominal signs of distress. The significance of these differences may become clear in the future, if substantial differences in deck durability and performance emerge over time. The visual distress surveys have found that the majority of the cracking that has occurred in the decks is near the integral abutments and that the Empirical deck had the most extensive cracking in this regard. The analysis presented herein generally serves as a baseline for the relative condition of the three bridges before prolonged demands from traffic and the environment. Should a follow-on project be initiated, data obtained from continued long-term monitoring and live load testing will likely provide a more complete body of evidence from which to ascertain which deck design offers superior performance. Relative to cost, initial expense for each deck was similar, thus the relative cost-to-benefit for the decks will be dependent on the service life that they offer.

17. Key Words Bridge deck instrumentation, long term monitoring, live load testing, durability, corrosion, field evaluation		18. Distribution Statement No restrictions. This document is available to the public through NTIS, Springfield, Virginia 22161.	
19. Security Classif. (of this report) Unclassified	20. Security Classif. (of this page) Unclassified	21. No. of Pages 302	22. Price

ACKNOWLEDGMENTS

DISCLAIMER

This document is disseminated under the sponsorship of the Montana Department of Transportation and the United States Department of Transportation in the interest of information exchange. The State of Montana and the United States Government assume no liability of its contents or use thereof.

The contents of this report reflect the views of the authors, who are responsible for the facts and accuracy of the data presented herein. The contents do not necessarily reflect the official policies of the Montana Department of Transportation or the United States Department of Transportation.

This report does not constitute a standard, specification, or regulation.

ALTERNATIVE FORMAT STATEMENT

MDT attempts to provide accommodations for any known disability that may interfere with a person participating in any service, program, or activity of the Department. Alternative accessible formats of this information will be provided upon request. For further information, call (406) 444-7693, TTY (800) 335-7592, or Montana Relay at 711.

UNIT CONVERSIONS

Measurement	Metric	English
Length	1 cm	0.394 in
	1 m	3.281 ft
	1 km	0.621 mile
Area	1 cm^2	0.155 in^2
	1 m^2	1.196 yd^2
Volume	1 m^3	1.308 yd^3
	1 ml	0.034 oz
Force	1 N	0.225 lbf
	1 kN	0.225 kip
Stress	1 MPa	145 psi
	1 GPa	145 ksi
Unit Weight	1 kg/m^3	1.685 lbs/yd^3
Velocity	1 kph	0.621 mph

EXECUTIVE SUMMARY

One major area of concern regarding concrete bridge deck performance is durability. It is generally acknowledged across the country that the service life of bridge decks designed by traditional procedures is often shorter than desired. Typically, the deck concrete cracks, allowing corrosive agents (notably deicers) to access the reinforcing steel. The steel subsequently corrodes and the expansive products of this corrosion further fracture the concrete. Cracks in the concrete also promote freeze-thaw damage, as they allow additional moisture and perhaps chlorides to penetrate the deck. Customary approaches used to mitigate these problems include, but are not limited to, coating the reinforcing steel with epoxy, reducing the amount of steel reinforcement, using denser concrete mixes, cathodic protection, and sealing the concrete surface. While these measures have all been used for several years, instrumented field tests to determine their performance has been sparse, due in part to the costs involved in conducting such tests and the difficulties encountered in finding appropriate sites. Nevertheless, field investigations of deck condition through time are frequently conducted and can be very useful to determine deck behaviors and performance.

While planning the replacement of three bridges on Highway 243 north of Saco, Montana, bridge engineers at the Montana Department of Transportation (MDT) recognized and seized a unique opportunity to evaluate the performance of different deck designs exposed to the same vehicular and environmental loads. The new bridges have identical geometries, and were constructed at the same time by the same contractor, which helped minimize the number of variables typically encountered in large-scale field investigations of comparative performance. The primary focus of this research project has been to investigate the behavior of the three different deck designs (that have different concretes and reinforcing configurations) used in these bridges under vehicle loads and long-term environmental exposure.

Two alternative deck designs were used in this project in addition to the standard bridge deck design used by MDT. The "Conventional" bridge deck (used as a control in this experiment) was designed using the standard practices of MDT's Bridge Bureau, and utilizes a conventional deck concrete and standard reinforcement layout. The "Empirical" bridge deck was designed using the empirical design approach specified by the American Association of State Highway and Transportation Officials (AASHTO) Load & Resistance Factor Design (LRFD) Specification for Highway Bridges, which allows for a significant reduction in the steel reinforcement in conjunction with the standard deck concrete (AASHTO, 2000). The high performance concrete, "HPC," bridge deck was designed using the standard reinforcement layout (as in the Conventional deck) but utilized a high performance concrete for the deck. Each of these bridges was constructed less than a mile from one another, so environmental and vehicle demands are the same on the three structures. The Western Transportation Institute was

contracted to conduct a comparative study of the performance of the three bridge decks and assess their long term durability.

To accomplish the research objectives, an array of strain and temperature instrumentation was embedded in each of the bridge decks prior to placing the deck concrete. Strains are measured both in the reinforcement and the concrete at strategic locations using three different technologies: resistance strain gages bonded directly to the reinforcing steel, resistance strain gages embedded directly in the concrete, and vibrating wire strain gages embedded in the concrete. Resistance strain gages are very suitable for responding to immediate changes in strain during live load events, while the vibrating wire strain gages respond slower but are more stable over longer periods of time corresponding to diurnal or seasonal strain fluctuations.

Basic structural behavior of the decks was characterized by subjecting the decks to controlled live load tests in which vehicles with known characteristics and weights were driven across the bridges while simultaneously monitoring the strain response. These tests were used to characterize how each type of deck structurally transferred wheel loads from their point of application into the supports and to determine the magnitudes of the strains that developed in the decks as they performed this function. Strain measurements were used to establish both the manner in which the decks carry loads from their point of application into the supports, and the magnitude of the demands that these loads placed on the decks relative to their capacity. This information helped determine the likelihood of immediate and/or long term crack development in the decks from vehicle loads.

Live load tests were conducted in July 2003 and July 2005, during which two heavily loaded three-axle dump trucks were used to load each of the bridge structures along nine longitudinal paths. Generally, tire loads were positioned to be either directly over a girder or at the midspan between girders to characterize deck response under the most critical load positions. Each bridge was subjected to 15 test runs: 8 low speed single-truck tests, 5 high speed single-truck tests, and 2 low speed two-truck tests.

The live load test data was first used to develop a fundamental understanding of how each bridge deck responds to vehicle loads. Simple observations in this regard were then used to compare the relative performance of the three decks. Comparisons between the reported data and expected responses derived from basic strength of materials concepts were also used in this analysis. This analysis focused more upon the transverse rather than the longitudinal deck response, as it was believed to be more significantly affected by the differences in construction of each deck, as well as to be less confounded by any incidental differences in the restraint to longitudinal movement offered by the abutment and bent supports of each bridge. Further, relative to transverse behavior, a typical deck panel defined by the end and middle transverse diaphragms in any span of each bridge was expected to represent the general behaviors across the entire bridge.

The analysis of the live load test results began with the 2003 tests, followed by a comparison of these results with those obtained from the tests conducted in 2005. In both cases, the aspects of deck behavior that were considered include:

- general load carrying behavior in the longitudinal and transverse directions,
- detailed analysis of transverse behaviors using shifts in the position of the neutral axis to investigate the presence/absence of cracking and in-plane stresses in the decks,
- stiffness analysis in the transverse and longitudinal directions, including calculation of girder distribution factors, and
- general linearity of the response as inferred by results obtained in the two-truck versus the single truck tests.

In each case, the common features observed in the response of all three bridges were identified and discussed, and comparisons were made of the more detailed features of the responses seen in each deck. Both qualitative and quantitative observations and comparisons were made, when possible and appropriate. Indeed, the important, qualitatively based conclusion that can be readily drawn in this case after reviewing the test data is that all three decks are behaving in a very similar fashion. The decks, however, are not behaving identically. Thus, the issue becomes whether or not consistent patterns exist in the small variations in the response between decks that reflect true differences in deck behavior.

Standardized techniques for processing strain data collected during live load tests on bridges have not been developed, particularly when the objective of the analysis is to compare the relative performance of three different bridge decks. In this investigation, the decision was made to use some of the principles of engineering mechanics coupled with the strain data to estimate several structural parameters for each deck, such as the position of the neutral axis across the depth of the deck, the magnitude of the in-plane axial forces acting in the deck, and the magnitude of the average strains in the deck. Some of these parameters were found to statistically differ between bridges and over time. Note that while these differences were detectable, their significance remains uncertain, as the bridges are relatively young, and they only exhibit signs of nominal distress. The significance of these differences may become clear in the longer term, if substantial differences in deck durability and performance emerge over time.

Long term monitoring consisted of measuring internal deck strains and temperatures, assessing corrosion potential, visual distress surveys, and detecting global movement of the bridge structures through periodic topographic surveys of the bridge decks. The data acquisition system was programmed to collect strain and temperature information from all of the embedded sensors on an hourly basis. All other effects were monitored through periodic visits to the bridge site.

The data available from the long term monitoring was studied to correlate changes in deck performance with the vehicle and environmental loads they experienced, and then to further evaluate the relative performance of the three types of decks. The primary "environmental" behaviors experienced by the decks are related to the dimensional changes they experienced due to changes in relative humidity (shrinkage of the concrete) and temperature (shrinkage and expansion of both the concrete and the reinforcing steel). The analysis of long term data utilized strain and temperature data from the vibrating wire sensors, as well as associated deformations of the decks in response to temperature changes.

Based on the long term strain analysis, the decks generally are all responding the same, where this response consists of temperature related diurnal strain cycles superimposed on broader seasonal temperature related strain cycles, all of which are superimposed on basic long term shrinkage strains. The long term shrinkage strain in the decks ranged from 300 to 350 microstrain, with the lowest shrinkage strains occurring in the HPC deck. The shrinkage strains in the decks are generally consistent with the shrinkage strains observed in concrete samples cast at the time of deck construction. Changes in strain associated with daily and seasonal temperature fluctuations are as expected based on the coefficients of thermal expansion of the deck concretes. Deck curvatures and net in-plane strains generated from the strain data were useful in picturing the behavior of the decks under different temperature conditions, and they produced deflected deck shapes that were consistent with those expected.

With the exception of the behavior of the decks over the bents (where major transverse cracks occurred), no obviously significant differences in behavior between the decks were observed in the long term strain data. Such differences may develop with time, as the decks experience more distress. The ability of the instrumentation in the decks to reflect the presence of such distress in the decks was demonstrated using the changes in the longitudinal strain data in the Conventional deck when it cracked in the transverse direction over the bent. The occurrence of this crack was directly captured by the gage at his location, and it may further have influenced the longitudinal response recorded at other locations in this deck.

Visual distress surveys revealed various types of cracking distresses within the Saco bridge decks. While overall, the cracking behaviors were similar between the three bridges, they also showed subtle differences. The most pronounced cracking generally was observed in the decks near the abutments at each end of each bridge, and directly over the bents. Smaller cracks and some crazing were observed elsewhere in the decks. In general, this cracking was of limited severity and extent. Cracking near the abutments and over the bents was generally more pronounced in the Empirical deck. The Conventional deck exhibited similar crack behavior, but not as acute. The HPC deck has not exhibited as much cracking near the abutments, however, edge cracking and underside hairline cracking are more pronounced on this deck. It appears that each of the decks is experiencing similar types of distress, and that current and subtle differences in the severity of these distresses may become more apparent as the bridge decks age.

Periodic corrosion monitoring indicated that the deck reinforcement and concrete have not shown potential for corrosion. Topographic surveys of each of the bridge decks did not reveal significant displacement over time or between decks, but did help explain behavioral differences in the HPC deck at Bent #2 when subjected to live loads.

The analysis presented herein generally serves as a baseline assessment of the relative condition of the three bridges before prolonged demands from traffic and the environment. Should a follow-on project be initiated, data obtained from continued long-term monitoring and live load testing will likely provide a more complete body of evidence from which to determine which deck design offers superior performance over time.

Based on all of the information obtained to-date, the HPC deck potentially will offer the most cost effective performance of the three deck configurations, followed closely by the Conventional deck, and more distantly by the Empirical deck. This conclusion is primarily based on the relative visual distresses observed in the decks and on the relative stability of their behavior over time, as inferred from the live load strain data. In making this statement, it is important to recognize that, as is emphasized above: a) the differences in performance between the decks were small; b) the various pieces of evidence related to their relative performance sometimes tell a conflicting story; and c) presently subtle differences in their performance could become significant in the future. Thus, this conclusion must be considered as "preliminary" in nature, until it can be confirmed (or refuted) based on additional study of the decks' performance over time.

TABLE OF CONTENTS

LIST OF TABLES

LIST OF FIGURES

1   INTRODUCTION

1.1   Background

There are a number of factors which contribute to the short service life of traditional concrete bridge decks. Most often the concrete in the decks cracks, which allows agents of corrosion (notably deicers) to penetrate to the reinforcing steel. The steel subsequently corrodes, and the expansive products of this corrosion crack the concrete even further. Cracks in the concrete also contribute to freeze-thaw damage, as they allow more moisture and potentially chlorides to penetrate the concrete. Approaches believed to mitigate these problems include coating the reinforcing steel with epoxy, using less reinforcing steel, using less permeable concretes, and sealing the concrete surface. The effectiveness of these and other methods to improve long term deck performance have been and continue to be investigated by field observations of deck condition (cracking, carbonation, chloride ion penetration, etc.) through time (e.g., Carrier and Cady, 1973; James et al., 1987; Pyć et al., 2000; Darwin, 2002; Russell, 2004; Lindquist et al., 2005). Investigations of deck behavior and long term performance using active instrumentation such as internal strain gages, however, are sparse, in part due to the costs involved in conducting such investigations and the difficulties encountered in finding appropriate sites. Nonetheless, investigations of this type (e.g., Ramakrishnan and Sigl, 2001; Hughes et al., 2000) do offer insights on internal deck behavior that may not be obvious from the periodic observation of deck conditions referred to above.

While planning the replacement of three bridges on Highway 243 north of Saco, Montana, bridge engineers at the Montana Department of Transportation (MDT) recognized and seized a unique opportunity to evaluate different deck designs built by the same contractor and subsequently exposed to the same environmental and vehicular conditions. Thus, variability in test articles and conditions between test sites typically encountered in large-scale field investigations was minimized in this situation. The primary focus of this research project has been to compare the performance of three different bridge deck designs.

All three bridges utilize a concrete slab on prestressed stringer construction, but incorporate a different concrete deck design. One bridge deck was designed using standard practices of MDT's Bridge Bureau and built using conventional concrete and reinforcement layout. As such, it is referred to as the "Conventional" bridge deck. The second deck, known as the "Empirical" bridge deck, was designed using the empirical design approach presented in the American Association of State Highway and Transportation Officials (AASHTO) Load & Resistance Factor Design (LRFD) Specification for Highway Bridges (AASHTO, 2000). This design allowed for an overall reduction in the reinforcing steel, but still used a conventional concrete mix design. The third bridge deck, referred to as the "HPC" bridge deck, was designed in the

same manner as the Conventional deck, but replaced the standard concrete with high performance concrete (HPC).

A variety of gages were embedded in the decks to monitor their relative performance. The instrumentation consists of strain and temperature gages bonded directly to the reinforcement and embedded in the concrete. Gages were placed at strategic locations within the deck to monitor various design features and structural behaviors. Data was collected from these gages during live-load testing to capture structural behaviors, and over time to monitor long term environmental effects.

1.2 Objectives and Scope

The objective of this project was to investigate the performance of three different types of concrete bridge decks, namely:

1. a conventionally reinforced deck made with standard concrete, designed and constructed following standard practices of MDT's Bridge Bureau,
2. a deck with reduced reinforcement made with normal concrete, designed following the empirical design approach presented in the AASHTO LRFD Specifications for Highway Bridges and constructed following standard MDT practice, and
3. a conventionally reinforced deck made with high performance concrete (HPC) developed following FHWA guidelines.

The structural behavior of these decks under vehicle live loads and their long-term durability under environmental and vehicular demands was studied using instrumentation embedded in the bridge deck, as well as through periodic on-site surveys of their condition. The performance of the decks was compared and contrasted with due consideration of the known and projected costs for each type of deck to ultimately determine which deck construction offered the best performance as a function of cost. Deck performance was monitored for a two-year period immediately after their construction. At the end of this period, the data was collectively analyzed to determine whether a recommendation could be formulated as to which configuration(s) should be built in the future.

1.3 Project Timeline

Prior to construction of the three new bridges on Route 243 near Saco, Montana, a temporary weather station was installed atop the Saco Public School in August 2002 to provide weather information during the life of the project, and provide a conduit for future data transmission from the bridges. Bridge construction at the Saco bridge site began during the winter of 2002-2003. While the old bridges were being removed and the new support structure for the replacement bridges was being constructed, an instrumentation plan was developed to

determine the layout of the embedded instrumentation. When this plan was completed, the reinforcement strain gages were bonded to the reinforcing bars at Montana State University. Additionally, the data acquisition system was assembled. By April 2003, the bridge superstructure was in place, and all deck forming was complete. The instrumented reinforcement was delivered to the Saco construction site and installed in the bridge decks. Soon after, the remaining instrumentation was tied in place in the decks, all instrumentation cabling was routed, the communication and power hardware was installed, and the instrumentation was activated.

The decks were cast in May and June of 2003. The bridges were subsequently allowed to cure, the deck forms were removed, saw-cuts were made over the south bents, the decks were grooved, the guardrail was installed, and the bridge approaches were paved. Figure 1 shows one of the finished Saco bridges. The first live load tests were conducted in late July 2003, as well as benchmark durability tests (i.e., half-cell tests and carbonation tests). Additionally, topographic surveys and visual distress surveys of the bridge decks were conducted. All three bridges were then opened to public use in early August 2003. Subsequent monitoring of the bridge decks (including visual distress surveys) occurred at regularly scheduled intervals as described in the individual sections in this report. A second set of live load tests was conducted in July 2005. Long term monitoring began when the decks were cast, and continued throughout the life of this project. The analysis of the long term data extends from July 2003 to July 2005. This report documents all of these activities, and includes an extensive analysis of the live load tests and long term data.

Figure 1: Completed Saco Bridge

Prior to beginning the work outlined above, available literature on bridge deck performance was collected, reviewed and summarized. This report begins with a summary of this review.

2   LITERATURE REVIEW

Reinforced concrete has emerged as a highly versatile building material in the modern age. For certain applications, it has several advantages over other building materials. Due to the combination of the steel and the concrete, the structure is effectively strong under both tensile and compressive demands. This strength is offered at a significantly reduced cost from steel alone. Additionally, reinforced concrete may be formed into countless structural and aesthetic forms not readily available when using steel or other building materials. As with all materials, reinforced concrete's benefits are accompanied by disadvantages. Within the reinforced concrete matrix, concrete is susceptible to brittle fracture, and the steel is susceptible to corrosion damage.

Historically, as the use of reinforced concrete became more widespread, it was important to test and understand its physical properties and behaviors under specific loading conditions. Due to the deterioration of transportation infrastructure in the United States, a renewed interest has emerged toward understanding reinforced concrete specifically as it applies to highway bridges (Lenett et al., 2001).

Cao (1996) states that about one-third of the nation's bridges have deficient decks. In this regard, one of the major problems that bridge decks face is corrosion of the reinforcing steel. This damage is generally initiated by cracking of the concrete in the top of the deck. These cracks allow moisture, deicing chemicals, and air to reach the steel and sustain the oxidation process. As the reinforcing steel corrodes, it debonds from the surrounding concrete, thereby reducing composite action, as well as overall structural integrity. Furthermore, due to the expansive nature of the corroding steel and the relatively low tensile strength of concrete, portions of the deck may spall as the corrosive activity proceeds. Many possible solutions to this problem are currently under investigation and include: epoxy-coated rebar, fiber-reinforced polymer (FRP) reinforcement, fiber-reinforced concretes (FRC), low-permeability concretes, and reduced amounts of reinforcement (Cao, 1996; Bakht et al., 2000). To date, full-scale, instrumented field testing of these damage mitigation techniques, as applied to bridge decks, has been sparse, mostly due to the high costs associated with such studies.

2.1   Bridge Deck Design Considerations

The deck-on-girder design used in the Saco bridges is typically comprised of a reinforced concrete slab supported by two or more girders made of steel, timber, or prestressed concrete, and is one of the most common bridge designs in use today (Cao et al., 1994). In this configuration, the deck directly supports tire loads by transferring them transversely to the adjacent girders. The bridge deck is compositely attached to the girders using shear connectors to better resist longitudinal moments and transfer loads to the supporting substructure.

Traditionally, the AASHTO (2000) bridge deck design method assumes that slab-on-girder deck sections behave as one-way slabs acting in the transverse direction (perpendicular to

traffic). In 1930, Westergaard represented the bridge deck as a continuous beam supported by rigid girders which are unable to deflect vertically (Mourad and Tabsh, 1999; Csagoly and Lybas, 1989; and Cao et al., 1994). It is generally acknowledged that Westergaard's model yields conservative designs relative to strength and safety. More recently, research has sought to make deck design more efficient by modeling the actual load carrying mechanisms more accurately. The discovery of a mechanism called "internal arching" allows designers and researchers to develop sufficiently strong designs using less reinforcing steel than is required in conventionally designed decks. This has become a popular technique since reducing the amount of reinforcing steel reduces the probability of corrosion damage and increases efficiency.

Contrary to traditional models, the deck slab does not actually support wheel loads completely in flexure. Instead, a 'compressive dome' forms due to cracking in the positive moment regions (i.e., bottom fibers) of the deck concrete (Csagoly and Lybas, 1989; Fang et al., 1990; AASHTO, 2000). This 'compressive dome' supports wheel loads by relying upon the lateral restraint provided by the surrounding deck concrete and other structural elements such as girders and diaphragms. Additionally, remaining flexural loads are carried by the reinforcing steel in the bottom mat (Csagoly and Lybas, 1989). In-plane compressive membrane forces found in the concrete near the tire generally helped to establish the presence of the arching phenomenon.

Canada has developed a deck design that takes advantage of this arching behavior, commonly referred to as the 'Ontario' deck design. For bridge decks meeting certain geometric criteria, the Ontario approach allows the total amount of reinforcing steel to be reduced by approximately 30%. The primary design guideline requires a minimum steel area of 0.3% of the concrete area in both the top and bottom reinforcing mats to help control cracking and maintain confinement within the deck. Based on component testing and finite element analysis (FEA), AASHTO (2000) has included provisions for an 'empirical design,' which is similar to the Ontario deck design except that a further reduction in the top layer of reinforcing steel is allowed. Minimum top and bottom-mat steel areas of 0.2% and 0.3% of the concrete area, respectively, are required to improve crack control and maintain confinement within the deck.

To evaluate the validity of the internal arching behavior, Fang et al. (1990) tested a full-scale bridge specimen at the University of Texas at Austin. The deck concrete had a compressive strength of approximately 29 MPa. At wheel loads up to three times the AASHTO service wheel load of 92.5 kN, no compressive membrane stresses (indicative of internal arching) were observed, however, membrane tension was observed. Above this load, cracking began to occur in the positive moment regions of the slab, initiating internal arching. As expected, internal arching and failure in punching shear were also observed in the specimen at higher loads.

To further validate the credibility of the empirical deck design method, Csagoly and Lybas (1989) reviewed several research projects related to internal arching behavior in bridge decks.

One laboratory experiment proved that bridge decks with two mats of reinforcement fail in punching shear at loads six times larger than the design wheel load. All of the reviewed studies confirmed that the ultimate capacity and serviceability of the empirical deck design is comparable to the traditional deck design methods.

Fenwick and Dickson (1989) conducted laboratory tests on reinforced concrete slabs to investigate structural benefits from membrane action. Their results indicated increased strength in confined plates, suggesting membrane action was potentially contributing to load carrying capacity. However, without further testing they were unable to conclusively establish the relationship between membrane action and increased strength.

A more aggressive approach to mitigate steel corrosion is to completely remove all steel from the top mat, as proposed by Cao (1996). The slab theory of Westergaard requires the placement of reinforcing steel near the top of the deck to resist negative moments that occur over the girders. However, Cao (1996) concluded that slab theory alone was not sufficient for use in deck design. Due to the underlying differential deflections between girders, the negative moments incurred in the deck slab were less than those predicted by a slab supported on rigid girders. Cao et al. (1994) performed live load testing on the South Platte River Bridge near Commerce City, Colorado to evaluate this conclusion. Based on his results, the top mat of reinforcing steel was not necessary to withstand the negative bending moment over the girders induced by truck loads. Although these conclusions have not been included in the bridge design provisions of AASHTO (2000), his findings are important and may help others properly understand and interpret live load test results.

Even more recently, Canadian engineers have developed 'steel-free' concrete bridge deck designs, which take advantage of arching action to completely eliminate all of the reinforcing steel within the deck (Bakht and Lam, 2000; Sargent et al., 1999; Bakht and Mufti, 1998). In lieu of the internal steel reinforcement, exterior steel 'straps' are connected between adjacent girders to provide the lateral confinement necessary to maintain arching action. Other steel-free deck designs utilize fiber-reinforced polymer (FRP) bars or grids within the deck concrete in place of traditional steel rebar (Bakht et al., 2000). Both steel-free methods effectively mitigate any damage due to corrosion of the reinforcing steel by completely removing it from inside the deck.

2.2 Live Load Testing of Bridges

It is important to evaluate how bridge decks respond to vehicle loads (namely heavy vehicles) and how that response affects the expected durability of the deck over time. Changing the amount and/or configuration of the reinforcing steel may influence the bridge deck's load-carrying capacity and/or load transfer path. Although the opportunity for cracking and corrosion may be reduced or eliminated, the overall stability and integrity of the bridge deck must not be

compromised. Live load tests are commonly used to evaluate the behavior and integrity of bridges. The majority of live load tests conducted on deck-on-girder bridges have focused mainly on the girder system to determine how loads are distributed among these members. Many studies generally attempt to quantify the load carrying capacity of the bridge based on properties of the girders, and how loads are globally transferred through the superstructure and substructure to the ground. Girder distribution factors (GDFs) are commonly reported as a measure of bridge performance (Nassif et al., 2003; Tabsh and Tabatabai, 2001; Yang and Myers, 2003; Amer et al., 1999).

Even though bridge decks are acknowledged as a primary source of deficiency, very few projects have focused specifically on the internal response and the durability of bridge decks under live and environmental loads. A limited number of projects have investigated bridge deck responses to these load types as part of a larger study. Lenett et al. (2001) installed instrumentation and conducted live load tests on the HAM-126-0881L bridge near Cincinnati, Ohio. The instrumentation for the project was extensive, monitoring nearly every aspect of the bridge – abutments, piles, stringers, and the deck. Most deck sensors were placed in the longitudinal direction to construct strain profiles in the deck-girder composite sections. Monitoring was conducted during construction of the bridge to evaluate what effects the bridge experienced prior to being commissioned. Before traffic was allowed on the bridge, it was subjected to live load tests (mostly static). Bending stresses in the girders and the distribution of longitudinal strains across transverse strips of the deck were the primary focus of the analysis. The response of the bridge to environmental fluctuations was then monitored over at least one full year.

Stallings and Porter (2002) performed live load tests on the Uphapee Creek Bridge in Alabama, in which some measurements of the deck response were made. This bridge deck was constructed using a high performance concrete (HPC) mix design. Comparisons of test results with AASHTO predictions were of greatest interest to the authors. Although deck strains recorded from strain gages attached to transverse reinforcement were measured and reported, little comment was offered with regard to their meaning. Typical deck strain results reported by Stallings and Porter (2002) are shown in Figure 2. Internal deck strains recorded from strain gages located at the longitudinal midspan and transversely between two girders are shown.
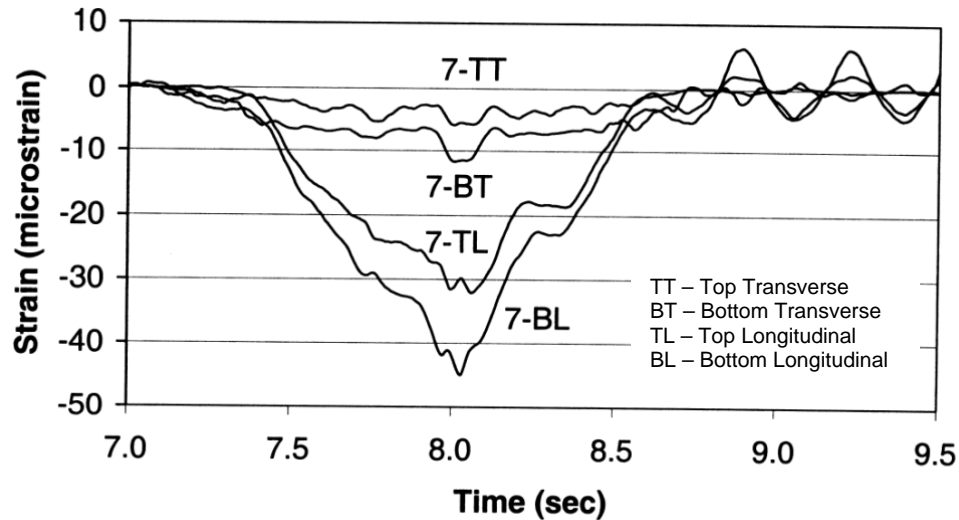
Figure 2: Reported Deck Strains at Midspan (adapted from Stallings and Porter, 2002)

Cao (1996) performed live load testing on the South Platte River Bridge near Commerce City, Colorado to validate a simplified method to analyze and model the behaviors of reinforced concrete bridge decks. The test truck used by Cao (1996) had a front axle weight of 73.4 kN, a combined rear tandem axle weight of 252 kN, and a total trailing axle weight of 145.5 kN. The total weight of the truck was 471.5 kN, which is 47% more than a standard HS20 truck, however, the wheel and axle spacing were similar. The bending moments in the bridge deck were calculated from strain data. This analysis helped to verify his hypothesis that negative moments in the bridge deck are reduced by differential girder deflections.

2.3   Instrumentation

Instrumentation is commonly used to monitor and understand the behavior of various structures. On reinforced concrete structures, instrumentation may be placed internally or externally depending on what types of information are desired. Typical sensors include strain gages, temperature sensors, tilt meters, accelerometers and displacement gages. Strain gages may be embedded in the concrete or attached directly to the reinforcing steel using a variety of configurations and techniques. Many research projects have utilized instrumentation, yet few have focused their attention on strains within the bridge deck. Following are a few examples of such projects.

In a study by Buckler et al. (2001), researchers at the Virginia Transportation Research Council (VTRC) developed a computational model to represent the behavior of a reinforced concrete bridge deck. They successfully validated their model using experimental results from the Willis River Bridge, an instrumented bridge deck in Buckingham County, Virginia. Instrumentation was designed to measure the displacement of the four stringers, longitudinal

strains in the flanges of the four stringers, transverse deck strains midway between the three sets of stringers, and the natural frequency of the bridge (Buckler et al., 2001).

Cantilever deflection gages (CDG) were attached to the lower flanges of each stringer to determine the deflection of all four steel stringers. The CDGs used in this research consisted of a triangular steel plate instrumented with strain gages. The plate was attached to the flange of the stringer at its midspan using C-clamps, and a weight suspended from the plate rested on the ground below. The suspended weight imparted an initial strain to the plate, so as the bridge deflected under a load, the strain in the CDG decreased. Strain in the CDGs was converted into deflections of the stringer at midspan.

Resistance strain gages were bonded to the flanges of the stringers using an epoxy to measure longitudinal strain. Two stringers had both top and bottom flanges instrumented, while the remaining stringers only had gages on the bottom flanges.

Five weigh in motion gages (WIM) were used to measure strain in the bottom of the concrete. Three gages were placed on the underside of the deck midway between each set of stringers to measure transverse strain. A fourth WIM gage was oriented in the longitudinal direction near the interface between the top flange of the second stringer and the bottom of the concrete deck. The fifth WIM gage was placed in the same location, but oriented in the transverse direction.

Accelerometers were used to determine the natural frequency of the bridge. A single accelerometer was placed on the top surface of the bottom flange of each girder at their midspan. All of the data mentioned were recorded near the middle of the first span, between the abutment and first pier.

For the field investigation of the South Platte River Bridge near Commerce City, Colorado (Cao et al., 1994), bridge deck response was monitored using strain gages embedded at different locations within the deck concrete. The stain gages were welded onto pieces of #4 rebar having several bends to ensure good bonding with the surrounding concrete. Five transverse gage lines were selected; three in the experimental portion of the deck, and two in a control section (Figure 3). In the experimental portion of the deck, the first and third gage lines were located near the ends of the span. The second gage line was near, but not exactly at the center of the span. In the control portion of the deck, the same gage lines were used, except that the gage line near the pier was not included. There were seven gage points within each gage line, as shown in Figure 4. At each gage point, gages were typically placed near the top and bottom of the bridge deck in either the transverse or longitudinal direction.
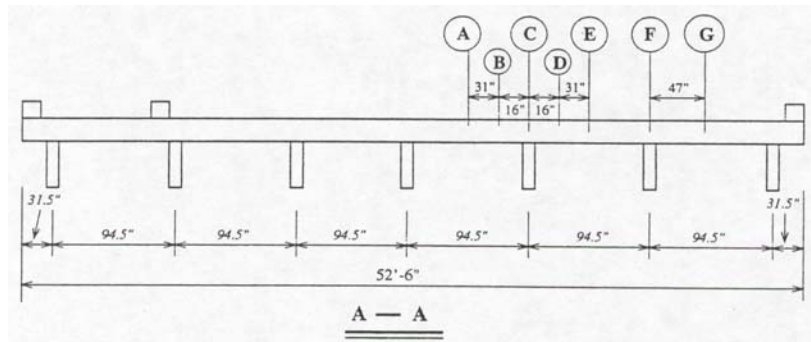
Figure 3: Plan View of Transverse Gage Lines (from Cao et al., 1994)
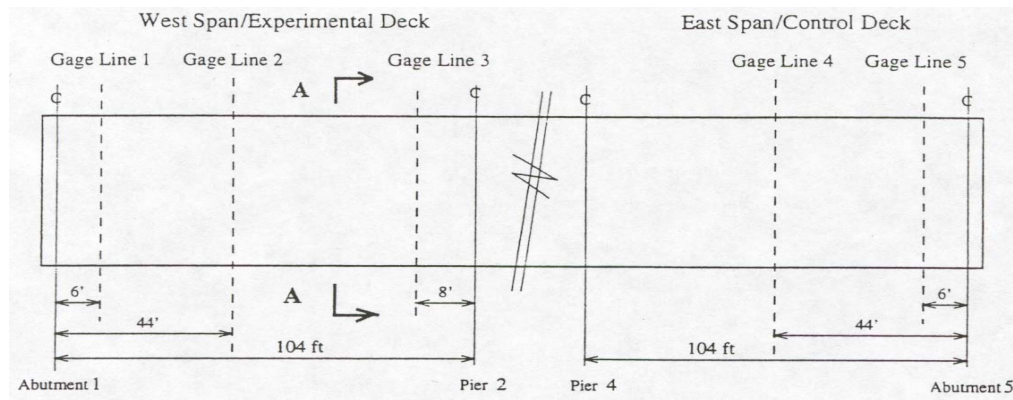
Figure 4: Typical Transverse Cross-Section Showing Gage Point Locations (from Cao et al., 1994)

2.4   Temperature Effects on Concrete Bridge Structures

The first comprehensive investigation of thermal effects on bridge decks in the United States was conducted in the mid-eighties through the National Cooperative Highway Research Program (NCHRP). Report 276 entitled *Thermal Effects in Concrete Bridge Superstructures* summarizes the results of this research project (Imbsen et al., 1985). An abridged version of this report was later published by the American Association of State Highway and Transportation Officials (AASHTO) as a recommended guide specification (rather than as a modification to the AASHTO design specifications). The current AASHTO LRFD Bridge Design Specifications incorporate the recommendations of NCHRP Report 276 (with slight modifications) (AASHTO, 2000).

2.4.1 Bridge Design Considerations

The temperature behavior of bridges is typically viewed as two superimposed effects. The first effect is from a uniform change in temperature that occurs over the entire superstructure. This temperature event causes an overall length change for an unrestrained structure. If the

structure is restrained, a uniform temperature change will produce internal stresses. The second event is a temperature gradient that occurs when the bridge superstructure is heated unevenly (such as when the sun substantially heats the deck surface or a freezing rain falls on a warm day). Temperature gradients in bridge decks are more commonly realized in the vertical direction; therefore, designs typically do not consider uneven temperatures in the horizontal direction.

The two primary temperatures used by bridge designers to account for thermal stresses from temperature changes throughout the bridges life are: 1) the concrete setting temperature and 2) the range of temperatures likely to be experienced by the bridge deck. The setting (installation) temperature, as defined by AASHTO, is determined by averaging the actual air temperature over the 24-hour period immediately before the setting event (AASHTO, 2000). The setting temperature is the reference temperature used to define the direction and magnitude of subsequent thermal behavior under temperature changes. This parameter is most critical when expansion bearings and deck joints are installed.

The range of temperatures the deck will experience throughout its life is also important. AASHTO divides the country into two regions to determine uniform temperature ranges that bridges will experience based on the number of expected freezing days (temperatures less than 0 °C). Moderate climates are defined as having fewer than 14 freezing days per year; conversely, cold climates have greater than 14 days below freezing. This method is merely a general indication of the length of time a bridge deck could be expected to be at a colder temperature but does not necessarily represent the number of actual days spent at a particular temperature. Bridge designs in varying climates account for this, as illustrated in Table 1. The temperature range considered in design also depends on the bridge material. Metal bridges have quicker response to changes in temperature, whereas the thermal mass of concrete bridges acts as a temperature regulator, reducing their reaction to rapid and extreme changes in temperature. The temperature sensitivity of wood bridges is further reduced because of wood's superior performance in colder temperatures (i.e., reaching critical strains in wood does not result in brittle failures).

Table 1: Uniform Temperature Ranges (from AASHTO, 2000)

Climate	Steel or Aluminum (°C)	Concrete (°C)	Wood (°C)
Moderate	-18 to 50	-12 to 27	-12 to 24
Cold	-35 to 50	-18 to 27	-18 to 24

Saco, Montana has a cold climate; thus, referring to Table 1, a uniform temperature range of -18 °C to 27 °C would be used for design (concrete deck in a cold climate). The deck concrete setting temperature for the Saco bridges was approximately 25 °C. These results imply that the

Saco bridges will likely experience a positive uniform temperature change (ΔT_{pos}) of 2 °C and a negative uniform temperature change (ΔT_{neg}) of 43 °C ($\Delta T_{pos} = 27 - 25 = 2$ °C and $\Delta T_{neg} = 25 - (-18) = 43$ °C).

Relative to temperature gradients, AASHTO divides the United States into four solar radiation zones, with zone 1 receiving the most and zone 4 the least solar radiation (Table 2) (AASHTO, 2000). Zone 1 encompasses most of the Western United States, giving the Saco bridges the temperature gradient shown in Figure 5. Three temperatures are used to define the gradient through the deck and superstructure: T_1 is the temperature at the top of the bridge deck, T_2 is the temperature 0.10 meters below the top of the bridge deck, and T_3 is the temperature at the bottom of the superstructure (defined as 0 °C).

Table 2: Gradient Temperatures for the United States (from AASHTO, 2000)

Zone	T_1 (°C)	T_2 (°C)
1	30	7.8
2	25	6.7
3	23	6
4	21	5
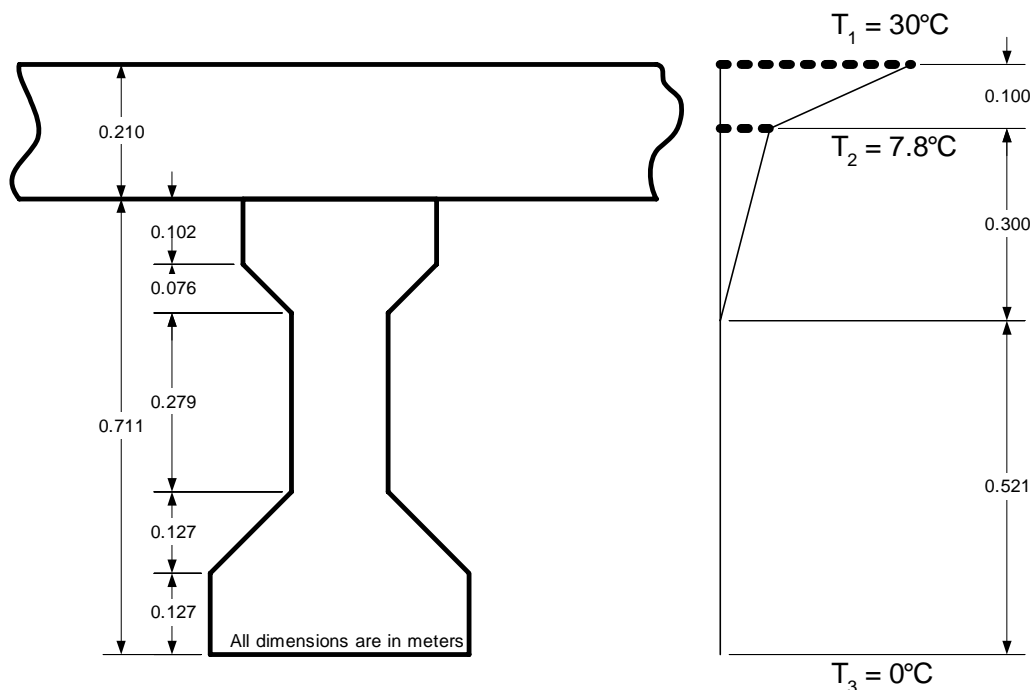
Figure 5: Positive Gradient Temperature Distribution in the Saco Bridges

Negative gradient temperatures (gradient under decreasing temperature) are obtained by multiplying the positive temperatures by -0.30. The lower magnitude negative temperature

gradient reflects the different heating and cooling events for the bridge decks. The positive temperature gradients occur when during the summer the top of the deck is warmer than the soffit; the negative temperature gradient develops on winter nights when the deck temperature is cooler than the soffit. The summer event develops a much larger temperature gradient than the winter event.

2.4.2 Bridge Response

Several methods of analysis exist to determine the effect of temperature changes on structures. The following assumptions are made when thermal analyses of bridge structures are conducted using the AASHTO bridge deck specifications (AASHTO, 1989):

1. The material is homogeneous and exhibits isotropic behavior.
2. Material properties are independent of temperature.
3. The material has linear stress-strain and temperature-strain relations. Thus, thermal stresses can be considered independently of stresses or strains imposed by other loading conditions, and the principle of superposition holds.
4. The Navier-Bernoulli hypothesis that initially plane sections remain plane after bending is valid.
5. The temperature varies only with depth, but is constant at all points of equal depth (except those points over an enclosed cell).
6. Longitudinal and transverse thermal responses of the bridge superstructure can be considered independently and the results superimposed; i.e., the longitudinal and transverse thermal stress fields are assumed to be uncoupled.

AASHTO LRFD Bridge Design Specifications (Section 4.6.6) provide the following method for examining the force effects due to temperature deformations. The structure's response is divided into three effects: 1) axial expansion, 2) flexural deformation, and 3) self equilibrating stresses (AASHTO, 2000). Axial expansion is caused by the uniform component of the temperature gradient. The uniform component of the temperature gradient is calculated as the average temperature across the cross section. Flexural deformation is a result of plane sections remaining plane under a linear temperature gradient. Structures that are externally unrestrained develop no external forces. In a fully restrained structure, however, axial forces and moment forces may also develop. The internal "self-equilibrating" stresses are determined by first allowing the free expansion of the material fibers for the temperature load; from this analysis the axial force developed for the uniform temperature case, and the moment developed for the gradient temperature case, are subtracted. The resulting stress distribution is termed the continuity stresses, which are required to keep plane sections plane.

2.4.3 Thermal Behavior of Concrete

The behavior of concrete during temperature changes is complex and has been shown to vary significantly between concrete mixtures. Concrete material models (including those that address thermal behaviors) are incomplete and subjective because concrete continues to change physically and chemically with, among other things, time, temperature, and stress. Furthermore, observed behaviors are related to the physical and chemical structure of the concrete on a nanometer scale. The various components of concrete that influence its behavior are illustrated in Figure 6.
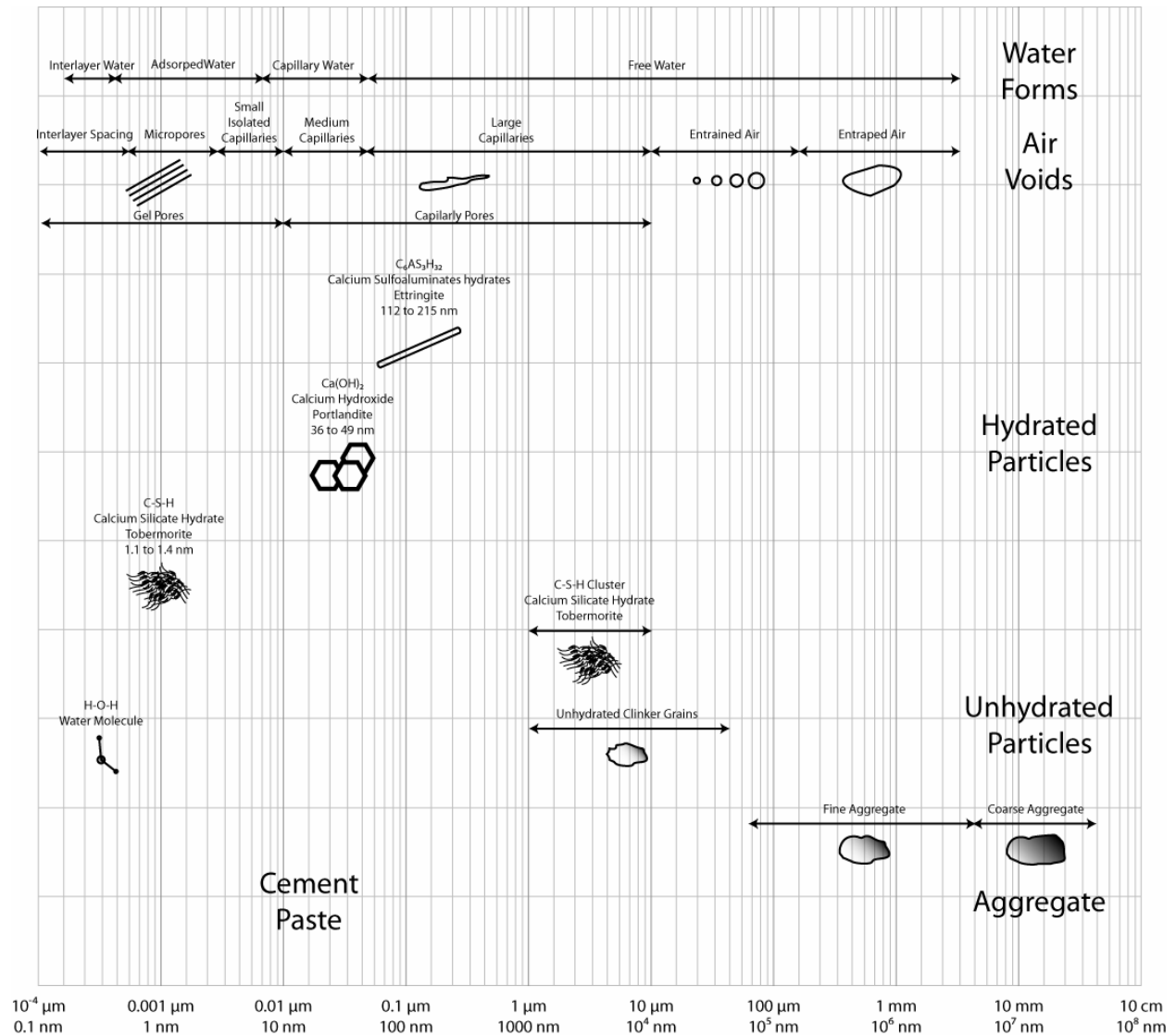
Figure 6: Scale of Structural Components of Concrete (adapted from Mehta, 1986)

2.4.3.1   Coefficient of Thermal Expansion

The thermal expansion of concrete varies with aggregate type, cement content, water-cement ratio, temperature range, concrete age and relative humidity (Kosmatka et al., 2002). The

coefficient of thermal expansion (CTE) for concrete is highly dependent on the type of aggregate from which it is made. This situation is not surprising, since the aggregate typically makes up approximately 75 percent of the concrete's total volume. For design, the CTE value of concrete is typically assumed to be constant, with a commonly reported value of 10.4 $\mu\varepsilon/°C$ (approximately midway in the reported range of 7 to 14 $\mu\varepsilon/°C$). This range is mostly a result of the aggregate used to make the concrete. A summary of concrete CTE values is shown in Table 3.

Table 3: Thermal Expansion Coefficients Various Concrete Mixes (adapted from Imbsen et al., 1985 and Zia et al., 1997)

Aggregate Type	Reported CTE from Various Publications ($\mu\varepsilon/°C$)				
	PCA, 1982	Emerson, 1979	Brown, 1968	Ontario, 1979	Turner Fairbanks, 2005
Quartzite	---	12.7	11.7 – 14.6	12.8	11 – 13
Quartz	11.9	---	9.0 – 13.2	---	---
Sandstone	11.7	11.7	9.2 – 13.3	9.5	11 – 12
Granite	9.5	9.6	8.1 – 10.3	9.5	7 – 9
Dolerite	---	9.6	---	9.5	---
Basalt	8.6	---	7.9 – 10.4	---	6 – 9
Marble	---	---	4.4 – 7.4	---	4 – 7
Limestone	6.8	7.3	4.3 – 10.3	7.4	6
Dolomite	---	---	---	---	7 – 10

The aggregate source for the three decks in Saco was a gravel pit near Malta, Montana. The aggregate was believed to be primarily composed of quartz, indicating a range of CTE values between 9.0 and 13.2 $\mu\varepsilon/°C$. The Turner Fairbanks Research Center determined common CTE values for all of the components of Portland cement concrete. Saturated cement paste having water-cement ratios between 0.4 and 0.6 have CTEs from 18 to 20, concrete mixes have CTEs from 7.4 to 13, and the CTE of steel is 11 to 12. The thermal properties of high performance concrete are within the same range as conventional concretes (Shah and Ahmad, 1994). This, again, is not surprising since the aggregate occupies the majority of the concrete's volume.

While the general thermal behavior of concrete is dictated by the aggregate type, several secondary behaviors can be attributed to the thermal behavior of the water within the cement paste. These behaviors typically occur when the water within the cement paste changes phase. Berwanger (1971) identified a change in the strain slopes at around the freezing point of water for concrete specimens undergoing a temperature change. Powers and Brownyard (1947) showed that the freezing point of water in concrete was typically 5 to 7 °C below the standard

freezing point. Powers associated this phenomenon with the alkali content of the water within the cement paste. In general, the water related temperature behaviors are deeply affected by the nanostructure of the cement paste. Cement paste is composed of three primary constituents: 1) the cement gel, which consists of the hardened hydration products, 2) un-hydrated cement particles and 3) pores of varying shape and size filled with water or air (excluding the gel pores, and interlayer spaces) (Mehta, 1986).

2.4.3.2 Freeze-Thaw Effects

Water in the cement paste affects the overall behavior and performance of a concrete on macroscopic level, and is associated with concrete's response to freezing and thawing cycles. Freeze-thaw damage is directly associated with the phase change of the water in the cement paste. There are three mechanisms that contribute to freeze-thaw damage: 1) hydraulic pressure, 2) osmotic pressure, and 3) capillary effect (Mehta, 1986).

The first mechanism, hydraulic pressure, is thought to typically develop in the capillaries and other larger voids. When water freezes, it expands approximately 10 percent. If the water content of the void is above the critical saturation level (91.7 percent water), the expansion will cause the void to enlarge and/or cause some of the water to exit the void. The pressure associated with this phenomenon is called hydraulic pressure, and it is proportional to the distance the water must travel to an 'escape boundary'. This boundary is typically provided by air entrained into the concrete.

Another phenomena that is believed to occur as the larger voids start to freeze, is that the salts (alkalis, chlorides, and calcium hydroxide) naturally occurring in the hydrated cement paste migrate into the adjacent water. The alkali concentration in the nearby water greatly increases as a result, which lowers its freezing point. Osmotic pressures develop from the differences in alkali concentrations, and adjacent water tries to flow towards the high concentration. This pressure may become high enough to rupture the cement paste near the surface, causing scaling.

The final mechanism that is believed to develop in the paste under freeze-thaw action results from the thermodynamic imbalance between the frozen water in the larger voids and the unfrozen water located in the gel pores. The interlayer and adsorbed water remains unfrozen at supercooled temperatures (to perhaps as cold as -78 °C in the smallest voids) due to its bonding with the calcium silicate hydrate (C-S-H) matrix, which greatly reduces its ability to rearrange into ice. As the temperature decreases, the forces drawing the unfrozen water towards the ice formation increase, causing a transmittal of water into more ice. Damage is done when the concrete's permeability is too low to allow the water transition needed to meet external demand. When the forces become large enough, the cement gel can rupture.

Air entrainment has historically shown to be the best remedy for concrete's susceptibility to freeze-thaw. The entrained air (typically assumed to be unsaturated) reduces pressures within

the matrix by allowing expansion of ice within the voids and by providing an escape boundary for water towards the lower energy state. Its effectiveness has been inferred from the differences observed in the temperature deformations of normal concrete and air entrained concrete. Normal concrete, when cooled, typically undergoes an expansion due to the formation of ice within the voids. Air entrained concrete when cooled typically contracts at a different rate, a result of the combination of the expansion of ice formations and the shrinkage of the C-S-H due to the removal of water.

High performance concretes typically have lower permeabilities and porosities when compared to standard concretes. The strength gains in high performance concretes are specifically attributed to the reduction in pore numbers and size. High performance concretes typically have less available water for freeze-thaw than conventional concrete, due to their relatively lower initial water to cement ratios. In addition, their lower permeability reduces the ability for water to infiltrate into the concrete from the external environment. Low permeability, however, also reduces the ability of the water to move through the cement paste under the mechanisms stated above. This situation could make high performance concretes more susceptible to damage from rapid freezing and thawing (Zia et al., 1997). The two characteristics work to offset each other. Research has suggested that non-air-entrained high performance concrete has good frost resistance (Shah and Ahmad, 1994; Zia et al., 1997).

Hammer and Sellevold (1990) proposed much of the damage in concretes caused by freeze-thaw could be attributed to thermal incompatibility of its components, instead of the formation of ice, based on calorimeter data that suggested little ice forms at temperatures above -20 °C.

3   DESCRIPTION OF THE BRIDGES

The three new bridges were constructed on Route 243 approximately one mile north of Saco, Montana. Route 243 is a Secondary route that has an average annual daily traffic count of 220 (1998), with 11.5% being trucks. Much of the anticipated loading will come from heavy farm machinery and trucks, which can impose high demands.

The concrete was placed in the HPC deck on May 28, 2003; in the Empirical deck on June 3, 2003; and in the Conventional deck on June 5, 2003. Concrete samples were collected from several trucks in the instrumented section of the bridges.

All three bridges are 44.5 meters long and 9.1 meters wide. The superstructure consists of three spans, as shown in Figure 7. The stringers that support the deck are standard, Type-I prestressed concrete I-beams spaced at 2.4 meters on center, as shown in Figure 8. The thickness of each deck is 210 mm. Design specifications for the bridge decks required 31 MPa strength concrete.
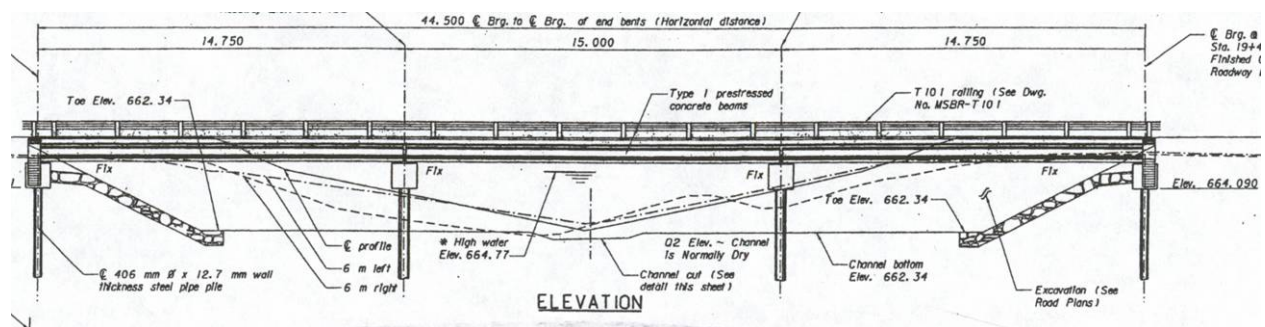
Figure 7: Elevation View of One of the Bridges
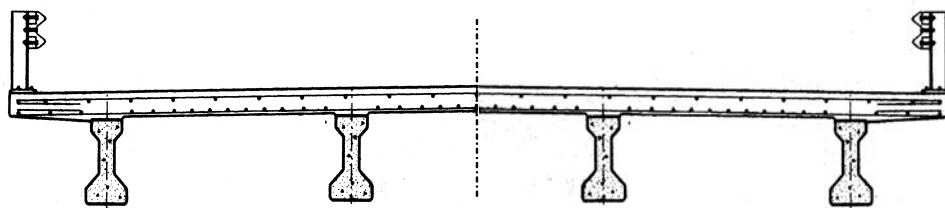
Figure 8: End View of Conventional Bridge Deck

While all three decks use epoxy coated reinforcing steel, the layout of the reinforcing steel varies between the three decks. The conventional and HPC decks are designed using the traditional strength approach described in the AASHTO specifications (AASHTO, 2000). The traditional strength design method treats the deck as if it were a beam in flexure spanning the stringers. This design results in the primary reinforcement oriented transversely to the length of the bridge.

The empirical design approach, which requires no formal analysis, is permitted by the AASHTO specifications for monolithic concrete bridge decks that satisfy specific conditions.

Using this design method, reinforcement ratios for the top and bottom mat in both the longitudinal and transverse directions are simply functions of the depth of concrete and length of span. AASHTO specifies a minimum reinforcement ratio equal to 3.8 cm^2/meter in each direction in the top mat, and 5.7 cm^2/meter in each direction in the bottom mat. The reason for the increased amount of steel in the bottom mat is for better crack control in the positive bending regions of the slab. Comparatively, in the construction drawings for the decks constructed as part of this research project, the Conventional and HPC decks require 3679 kg more steel than the empirical deck. Figure 9 shows the difference in the density of the reinforcement between the two deck designs, taken at the same place in the deck. Reducing the amount of steel in the empirical deck, especially in the top layer, decreases the opportunity for, and the affects of reinforcement deterioration.

a)   b)
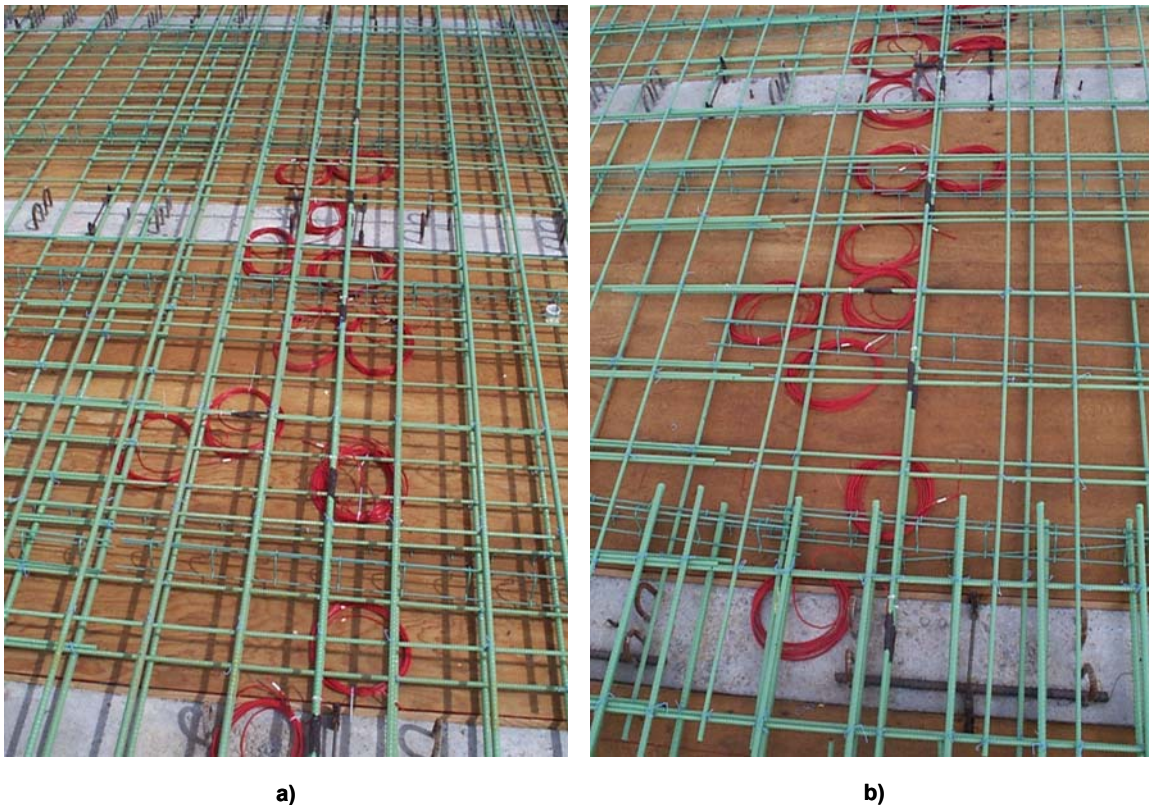
Figure 9: Example Reinforcement Densities of the Conventional and HPC Decks (a), and the Empirical Deck (b)

3.1 Concrete Bridge Deck Mix Designs

The concrete mix designs used by the Montana Department of Transportation for each of the bridge decks are detailed in Table 4. The Conventional and Empirical decks used the "Special Deck" recipe while the HPC deck used the high performance recipe. A 19 mm minus aggregate mixture was used in conjunction with these mix designs.

Table 4: Mix Designs for Deck Concrete Used in the Saco Bridges

Components	Special Deck Concrete Batch Quantities	HPC Deck Concrete Batch Quantities
Cement	366 kg/m^3	366 kg/m^3
Silica Fume (Rheomac SF100)	---	22.3 kg/m^3
Water	151.1 kg/m^3	129 kg/m^3
Coarse Aggregate (#4 – ¾")	1061 kg/m^3	1094 kg/m^3
Fine Aggregate (sand)	719 kg/m^3	693 kg/m^3
Air Entraining Solution[a]	127 ml	325 ml
Water Reducing Agent[b]	910.9 ml	911 ml
Superplasticizer[c]	---	1455 ml
Properties		
Final Slump	40 – 80 mm	100 – 200 mm
Air Content	6% ± 1%	5 – 7%
Minimum 28-Day Strength	31 MPa	31 MPa

3.2   Materials Sampling and Testing

Concrete was poured into the decks using a two-yard bucket and a crane, and was leveled using an automatic screed (Figure 10). During construction of the bridge decks, MDT performed air content tests, slump tests, and collected test specimens from selected trucks on each bridge to make concrete test cylinders. Average results from slump and air content tests are provided in Table 5, and the detailed results from all tests are summarized in Appendix A. In addition, the Western Transportation Institute (WTI) collected concrete test specimens from a representative portion of the concrete used to cast the instrumented section of each deck. Sufficient samples were collected to be tested at three distinct time intervals: 28-days, at the first live load test, and at the second live load test. All material sampling and testing was conducting in substantial compliance of ASTM specifications listed in Appendix B.

Table 5: Average Slump and Air Content from Bridge Deck Concrete

Bridge Deck	Average Slump (mm)	Average Air Content (%)
Conventional	79.4	6.3
Empirical	92.1	6.5
HPC	168.3	5.1

Sixteen to eighteen truckloads of concrete (approximately 96 cubic meters) were used to cast each bridge. In general, the instrumented areas of each bridge were cast with concrete from the fourth truck through the eighth truck. Rather than sampling from a single truck in the instrumented region of the decks, as was originally proposed, the decision was made at the time of the deck pours to collect samples from three of the trucks from the instrumented region of each deck (samples were actually collected from four trucks for the Conventional deck). For the most part, one truck from each bridge was more heavily sampled than the remaining trucks. Table 6 summarizes the number of each type of sample collected from each bridge.

Figure 10: Placing the Deck Concrete

Table 6: Concrete Samples Collected during Construction

Bridge	Cylinders	Rupture Beams	Shrinkage Beams
Conventional	35	9	3
Empirical	26	9	3
HPC	18	9	3

Concrete test cylinders 152 mm diameter by 305 mm long were used to determine uniaxial compressive strength, elastic modulus, and splitting tensile strength. Rectangular beams 152 mm wide by 152 mm deep by 508 mm long were used to determine modulus of rupture. Shrinkage properties were determined using rectangular beams 76 mm wide by 76 mm deep by 406 mm long. Selected concrete specimens were cured in a moist cure room at Montana State University

(for 28-day testing) while the remaining samples were cured near the bridge decks. A complete summary of the samples collected from each bridge, the conditions under which these samples were cured, and the tests to which these samples were subjected is presented in Tables 7, 8, and 9.

Table 7: Concrete Sampling and Testing Matrix – Conventional Deck, Cast 6/05/03

Truck No.	Type of Specimen[a]	Number of Specimens	Curing	Times Tested	Type of Test
C-4	cylinder	3	moist	28 days	compression
	cylinder	3	with deck	1st live load	compression
	cylinder	3	with deck	2nd live load	compression
	beam	2	with deck	1st live load	bending
C-5	cylinder	2	with deck	1st live load	compression
	cylinder	2	with deck	2nd live load	compression
C-6	cylinder	3	moist	28 days	compression
	cylinder	3	with deck	1st live load	compression
	cylinder	3	with deck	1st live load	split cylinder
	cylinder	3	with deck	2nd live load	compression
	cylinder	3	with deck	2nd live load	split cylinder
	beam	2	with deck	1st live load	bending
	beam	2	with deck	2nd live load	bending
	shrink	3	with deck	periodically	shrinkage
	shrink	3	moist	periodically	shrinkage
C-7	cylinder	3	moist	28 days	compression
	cylinder	3	with deck	1st live load	split cylinder
	cylinder	3	with deck	2nd live load	compression
	beam	2	with deck	2nd live load	bending

[a] *cylinder – 152 mm diameter by 305 mm long cylinder*
beam – 152 mm wide by 152 mm deep by 508 mm long beam
shrink – 76 mm wide by 76 mm deep by 406 mm long beam

Table 8: Concrete Sampling and Testing Matrix – Empirical Deck, Cast 6/02/03

Truck No.	Type of Specimen[a]	Number of Specimens	Curing	Times Tested	Type of Test
E-5	cylinder	3	moist	28 days	compression
	cylinder	3	with deck	1st live load	compression
	cylinder	3	with deck	2nd live load	compression
	beam	2	with deck	1st live load	bending
E-7	cylinder	3	moist	28 days	compression
	cylinder	3	with deck	1st live load	compression
	cylinder	3	with deck	1st live load	split cylinder
	cylinder	3	with deck	2nd live load	compression
	cylinder	3	with deck	2nd live load	split cylinder
	beam	2	with deck	1st live load	bending
	beam	2	with deck	2nd live load	bending
	shrink	3	with deck	periodically	shrinkage
	shrink	3	moist	periodically	shrinkage
E-9	cylinder	3	moist	28 days	compression
	cylinder	3	with deck	1st live load	compression
	cylinder	3	with deck	2nd live load	compression
	beam	2	with deck	2nd live load	bending

[a] *cylinder – 152 mm diameter by 305 mm long cylinder*
beam – 152 mm wide by 152 mm deep by 508 mm long beam
shrink – 76 mm wide by 76 mm deep by 406 mm long beam

Table 9: Concrete Sampling and Testing Matrix – HPC Deck, Cast 5/28/03

Truck No.	Type of Specimen[a]	Number of Specimens	Curing	Times Tested	Type of Test
H-4	cylinder	1	moist	28 days	compression
	cylinder	2	with deck	1st live load	compression
	cylinder	2	with deck	1st live load	split-cylinder
	cylinder	2	with deck	2nd live load	compression
	beam	2	with deck	1st live load	bending
	beam	1	with deck	2nd live load	bending
	shrink	3	with deck	periodically	shrinkage
	shrink	3	moist	periodically	shrinkage
H-6	cylinder	2	moist	28 days	compression
	cylinder	2	with deck	1st live load	compression
	cylinder	2	with deck	2nd live load	compression
	beam	2	with deck	1st live load	bending
	beam	1	with deck	2nd live load	bending
H-8	cylinder	1	moist	28 days	compression
	cylinder	2	with deck	1st live load	compression
	cylinder	2	with deck	2nd live load	compression
	beam	1	with deck	1st live load	bending
	beam	2	with deck	2nd live load	bending

[a] *cylinder – 152 mm diameter by 305 mm long cylinder*
beam – 152 mm wide by 152 mm deep by 508 mm long beam
shrink – 76 mm wide by 76 mm deep by 406 mm long beam

The Western Transportation Institute (WTI) conducted 28-day compression tests on all moist cured test cylinders from all the bridges. Load and displacement data was collected from most of the specimens, and the stress-strain behavior of the concrete was determined. Average strength values from the 28-day compression tests conducted by WTI and MDT are provided in Table 10. Conflicting values between MDT and WTI may be associated with different curing and end cap conditions. Table 11 lists the moduli of elasticity from tests conducted at 28 days, during the first live load tests and during the second live load tests. Results from all unconfined compression tests are presented in Appendix A. A plot of the average stress-strain relationships are shown in Figure 11 for all three decks tested at 28 days, during the first live load and during second live load.

Table 10: Average 28-Day Concrete Strengths

Testing Entity	Conventional (MPa)	Empirical (MPa)	HPC (MPa)
MDT	37.8	33.0	54.0
WTI	28.0	27.4	46.0

Table 11: Modulus of Elasticity of Deck Concrete

Bridge	28-day (GPa)	1st Live Load (GPa)	2nd Live Load (GPa)
Conventional	29.3	29.9	28.8
Empirical	27.8	24.8	25.7
HPC	31.5	30.8	29.4
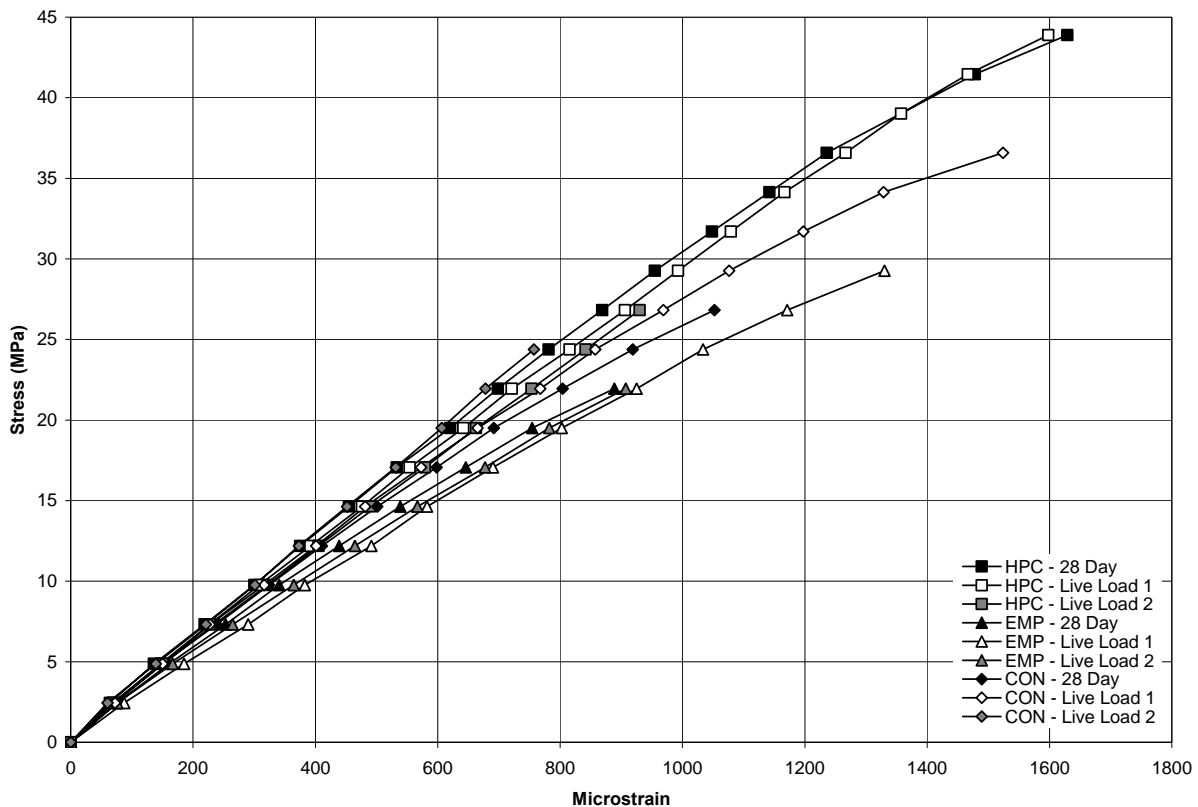
Figure 11: Average Stress/Strain Plots for All Bridge Decks

Shrinkage of the deck concrete was monitored using special beams cast during the deck pour. Some of the shrinkage beams were cured in a moist environment while the remainder were cured with the deck. Shrinkage is highly dependent upon humidity, therefore, the shrinkage beams cured with the bridge decks in Saco most closely represent true shrinkage of the deck concrete. Length measurements were made using a very accurate digital micrometer. Figure 12 shows the shrinkage of the site-cured specimens (negative microstrain indicates compressive or shrinkage strains) during the monitoring period. Initial measurements were made just after the decks were cast, and the second and third measurements were made during summer 2004 and 2005. Measurements revealed that the shrinkage was different between the HPC deck and the other two decks. These differences are most apparent from the last measurements made in 2005.

3.2.1 Steel Reinforcement

Epoxy-coated, Grade 60 steel rebar was specified for each of the bridge decks. Mill test reports were obtained from MDT for the rebar used in the project. The average yield strength is 478.5 MPa, the average tensile strength is 740.1 MPa and the elongation at failure is 14.5%. Tests to evaluate the epoxy coating yielded acceptable results. Raw data is provided in Appendix C.
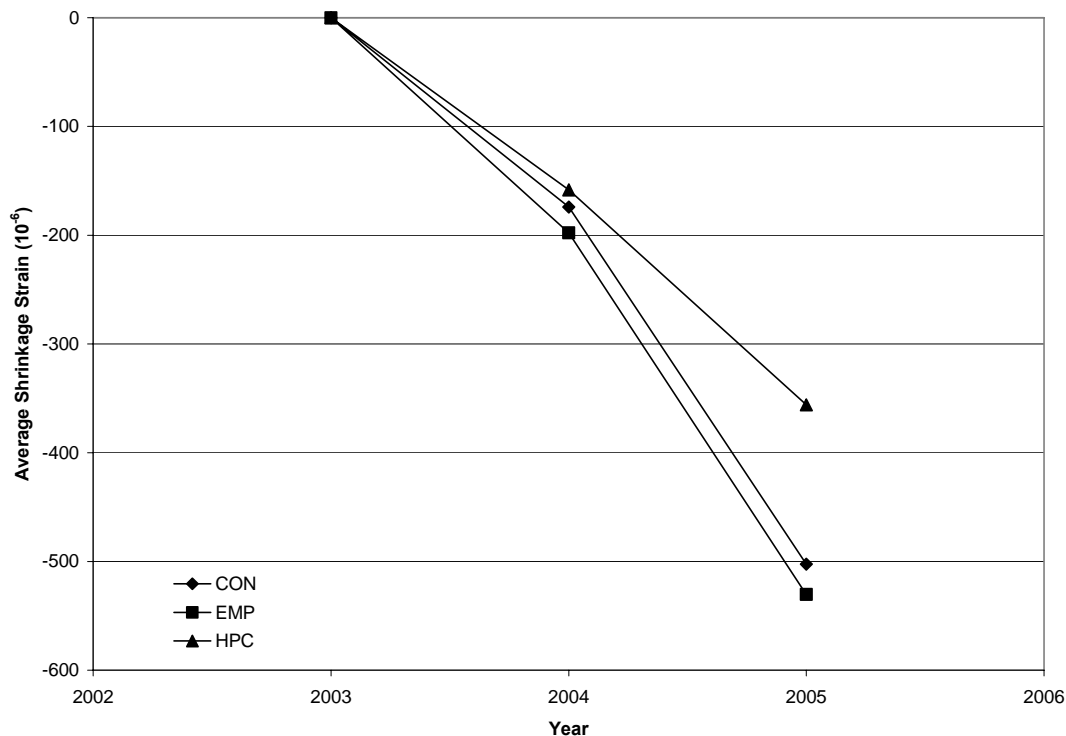
Figure 12: Shrinkage of the Deck Concrete over Time

3.2.2 Prestressed Girders

Type I prestressed concrete beams were used to support the bridge deck. The dimensions and sectional properties of these beams are shown in Figure 13. The results of the concrete compressive strength tests for the prestressed girders (obtained from MDT) were averaged and are summarized in Table 12. The raw data is provided in Appendix D.
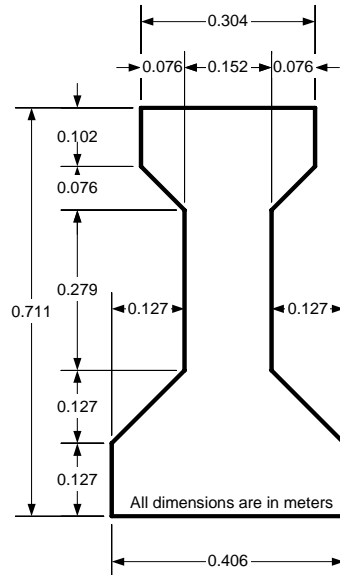
Figure 13: Dimensioned Cross-Sectional View of Saco Bridge Girders

Table 12: Average 28-day Prestressed Girder Concrete Compressive Strengths

Bridge	Prestressed Girder (MPa)
Conventional	63.0
Empirical	61.0
HPC	64.2

4   DEVELOPMENT AND IMPLEMENTATION OF THE INSTRUMENTATION PLAN

The instrumentation in the Saco Bridge Project was configured to fulfill multiple project goals. The two primary objectives were to observe long-term environmental and short-term live load deck responses. It was also desirable to separately monitor strain in the concrete and in the reinforcement, especially in areas prone to cracking. To meet these objectives, a detailed instrumentation plan was produced to determine general and specific gage locations. The instrumentation and data acquisition system were chosen based on durability, reliability and flexibility. Redundancy was necessary to ensure critical measurements were not missed. The following subsections detail 1) how gage locations were selected, 2) the various types of instrumentation, 3) the data acquisition system capabilities and setup, and 4) how each of these components were installed and assembled.

4.1   Gage Locations

A three-dimensional analytical model of the bridges was used to help select critical instrumentation locations. The model was created using Visual Analysis, a multipurpose finite element program. The model was constructed using four-node plate elements to represent the bridge deck and beam elements to represent the stringers. All elements were linked together using stiff beam elements to simulate the composite action of the deck-girder superstructure system. Further care was exercised in developing the model so that the details of the deck and stringer configurations were accurately portrayed at the interior supports. The model was loaded with a three-axle truck placed at predetermined longitudinal and transverse positions of the bridge deck using point loads. Stress contour plots of the deck were generated for each truck position. These plots were then used to verify locations of high and low stress, and to identify any unexpected locations with high stresses, where instrumentation should be placed. Gage locations were selected to 1) capture the extreme response, 2) characterize the response in general, and 3) characterize the response at specific features/locations of interest. Gage locations were also selected to study the interaction between the deck and the supporting structure. For added verification, candidate instrumentation locations were compared with locations chosen by other researchers in similar bridge test programs.

To identify precise locations for instrumentation, envelopes of extreme fiber stresses were generated for the bridge deck in both the longitudinal and transverse directions. Using this information, specific reinforcing bars within these areas were chosen to be instrumented. When appropriate, instrumentation was embedded in the concrete near these instrumented bars to duplicate or augment strain information from the instrumented rebar. From this work, a formal instrumentation plan that detailed gage type, location, and expected level of response was generated (Appendix E).

The final instrumentation suite used three types of instrumentation to monitor strains in the bridge decks. Each bridge deck contained 35 strain gages bonded directly to the reinforcement, 9 strain gages embedded in the concrete, and 20 vibrating wire gages embedded in the concrete. During live-load testing, four external strain gages were attached to the underside of the stringers.

General locations selected for instrumentation are between the south abutment and Bent #2 (southernmost interior bent). The approximate positions of the deck gages oriented in the longitudinal and transverse directions are shown in Figures 14 and 15, respectively. The positions of the external strain gages, oriented in the longitudinal direction and attached to the bottom of the stringers, are shown in Figure 16. In the longitudinal direction, gage locations were primarily concentrated near the bents and diaphragms, while the transverse gages were focused in the area between the diaphragm and the bent. Most locations have gages placed at the top and bottom of the cross-section. Overall, these locations were chosen to study:

- stringer-bent interaction,
- bending across the bent,
- effects of the diaphragm,
- continuity effects,
- global bending,
- effect of saw cut,
- stringer effects,
- bent effects, and
- local deck behavior.
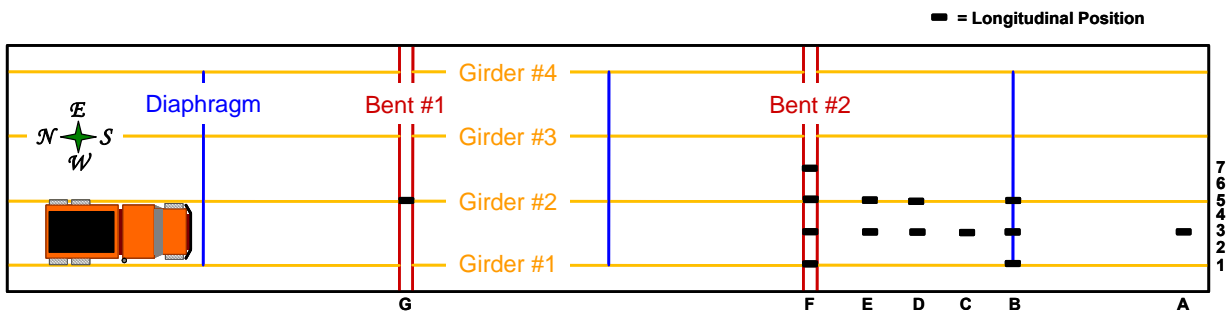
Figure 14: General Location of Strain Gages Oriented in the Longitudinal Direction (plan view)
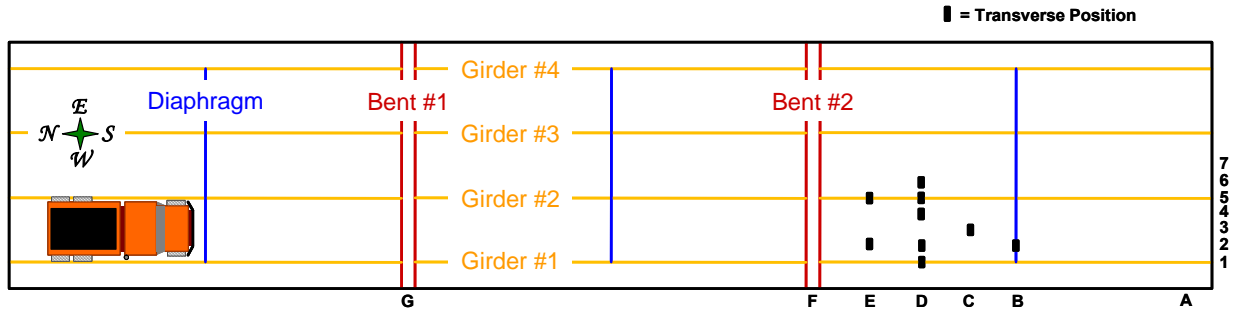
Figure 15: General Location of Strain Gages Oriented in the Transverse Direction (plan view)
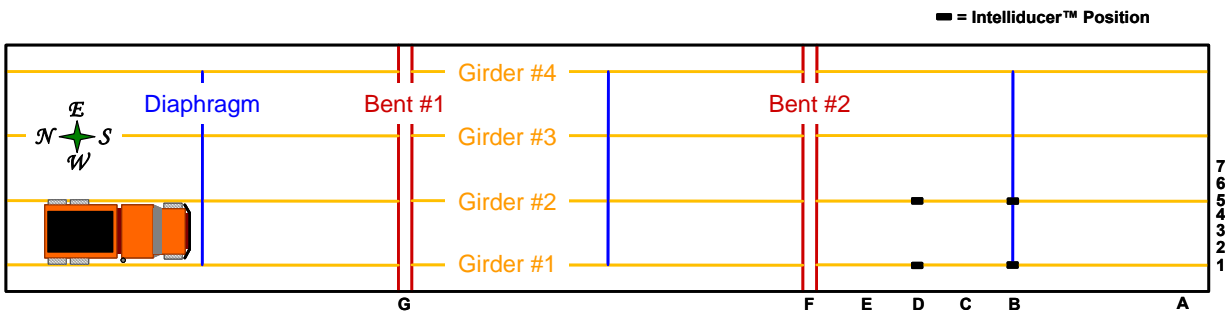
Figure 16: General Location of Intelliducer™ Gages Oriented in the Longitudinal Direction (plan view)

4.2   Position Referencing Nomenclature

A reference numbering system was created to help organize and distinguish each gage based on its location, orientation, type, and relative position. Altogether, the gage numbering system consists of six characters, as illustrated in Figure 17. The global location indicates which bridge the sensor is embedded in: Conventional (C), Empirical (E), and HPC (H). Gages are oriented either longitudinally (L) or transversely (T) with respect to the direction of traffic. Gage types are either strain gages bonded to the reinforcement (R), vibrating wire gages (V), or embedded concrete gages (E). Positions of the gages are referenced from the southwest corner of the bridge. Longitudinal distances from the south end of the bridge are denoted by the letters A through G. Transverse positions of the gages from the west side of the bridge are denoted by the numbers 1 through 7. Finally, the vertical position of each gage within the deck is described as bottom (B), middle (M), or top (T). The example in Figure 17 (C-LV-F-3-B) corresponds to a **L**ongitudinally oriented **V**ibrating wire gage in the **C**onventional bridge deck, located at Gage Line **F** (approximately 14.625 meters from the south end of the bridge), transverse position **3** (approximately 2.15 meters from the west side of the bridge), and in the plane of the **B**ottom mat of reinforcement. These unique reference numbers are used throughout the remainder of the report.

C-LV-F-3-B

Global Location
C = Conventional (Sta. 19+23.24)
E = Empirical (Sta. 16+81.74)
H = HPC (Sta. 11+57.24)

Gage Orientation
L = Longitudinal gage
T = Transverse gage

Gage Type
R = Reinforcement gage
V = Vibrating wire gage
E = Embedded gage

Longitudinal Position*
A = 1.00
B = 7.25
C = 9.06
D = 10.875
E = 12.688
F = 14.625
G = 29.625

Transverse Position*
1 = 0.95
2 = 1.75
3 = 2.15
4 = 2.55
5 = 3.35
6 = 4.15
7 = 4.55

Vertical Position
B = Bottom
M = Mid
T = Top

* Length in meters

Figure 17: Gage Reference Numbering System

4.3   Instrumentation

Three types of strain gages were used to internally instrument the bridge decks and one type was used to instrument the bottom of the stringers. Resistance strain gages (a.k.a. foil gages) were used to measure strain in the reinforcement, vibrating wire gages were used to measure long term strains in the concrete, and pre-manufactured resistance gages encased in a rigid polymeric housing were used to measure strain in the concrete. Specially made Intelliducers™ manufactured by Bridge Diagnostics, Inc. (Boulder, Colorado) were used to measure strains at the bottom of the bridge stringers during live load testing only.

4.3.1 Resistance Strain Gages

Direct measurements of local strain in the reinforcement were made using resistance strain gages.   These strain gages were bonded directly to the top and bottom surface of the reinforcement using a special epoxy. Bonding them to the top and bottom surface reduces the effects of local bending, so that only axial forces are recorded. Gage installation was done in College of Engineering laboratories at Montana State University (MSU). Each bridge deck had 35 resistance strain gage locations.

Resistance strain gages are composed of a thin layer of metal foil bonded atop a thin polymer backing. The foil acts as an electrical resistor, and when attached to a material's surface, changes in the length of the material will result in a nearly identical change of length of the foil. These length changes result in a change in the gage's electrical resistance. Such

changes are quite small and are generally detected using a special circuit arrangement called a Wheatstone bridge, as discussed below.

The strain gages purchased from Micro-Measurements Group, Inc. (Raleigh, North Carolina) are designated as type CEA-06-250UN-350 (using their nomenclature). Figure 18 shows a resistance strain gage prior to installation. CEA gages are general-purpose gages made of a constantan foil that are widely used in experimental stress analysis. The foil grid is fully encapsulated and includes exposed copper-coated integral solder tabs. The temperature range at which these gages will self-temperature-compensate is -75 to +175 °C for static measurements on steel. The active gage length of these gages is 6.35 mm (0.250 inches) and their resistance in ohms is 350 ±0.3%. Strain in these gages should not exceed approximately ±5000 microstrain (με) and fatigue life will be approximately 10^5 cycles at ±1500 με.

Not to scale
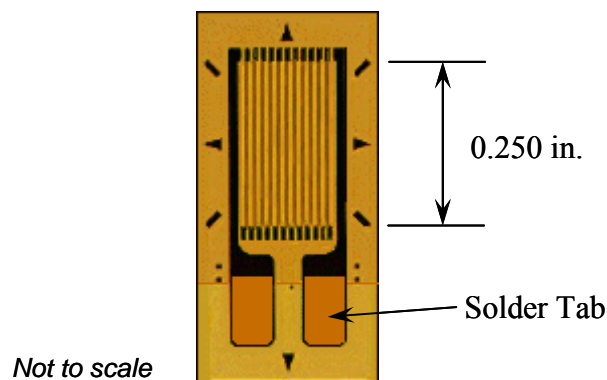
Figure 18: Resistance Strain Gage from Micro-Measurements Group, Inc. (CEA-06-250UN-350)

Bonding resistance strain gages to the epoxy-coated reinforcement followed several steps. This process included:

1. locating and marking the desired location,
2. grinding away the epoxy coating and steel ribs to make a smooth bonding surface,
3. cleaning and neutralizing the area,
4. gluing the gage onto the bar,
5. soldering the lead wires to the gage,
6. cleaning the area of any contaminants, and
7. covering the area with a coating to provide environmental and mechanical protection.

A two-part, medium viscosity epoxy (M-Bond AE-10) was used to attach the gages to the reinforcing steel. This epoxy system is highly resistant to moisture and chemicals and is used for general-purpose stress analysis, having improved longevity over other epoxies. Cure time was about six hours at 24 °C.

A two-part polysulfide liquid polymer compound (Micro-Measurements M-COAT J) was used to environmentally protect the strain gages from damage during and after construction. This tough, flexible, black coating was mixed and applied over the strain gaged area in the lab and allowed to dry overnight before moving. M-COAT J provides good protection against oil, grease, most acids and alkalies, and most solvents. Figure 19 shows a strain gage bonded to the reinforcement before and after the environmental protection was installed.
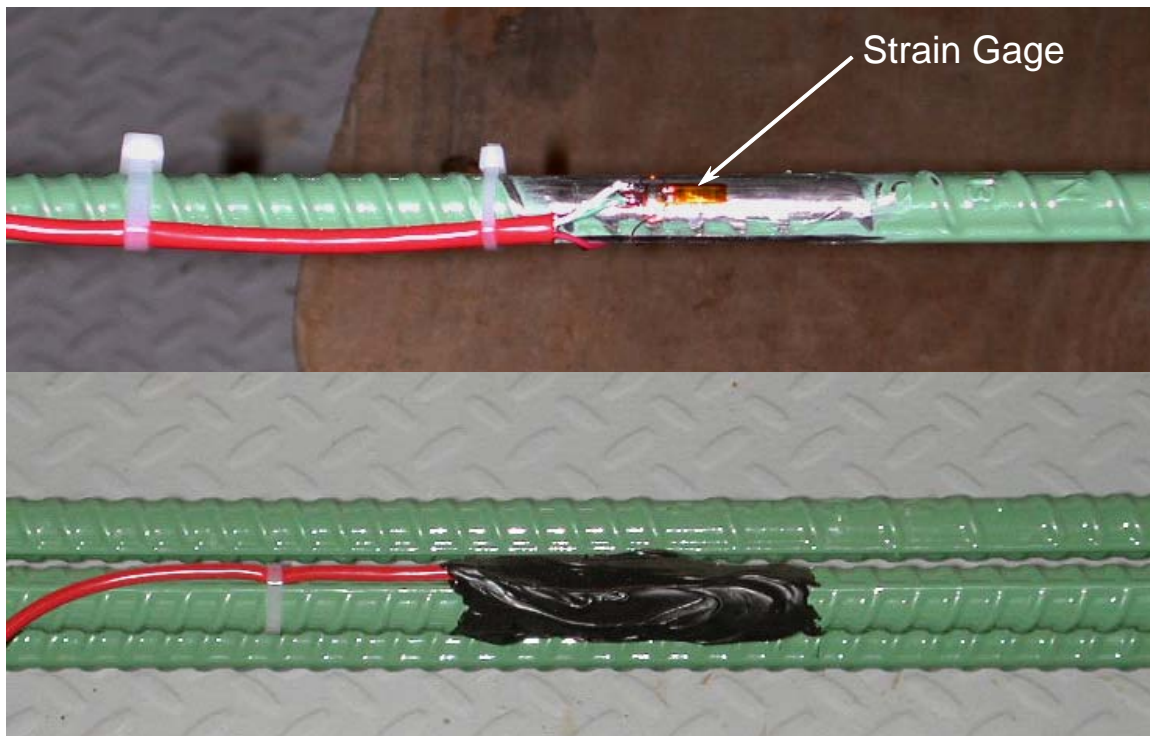
Figure 19: Strain Gage Bonded to the Reinforcement before (Top) and after (Bottom) Environmental Protection

Reinforcing bars scheduled for use during construction of the bridge decks were ordered directly from the manufacturer and shipped to MSU so that the resistance strain gages could be installed under controlled laboratory conditions rather than in the field. The instrumented rebar was installed in the bridges by Sletten Construction (the prime contractor on the job) under the Western Transportation Institute's (WTI's) supervision.

The resistance strain gages were quite durable, having a survival rate of 85% after construction. Similar to the embedment gages, the gage locations that experienced the greatest losses were over the bents. Losses in this area were more frequent due to cracks that had developed over the bent. The crack allows larger daily strain shifts due to temperature swings and higher strains during vehicle loads. Losses were sustained at a few other gage locations, which could have occurred during installation or due to wire breaks.

4.3.2 Vibrating Wire Strain Gages

The 20 vibrating wire strain gages (Model VCE-4200) that were embedded in the bridge deck concrete for long term monitoring were purchased from Geokon (Lebanon, New Hampshire). This standard model, shown in Figure 20, has a 153 mm gage length, 3000 microstrain range, and 1 microstrain sensitivity. They are designed to be embedded directly in concrete and are typically used to monitor long-term strain and temperature in structures such as foundations, piles, bridges, dams, containment vessels, and tunnel liners. Survival of these gages was excellent, having no losses due to construction activity.
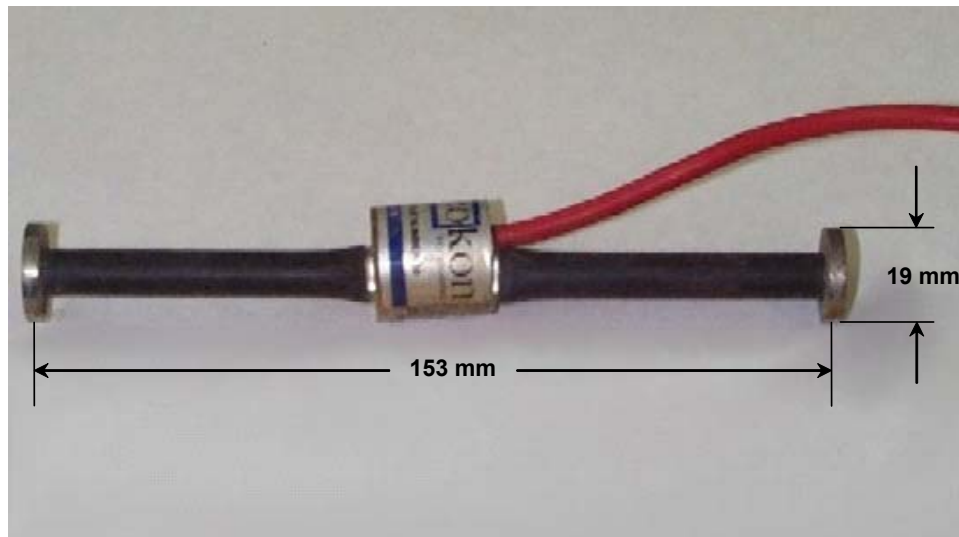
Figure 20: Vibrating Wire Strain Gage (VCE-4200)

The gages use a steel wire in tension between two circular end plates, to measure length changes in the concrete. As the concrete contracts or expands, the wire responds accordingly, thereby changing its resonant frequency of vibration. The wires are excited by electromagnetic coils, which also detect their resonant frequencies of vibration. Frequencies detected by the coil are converted to a DC voltage using a Campbell Scientific, Inc. (Logan, Utah) AVW1 unit and recorded by the data logger. The AVW1 unit will accommodate a single vibrating wire gage or, if a multiplexer is used, up to 16 vibrating wire gages may be sequentially converted and recorded. The time required for the frequency sweep and the slow speed of the multiplexer makes it impractical to log data from the vibrating wire gages during live load testing with a moving vehicle (hence their focus on capturing long term environmental effects). Each vibrating wire gage is also equipped with a thermistor to record temperature. Temperature measurements are used to apply temperature corrections to measured strains. Differences between the thermal expansion coefficients of steel and concrete necessitate these temperature corrections.

Using plastic coated steel wire, each vibrating wire strain gage was suspended in the concrete between the reinforcing bars (Figure 21). As suggested by Geokon, a thin rubber pad

was placed between the gage body and the tying wire to damp resonant vibrations in the steel wire and rebar cage.
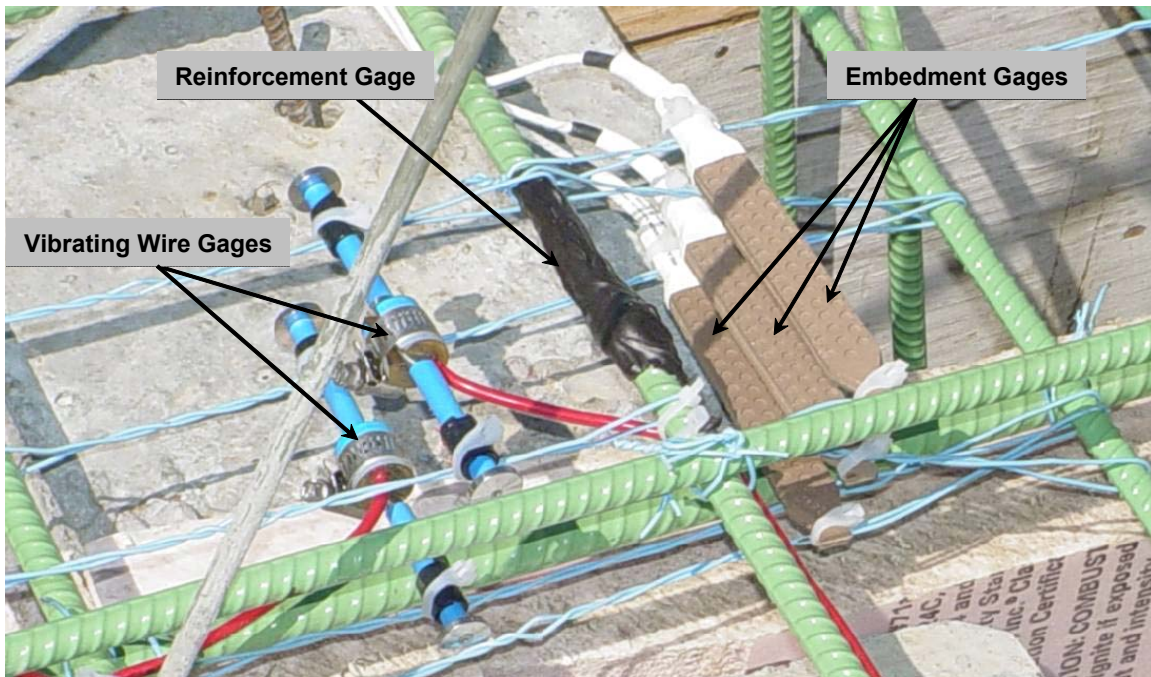
Figure 21: Illustration of Finished Gage Location Showing All Three Embedded Gages

4.3.3 Concrete Embedment Strain Gages

Nine concrete embedment gages, specially made to measure strains inside concrete structures, were used in each of the bridge decks. These gages (EGP-5-350), shown in Figure 22, were purchased from Micro-Measurements Group, Inc. Each embedment gage contains a single 350 ohm bonded-foil resistance strain gage (functionally similar to the ones described earlier). The sensing grid has an active gage length of 100 mm and is self-temperature-compensated to minimize thermal output when installed in concrete structures. The gage is set in a proprietary polymer body to protect them from corrosion, moisture and mechanical damage during construction and use. The outer body has a length of 130 mm and is dimpled to ensure proper adherence to the surrounding concrete. Embedment strain gages utilize a ¼ Wheatstone bridge (described later), since there is only a single resistance strain gage housed in the polymer body.
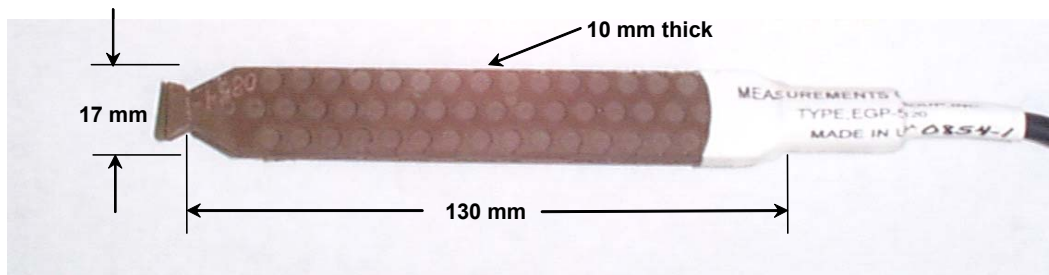
Figure 22: Concrete Embedment Strain Gage (EGP-5-350)

The concrete embedment gages were installed similar to the vibrating wire gages by suspending them from the reinforcing cage using plastic-coated tie wire, as shown in Figure 21. The embedment strain gages suffered the worst mortality, having only a 56 % survival rate after construction. Many of the embedment gages were located in the continuous deck over the bent, which cracked in all three decks several days after the deck concrete was poured. The cracking likely occurred due to flexural bending and axial stresses in response to diurnal temperature changes. At the crack, strains exceeded the maximum strain threshold of the embedment gage, causing them to fail.

4.3.4 Intelliducers™

During the live-load experiment only, Intelliducers™ manufactured and sold by Bridge Diagnostics, Inc. (BDI) of Boulder, Colorado were temporarily mounted to the bottom of the stringers of the bridges. Intelliducers™ are used to measure strain at the surface of structural elements. They are made of aluminum and have a 76.2 mm effective gage length. Extensions are available for averaging strain over a longer gage length, and in this application, a 228.6 mm gage length was used. Figure 23 shows an Intelliducer™, and Figure 24 shows an Intelliducer™ mounted to the bottom of a girder with the extensions used in this test program. The circuitry for monitoring the response of these gages consists of a full Wheatstone bridge with four active 350 Ω resistance gages. BDI states that the gages have an accuracy of ± 2 %, a range of ±4000 µε, and should not be used below 30 µε. The Intelliducer™ gages suffered no mortality during the live load tests.
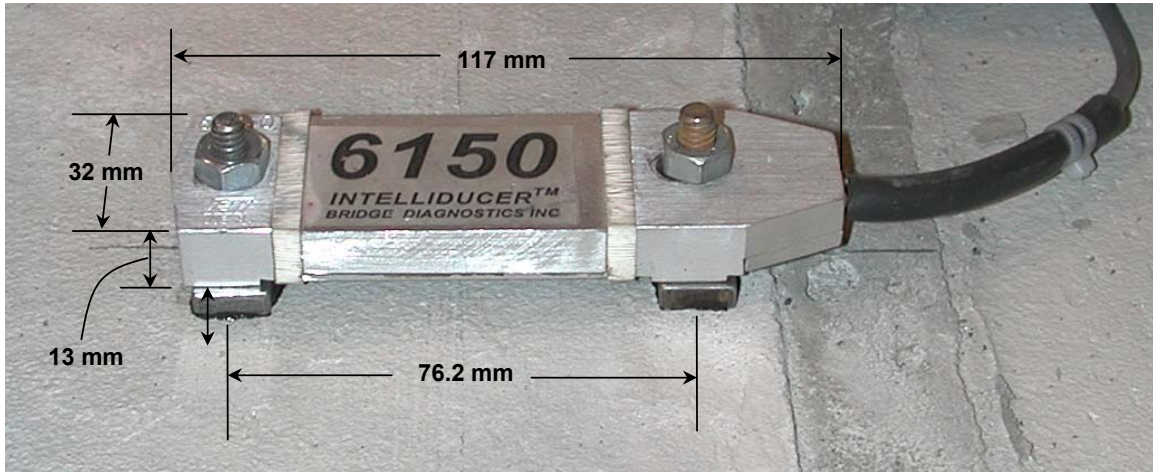
Figure 23: Intelliducer™ Mounted on Concrete Surface
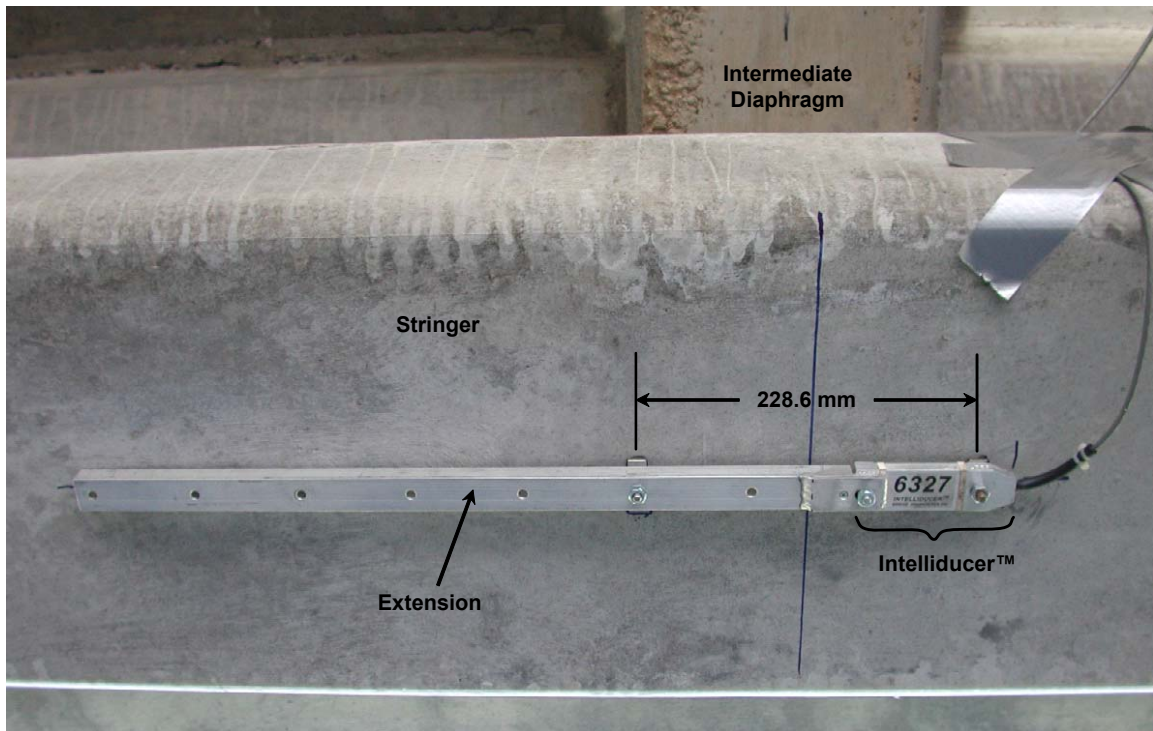
Figure 24: Intelliducer™ Mounted to Bottom of Concrete Girder with Extensions

4.3.5 Gage Durability

Success of this project partly depends on the instrumentation installed in the bridge decks. Therefore, rugged strain gage technologies were chosen to withstand construction and the environment. In addition, great care was taken during installation of the reinforcing gages to rigorously use the materials and methods recommended by Micro-Measurements Group for installing their gages. Furthermore, these gages were all installed at MSU in the lab under a

controlled environment. In any event, gage failures cannot be prevented, and they are likely to continue in all of the decks given enough time. Each of the three strain gage types embedded in the deck concrete performed differently in this regard. Survivability immediately after the decks were cast was difficult to quantify; therefore, the first assessment was conducted the following spring after the decks were cast (May 2004). The second assessment was conducted in summer 2005. The results of these assessments are provided in Tables 13 and 14, and consist of the cumulative number and percent of failure of each gage type, respectively, in each of the bridge decks. The values of percent in Table 14 are based on the total number of gages installed (Table 15 lists the number of gages installed and monitored within each bridge). Referring to these tables, gage failures are increasing with time, as expected. The greatest failure rates are for the concrete embedment gages and those bonded to the reinforcing steel. Almost half of the embedded gages had failed by summer 2005 (with the majority of these failures having occurred by summer 2004). Reinforcement gage failure is the greatest in the HPC deck (approximately 69%), with fewer failures occurring in the Conventional and Empirical decks (49% and 14%, respectively). The majority of these failures occurred between spring 2004 and summer 2005. The vibrating wire gages have performed very well (only 10% failure by summer 2005) and will likely perform well into the future. Overall, approximately one-third of all the gages installed in the bridges have failed as of summer 2005. An addendum located at the end of Appendix E shows a list of gages that have failed over the course of this project.

Table 13: Cumulative Number of Gage Failures over Time

	Gage Type							
	Reinforcement		Embedded		Vibrating Wire		All Gages	
Bridge Deck	Spring 2004	Summer 2005	Spring 2004	Summer 2005	Spring 2004	Summer 2005	Spring 2004	Summer 2005
CON	7	17	5	5	1	3	13	25
EMP	3	5	2	3	2	3	7	11
HPC	5	24	4	5	0	0	9	29
All Decks	15	46	11	13	3	6	29	65

Table 14: Cumulative Percent of Gage Failures over Time

	Gage Type							
	Reinforcement		Embedded		Vibrating Wire		All Gages	
Bridge Deck	Spring 2004	Summer 2005	Spring 2004	Summer 2005	Spring 2004	Summer 2005	Spring 2004	Summer 2005
CON	20%	49%	56%	56%	5%	15%	7%	13%
EMP	9%	14%	22%	33%	10%	15%	4%	6%
HPC	14%	69%	44%	56%	0%	0%	5%	15%
All Decks	14%	44%	41%	48%	5%	10%	15%	34%

Table 15: Number of Gages Installed and Monitored per Bridge

Gage Type	No. Gages Installed	No. Gages Monitored
Reinforcement	35	35
Embedment	9	7
Vibrating Wire	20	16
Total	64	58

While there are a variety of reasons for the reinforcement gages to fail (e.g., faulty installation, transportation and handling of instrumented bars, installation of reinforcement at jobsite, placement of concrete), failure in this case is most likely due to moisture intrusion, since 1) most of the failed gages worked properly for at least a year, and 2) strain traces reviewed by the manufacturer of the strain gages indicated that moisture intrusion is likely the cause. The reason the reinforcement gages in the HPC deck have been particularly vulnerable (while the gages in the Empirical deck have been more successful), may be due to available pore space within the microstructure of the concrete. Freeze-thaw cycles drive the water into and out of the pores of the concrete. In this case, because the HPC deck concrete is less permeable than the other decks, the gaged areas and lead wires may be convenient conduits for the migration of moisture under changing climatic conditions.

4.4 Data Acquisition System

Each bridge site required an independent data acquisition system to store and transfer data. Each system consisted of a single data acquisition computer, two multiplexers, supporting circuitry, a 12-volt battery connected to a solar panel through a regulator, and a radio unit connected to an antenna. The CR5000 data acquisition computer, AM16/32 multiplexers, AVW1 vibrating wire conversion unit, and RF400 spread spectrum radios were purchased from Campbell Scientific, Inc. Solar panels, batteries, radio antennas and regulators were purchased from other sources. A weather-resistant steel enclosure was used to house the data acquisition computer, radios, multiplexers, and other peripheral circuitry. The various components contained within each data acquisition enclosure at each bridge are illustrated in Figure 25, and are discussed in more detail below.
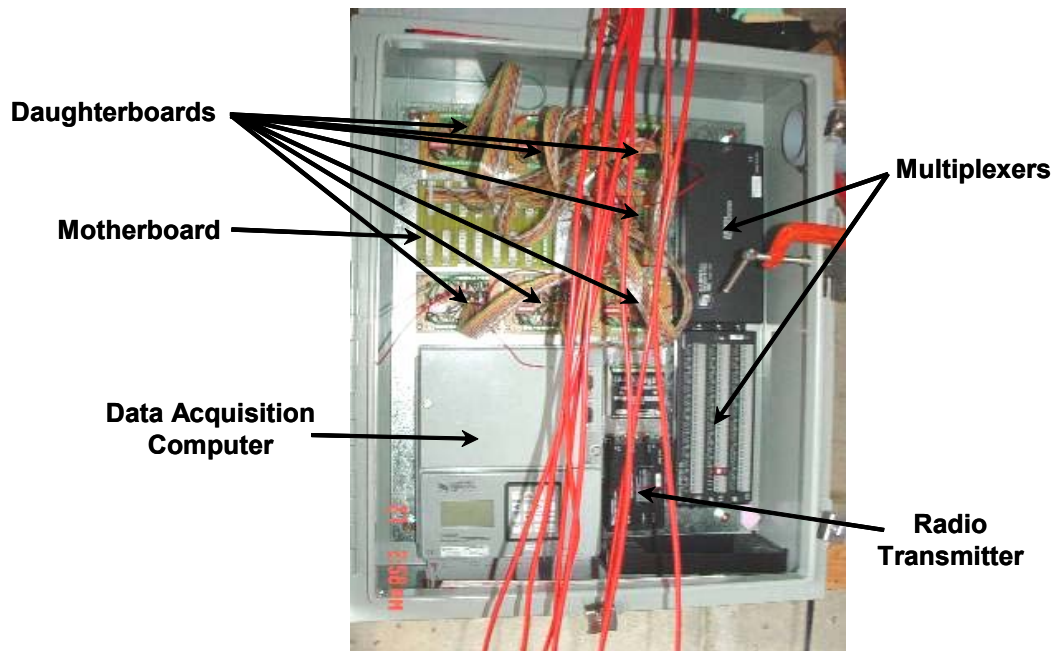
Figure 25: Various Components within a Data Acquisition Box

4.4.1 Data Acquisition Computer

The CR5000 measurements and control system from Campbell Scientific, Inc. is a rugged, high-performance data acquisition system. This system was selected for its durability, wide range of temperature operation, and internal computing and storage capabilities. Some of its other features include:

- a graphical display,
- low power draw,
- twenty differential (40 single-ended) input channels,
- 16 bit measurement resolution,
- 5-volt and 12-volt terminals to power sensors,
- 1,000,000 data point storage capacity,
- a maximum throughput of 2000 to 5000 measurements per second (depending on configuration), and
- an operable temperature of -40 to +85° C.

The data acquisition system uses a proprietary computer code to operate. A computer program was written to control data collection activities at the bridge site. Prior to installing the final program on the data acquisition computers, the program was tested at MSU to ensure that it was working properly. In general, the long term monitoring program was written to deliver excitation voltage to each of the sensors at predetermined times (i.e., each hour), capture each sensor's response and store that information in memory. Collected and stored data is transferred on command to MSU using a dedicated Internet connection via the RF400 radios and a series of

900 MHz antennas. For live load testing, a different computer program was required. This program was designed to record only the bonded-foil and embedded gages at a higher rate of speed (~50 Hz) during each test. Data sets collected during testing were transferred and stored on-site to a laptop computer.

4.4.2 Multiplexers

Multiplexers are used to increase the number of sensors that can be monitored by a single data acquisition computer. The CR5000 dataloggers can only directly accommodate 20 differential inputs. The AM16/32 multiplexer can accommodate up to 32 differential measurement channels. It acquires data at a slow rate (approximately 1 Hz) by switching through its channels and simultaneously transferring and storing the data through a single port on the face of the datalogger.

Two multiplexers are required at each bridge site to accommodate 16 vibrating wire gages, 16 temperature measurements, and 30 resistance strain gages during long term monitoring. The remaining resistance gage measurements are connected directly to the front face of the data logger. In this case, the advantage of using multiplexers is the increase in the number of available data ports without the expense of purchasing a second datalogger; the disadvantage is the relatively slower acquisition speed compared to a datalogger alone. Multiplexers were not used during the live load experiments because of their slow data acquisition rate.

4.4.3 Communication and Power

A spread spectrum radio (RF400) is used to transfer data to and from each of the bridges during the long term monitoring. Antennas connected to these radios communicate at 900 MHz to a single receiving antenna collocated with the weather station at the Saco Public School. Information is transferred from the school to WTI via the Internet. This communication path is illustrated in Figure 26. The antennas near the bridges are attached to a wooden pole along with the solar panel.
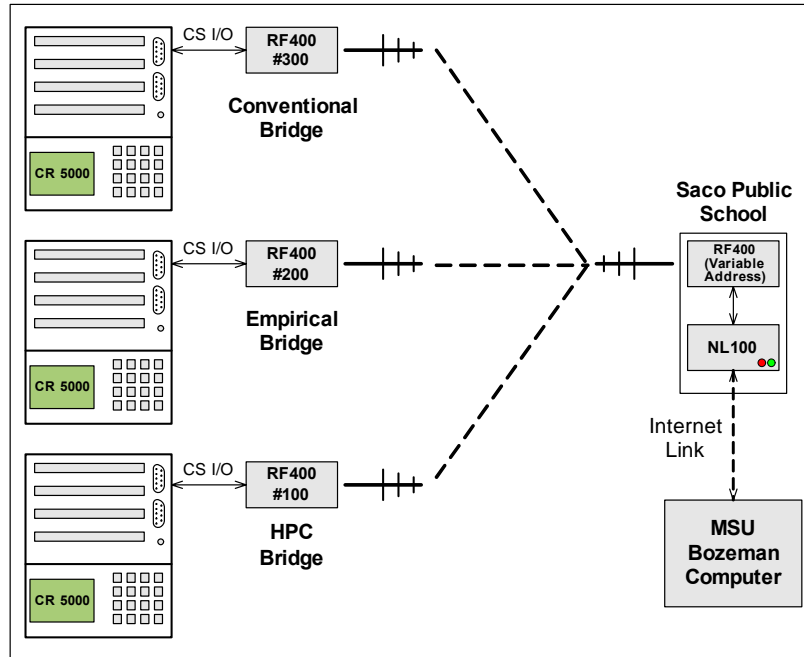
Figure 26: Communication Path for Long Term Monitoring

Power components consist of a 12 volt battery and a 60 Watt solar panel connected through a regulator to maintain a specific battery voltage over time. Each solar panel measures approximately 1.1 m by 0.5 m and is rigidly connected to a wooden pole near the southeast corner of each bridge. Deep-cell 12-volt batteries are being used because they are able to resist voltage decay during cold weather. A single battery at each bridge is housed under the bridge on top of the pile cap near the data acquisition cabinet. Each battery has approximately two weeks of life in the event the solar panel malfunctions or is damaged. Wiring for the communications and power were run through conduit and buried in soil to protect them from varmints and the environment. In addition, a lightning rod was connected to this pole to provide lightning protection.

4.4.4 Supporting Circuitry

Each bridge deck contains 35 resistance gages bonded to the reinforcement, 9 embedment gages, and 20 vibrating wire strain gages. The components used to support operations of the vibrating wires were discussed above. The circuitry that supports the resistance and embedded strain gages utilizes a Wheatstone bridge circuit. Seven identical circuit boards containing six Wheatstone bridge circuits were designed and built to service five resistance strain gages and one embedment strain gage. These seven boards are referred to as "daughterboards," since they complete the necessary circuitry for the strain gages and relay the final output to the datalogger through the "motherboard." This connection scheme facilitated rapid and accurate reconfiguration of the system, notably for the short turnaround time between live load tests on the three bridges. Due to limitations on the available number of connection points on the face of

the datalogger, two different arrangements were required based on the unique data acquisition needs of the long-term and the live load testing arrangements. These two arrangements will be discussed in further detail below.

4.4.4.1   Wheatstone Bridge Circuitry

The Wheatstone bridge arrangement is useful for detecting small changes in resistance elements, such as strain gages. Two of the four gage types employed in the instrumentation system for this project operate using a Wheatstone bridge arrangement: the bonded resistance strain gages and the embedment gages.

In its simplest form, the Wheatstone bridge is composed of four resistors, as depicted in Figure 27. A voltage E_{in} is applied to the circuit; for this project, +5V was used. If the resistances in the upper arms of the bridge are identical (i.e., $R_1 = R_2$), the voltage-divider theory dictates that the voltage at point A will be exactly half of the input voltage (i.e., +2.5 V). The same relationship holds true for the lower arm. Therefore, if $R_1 = R_2$ and $R_3 = R_4$, points A and B have equal voltages. Thus, the bridge is perfectly balanced, and E_{out} equals zero volts. However, a change in resistance in any one of the four arms of the bridge (i.e., if one of the arms is a strain gage) results in a voltage difference between points A and B. The resulting imbalance is detectable using sensitive voltage-reading equipment. Using theoretical calculations, the resistance change may be calculated using E_{out}. The resistance change is proportional to the strain experienced by the gages and may be converted to a real strain using the manufacturer's published gage factor.
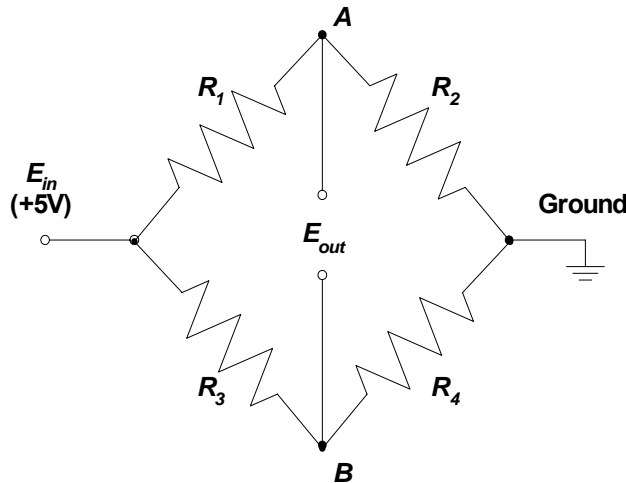
Figure 27: Ideal Wheatstone Bridge Circuit Arrangement

For this project, only axial strain is desired from the rebar strain gages. Thus, it is important that any effects due to local bending in the gaged portion of the bar be negated. This is electrically possible by using the arrangement shown in Figure 28(a) for all the strain gages bonded to the reinforcement. Notice that the two strain gages bonded to the rebar are connected

in series, and occupy a single arm of the bridge. If local bending does exist, bending strains of opposite sign occur at the top and bottom of the bar. Due to the symmetrical location of the gages about the neutral axis of the bar, these strains have an equal magnitude, but opposite sign. The tensile strain due to bending in one gage cancels out the equal bending compressive strain in the other gage. For that arm of the bridge, the net result yields only the amount of axial strain in the bar.

Practically, this arrangement is termed a "quarter bridge": only one arm of the bridge is occupied by strain gages, while the other three arms are occupied by stable resistors. The arm with the strain gages is balanced by the 700 Ω resistance arm. Although other arrangements of the Wheatstone bridge also negate bending effects, this particular arrangement experiences the least sensitivity to changes in temperature – an important consideration for long-term monitoring. The two resistors comprising the 700 Ω resistance arm were unmatched precision resistors, having a tolerance of ±0.01%, manufactured by Micro-Measurements Group. The two 350 Ω resistors used in the two lower arms of the Wheatstone bridge were a matched pair, having a tolerance of ±0.005%.

A second notable feature of this Wheatstone bridge arrangement is the use of the three-wire system. This technique was employed to compensate for the resistive imbalance in the circuit due to the long lengths of the gage lead wires. If only a single wire was used, that wire would be susceptible to an unknown change in resistance under temperature changes, affecting the resistance of the gaged arm of the bridge. By adding a second wire of identical length to the other 700 Ω resistor arm, any temperature effects in the wire are present in both arms and the bridge remains balanced.

The quarter bridge Wheatstone bridge circuit was also used with the embedded gages (Figure 28(b)). The fundamental theory and operation are the same in this case, except all arms of the bridge are 350 Ω. The three-wire system was also used for these gages.
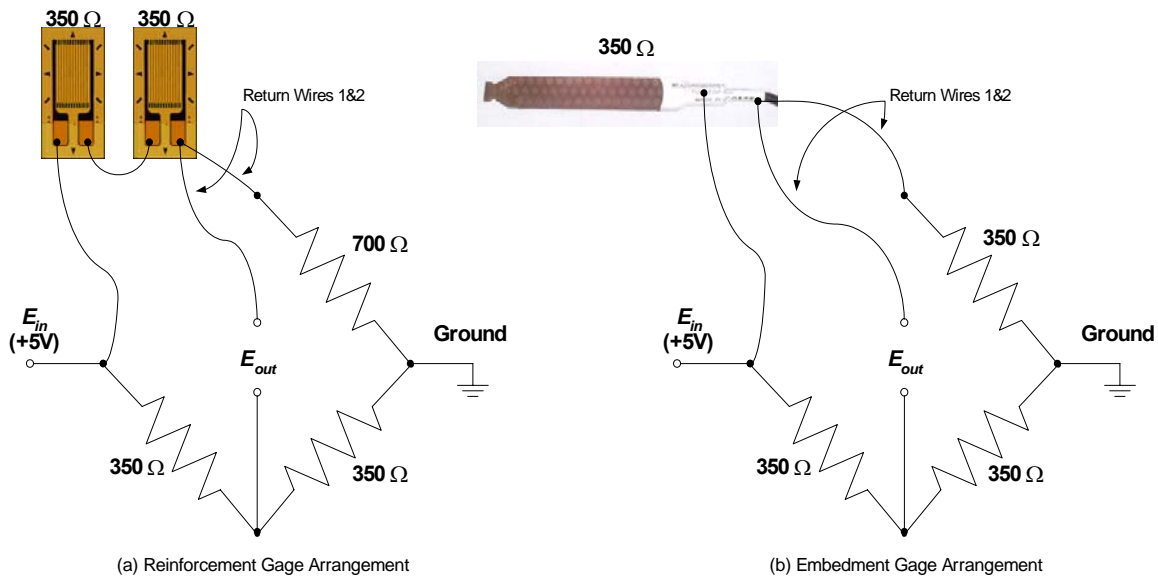
Figure 28: Wheatstone Bridge Arrangements Used on Saco Bridges

Prior to recording strains in the bridge decks, baseline voltage measurements were recorded and subtracted from all readings to set the initial strain to zero. A process called "shunt calibration" was used to calibrate the relationship between the voltage output from the Wheatstone bridge and the strain sensed by the gage. By applying a very large resistance (176 kΩ) in parallel with the 700 Ω arm of the Wheatstone bridge, it simulates a particular strain value – approximately 1900 $\mu\varepsilon$ in this case. The output voltage at this point is then the upper bound of the linear ratio measurement.

The Wheatstone bridge circuitry was assembled on each daughterboard to accommodate six gage locations: five resistance strain gage locations and one embedment gage location, in the configuration shown in Figure 29. Thus, seven daughterboards were required to accommodate 35 bonded and 7 embedment gages. A single +5 V voltage regulator (LM78L05) was used to ensure that a low-noise, constant supply voltage was provided to the six Wheatstone bridges on each board.
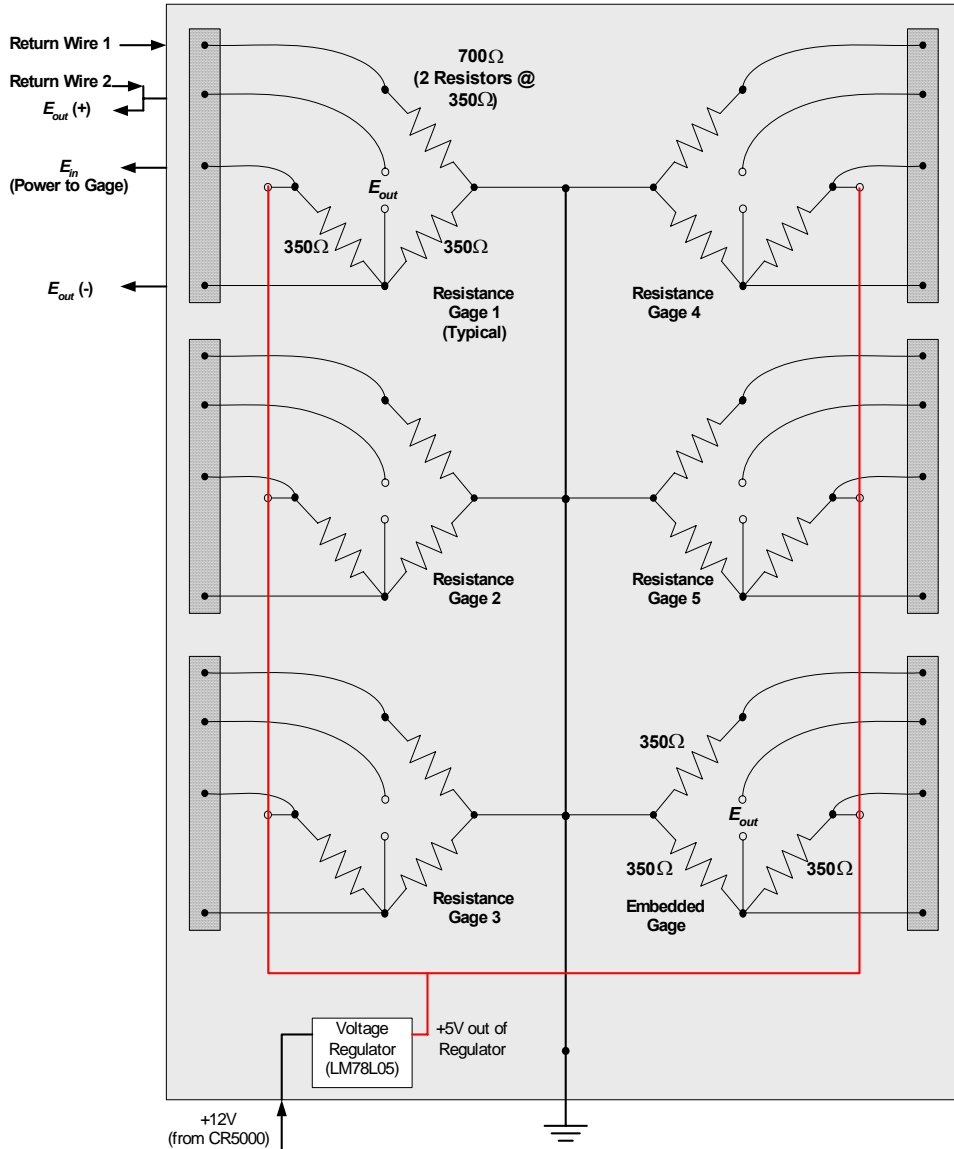
Figure 29: Diagram of Daughterboard Circuitry

4.4.4.2 Circuit Alternatives and Testing

All of the Wheatstone bridge arrangements require that a differential (two-wire) measurement be made to determine E_{out}. The CR5000 data acquisition unit used for this project is limited to 20 direct differential measurements. To accommodate more sensors, a multiplexer is generally used, however, multiplexers require additional cost, are relatively slow, and create one more connection through which noise may be introduced to the signal. Therefore, in the early stages of the project, several alternatives were investigated to increase the capacity of the datalogger without sacrificing accuracy and precision of the strain gages. One alternative was to use an instrumentation amplifier to convert differential analog outputs (a two-wire system) to single analog outputs (a one-wire system), as illustrated in Figure 30. By regulating one output

arm of the instrumentation amplifier at zero volts (i.e., ground), the other terminal can be read as a single-ended signal. This setup was attractive because the datalogger is able to accommodate 40 single-ended measurements, thereby doubling its capacity. However, based on the preliminary testing described below, this arrangement was not used in the final design.
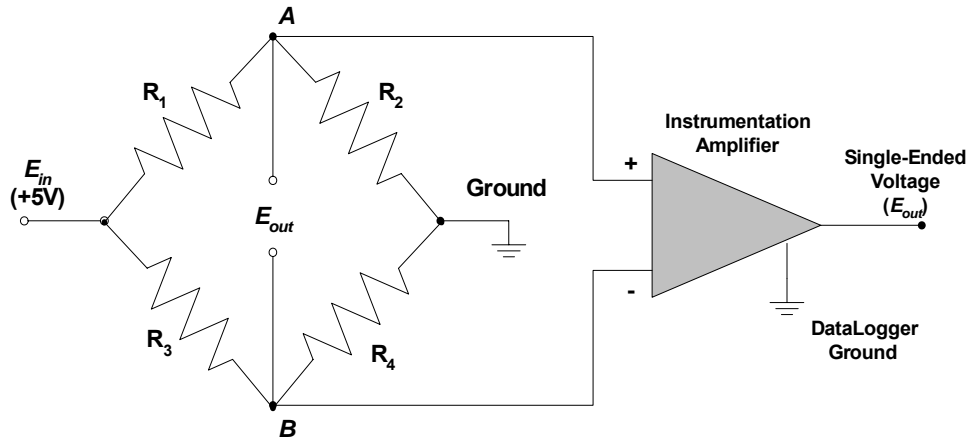
Figure 30: Alternative Circuit Design for Single-Ended Measurements

Items of concern regarding both types of circuitry (differential and single-ended) included: accuracy of outputs compared to theoretical calculations, electronic stability over time and temperature variation, and noise abatement. Initial tests found that the gage output from both circuit arrangements matched the theoretical predictions reasonably well, and that noise was generally controllable using various modifications to the circuits and datalogger programming.

To further investigate the relative performance of the two wiring configurations, a small-scale, reinforced concrete test beam (.25 m deep by .15 m wide by 1.52 m long) was designed and fabricated at MSU. In addition to testing the strain gage circuitry in a more realistic setting, this beam also afforded researchers an opportunity to evaluate the durability of the gage installations on the reinforcing steel. Other issues tested with this beam included: gage survivability during construction, cabling issues, and durability of the gages under loading.

To test gage durability, the gages at one location in the beam were purposefully abused during the construction process. All of the strain gages survived construction, confirming the durability of the installation procedure. Initial testing of the relative gage response found that the output matched the theoretical predictions reasonably well, and that noise was generally controllable using various circuits and programming modifications. However, it was difficult to assess electronic stability for long periods of time and at various temperatures due to the cumbersome nature of the concrete beam. Consequently, a small segment of rebar was instrumented at two locations along its length to further study the electrical stability, accuracy and reliability of the strain gage circuitry for longer periods of time and under more controlled conditions. One gage location was connected to a differential circuit and the other to a single-

ended circuit. Over a period of several days, a constant weight was suspended from the bar and the stability of the constant measurements evaluated against one another.

The single-ended circuit arrangement offered a significantly refined signal, with a low electrical noise band. This performance was attributed to the filtering characteristics of the instrumentation amplifier. However, performance of the single-ended voltage was too erratic over time for the long-term monitoring purposes of this project. The likely reason for this behavior was minor fluctuations in the electric potential of the ground. Small changes in the electric potential would create significant changes in the gage output since the magnitudes of the recorded signal were typically very small.

Overall, it was concluded from these laboratory experiments that the differential analog circuitry offered better stability and accuracy than the single-ended circuitry. Furthermore, this circuitry offered adequate noise abatement for the purposes of this project, although the single-ended circuit did have a better signal-to-noise ratio. Note also that additional time and cost would have been required to convert to single-ended measurements. Therefore, the final circuit design employed the differential outputs with a multiplexer.

4.4.5 Long-Term Monitoring Circuit Arrangement

For long-term monitoring, the available ports on the datalogger were inadequate to service all the necessary gages. As mentioned previously, multiplexers (Mux) were employed to expand the number of gages that could be monitored at hourly intervals. Using the daughterboard-motherboard arrangement seen in Figure 31, the voltage signals for the reinforcement and embedded gage readings were transmitted to the CR5000 directly or via the multiplexer. All of the vibrating wire readings were accommodated using a second multiplexer in conjunction with the AVW1 vibrating wire conversion unit. This daughterboard-motherboard arrangement offered flexibility for performing zeroing/calibration activities without the need for rewiring. Five of the daughterboards are used to monitor long-term strains only, as they are routed through the multiplexer. The remaining two daughterboards are connected directly to the face of the datalogger, allowing the gages wired into these boards to be logged at a relatively rapid rate. Events involving the passage of large vehicles are being recorded on each of the bridges using the 12 gages wired through these two boards.
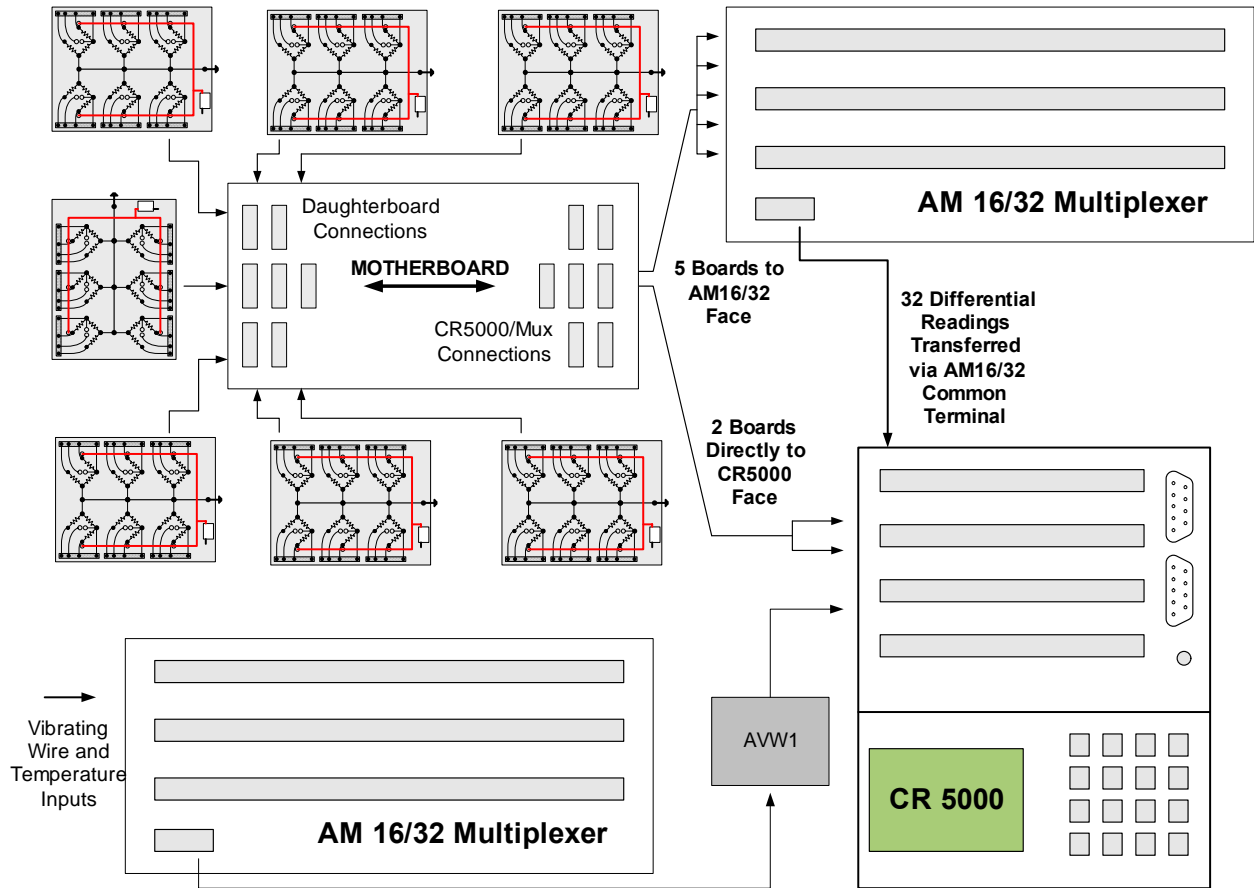
Figure 31: Data Acquisition Layout during Long-Term Monitoring

4.4.6 Live Load Testing Arrangement

During the live load testing, the instrumentation system was temporarily reorganized to accommodate a large number of sensors at the higher data acquisition speeds. As previously mentioned, the multiplexers could not be used during these tests since they were too slow. Consequently, all resistance gage measurements were connected directly to the loggers. All three CR5000 dataloggers were used together on a single bridge to simultaneously monitor and record 53 differential channels during live load testing, as shown in Figure 32.
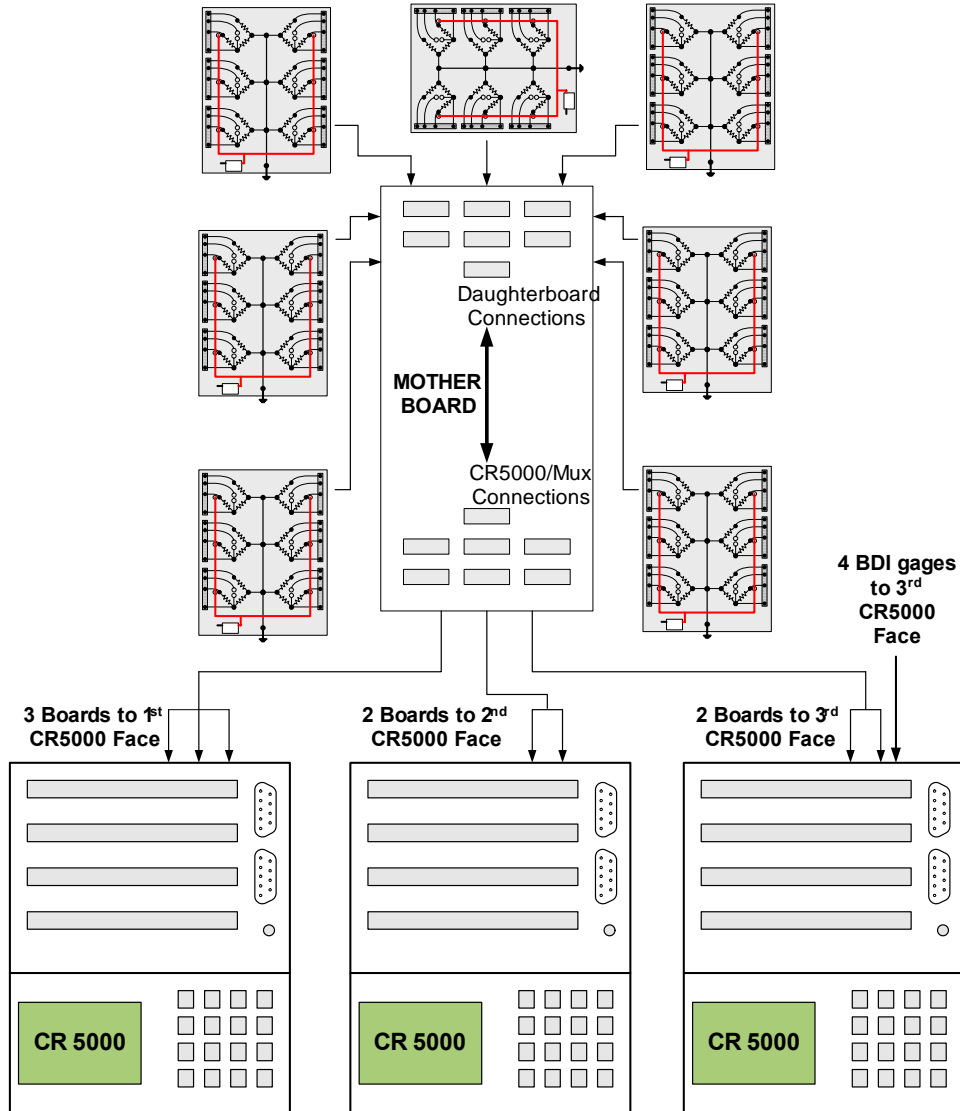
Figure 32: Data Acquisition Layout during Live Load Testing

For the live load tests only, Intelliducers™ were used to monitor strains at the bottom of the girders under the gaged section of each bridge; these gages were directly connected to the face of the third datalogger. Vibrating wire strain gages were not monitored during live load because they are only able to accurately monitor strain at approximately 0.5 Hz (100 times slower than what is necessary during live load testing). Once again, the daughterboard-motherboard interface allowed speedy transitions during live load testing by reducing the amount of physical rewiring required to modify the system to acquire data without multiplexers.

4.5   Installation and Assemblage

The instrumented reinforcing bars were bundled securely together and shipped to the construction site. The bars were then installed as the reinforcing cages were assembled in-place for each deck (in April 2003). The embedded resistance strain gages and the vibrating wire

strain gages were installed once the reinforcing cage for each bridge was complete. Lead wires were routed out through the bottom of the decks through predrilled exit ports. Cabling was bundled together and tied to the underside of reinforcing bars or to the chairs used to space the top mat of reinforcement from the bottom mat, as shown in Figure 33.

Figure 33: Example of Cable Run

Precise coordinates of each instrument location were documented after they were installed and prior to the deck concrete being placed. Once all sensors were in place, small plastic inserts were attached to the sides of the longitudinal formwork to indicate the approximate location of the transverse gage lines. The plastic inserts left a permanent indentation in the concrete when the forms were removed. These indentations will help to locate the gage lines in the future. In addition, longitudinal and transverse measurements were made to document the locations of all the gages. Photographs were also taken to record the orientation and layout of each gage.

When the decks were cast, all gage installations were flagged so that the construction workers would know where to exercise greater care during concrete placement. The flags were constructed using thin dowels tied in the shape of a teepee. They were connected to the reinforcing cage near each gage location using plastic zip ties. Once the concrete was placed and vibrated, the flags were simply pulled free from the reinforcing cage.

The data acquisition box for each deck was temporarily installed under the bridge near the south bent prior to placing the bridge deck concrete. The lead wires from the gages were connected to the data acquisition system after being routed through the exit ports in the deck forms. After the deck concrete had set up, the forms were removed from the bottoms of the bridge decks and the data acquisition and power enclosures were permanently mounted to the diaphragm and pile cap, respectively. All lead wires were then trimmed and permanently plumbed in PVC conduit between the exit ports and the data acquisition boxes. The final

arrangement of the data acquisition system and power enclosures with the plumbing in place is shown in Figure 34.

Figure 34: Data Acquisition and Power Enclosure Arrangement under the Bridge Decks

5 WEATHER STATION
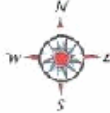
A weather station with a data acquisition system was installed at the Saco Public School in August 2002. Weather sensors were mounted to an existing communications tower located on the roof of the school. Weather sensors include a combination temperature/relative humidity probe, a wind speed and direction sensor, and a barometric pressure sensor. Power and Internet connections are being supplied by the school in return for allowing them free access to the data. Weather data was used in conjunction with strain and internal temperature data collected from the bridges to help understand the effect of environmental factors on the behavior of the structures.

Remote communication with the data acquisition system was established using a dedicated, on-site, Internet connection. Automatic storage and downloading capabilities have allowed the data to be retrieved via the Internet. A rudimentary website was created to allow remote monitoring and retrieval of the weather data. This website has been integrated into an existing website maintained by the Western Transportation Institute. Additionally, a database was developed to store and organize data collected from the weather station.

The active Internet link to view current and historical weather conditions at Saco, Montana is http://wtigis.coe.montana.edu/saco/Saco_Current.htm. Figure 35 shows a screenshot of the weather website. Specific features of this website include:

- 15 minute updates of temperature, wind speed and direction, relative humidity, dew point, and barometric pressure;
- a collection of the past 24 hours of data updated every 15 minutes;
- 1 month of daily averages;
- 1 month of daily maximums;
- 1 month of daily minimums;
- various pictures associated with the project; and
- links to the other project related information.

Figure 35: Internet Screenshot of Real-Time Weather Data from the Saco Weather Station

6 LIVE LOAD TESTING

The objective of the live load testing of the Saco bridge decks was to determine how each type of deck structurally transfers wheel loads from their point of application into the supports and to determine the magnitudes of the stresses and strains that develop in the decks as they perform this function. This information can be used to understand whether the current approaches used for deck design reasonably represent actual structural behavior (with respect to the both the manner in which the load is carried and the levels of stress generated in the system) and to assess the likelihood of immediate and/or long-term crack development in the decks from vehicle loads. The primary focus of the live load tests was to determine a) the manner in which wheel loads are locally transmitted from the deck transversely into the bridge stringers, b) how this load flow varies between the three different decks, and c) how data from the live load tests can be used to identify changes in the condition of the decks over time.

The first live load tests were conducted on the three bridges the week of July 28, 2003 (approximately one month after placing the bridge deck concrete). These tests were conducted after the decks were grooved and sealed and shortly after the bridge approaches were paved, but prior to being opened to traffic. The second set of live load tests were conducted during the week of July 18, 2005 (approximately two years after the bridges were put into service). The vehicles used in these tests were 3-axle dump trucks provided by MDT Maintenance in Malta, Montana. Most test runs were conducted with a single truck, at slow and high speeds. Additional tests were conducted using two trucks traveling adjacent to each other at slow speed.

6.1 Test Vehicles

Calculations were performed prior to live load testing to determine a desirable truck weight and configuration. The design moments for the deck were determined using an AASHTO standard HL-93 truck configuration (3-axle truck) with a 145 kN single axle, positioned to generate the highest possible transverse moment in the deck. Several vehicle configurations were investigated to generate demands in the bridges during the live load tests on the same order of magnitude as the design moments. These configurations included grain trucks, farm tractors, and tractor semi-trailers. These configurations were found to offer little advantage over a three-axle dump truck with respect to maximizing demands on the deck. A three-axle dump truck operating at a gross vehicle weight of 300 kN with 112 kN per axle on the back tandems was calculated to generate transverse moments in the deck equal to 90 percent of the design moments. At this load, the maximum longitudinal moment in the deck was estimated to be 104 percent of the longitudinal design moment generated by the HC-93 design vehicle. As this load was estimated to be approximately the maximum load a three-axle dump truck can physically carry, it was selected for test purposes.

Using a heavier vehicle for the live load tests pushed the decks closer to their design demands, with the intent of possibly amplifying any differences in behavior between the three deck configurations. A review of prior research found that other researchers have utilized heavy three-axle dump trucks with wheel loads on the same order of magnitude as the proposed load set (Yang and Myers, 2003; Stallings and Porter, 2002; Nassif et al., 2003). The weights and dimensions of the actual trucks used in the live-load experiments (a Sterling and a Volvo truck) are summarized in Figures 36 and 37, respectively. The same two trucks were used for both the 2003 and 2005 live load tests. Weights for each year are denoted accordingly. Figure 38 shows the Sterling truck which was used for all the single truck tests.
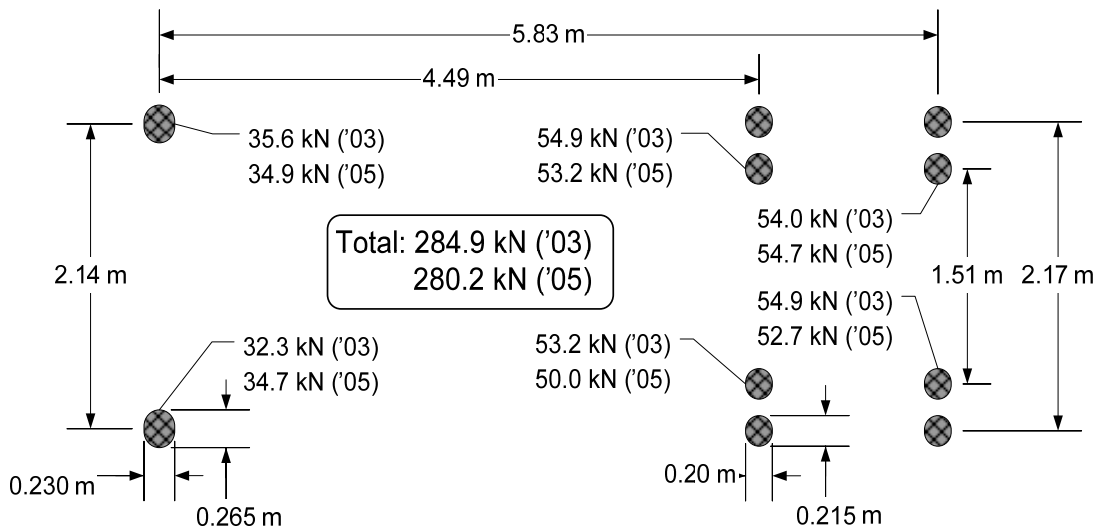
Figure 36: Dimension and Weight of the <u>Sterling</u> 3-Axle Dump Truck Used during Live Load Tests
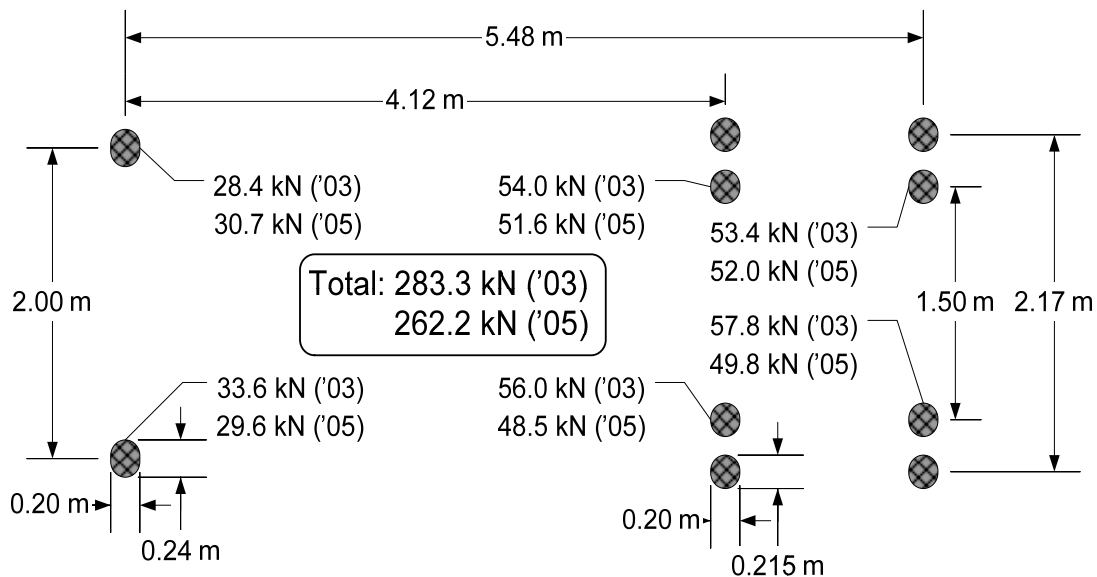
Figure 37: Dimension and Weight of the <u>Volvo</u> 3-Axle Dump Truck Used during Live Load Tests

Figure 38: Sterling 3-Axle Dump Truck

6.2   Testing Procedure

An identical regimen of live load tests was performed on each of the three Saco bridges. Each bridge was subjected to 15 test runs: 9 low speed single-truck tests, 5 high speed single-truck tests, and 2 low speed two-truck tests. Throughout the remainder of this document, low speed single-truck tests will be referred to simply as 'Single Truck' (ST) tests; high speed single-truck tests will simply be referred to as 'High Speed' (HS) tests; low speed two-truck tests will simply be referred to as 'Two Truck' (TT) tests.

Nine longitudinal truck paths were used in the live load tests. The positions, labeled R, S, T, U, V, W, X, Y, and Z, indicate the path of the front tire on the driver's side of the truck as it traverses the bridge in each test (see Figure 39). To record the longitudinal position of the truck as it crossed the bridge, transverse lines were painted on the deck at two-meter intervals. As the truck traversed the bridge during the slow-speed tests (ST and TT), a hand-held button was depressed to electronically record each time the front axle of the truck reached each successive two-meter mark.
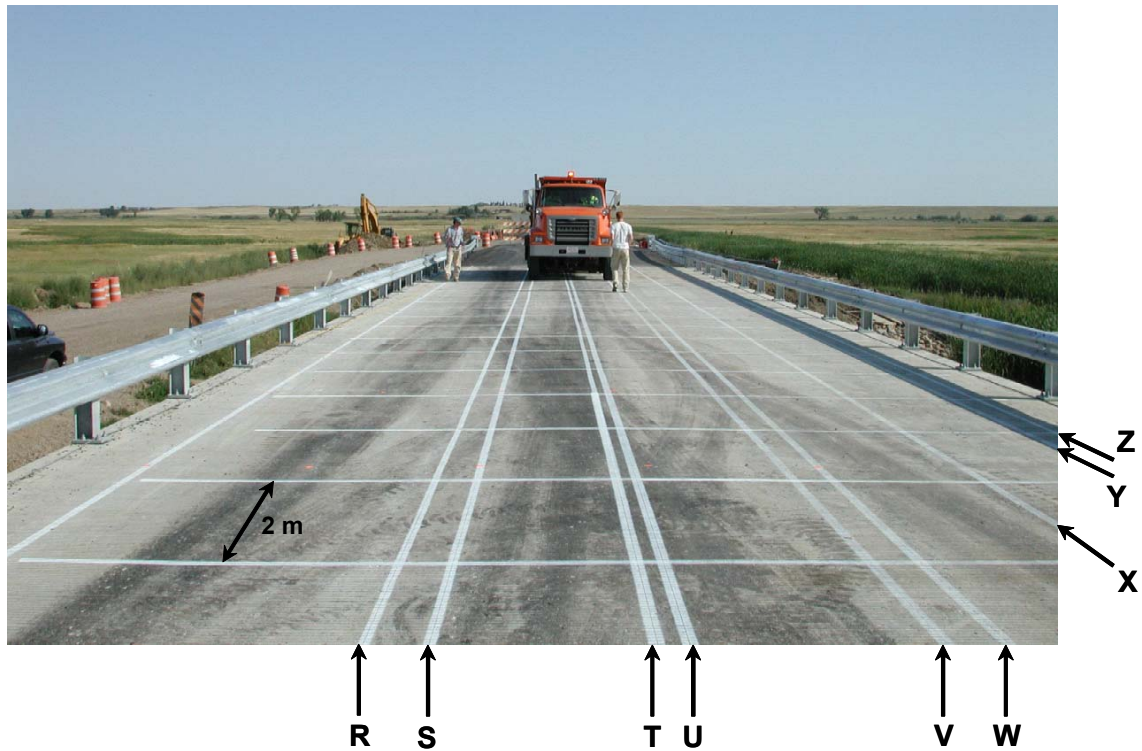
Figure 39: Photograph of Longitudinal Lines Used for Truck Positioning during Live Load Testing

The nine truck paths were selected to characterize deck response under the most critical load positions. Generally, tire loads were positioned to either be directly over a girder or at the midspan between girders, as shown in the cross-section views of Figure 40. Truck paths U and X position the center of the truck directly over a girder, such that the tires symmetrically straddle the girder. In Figure 40(a), the 'Single Truck' (ST) tests are followed by the letter of the appropriate truck path – R through Z. For example, ST-V represents a low speed single-truck test along the V truck line, as pictured in Figure 39. Likewise, positions in the two-truck and high-speed tests are shown in Figures 40(b) and 40(c), respectively.
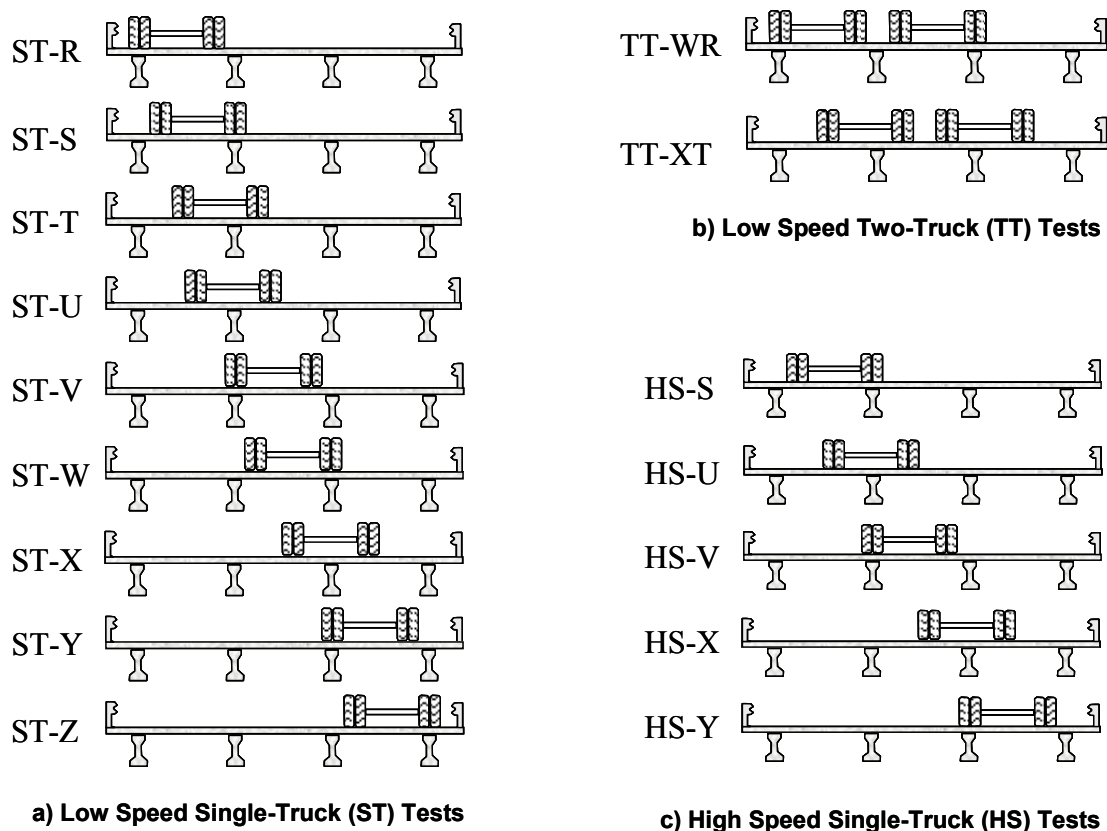
Figure 40: Truck Positions for Live Load Tests

Low-speed or "crawl" test were used in this investigation rather than statically stopping the truck at various locations and logging the data, as has been done in several bridge investigations. The information collected during such tests consists of a continuous stream of strain data as a function of longitudinal truck position. This approach is more efficient and provides more complete live load response information than static placement at discrete locations. Dynamic effects are negligible at the slow speeds used for these tests. The disadvantages of using a crawl test are the potential for minor deviations in the truck position and the inability to use certain types of gages (in this case the vibrating wire strain gages).

During the low-speed single-truck (ST) tests, the Sterling dump truck was driven along each of the nine selected longitudinal truck paths shown in Figure 40(a). One person marked the position of the front wheels using the hand-held button while the other guided the truck along the proper longitudinal path. Slow-speed tests were performed at a speed of approximately 2 miles per hour For the low speed, two-truck (TT) tests, both the Sterling and Volvo dump trucks were driven across the bridges side-by-side at two sets of longitudinal truck paths: truck lines W and R, and X and T, as shown in Figure 40(b).

Five high speed single-truck (HS) tests were conducted using the Sterling truck. The truck was driven across the bridge at a speed of approximately 100 kilometers per hour along each of the five selected longitudinal lines shown in Figure 40(c). Due to the relatively short duration of

these tests and the high speeds involved, no correlation between strain response and truck position was electronically recorded. Truck lines R, Y and Z place the truck very close to the guardrail and thus were not used in the high speed tests due to safety concerns. The actual positioning of the truck in the high speed tests was not as precise as during the slow tests, but was within approximately 30 cm from the longitudinal lines. Lines that were close together, such as T and W, were omitted because of their close proximity to test lines U and V.

6.3 Data Processing

To facilitate analyses of the live load data, it was manipulated to output deck response as a function of vehicle position, rather than a function of the elapsed time (which was how the data was recorded). Notably, due to differences in the travel speeds of the vehicle during the various tests, the data arrays from all the tests were difficult to correlate. Utilizing the position stamps created by the hand-held push button, a routine was written to estimate, from the time histories, the strain data at specific longitudinal truck positions. In this way, all data sets consisted of strain response information at identical spatial positions of the truck. Additionally, it was determined that minimal changes occurred over the short duration of each test (less than 2 minutes) due to changes in ambient conditions (i.e., temperature variation). As such, all strain histories were shifted as necessary so that initial strains were zero for each experiment.

7   RESULTS AND ANALYSIS OF LIVE LOAD TEST DATA

The primary goal of this project is to compare the relative performance of the three bridge decks. As part of this process, the live load test data can be used to develop a fundamental understanding of how each bridge deck responds to vehicle loads. Simple observations in this regard allow useful comparisons to be drawn between the performance of the three decks when more complex behaviors arise. Comparisons between the reported data and expected responses derived from basic strength of materials concepts are also useful in this analysis. To analyze the live load test results, an attempt was made to isolate the behavior of the deck from the contributions of other structural elements in the bridges. In the longitudinal direction, the decks act in concert with the girders; while in the transverse direction, the decks are the primary structural element. Consequently, this analysis focused more upon the transverse rather than the longitudinal deck response, as it was believed to be more significantly affected by the differences in construction of each deck, as well as to be less confounded by any incidental differences in the restraint to longitudinal movement offered by the abutment and bent supports of each bridge. Further, relative to transverse behavior, a typical deck panel defined by the end and middle transverse diaphragms in any span of each bridge was expected to represent the general behaviors across the entire bridge.

The analysis of the live load test results begins with the 2003 tests, followed by a comparison of these results with those obtained from the tests conducted in 2005. In both cases, the aspects of deck behavior that are discussed include:

- general load carrying behavior in the longitudinal and transverse directions,
- detailed analysis of transverse behaviors using shifts in the position of the neutral axis to investigate the presence/absence of cracking and in-plane stresses in the decks,
- stiffness analysis in the transverse and longitudinal directions, including calculation of girder distribution factors, and
- general linearity of the response as inferred by results obtained in the two-truck versus the single truck tests.

In each case, the common features observed in the response of all three bridges are identified and discussed, followed by comparisons of the more detailed features of the responses seen in each deck. Both qualitative and quantitative observations and comparisons are presented, as possible and appropriate. While qualitative assessments are valuable in generally describing differences in performance between test articles, they are of limited use unless these differences are pronounced in nature. That is, subtle differences in behavior may be impossible to detect simply by qualitative observation. Indeed, the important, qualitatively based conclusion that can be readily drawn in this case after reviewing the test data is that all three decks are behaving in a very similar fashion. The decks, however, are not behaving identically. Thus, the issue becomes whether or not consistent patterns exist in the small variations in the response between decks that

reflect true differences in deck behavior. This question can possibly be answered through some form of quantitative analysis of the data.

Standardized techniques for processing strain data collected during live load tests on bridges have not been developed, particularly when the objective of the analysis is to compare the relative performance of three different bridge decks. In this investigation, the decision was made to use some of the principles of engineering mechanics coupled with the strain data to estimate several structural parameters for each deck, such as the position of the neutral axis across the depth of the deck, the magnitude of the in-plane axial forces acting in the deck, and the magnitude of the average strains in the deck. Some of these parameters were found to statistically differ between bridges and over time. Note that while these differences were detectable, their significance remains uncertain, as the bridges are relatively young, and they only exhibit signs of nominal distress. The significance of these differences may become clear in the longer term, if substantial differences in deck durability and performance emerge over time.

In performing quantitative comparisons between bridge behaviors, generally a two sample t-test was used. This test evaluates the statistical significance of the difference in the means of two sample populations (e.g., the mean strain response observed in two bridges during the 2003 live load tests, or the mean strain responses for a single bridge observed in the 2003 and 2005 live load tests). The results of this test can be expressed in a variety of forms, and the decision was made to cite the p-value for each comparison when their result is stated. The p-value for the test ranges between zero and one; values approaching zero indicate a greater likelihood that the sample means are different, while values approaching one indicate a greater likelihood that the means are the same. This methodology and its results are described in more detail in Appendix F.

7.1 Results of First Live Load Tests – 2003

7.1.1 General Behaviors

Before proceeding with a detailed analysis of the data from the 2003 live load tests, it was critical to validate that behavioral responses reported in the data matched the direction and relative magnitude of the expected response. One unique aspect of this project was the availability of several live load tests on three different bridges. Certainly, some behavioral differences were expected between the three decks, which are examined later in this chapter. Nonetheless, general behaviors were expected to be similar. These similarities build confidence in the data and what it reveals. The response patterns and magnitudes were also compared with published data from other bridge live load tests to validate that they were "reasonable".

In general, similar responses were seen in all three decks during the live load tests. Furthermore, with the exception of the longitudinal strains over the bents, all of the measured strains were below the expected tensile cracking strains of the concretes.

7.1.1.1   Longitudinal Response

Presumably, the longitudinal bridge response is best understood conceptually. Interest in this response focused on effects generated in the third span (the instrumented span) of each bridge as a vehicle successively traversed all three spans of the bridge. When a vehicle entered the first span of each bridge, little response was expected in the third span (see Figure 41a), as the only continuity between the spans was provided by the deck (the girders ended at the abutments and bents). As the vehicle moved on to the center (the second) span, the deck was expected to deflect downward, generating positive moments (compression top, tension bottom) in the loaded span, as illustrated in Figure 41b. Under the same load, the curvature reverses over the interior bents, due to the continuity of the decks over the bents, creating negative moments (tension top, compression bottom) over the bent and in adjacent spans, eventually transitioning to positive bending moment furthest from the load at the integral (quasi-fixed) supports. As the vehicle moved onto the instrumented third span (see Figure 40c), the longitudinal strain response in that span was expected to significantly increase in magnitude, with positive moment in the middle of the span and nominal negative moments over the bent and adjacent to the integral abutment (which tend to restrain rotation at these locations).

a)

b)

c)
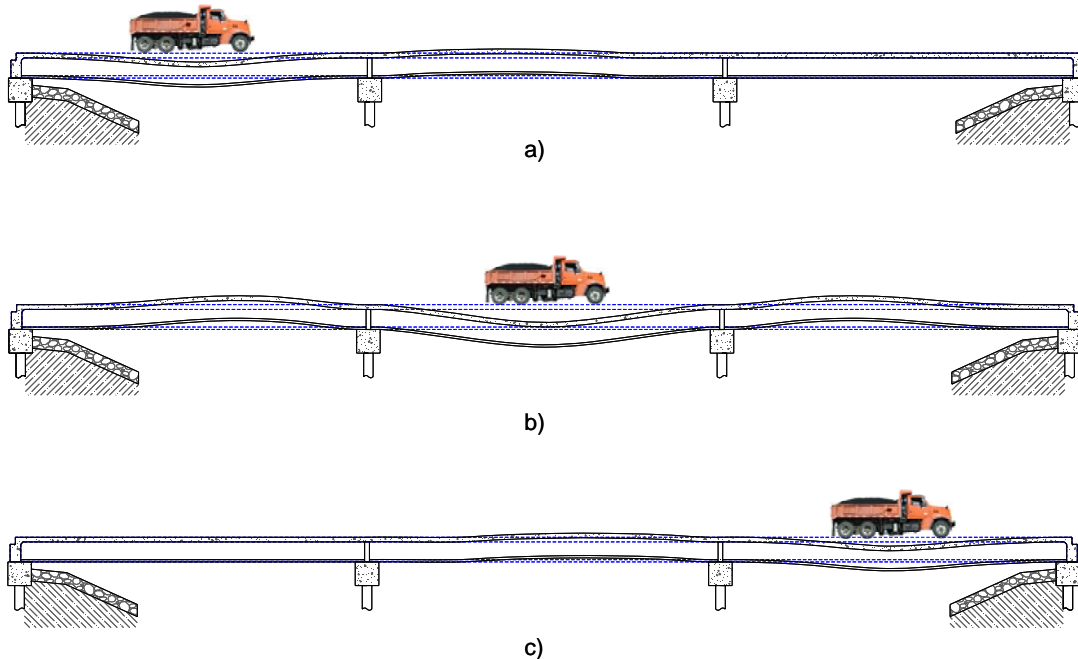
Figure 41: Expected Longitudinal Behavior of the Bridges

Relative to the expected behavior described above, a typical longitudinal strain history recorded in the third span is shown in Figure 42 (in this case, at the longitudinal quarter-span (Gage Location D-3)). For this style of plot, the positions denoted along the horizontal axis refer to the position of the test truck's front tire as it traverses the bridge. The strain trace is the record of the strain at a single, stationary gage location when the truck is at various longitudinal

positions along the deck. Thus, for example, the peaks corresponding to the tandem axles are later in the strain history than the front axle (i.e., the front axle passes over the fixed gage location first, followed by the tandem axles – about 5m later). The beginning and end of the decks are denoted by dashed lines in conjunction with the illustration of the elevation view of the bridge, above the graph. The strain response continues even after the front axle of the truck leaves the south end of the deck, since the rear tandem axles are still on the deck for approximately five more meters.
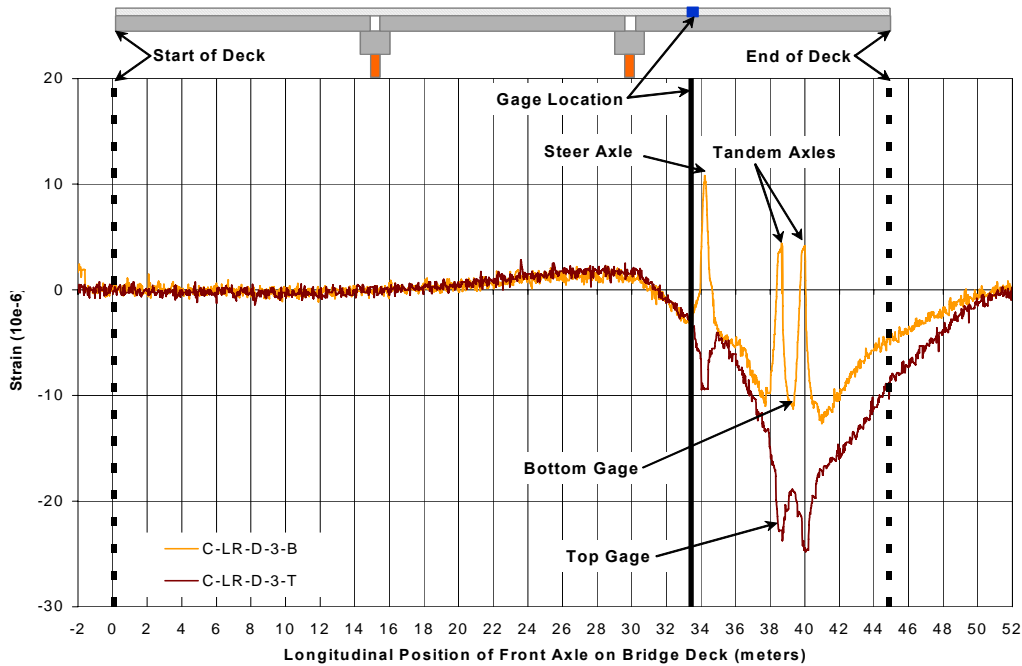
Figure 42: Strain History – Conventional Deck longitudinal Gage Location D-3 (ST-T Test)

Returning to Figure 41b, when the truck loads the center span of the bridge (longitudinal positions 15 m - 30 m), negative moments are induced as expected in the adjacent instrumented span, as shown by the nominal tensile strains at Gage Location D-3 (Figure 42). Note that in longitudinal bending behavior, the deck acts like the flange of a T-beam in concert with the stringers which act as the stem. As such, positive (tensile) strains in the deck indicate negative moment, while negative (compressive) strains in the deck indicate positive moment. As the truck tires enter the instrumented span, the response quickly changes to the expected positive bending moment response. Under positive moment, the top and bottom gages are both in compression. Also notable is the sharp positive moment peak in the gage response when each axle passes over the gage line. This characteristic response is caused by the local positive moment in the deck in the immediate vicinity of each tire footprint (i.e., a small 'dish' is formed around each tire load). These behaviors are not unexpected, since Gage Location D-3 is not directly supported by a girder; therefore, the deck experiences local deformation superimposed on the global response when the applied load is in the immediate vicinity of the gage. The shape

and magnitude of this phenomenon is similar to longitudinal deck strains observations by Stallings and Porter (2002) (see Figure 2).

The longitudinal response at Gage Location D-3 for all three bridges is shown in Figure 43. Notably, all three bridges exhibit similar shapes and magnitudes of response, thereby building confidence in the data. Also note that relative to magnitude, the peak strains were small, with maximum tension and compression values between 15 to 18, and 18 to 28 microstrain, respectively. The strains in the HPC deck were at the lower end of this range, while the strains in the Empirical deck were at the upper end of this range.
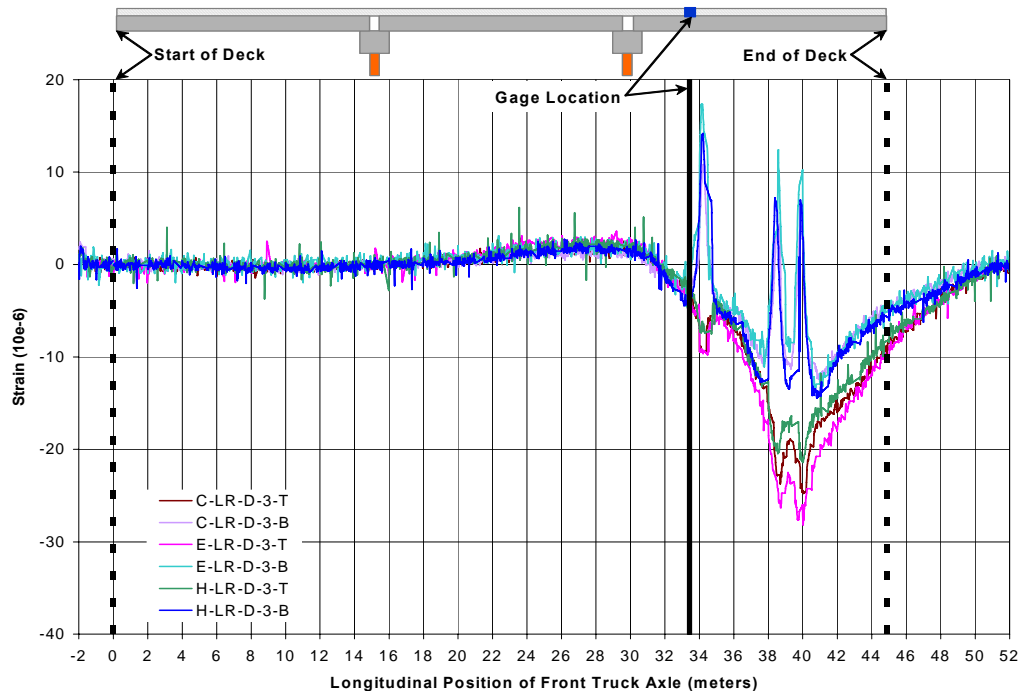
Figure 43: Strain History – All Three Decks Longitudinal Gage Location D-3 (ST-T Test)

A typical longitudinal strain history recorded in the third span close to the end of the bridge (Gage Location A-3) is shown in Figure 44. At this location, the longitudinal strain response was similar to that observed at location D-3, consisting of nominal negative bending moment when the vehicle was in the middle span (the deck gages nominally went into tension), followed by global positive bending moment when the vehicle enters the third (instrumented) span (the deck gages went into compression). Once again, superimposed on the global longitudinal response was a local positive bending moment response as the axles of the test vehicle traversed the gage location (the top gages spiked in compression, while the bottom gages spiked in tension). The maximum global positive moment response at location A-3 was considerably smaller in magnitude then at location D-3, as would be expected based on their relative positions along the span (location A-3 is considerably closer to the supports). The fact that positive global bending moments were observed at location A-3 indicates that the integral

abutment was relatively free to rotate, eliminating the existence of a significant negative moment zone along the girders adjacent to the abutment. If the integral abutment was fixed relative to rotation, a point of inflection would have occurred approximately 4 m from the end of the span, and negative rather than positive bending moment would have occurred at location A-3 (for the case of the test vehicle in the middle of the third span). The spike in the positive moment in the deck when the axles of the vehicle crossed directly above location A-3 was very similar in character and magnitude to the spike in response seen at location D-3. This behavior was in response to the local effect of the wheels, and thus it was expected that its magnitude and character would not be significantly influenced by position along the span.
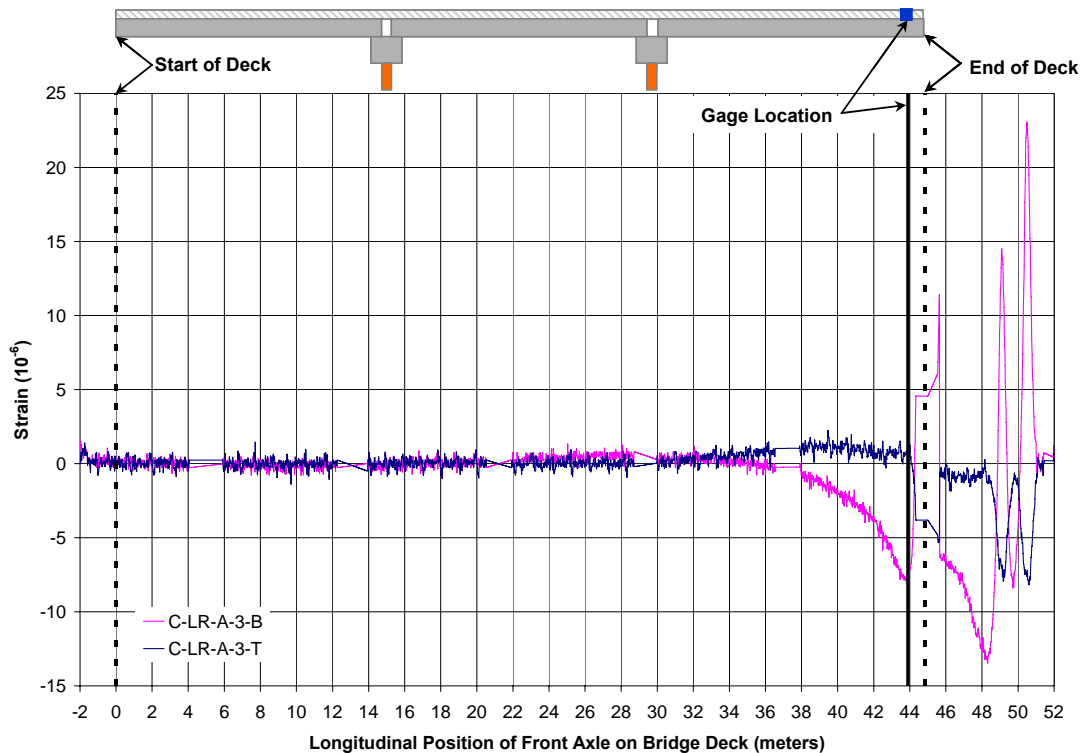
Figure 44: Strain History – Conventional Deck Longitudinal Gage Location A-3 (ST-T Test)

The longitudinal response at Gage Location A-3 for all three bridges is shown in Figure 45. As was observed at Location D-3, the strains recorded in each deck were generally similar in character, but varied somewhat in magnitude, with the smallest strains occurring once again in the HPC deck. The tensile strains in the HPC deck, for example, peaked at 12 microstrain, while the tension strains in the Empirical and Conventional decks peaked at 23 microstrain. All of these magnitudes are well below the tensile cracking strain of the concrete (estimated at around 150 microstrain). Note that these strains were measured in the interior of the deck, rather than at its surface, as is the case for all the measured strains presented in this report. Assuming a linear strain profile, larger strains would be expected at the surface of the decks, as is further discussed in Section 7.1.2.2. Nonetheless, the strains extrapolated at the surface of the deck from these values were still well below the tensile cracking strain of the concrete.
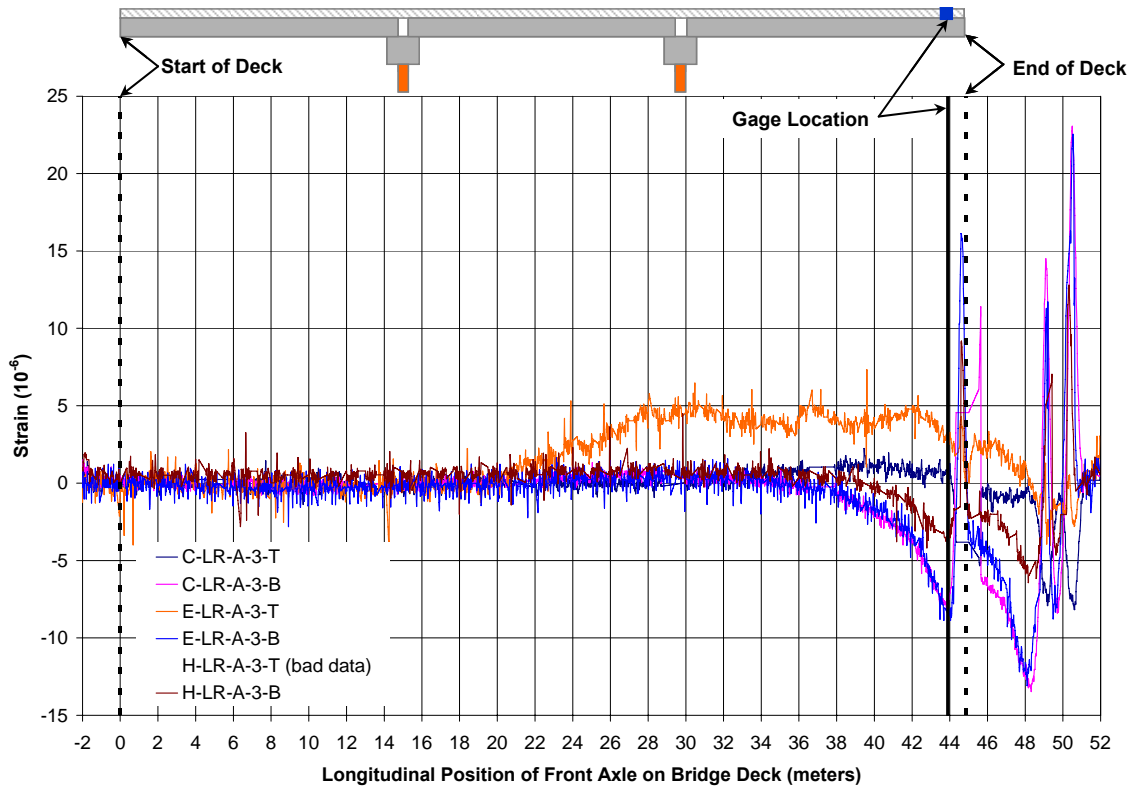
Figure 45: Strain History – All Three Decks Longitudinal Gage Location A-3 (ST-T Test)

At the bents (Gage Line F), negative moment was expected in the longitudinal direction due to global bending behaviors when the test vehicle was positioned on the center span of the bridge (see Figure 41b). A strain history recorded over the bent is shown in Figure 46 (this record specifically is from the Empirical deck, longitudinal Gage Location F-1, immediately over Bent 2 (the interior bent containing the instrumentation)). In contrast to the longitudinal strain histories at Gage Locations D-3 and A-3 (Figures 43 and 45), negative bending moment (tension top, compression bottom) dominates the deck response at Gage Line F. Recall that the deck is continuous across the bents, but the girders are not. Therefore, unlike at gage lines D and A, the depth of the cross-section is simply that of the deck, not the composite deck and girder section. The reduction of the moment output when the tandem axles of the truck are directly over Gage Line F (front axle at approximately 35 to 36 m) is because, at this truck position, only the front axle is loading the deck away from the bent, thereby reducing the negative moment over the bent.
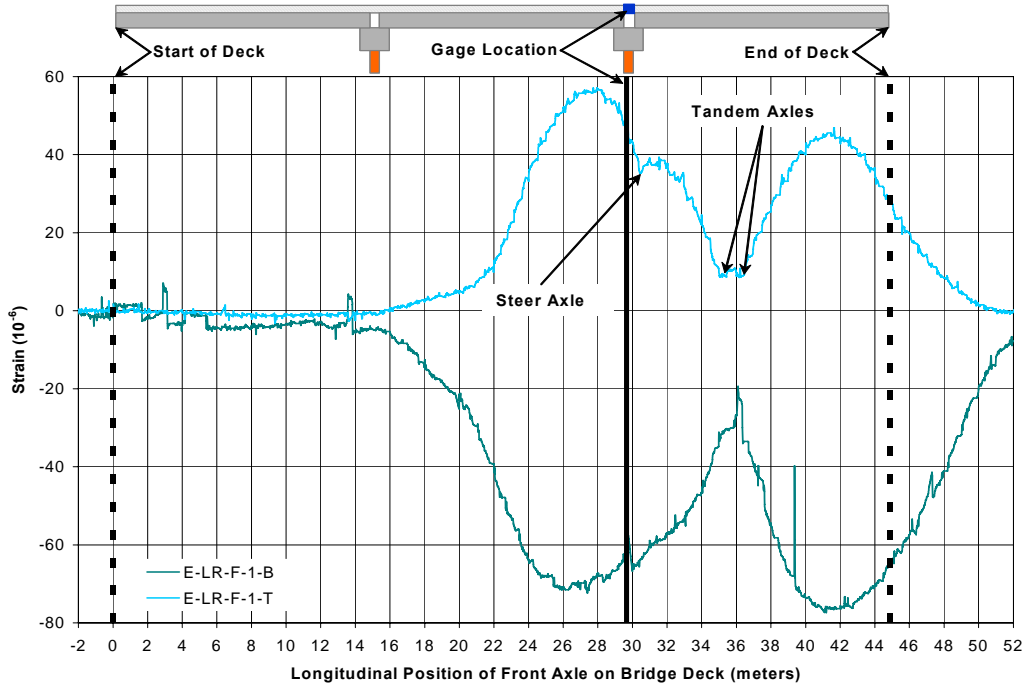
Figure 46: Strain History - Empirical Deck Longitudinal Gage Location F-1 (ST-T Test)

Strain histories for all three bridges at Gage Location F-1 are shown in Figure 47. Negative moments are evident in all three decks under the same load at this location. That is, the strains recorded in the top mat of reinforcement are all more tensile than the strains in the corresponding bottom mat, and the magnitude of the bending moment is similar for each deck (i.e., the difference between the top and bottom strains). In the case of the Conventional and HPC decks, this bending behavior is superimposed on an obvious in plane axial force effect, with this effect being tensile in the case of the Conventional deck and compressive in the case of the HPC deck. The in-plane axial force effect in the Conventional deck at Gage Location F-1 could result from T beam like action in which negative moment is being carried across the discontinuity at the bents through a couple consisting of a tension resultant in the deck in concert with a compression resultant acting through the anchor points of the girder, as illustrated in Figure 48. The greatest tensile strains at any location in any bridge in any test are seen here, with a magnitude of approximately 150 microstrain in the top of the deck. These strains are at a level at which cracking would be expected, and indeed this deck (like all the decks) was cracked in the transverse direction over the bent.
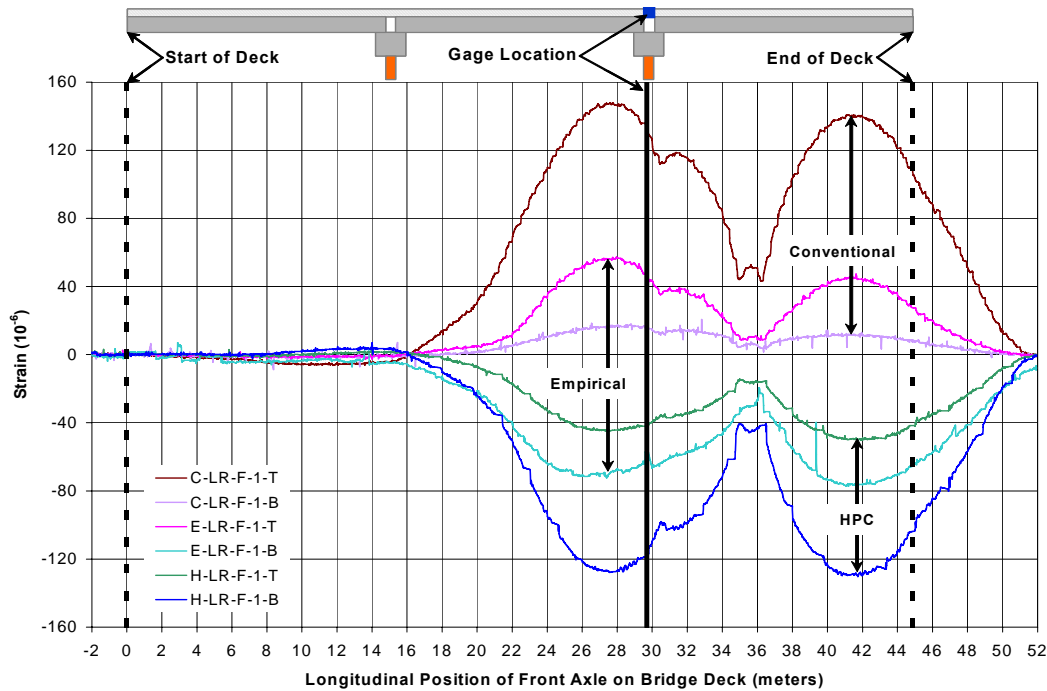
Figure 47: Strain History – All Three Decks Longitudinal Gage Location F-1 (ST-T Test)
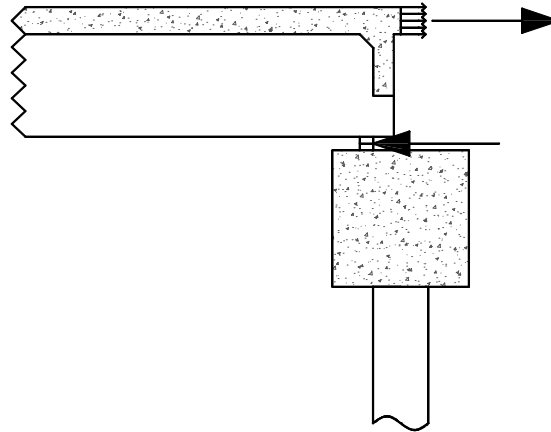
Figure 48: Possible Tension/Compression Couple at Bent 2 in the Conventional Bridge

The axial in plane compression behavior seen in the HPC deck at Gage Location F-1 may be related to the initial camber in the deck girders on the HPC deck. The topological survey data (reported in Section 8.4) clearly shows that the HPC deck has a greater camber than the Conventional and Empirical decks. As a result of this camber, this deck may exhibit some arching action, producing in-plane compression stresses across the depth of the deck. In this regard, a simple finite element analysis was done on a model of an interior girder that included the curved geometry of the actual cambered beam. In plane compression stresses and strains on the order of magnitude of those seen in the HPC deck over the bents were generated in this model.

With the exception of the response over the bents, little difference was observed qualitatively in the longitudinal strain response of the three bridges. In an effort to discern any subtle differences that might actually exist between these responses, the mean longitudinal strains measured in the bridges were calculated for all the longitudinal gage locations (except for the gages in the F-Line over the bents, which were believed to represent specific local behaviors) for selected test runs (specifically, runs ST-S, T, and U, and TT-WR, in which the test trucks were in the immediate vicinity of the instrumented deck sections). In light of the fundamental differences in the character of the response in the top and bottom of the decks, only the top gages at each location were used in the mean calculations (note that the bottom gages could just have easily been selected). The results of this comparative analysis were somewhat inconclusive. The mean strains in the HPC and Empirical decks were found to be the most similar (p-value of 0.77), while the mean strains in the Conventional and Empirical decks were least similar (p-value of 0.28).

7.1.1.2 Transverse Response

The deck was expected to transmit wheel loads transversely from their point of application into the adjacent girders. While often the deck is modeled as a continuous beam spanning pinned supports provided the girders (AASHTO, 2000), the girders are not fixed supports in the vertical direction, but rather they themselves deflect under the applied loads (see Figure 49). Thus, a more appropriate model for this situation is that of a beam on elastic supports (Cao, 1996), and the resulting distribution of bending moments in the deck is more complicated than that portrayed by the simple model first mentioned above. The deflected shape of the deck and the associated distribution of moments in the transverse direction are significantly influenced by the rigidity of the girders compared to the deck and the proximity of section under consideration to the concentrated wheel loads causing the deflection and moments.
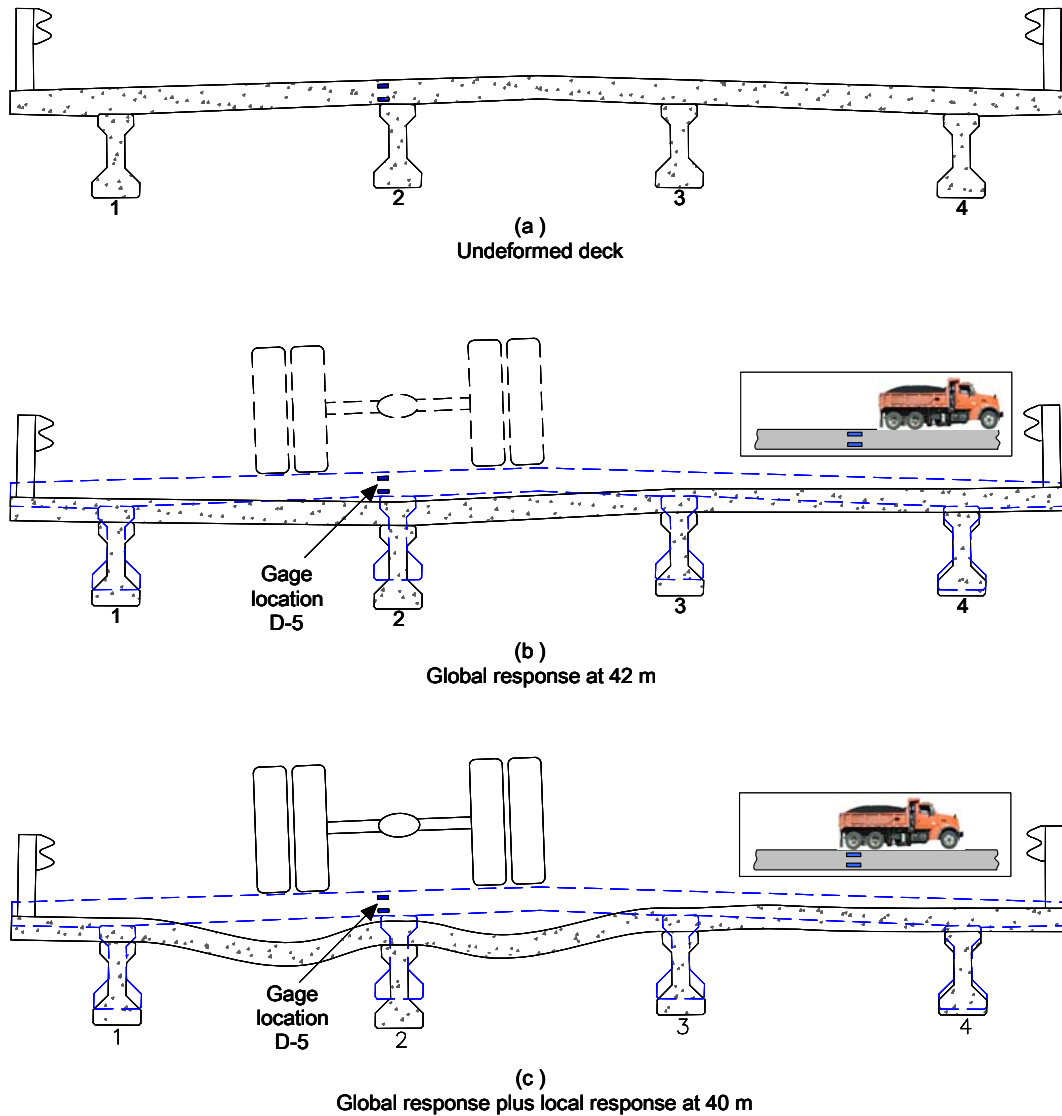
Figure 49: Expected Transverse Behavior of the Deck

The expected deflected shape of the deck at the location of a typical set of wheel loads is shown in Figure 49 (for the case of a vehicle straddling the girders). The expected response consists of two distinct components. The first component consists of a global deflection downward of both the deck and the supporting girders in the general vicinity of the loaded axle (see Figure 49b). The second component consists of a localized downward deflection of the deck relative to the girders immediately under the concentrated loads from the wheels at each end of the axle (see Figure 49c). The net transverse moment in the decks was expected to be a simple superposition of these two effects, with the positive global moment in the deck adding to the positive local moment in the deck at midspan between the girders, and acting opposite to the negative local moment in the deck at the face of the girders. This superposition of effects was

expected to result in a beneficial reduction in the transverse tensile strains experienced in the top of the deck over the face of the girders (Cao, 1996).

Relative to this expected behavior, typical transverse strain histories at a location in the deck between two girders are presented in Figure 50 for a run in which the test vehicle straddled the girders (much like the situation illustrated in Figure 49). The specific traces presented in this figure are for run ST-U for the Conventional deck at Gage Location D-4. As expected, as the test vehicle came on to the instrumented span, global positive moments were observed at this location (tension strains in the bottom of the deck, compression strains in the top of the deck) under the general dishing down of the deck and girders in the vicinity of the axle loads. As each axle passed directly over the gaged section, a further and distinct increase occurred in the positive moment response from the wheels additionally deflecting the deck downward in their immediate vicinity.
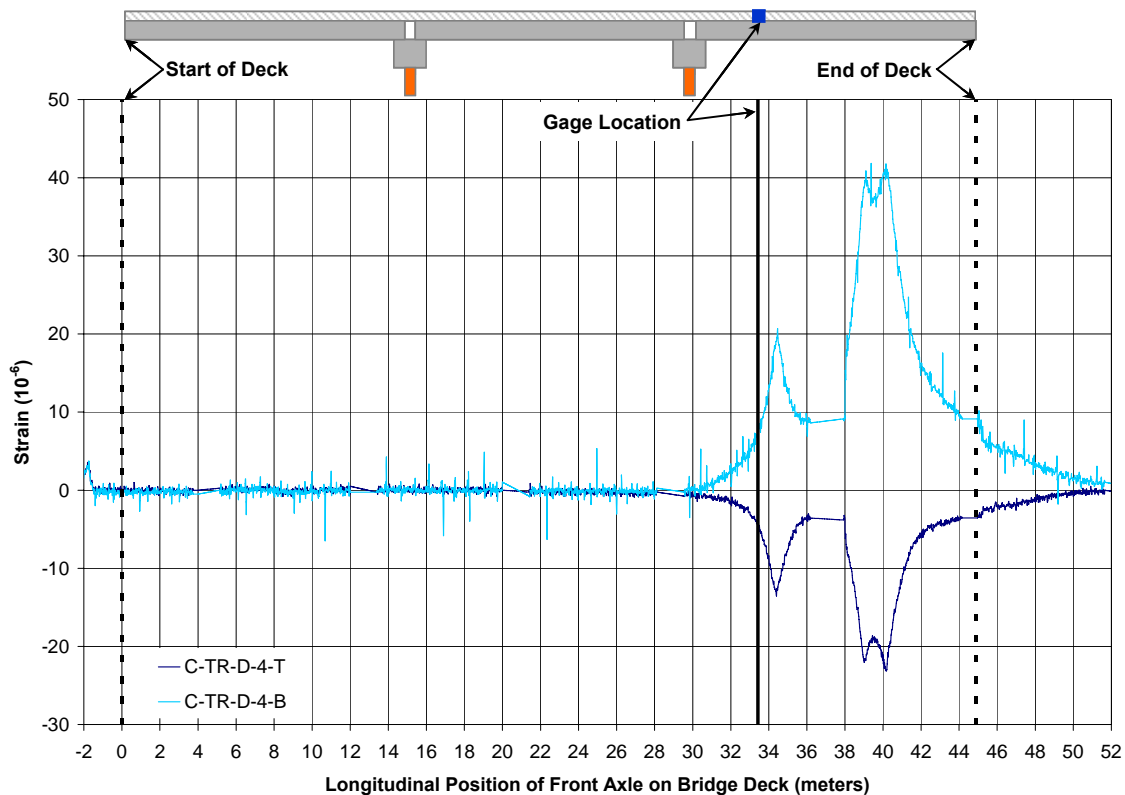
Figure 50: Strain History – Conventional Deck Transverse Gage Location D-4 (ST-U Test)

Transverse strain histories are presented for all three decks at Gage Location D-4 in Figure 51 for the same vehicle run (ST-U). Referring to Figure 51, the similarity in the general response of all three decks once again is apparent. In this case, the tension and compression responses from all three bridges are closely grouped around 43 and 15 microstrain, respectively. These tension strains were among the largest strains seen in the decks throughout the live load tests, with the exception of the strains observed in the cracked regions over the bents (Gage Line

F). Once again, these tensile strains (as well as the tensile strains extrapolated for the surface of the deck from these values) were well below the expected tensile cracking strain of the deck concretes.
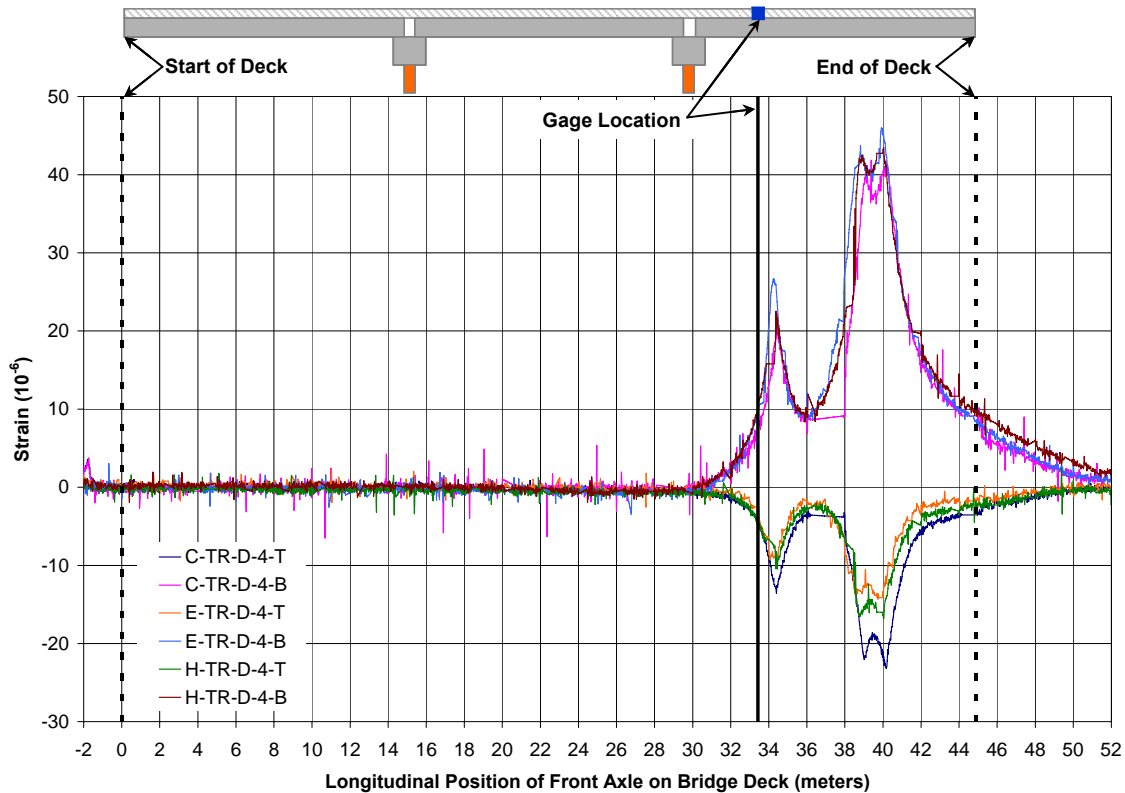
Figure 51: Strain History – All Three Decks Transverse Gage Location D-4 (ST – U Test)

Typical transverse strains measured in the deck at the face of the girder (Gage Location D-5) are presented in Figure 52. The response begins in positive moment when the front axle of the test truck moves onto the third span (at a position of approximately 30 m), as evidenced by the compression strains in the top gages and tension strains in the bottom gages of the deck. When the front axle reaches Gage D-5 (at 34 m), the moment reverses and becomes negative, in response to the wheels exactly straddling the gage location and locally reversing the bending moment at the face of the girder. The moment subsequently again becomes positive, until the rear axles are directly over the gages, where the moment reverses and becomes negative. Once the rear axles have passed over the gage line, the moment again reverses and becomes positive.
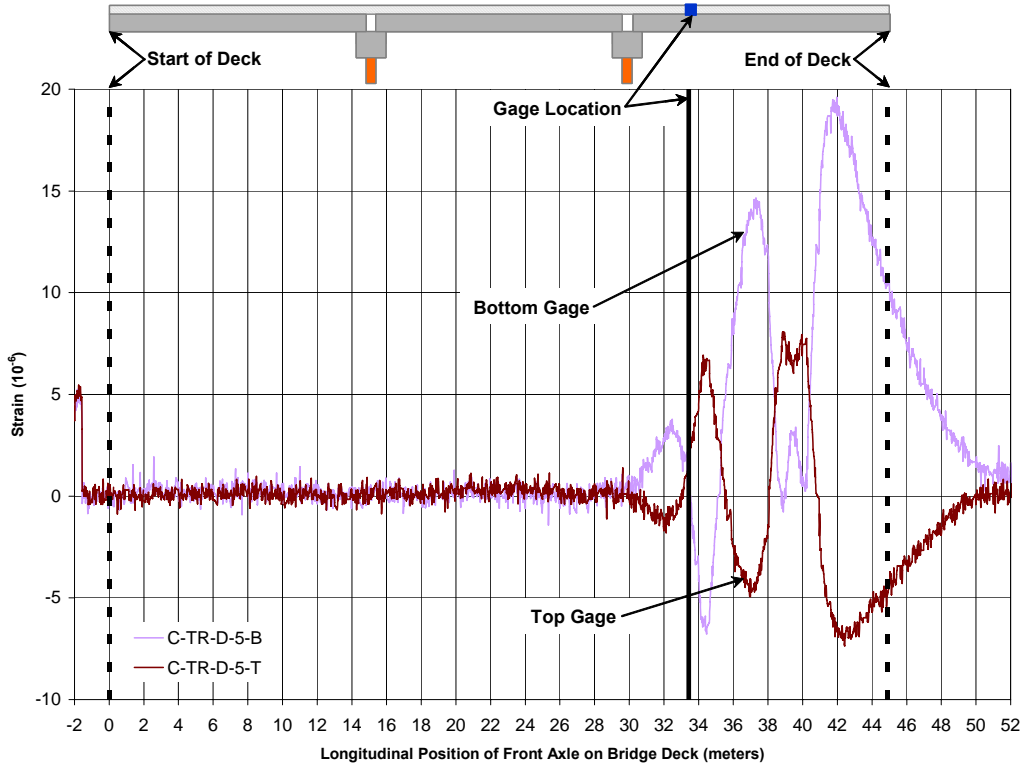
Figure 52: Strain History – Conventional Deck Transverse Gage Location D-5 (ST-U Test)

The transverse strain histories at Gage Location D-5 during test ST-U from all three bridges are overlaid in Figure 53. Once again, the response from all three bridges is very similar in character and magnitude. In this case, the maximum tensile and compression strains only ranged from 14 to18 and 7 to 10 microstrain, respectively, across all three bridges.
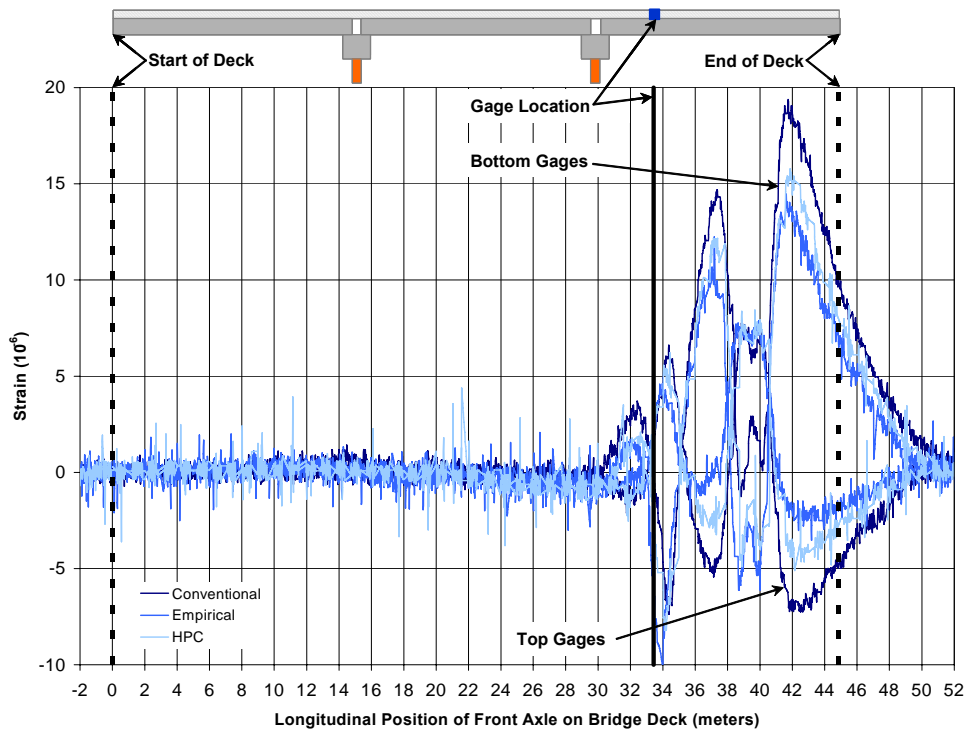
Figure 53: Strain History – All Three Decks Transverse Gage Location D-5 (ST – U Test)

In an effort to detect subtle differences in the response between the three bridge decks, the mean strain measured in each deck was calculated from the data collected from the bottom gages in the D Gage Line during selected tests (specifically, tests ST -S, T, and U, and TT-WR, which once again were selected due to their proximity to the instrumented deck section). The magnitude of the mean strains measured in the bottom of the decks for these gages and test runs were 2.0, 1.6, and 1.7 microstrain, respectively, for the Conventional, Empirical, and HPC decks. Despite the variation in these values, statistically the mean strains in the three decks were similar (p-values of 0.74 and greater for all comparisons).

In all of the transverse strain data presented above, the tension and compression response in the top and bottom mats of steel in the deck at any given location are not equal in magnitude. Specifically, the tension strains in the decks, whether they occurred in the bottom of each deck under positive bending moment, or in the top of each of deck during negative bending, were consistently two to three times greater than the corresponding compression strains that occurred simultaneously in the opposite mat of steel in the deck. This difference in the magnitudes of the tension and compression strains measured on opposing reinforcing mats across the depth of the decks could result from a) asymmetry in the amount and arrangement of the reinforcing steel in the cross-section, b) the presence of in-plane axial forces superimposed on the bending response of the decks, c) longitudinal cracking of the cross-section, and/or d) some combination of these effects. Which one of these effects is responsible for the stress differential observed in this case is explored in detail in the next section of this report. Asymmetry in the amount and placement

of the reinforcing bars in the top and bottom mats of steel does explain some of the observed differences in the magnitudes of the tension and compression strains experienced in the decks. The remaining difference in the magnitude of the tension and compression strains across the depth of the decks is attributable to net in-plane axial tension forces that develop in the deck in the transverse direction under vehicle loads.

7.1.2 Neutral Axis Position: Cracking and In-Plane Strains in Bridge Decks

Locating the actual and theoretical positions of the neutral axis across the depth of the deck cross-section under live load demands is a useful step in determining why the observed compression and tension strains in the top and bottom mats of reinforcing steel differ significantly in magnitude, and notably to identify if this difference is related to either cracking or the presence of in-plane stresses in the decks. Differences in the neutral axis position between bridges, and changes in this position over time, could further reflect underlying differences in the performance between bridges and changes in this performance over time.

The neutral axis location is easily determined from the strain data collected in the Saco bridge decks. As previously mentioned, the best opportunity to evaluate the effects of deck construction independent of other confounding factors is to look at their behavior in the transverse direction in the middle of the deck panel bounded by the diaphragms at the end and middle of each bridge span. Thus, this neutral axis analysis was conducted using the five transverse gages bonded to the top and bottom reinforcing mats along Gage Line D (see Figure 54). This analysis began with the determination of the location of the theoretical bending neutral axis for each deck based on the actual geometry and material properties of each deck. The actual position of the neutral axis in each deck during the live load tests was then determined from the strain data. This information was subsequently used to evaluate the condition of each deck and to investigate the presence of in-plane axial forces during the live load tests. A brief review of the concept of the neutral axis is presented below prior to beginning this analysis.

(a)
Plan view of transverse deck gages

(b)
Cross-section X-X showing D-line transverse gages
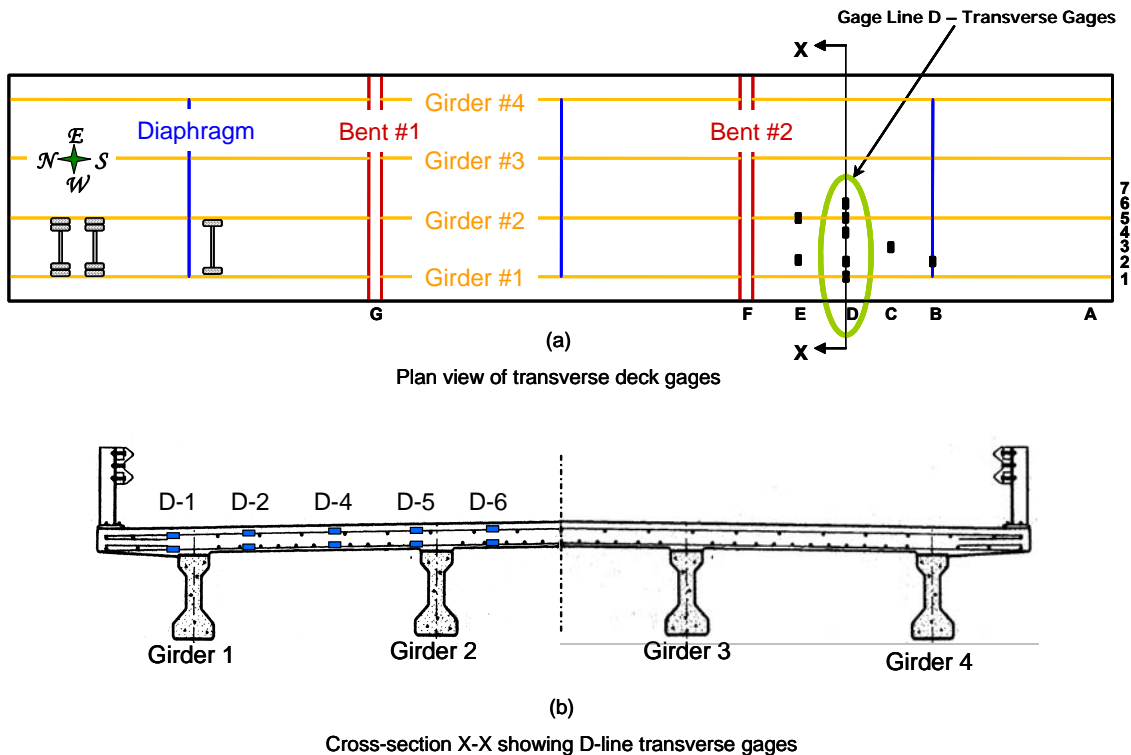
Figure 54: Transverse Gages of Interest (Gage Line D)

7.1.2.1   Background on Neutral Axis

The neutral axis of a beam is simply the height within its cross-section at which it experiences zero normal stress when loaded in bending. The **bending neutral axis** is the height of the beam's neutral axis under pure bending (i.e., no axial forces present). For beams composed of homogeneous materials, the height of the bending neutral axis can be determined from the geometry of the cross section, by using the first moments of areas. For example, the bending neutral axis of a rectangular homogeneous cross-section lies exactly at mid-depth, through the centroid, as shown in Figure 55.

For composite materials such as reinforced concrete, the relative amount, location, and stiffness of the two materials each factor into the position of the bending neutral axis. The standard procedure used to locate the bending neutral axis is called the Method of Transformed Areas. This method converts the actual area of steel to a theoretical area of concrete that would provide equivalent flexural resistance. Thus, the 'transformed' cross-section is composed of a homogeneous material; and the location of the bending neutral axis can be determined by taking the first moments of area (Wang and Salmon, 1985).
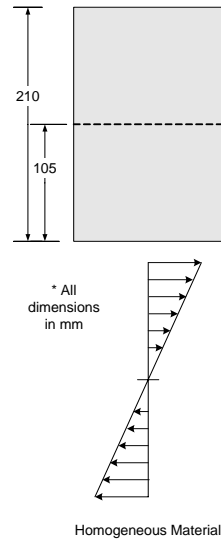
Figure 55: Homogeneous Deck Cross-Section Geometry with Calculated Bending Neutral Axis and Expected Bending Strain Profile (uncracked)

In typical design practice, it is common to neglect the area of concrete in tension when determining the position of the bending neutral axis, since its tensile load carrying capacity is minimal when compared to the compressive region. However, the material research of Gopalaratnam and Shah (1985) and Fenwick and Dickson (1989) indicate that concrete does, in fact, provide a substantial contribution in the tensile regions of the cross-section. Specifically for bridge decks, Fang et al. (1990) observed that under typical service loads, the tensile regions of the bridge deck remained uncracked. Thus, in the following analyses, the tensile contribution of the concrete was included as part of the cross-section when calculating the bending neutral axis. However, it is important to realize that the integrity of the concrete could greatly affect the position of the bending neutral axis, and if for any reason significant cracking is expected to have occurred, this assumption should be revisited.

7.1.2.2 Theoretical Position of the Bending Neutral Axis in the Saco Bridge Decks

Assuming that the concrete is uncracked, the expected location of the bending neutral axis was calculated for the Saco bridge decks using the Method of Transformed Areas (described above). All three decks had a specified thickness of 210 mm. For both the Conventional and HPC decks, the size (19 mm diameter) and distribution (230 mm on center) of the transverse steel is identical in the top and bottom reinforcing mats. However, the mats are not symmetrically located in the depth of the cross-section; the clear cover on the top surface (60 mm) is larger than at the bottom (25 mm).

Taking into consideration the different Young's moduli for the concrete in the two decks, and using a value from the initial portion of the stress curve (see Appendix A) appropriate for the small strain levels observed during the live load tests, the bending neutral axes for the

Conventional and HPC decks were calculated to be 104.2 mm and 104.4 mm above the bottom fiber of the deck, (Figure 56(a) and 56(b), respectively) – nearly the same height, lying just below mid-depth. As bending strains are directly proportional to distance from the neutral axis, the theoretical ratio of bending strains in the bottom steel versus in the top steel were calculated to be 1.92 for the Conventional deck and 1.94 for the HPC deck, due to the asymmetric placement of the reinforcing mats. Further note that although strains recorded in the rebar were expected to have different magnitudes, strains in the concrete at the extreme fibers of the deck were expected to have approximately equal magnitudes under pure bending, but be opposite in sign.

The Empirical deck cross-section has a slightly different geometry from the Conventional and HPC decks. The transverse steel in this deck is not identical in the upper and lower mats, as shown in Figure 56(c). Although the specified clear covers are the same as the other two decks, the bottom mat of transverse rebar is made up of 16 mm diameter bars spaced 345 mm on center and the top mat of transverse rebar is made up of 13 mm diameter bars spaced 330 mm on center. Despite this difference, the bending neutral axis for the uncracked Empirical deck was also predicted to lie relatively close to mid-depth, at 104.4 mm. Although the bending neutral axis was nearly identical to those of the Conventional and HPC decks, the predicted ratio of bottom rebar strains to top rebar strains is 1.82. This difference stems from the smaller bar sizes in the Empirical deck – given the same clear cover; the smaller bars place the mid-plane of each bar farther from the neutral axis. Again, the concrete strains at the extreme fibers will have approximately the same magnitude, with opposite sign.
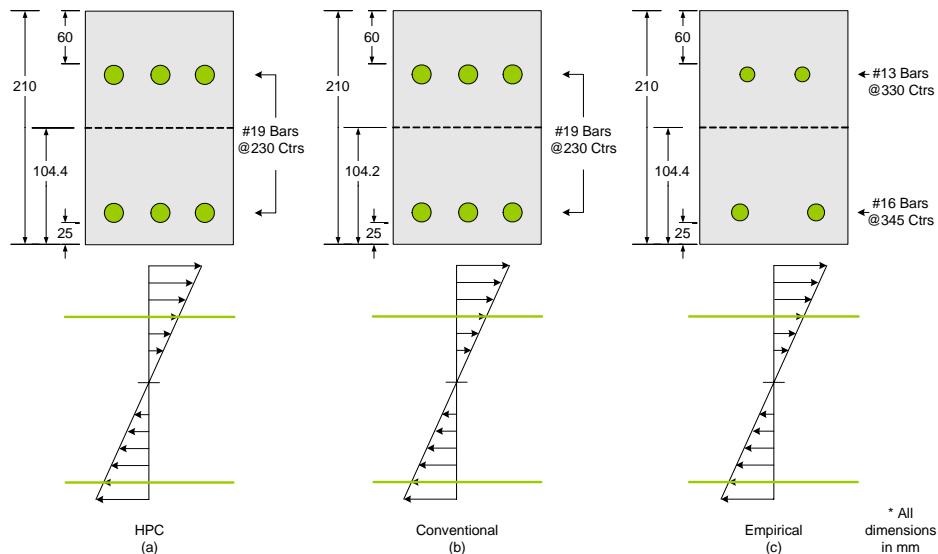
Figure 56: Saco Bridge Deck Cross-Section Geometries with Calculated Bending Neutral Axes and Expected Bending Strain Profiles (uncracked)

7.1.3 Actual Position of the Neutral Axis During the Live Load Tests

The location of the bending neutral axis in the bridge decks was determined using strain data recorded during live load testing. This neutral axis will be referred to as the **actual neutral axis** throughout the reminder of this report. Differences between the actual neutral axis and the predicted bending neutral axis are subsequently used in explaining deck behaviors observed under the live load events. Before looking at the specific neutral axis position, it is informative to review what these gages indicate relative to the general behavior of the deck during a typical live load test (ST-S). Referring to the response at Gage Location D-4 (see Figure 51), the gages located in the bottom mat show tensile strains approximately twice as large in magnitude as the compressive strains in corresponding top gages, which is generally consistent with bottom-to-top strain ratios predicted above for pure bending in the decks (1.92:1, 1.94:1 and 1.82:1 for the Conventional, HPC and Empirical decks, respectively). This general behavior is evident in all of the free-span areas under the influence of positive moments (i.e., it is not unique to Gage Location D-4). In addition, this behavior is also verified by strains reported from collocated concrete embedment gages at mid-depth and in the plane of the upper mat of reinforcing steel (not shown in Figure 51). Namely, in situations where positive moments are imparted by the test truck, tensile strains are recorded by gages located at mid-depth, which qualitatively indicates that the actual neutral axis is nearer to the top mat of steel than to the bottom.

The actual position of the neutral axis during the live load tests was more quantitatively established using the paired strain values from the top and bottom of the deck during each truck test. Assuming a linear strain distribution across the depth of the deck, the point of zero strain can be determined from the two strain values available from the test data, as illustrated in Figure 57. Referring to Figure 57, the angle φ is the interior angle formed between the internal linear strain profile and the vertical zero-strain-axis. Coincidently, the value of φ is directly related to the strength-of-materials value of curvature, κ, and is also proportional to the bending moment (assuming elastic behavior). Larger values of φ indicate larger magnitude moment, assuming the stiffness remains unchanged; positive values of φ are counter-clockwise and indicate positive moment, while negative values of φ indicate negative moment.
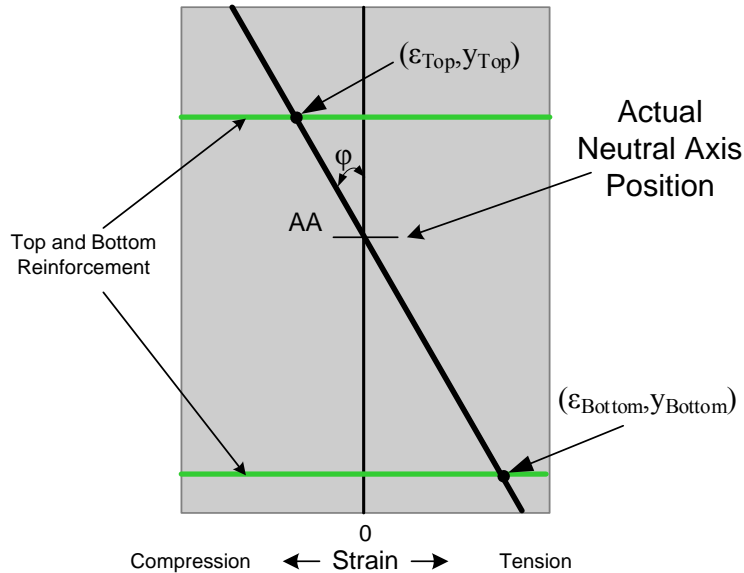
Figure 57: Illustration of How Actual Neutral Axis Height is Determined

Using the methodology described above, actual neutral axis positions were determined from for the Conventional, Empirical, and HPC decks, as reported in Tables 16, 17, and 18. All values are height (in mm) of the actual neutral axis above the bottom fiber of the deck concrete. The actual neutral axis positions were determined for a single truck tests at two separate positions of the test vehicle along the bridge deck. In the first position, the front axle is at 40 m and the back tandem axle is directly over Gage Line D. In the second position the front axle is at 42 m, and the back tandem axle is two meters south of Gage Line D. Hereafter, these two positions are simply referred to as the 40 m and 42 m truck positions, as shown in Figure 58. As might be expected, distinct behaviors were sometimes observed in the immediate vicinity of the concentrated wheel loads (evident in the 40 m response), relative to the global effects observed away from the vicinity of the wheel loads (observed in the 42 m response).
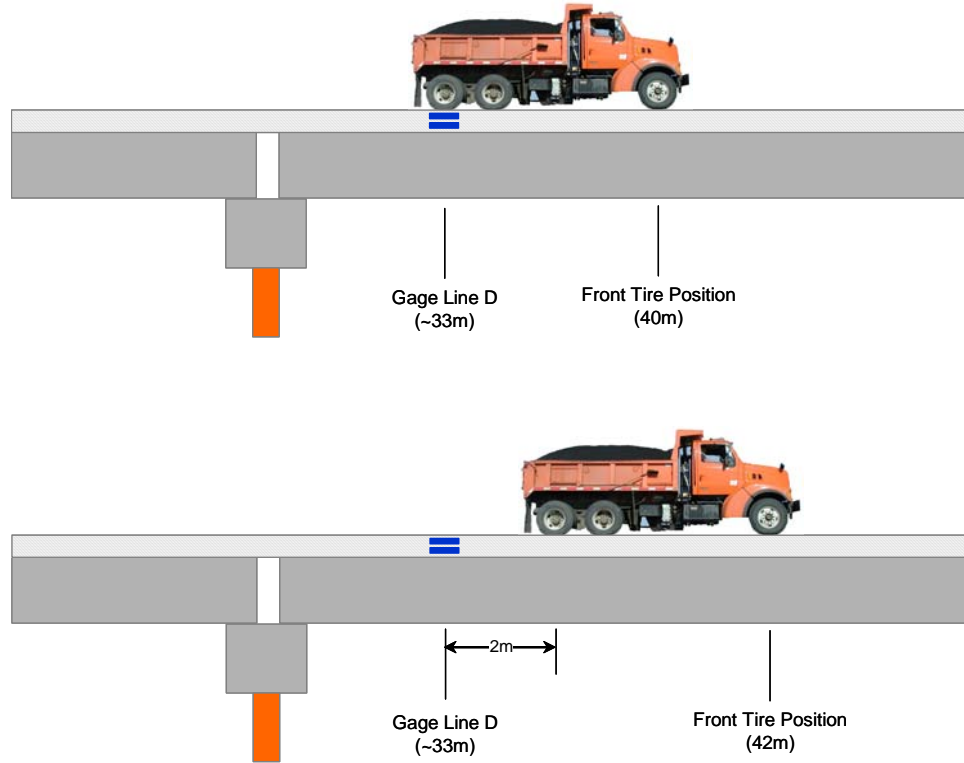
Figure 58: 40 m and 42 m Truck Positions, Relative to Gage Line D

Table 16: Actual Neutral Axis Positions for the Conventional Bridge Deck – 2003

Truck Position	Strain Gage Location	Single-Truck Tests * (mm)								Two-Truck Tests * (mm)	
		ST-R	ST-S	ST-T	ST-U	ST-V	ST-X	ST-Y	ST-Z	TT-XT	TT-WR
40 m	D-1	-248	-3	41	41	35	62	92	16	52	-60
	D-2	118	115	117	117	67	89	104	131	116	167
	D-4	110	110	104	104	134	92	102	109	107	114
	D-5	185	144	35	23	125	88	101	103	71	872
	D-6	78	149	120	119	119	123	112	116	121	122
42 m	D-1	326	-655	-56	-22	-26	55	114	20	9	-61
	D-2	134	126	126	128	53	89	97	131	134	173
	D-4	122	118	109	111	122	84	95	105	115	121
	D-5	138	127	122	118	113	60	94	101	140	131
	D-6	-266	139	122	121	121	124	106	115	125	127

* shading indicates negative moment

Table 17: Actual Neutral Axis Positions for the Empirical Bridge Deck – 2003

Truck Position	Strain Gage Location	Single-Truck Tests * (mm)								Two-Truck Tests * (mm)	
		ST-R	ST-S	ST-T	ST-U	ST-V	ST-X	ST-Y	ST-Z	TT-XT	TT-WR
40 m	D-1	-131	-60	42	50	53	70	144	121	26	-91
	D-2	129	120	113	115	97	106	115	113	131	213
	D-4	120	121	119	117	141	109	114	114	122	124
	D-5	525	211	82	64	155	109	109	106	86	37
	D-6	83	209	125	124	124	98	122	119	125	130
42 m	D-1	392	453	-299	-4	27	33	102	121	-146	-225
	D-2	141	132	146	147	70	95	112	113	184	184
	D-4	137	131	128	122	139	96	112	107	135	135
	D-5	174	148	141	136	130	50	108	98	156	174
	D-6	-1072	154	131	131	129	126	117	116	136	141

* shading indicates negative moment

Table 18: Actual Neutral Axis Positions for the HPC Bridge Deck – 2003

Truck Position	Strain Gage Location	Single-Truck Tests * (mm)								Two-Truck Tests * (mm)	
		ST-R	ST-S	ST-T	ST-U	ST-V	ST-X	ST-Y	ST-Z	TT-XT	TT-WR
40 m	D-1	-400	-34	22	30	28	194	†	289	38	-106
	D-2	114	107	109	111	75	96	113	113	108	162
	D-4	110	115	113	113	133	103	122	130	112	118
	D-5	278	152	64	55	141	96	170	102	88	7
	D-6	102	241	124	132	124	122	121	118	122	124
42 m	D-1	264	315	-253	-91	-33	123	88	300	-189	925
	D-2	133	120	119	123	8	89	96	105	123	184
	D-4	118	123	117	121	129	101	118	108	120	133
	D-5	139	127	126	131	120	88	100	101	169	126
	D-6	-36	150	126	129	127	165	112	116	127	133

† values are very large due to small strains
* shading indicates negative moment

In many cases, the actual neutral axis locations reported in Tables 16, 17, and 18 are quite different from the predicted bending neutral axis position of approximately 104 mm. In general, the actual neutral axis is higher than the bending neutral axis, under positive bending moments. Furthermore, the mean neutral axis height of the Empirical deck under positive moment of 158 mm may be statistically higher than the mean neutral axis height of the Conventional deck under positive moment of 139 mm (p-value of 0.30). The mean neutral axis height for the HPC deck under positive moment rests somewhere between the means of the other two decks, but it is not statistically different from either of them (p-values of 0.50 and 0.82, when compared with the Conventional and Empirical decks, respectively).

The neutral axis positions reported under negative moment were scattered, having many values higher and lower than the predicted bending neutral axis (see Tables 16, 17, and 18). These outliers made it difficult to assess trends in these values with any confidence. In general, however, most of the negative moment neutral axis heights for the Conventional deck were below the predicted value of 104 mm; most of the Empirical and HPC values were above 104 mm. Nonetheless, in the presence of negative bending moment, the actual neutral axis heights appear generally lower than for positive moment.

Comparing the localized effects and the more generalized global effects, the 42 m neutral axis heights seem generally higher than those at 40 m, although this observation is not consistently supported with statistical significance. In most cases, the neutral axes obtained during Two-Truck tests appear about the same or nominally higher than the Single-Truck experiments.

Perhaps the most important conclusion that can be drawn is that the actual height of the neutral axis differs from the predicted height of the bending neutral axis. This difference in the neutral axis location could be the result of either of two distinct phenomena (or a combination of both): 1) a geometric shift of the bending neutral axis due to cracking or other irregularities in the cross-section, or 2) the presence of in-plane axial tension or compression forces. Two separate analyses were conducted to investigate which of these phenomena is most dominant. Due to the different transverse locations of the gages across the deck, they are difficult to compare directly. Therefore, each gage location is considered separately, based on the surrounding geometry and presumed behaviors at that position in the bridge deck. The most conclusive evidence used to evaluate each bridge deck for cracking and axial effects was found in the data from Gage Locations D-4 and D-1, respectively. Specific evidence from these two gage locations is presented below. Data obtained from the remaining three gage locations (D-2, D-5, and D-6) corroborate and support the evidence from the other two gages locations, but do not offer any unique insights.

The presence of cracks throughout the deck cross section will cause an apparent shift in the neutral axis. Cracks located in the underside of the bridge deck will cause the bending neutral axis to shift upward under positive moments; similarly, cracks located on the topside of the deck will cause the bending neutral axis to shift downward under negative moments. The amount of this shift depends on the height of the crack. Three theoretical cracking scenarios are presented in Figure 59 for the positive moment case: uncracked, cracking up to the lower mat of reinforcement, and all tensile concrete cracked. When the concrete cracks in the bottom fibers due to a positive moment, the cross-section geometry changes and the neutral axis is expected to shift upward in the cross-section. The heights of bending neutral axes for these three theoretical conditions in each of the bridge decks are provided in Table 19.

(a)	(b)	(c)
Uncracked	Cracked up to Lower	All Tensile Concrete
	Reinforcing Mat	Cracked
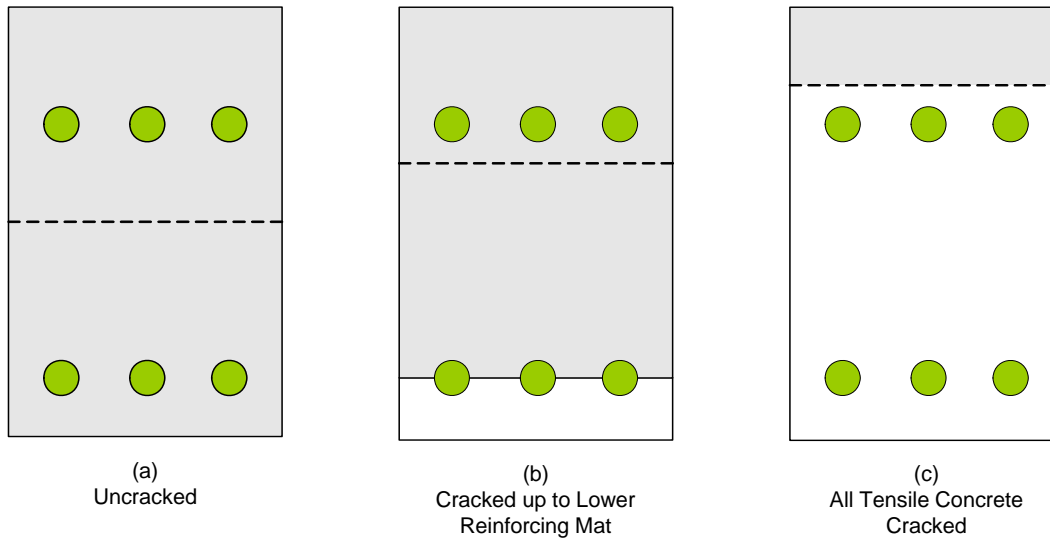
Figure 59: Theoretical Cracking Scenarios

Table 19: Bending Neutral Axis Heights at Various Cracking Levels under Positive Moment

Bridge Deck	Height of Bending Neutral Axis (mm)		
	Uncracked	Cracking up to Lower Reinforcing Mat	All Tensile Concrete Cracked
Conventional	104.2	120.0	165.6
Empirical	104.4	120.0	174.4
HPC	104.4	120.5	169.4

Many of the actual neutral axis heights calculated from strain data are similar to the height of the bending neutral axis for cracking up to the lower reinforcing mat (~120 mm), suggesting that the decks might be cracked, although no evidence of any such cracks was seen before, during, or after the tests (it is possible that such cracks could be small in magnitude and close in the unloaded condition). Conversely, cracking of all tensile concrete (approximately 85% of the cross-section height) would certainly have been noticed.

If a crack exists near the bottom of the bridge deck, the height of the bending neutral axis is expected to increase when compared to an uncracked section, under increasing positive moments. Increasing positive moments in the deck will increase the height of the bending neutral axis if the crack is unstable (i.e., the crack propagates upward under increasing positive moment), or the height of the bending neutral axis will remain constant if the crack is stable (i.e., the crack does not propagate upward under increasing positive moment). In the presence of a crack in the bottom fibers, it is not expected that the height of the bending neutral axis will reduce under higher positive moments.

Recall that φ (interior angle formed between the internal linear strain profile and the vertical zero-strain-axis – illustrated in Figure 57) is an indicator of the magnitude of moments in the deck cross section. To compare magnitude of positive moments within each bridge deck, several values of φ determined from strain data at Gage Location D-4 are shown in Table 20 for truck tests ST-R, ST-S, ST-T, and ST-U. Gage Location D-4 offers the best location to investigate deck cracking, since it is positioned relatively close to the midspan between Girder 1 and Girder 2. At this location, the expected behaviors are presumably the best understood, with the deck behaving most like a beam spanning between the adjacent girders. Values of φ are also provided for the 40 m and 42 m longitudinal positions (refer to Figure 58) to illustrate that φ decreases as the load moves away from the gage location, as expected.

Table 20: Values of φ at Gage Location D-4

Longitudinal Position	Deck	φ (degrees)			
		ST-R	ST-S	ST-T	ST-U
40 m	Conventional	15.6	14.1	28.8	28.7
	Empirical	15.2	14.0	27.3	27.1
	HPC	16.3	14.5	27.8	28.5
42 m	Conventional	9.4	10.9	18.3	16.6
	Empirical	8.5	9.8	14.6	15.9
	HPC	8.6	9.3	14.7	17.3

Based on these φ angles, the positive moments induced at Gage Location D-4 are higher during the ST-T and ST-U tests than the ST-R and ST-S tests (assuming stiffness remains constant). In fact, the positive moments observed at Gage Location D-4 during ST-T and ST-U, are the largest of all the live load tests. Therefore, if cracking had occurred, it would be most pronounced in these live load tests. However, the actual neutral axis heights in these tests do not show that cracking occurred, since they are generally lower under greater positive moment. The actual neutral axis heights determined using strain data from Gage Location D-4 in all the decks during tests ST-R, ST-S, ST-T, and ST-U, are presented in Table 21. The reported neutral axis heights are lower for tests ST-T and ST-U than for the corresponding ST-R and ST-S tests, with the exception for the HPC deck, notably for the ST-R truck test. This relative anomaly in the results for the HPC, ST-R test is under investigation, and could result from the manner in which this test was conducted or an actual difference in structural behavior. Nevertheless, in the Saco decks, higher positive moments generally are associated with lower neutral axis heights. Additionally, neutral axis heights are reportedly higher at the 42 m truck position than at the 40 m truck position, which is counterintuitive. For a partially cracked cross-section, recall that lower neutral axis positions are not expected under higher positive moments. This expected

behavior is not supported by the data presented here. Thus, it is unlikely the bottom of any of the decks has cracked.

Table 21: Actual Neutral Axis Heights (Gage Location D-4)

Longitudinal Position	Deck	Actual Neutral Axis Height (mm)			
		ST-R	ST-S	ST-T	ST-U
40m	Conventional	110	110	104	104
	Empirical	120	121	119	117
	HPC	110	115	113	113
42m	Conventional	122	118	109	111
	Empirical	137	131	128	122
	HPC	118	123	117	121

The absence of cracking in the negative moment regions of the deck can also be inferred from an analysis of the location of the neutral axis in negative bending (similar to the analysis done above for the positive moment case). In most cases, as previously commented, the neutral axis shifted down in negative moment regions during the live load tests relative to its theoretical position in pure bending. While such a shift might be expected if cracking occurred in the top of the deck, no such cracking was visibly evident in the decks. Furthermore, as in the case of positive moment, the neutral axis position was expected to either remain unchanged or move even lower in the cross-section in the presence of larger moments, if the top of the deck was cracked. This was not the case for the negative moments at the D-1 Gage line, where under larger moments, the neutral axis shifted upward in the cross-section.

In light of these observations regarding the relationship between moment and the actual neutral axis position, it is unlikely that cracking occurred in the top or bottom fibers of any of the three decks during live load testing. If cracking is not responsible for the observed shifts in the position of the neutral axis in the decks during the live load tests, the only remaining explanation is that in-plane axial forces are generated in the decks during the tests.

With or without the presence of cracks, axial forces acting within the plane of the bridge deck will result in an apparent neutral axis shift. When a member is loaded in pure bending, no net axial stress exists, and the strain profile for each deck will resemble those presented in Figure 56. Because the bridge deck is rigidly anchored to the girders, a mechanism does exist for in-plane axial stresses to be developed in the deck, superimposed on any bending behaviors. This results in a strain profile that is parallel to the predicted profile, but is shifted horizontally along the strain-axis, as shown in the two cases of Figure 60 for positive and negative moment situations.
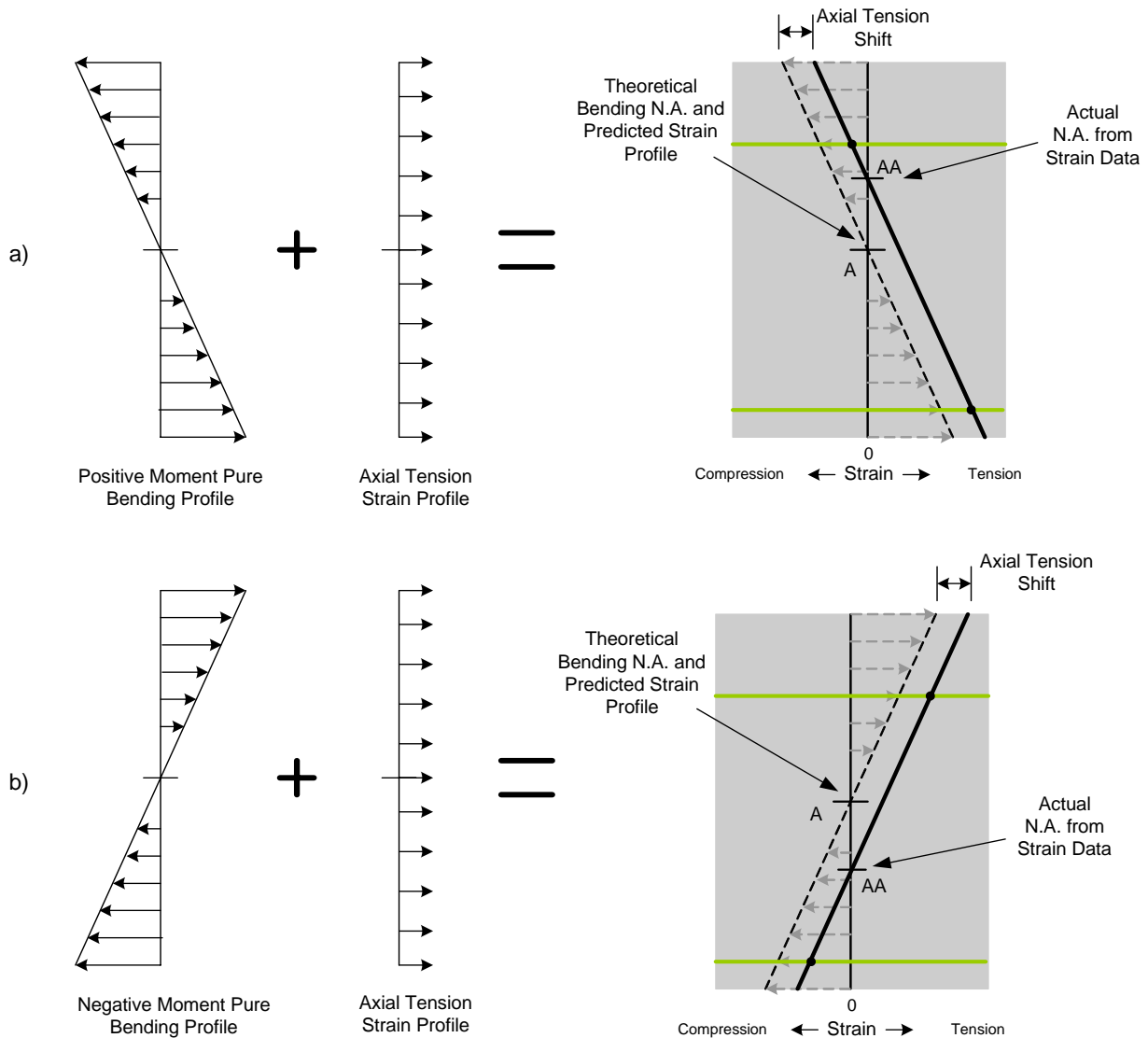
Figure 60: Illustration of Neutral Axis Shift Due to In-Plane Axial Strains under a) Positive Moment and b) Negative Moment

The addition of a uniform axial force effectively changes the height of the actual neutral axis from Point A (the height of bending neutral axis) to Point AA (the height of the actual neutral axis). In the presence of positive moments, the neutral axis shifts upward under axial tension (Figure 60a); correspondingly, it shifts downward in the presence of negative moments (Figure 60b). The neutral axis would shift in the opposite direction in a uniform axial compression field (not shown).

The expected direction of the neutral axis shift for the case of in-plane axial tension force matches the actual direction of the shift seen in the live load strain data in the transverse direction. That is, as previously reported, the neutral axis generally shifted upward in positive

moment zones and downward in negative moment zones. The uniform axial strains necessary to shift the neutral axis from the theoretical bending position to the actual position observed during the tests were determined for all truck runs on each bridge. These strains are presented in Tables 22, 23, and 24 for the Conventional, Empirical, and HPC decks, respectively. To calculate this axial strain shift, strain data from the live load tests were used to determine the slope of the linear strain profile at each gage location. Rebar strains for pure bending were then predicted by drawing a parallel profile through the theoretical uncracked bending neutral axis (the dashed profile shown in Figure 60). The amount of superimposed axial strain necessary to shift the strain profile to the actual neutral axis was simply the strain difference between the pure bending profile and the actual profile. In Tables 22, 23, and 24, a positive sign indicates a tensile axial strain, while a negative sign indicates a compressive axial strain. Shaded cells indicate negative moment.

Table 22: Back-Calculated Axial Strains for the Conventional Deck – 2003

Truck Position	Strain Gage Location	Single-Truck Tests * (µε)								Two-Truck Tests * (µε)	
		ST-R	ST-S	ST-T	ST-U	ST-V	ST-X	ST-Y	ST-Z	TT-XT	TT-WR
40 m	D-1	5.0	5.7	3.7	4.1	1.4	0.7	0.1	-3.8	4.4	8.4
	D-2	2.5	3.3	1.3	1.1	1.7	0.8	0.0	-0.9	1.5	3.8
	D-4	1.7	1.5	-0.1	0.0	1.5	0.9	0.1	-0.3	1.3	2.5
	D-5	4.6	4.3	4.7	5.0	2.8	1.7	0.3	0.1	6.4	7.2
	D-6	1.2	2.1	5.7	4.9	5.0	1.2	-0.7	-1.4	7.0	7.2
42 m	D-1	3.3	4.3	3.2	3.3	1.7	1.0	-0.1	-3.6	3.8	6.2
	D-2	3.2	3.6	2.3	2.0	2.0	0.8	0.3	-0.8	2.9	4.8
	D-4	2.9	2.7	1.5	2.0	1.4	0.8	0.5	0.0	3.1	3.9
	D-5	3.4	3.2	3.2	2.8	1.6	1.2	0.7	0.2	4.3	5.4
	D-6	2.1	2.2	5.1	4.4	5.3	1.7	-0.1	-1.2	7.4	5.3

* shading indicates negative moment; positive values = axial tension; negative values = axial compression

Table 23: Back-Calculated Axial Strains for the Empirical Deck – 2003

Truck Position	Strain Gage Location	Single-Truck Tests * (με)								Two-Truck Tests * (με)	
		ST-R	ST-S	ST-T	ST-U	ST-V	ST-X	ST-Y	ST-Z	TT-XT	TT-WR
40 m	D-1	5.3	5.5	4.0	3.1	1.0	0.3	0.0	-0.2	5.4	7.2
	D-2	4.3	4.6	0.7	0.7	0.3	-0.1	-0.4	-0.3	2.5	3.9
	D-4	4.2	4.2	7.4	6.7	1.5	-0.3	-0.6	-0.5	6.9	4.8
	D-5	4.2	4.7	2.5	3.6	3.8	-0.3	-0.2	-0.1	3.3	5.6
	D-6	1.2	2.6	6.8	6.0	5.6	-0.2	-1.8	-1.5	7.4	8.4
42 m	D-1	3.1	3.2	1.5	2.1	1.3	0.7	0.0	-0.2	4.8	5.4
	D-2	3.9	4.0	3.0	2.6	0.8	0.4	-0.3	-0.4	3.9	4.9
	D-4	4.8	4.6	6.1	5.1	2.2	0.3	-0.4	-0.1	6.8	7.0
	D-5	3.2	3.8	4.1	4.1	3.1	1.3	-0.1	0.3	5.0	6.1
	D-6	2.1	2.9	5.6	5.5	5.2	0.7	-1.1	-1.0	7.6	6.2

* shading indicates negative moment; positive values = axial tension; negative values = axial compression

Table 24: Back-Calculated Axial Strains for the HPC Deck – 2003

Truck Position	Strain Gage Location	Single-Truck Tests * (με)								Two-Truck Tests * (με)	
		ST-R	ST-S	ST-T	ST-U	ST-V	ST-X	ST-Y	ST-Z	TT-XT	TT-WR
40 m	D-1	4.8	5.2	4.0	3.6	1.2	-0.3	-0.8	-0.9	4.2	7.3
	D-2	1.5	0.8	0.7	0.6	0.7	0.4	-0.3	-0.3	0.6	3.4
	D-4	1.6	2.7	4.4	4.8	1.1	0.1	-0.9	-1.0	3.0	3.9
	D-5	4.4	4.2	3.7	3.9	3.0	0.9	-2.7	0.1	3.8	6.0
	D-6	0.2	2.7	6.7	8.9	6.0	1.0	-1.6	-1.7	7.9	8.6
42 m	D-1	2.7	2.8	2.4	2.0	1.4	-0.1	0.0	-0.4	2.5	3.9
	D-2	2.6	2.2	1.4	1.6	1.1	0.6	0.3	0.0	1.8	4.0
	D-4	2.1	3.1	3.4	5.3	1.7	0.1	-0.6	-0.1	3.8	4.4
	D-5	2.7	2.8	3.2	3.5	2.2	0.6	0.3	0.2	3.8	3.5
	D-6	0.8	2.4	4.7	5.7	4.7	1.7	-0.6	-1.3	6.4	5.1

* shading indicates negative moment; positive values = axial tension; negative values = axial compression

Notably, most of the axial strains calculated from the live load data were tensile (although there is a systematic change in the behavior of the instrumented test section when the test vehicle is on the opposite side of the bridge (test runs Y and Z), when the in-plane force in the deck is almost uniformly compressive rather than tensile). Recall that Fang et al. (1990) observed no deck cracking and observed in-plane tension membrane stresses in the decks up until cracks occurred at three times the AASHTO service load. The estimated tensile strains were small in magnitude, with a maximum value of approximately 9 microstrain, and a mean value of 2.5 microstrain. All the decks reveal fairly similar magnitudes and directions of axial strains, although the Empirical deck appears to show generally higher strains than the other two decks. The statistical tests described in Appendix F were used to compare the means of axial strains in

the three decks under positive moment only. The means of the axial tension strains in the Empirical deck under positive moment were statistically different from the other two decks (p-value of less than 0.01 for both comparisons). The mean axial tension strains in the HPC and Conventional decks may be different (p-value of 0.28).

One explanation of this tension is that as the truck nears the region of the gages, the deck exhibits a small amount of membrane behavior (superimposed on the flexural behavior), "drawing in" toward the tire location. However, because the bridge deck is supported laterally by the girders, diaphragms, and surrounding deck concrete, this "drawing in" action is resisted by tensile membrane forces, and concomitant axial tensile strains develop in the deck. This behavior can occur in a linear-elastic fashion if the deck has already transversely deflected under the action of other loads (i.e., self-weight).

For the Saco bridge decks, the data reported at Gage Location D-1 presents further evidence that axial forces are indeed present. Gage D-1 is located in the cantilevered portion of the bridge deck, just outside Girder 1 (refer to Figure 54). Many of the actual neutral axes calculated from strains at Gage Location D-1 fall outside of the geometric limitations of the cross-section (refer to Tables 16, 17, and 18). This phenomenon is physically impossible without the presence of axial forces. To illustrate this point, the diagram presented in Figure 61 shows a strain profile resulting from a positive bending moment coupled with a uniform axial tension field. In this case, the position of the neutral axis can be above the upper fiber of the cross-section.

The net tension in the deck at Gage Location D-1 is obvious in the transverse strain profile recorded from all three bridges at 40 m (truck tires in the vicinity of Gage Line D) for test ST-S, as shown in Figure 62. The moments induced at Gage Location D-1 are relatively small, as indicated by small φ angles. As such, bending and/or cracking effects are not expected to be very dramatic in this region. Therefore, it is reasonable to conclude that axial strains are predominantly governing the position of the actual neutral axis at Gage Location D-1.
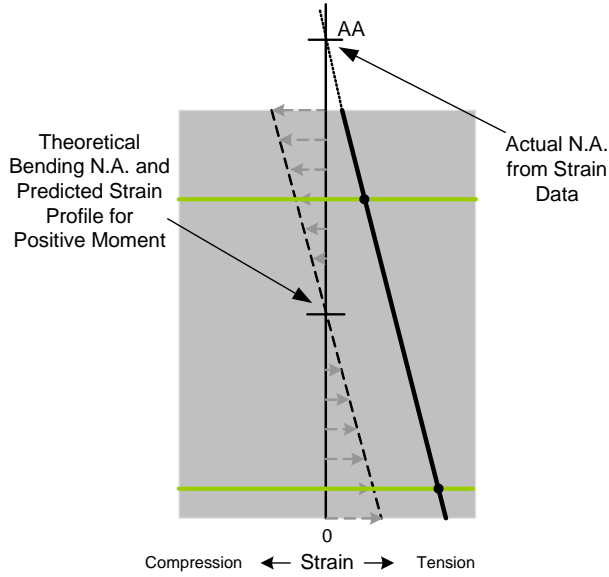
Figure 61: Illustration of Axial Tension Behavior at Gage Location D-1
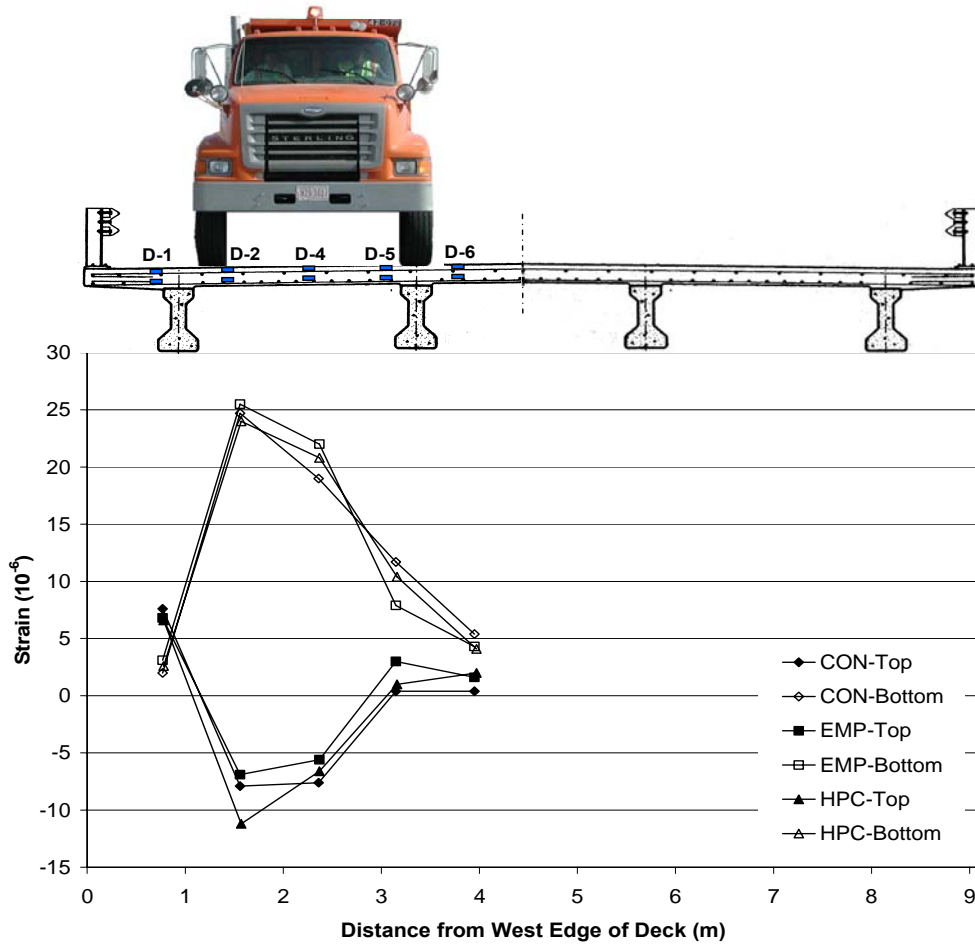
Figure 62: Transverse Strain Profile Revealing Axial Tension (ST-S Test at 40 m Truck Position)

Net tension is also evident at Gage Locations D-5 and D-6 in the transverse strain profile shown in Figure 62, further supporting the evidence of in-plane axial tension in the bridge decks. Although not as obvious from Figure 62, net axial tension is present in Gage Locations D-2 and D-4 as shown in Tables 22, 23, and 24. Similar results were found from all the bridge decks. That is, in-plane axial forces were present in all of the bridge decks, and that these axial forces were likely to have been responsible for shifting the neutral axis.

In summary, the shift in the position of the neutral axis from its theoretical position is most likely due to in-plane axial forces rather than deck cracking. Evidence presented using Gage Location D-4 (and supported by the other locations) consistently shows that cracking has not occurred in any depth of the deck. Convincing evidence was found to support this conclusion in the data of Gage Location D-1 and others. Undeniably, certain anomalies exist in the data, which limit the development of patterns or predictive models regarding these axial effects. Furthermore, while the effect is seen in all the decks, it is not the same in all the decks.

7.1.4 Deck Stiffness

Differences in the stiffnesses of the bridge decks could be responsible for some of the differences in the magnitudes of the strains experienced in each deck. In general, if two structural elements experience the same internal force demands, the relative magnitudes of the stress-related strains generated in them will be proportional to their relative stiffnesses, with the stiffer structure experiencing smaller strains. Structural stiffness generally can be quantified as the product of the material and geometric stiffnesses for the type of response being considered (e.g., bending). In the case of bending/flexural stiffness, these parameters specifically are the modulus of elasticity, E, and the moment of inertia, I. The theoretical stiffnesses of each bridge in the longitudinal and transverse directions were quantified in terms of EI assuming a common geometry and using the measured material properties. These stiffnesses are presented in Table 25 for a typical interior girder in the longitudinal direction (for composite deck and girder action) and for a unit width of the deck in the transverse direction.

Table 25: Bridge Deck Stiffness Parameters

Bridge	E-Girder (GPa)	E-Deck (GPa)	Longitudinal Direction		Transverse Direction	
			I (10^8 mm^4)	EI (10^7 N·m^2)	I (10^8 mm^4)	EI (10^7 N·m^2)
CON	37.6	30.2	413	155	8.145	2.546
EMP	37.0	24.8	394	146	7.979	1.983
HPC	37.9	30.8	415	158	8.135	2.504

Referring to Table 25, the Empirical deck has a longitudinal stiffness that is approximately 94 percent of the HPC and Conventional deck stiffnesses (which are similar). This reduction in

stiffness for the Empirical deck is primarily due to the lower value of the modulus of elasticity of the concrete in this deck, rather than the reduced amount of longitudinal reinforcement used in the deck. In the transverse direction, once again the HPC and Conventional decks have similar stiffnesses, and are both approximately 25 percent stiffer than the Empirical deck. The difference in transverse stiffnesses between the bridges is primarily the result of the differences in the modulus of elasticities of the three deck concretes (see Table 25). As mentioned previously, the reduced amount of reinforcing steel in the Empirical deck compared to the other decks had only a nominal influence on the moments of inertia of the uncracked cross-sections.

Before attempting to correlate any observed differences in the magnitudes of the strains in each deck with these differences in their calculated stiffnesses, it is important to establish the relative nature of the force flow through the decks when vehicle loads are applied. Notably, the bridge superstructures are indeterminate; that is, multiple load paths are available to transmit the vehicle loads into the bents and abutments depending on the stiffness characteristics of each bridge. Thus, differences in the magnitudes of the strains measured on the different decks could reflect differences in the load paths exercised in each bridge, as well as direct differences in their stiffnesses. Referring to Table 25, for example, the HPC deck is stiffer in the longitudinal direction than the Conventional deck. If all other parameters were constant between the bridges, more load would be attracted to the individual girders directly under the vehicle in the HPC deck, relative to the conventional deck.

The load flow situation, however, is more complicated than described above, as "all other parameters" are not constant between the bridges. Notably, the transverse stiffnesses of the three decks are not the same, which affects the manner in which they transfer vehicle loads transversely into the stringer system. The HPC deck, for example, is stiffer than the Conventional deck in the transverse direction, which would result in a more effective sharing of vehicle loads transversely across all the girders in this bridge, relative to the situation in the Conventional bridge. This increased load sharing in the HPC bridge, however, is counterbalanced by the previously mentioned load focusing associated with the increased longitudinal stiffness of this deck. As a result of these two effects, the load flow through the HPC deck is expected to be similar to that in the Conventional deck. The Empirical deck has both lower longitudinal and transverse stiffnesses relative to the Conventional deck. Once again, these two individual effects counterbalance each other, meaning that the load flow in this deck is similar to that in the Conventional deck. Thus, despite the differences in the stiffnesses of the three bridges in both the longitudinal and transverse directions, the load flow through the elements of the superstructure into the abutments and bents are expected to be similar in all three bridges.

This discussion of load flow as a function of the relative stiffnesses of each bridge in the longitudinal and transverse directions can be quantified using the AASHTO girder distribution factor concept. Bridge engineers and analysts characterize the manner in which structural

demands are shared across the girders in a bridge using a parameter called the Girder Distribution Factor (GDF). GDF is often expressed as a percentage, which indicates the proportion of total structural demand carried by each girder in the superstructure. Equations are available to calculate GDFs in terms of, among other things, the longitudinal and transverse stiffness of a bridge, and they can also be readily determined experimentally from strain or displacement measurements taken on the girders of bridge as it is loaded. Conceptually, the stiffness of a structure can be correlated with the GDFs in the following manner. Greater longitudinal stiffness results in an overall stiffer longitudinal response, and relatively softer behavior of the deck in the transverse direction. As a result, the load picked up by an individual girder increases (less sharing between girders occurs), resulting in a higher GDF. As the transverse stiffness of the deck increases relative to the longitudinal stiffness of the girder-deck system, more uniform load sharing occurs across the girders, resulting in lower magnitude and more uniform GDFs for each girder.

7.1.4.1 AASHTO LRFD Girder Distribution Factors

The AASHTO LRFD Bridge Design Specification provides an approximate method for determining the girder distribution factors for interior and exterior girders. These empirical equations were developed under NCHRP Project 12-26, whose objective was to determine how various bridge parameters affected GDFs (Zokaie, 1991). In light of the manner in which they were developed, the equations can only be applied to certain bridge geometries (which include the geometry of the Saco bridges). The GDF values determined by these equations are expected to be more than 5% greater than the actual values.

GDFs were calculated for the three bridges under investigation using LRFD Tables 4.6.2.2.2b-1 and 4.6.2.2.2d-1 in the Design Specifications. Girder distribution factors were calculated using the geometry and actual material properties for each bridge.

The only distinctly different material parameter between bridges is the modulus of elasticity for the concrete in the Empirical deck, which is only around 80% of that of the concrete in the other two decks (see Table 25). This difference ultimately had little effect on the distribution factors calculated for the bridges, which are presented in Table 26. This result can be attributed to the insensitivity of the GDF equations to girder and beam stiffnesses. The applicable distribution factor equations are primarily dependent on girder spacing.

Table 26: AAS0HTO LRFD Distribution Factors

Load Type	Bridge	Interior Girder	Exterior Girder
Single Truck	Conventional	49%	29%
	Empirical	49%	29%
	HPC	49%	29%
Double Truck	Conventional	65%	64%
	Empirical	66%	65%
	HPC	65%	64%

7.1.4.2   Measured Girder Distribution Factors

Actual GDFs were calculated using strain and/or displacement data from the live load tests. Live load tests conducted in 2003 used only strain data collected from the Intelliducer™ gages provided by Bridge Diagnostics Inc. (BDI). These gages were fixed to the bottom of the two western most girders (referred to as Girders #1 and #2, as shown in Figure 63). Bonded reinforcement gages located in the bridge deck were also used to validate the results from the BDI gages.
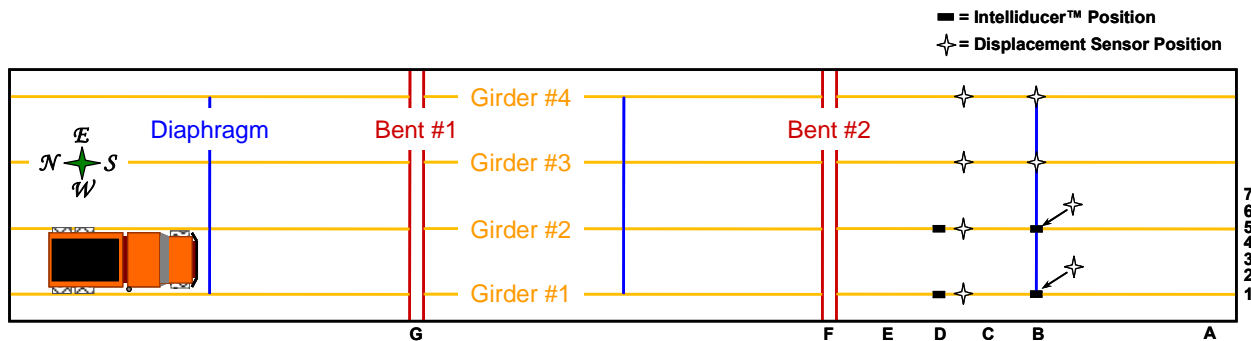
Figure 63: General Location of Intelliducer™ Gages and Displacement Sensors Used in the Live Load Tests

In this analysis of GDFs, the bridges were assumed to respond elastically with small global deflections. This assumption allows for the superposition of results from different tests. In addition, distributed lane loads as specified in the LRFD were ignored and assumed to have minimal impact on the distribution factors due to their inherent nature.

Multiple presence factors from the AASHTO LRFD were used in this analysis (LRFD Table 3.6.1.1.2-1). In cases where two lanes were loaded, a multiple presence factor of 1.0 was used. In single lane loading a multiple presence factor of 1.2 was used.

Results for girders #3 and #4 were determined by enforcing symmetry on the structure. For example; the response of girders #3 and #4 for truck path R should be the same as the response of girders one and two for truck path Z (refer to Figure 40). Similarly, girder responses can be found for longitudinal truck paths S and U, which correspond to truck paths Y and X, respectively. In this fashion, the strain in each girder was determined for a given loading condition. The fraction of that load carried by each girder was then simply calculated as the strain in the girder divided by the sum of the strains across all the girders, as illustrated in Table 27. The strain values used in this calculation were the absolute maximum values observed during the test, which typically occurred within a meter of each other and when the tandem axle was centered in the bridge span. Girder distribution factors were determined for several truck load paths (with some adjustments to the methodology for the two truck tests), and a worst case scenario emerged that consisted of placing two trucks on the bridge as close as possible to each other and as close to the railing as possible, as shown in Figure 64. The GDFs for this scenario are given in Table 28, along with AASHTO-calculated GDFs.

Table 27: Typical GDF Calculation, Single truck Test R (ST-R) on the Empirical Deck

Parameter	Girder 1[a]	Girder 2[a]	Girder 3[b]	Girder 4[b]	Sum
Girder Strains	76	46	21	8	151
Fraction of Total Strain	50%	30%	14%	5%	100%

a) directly measured in test R
b) inferred from test Z
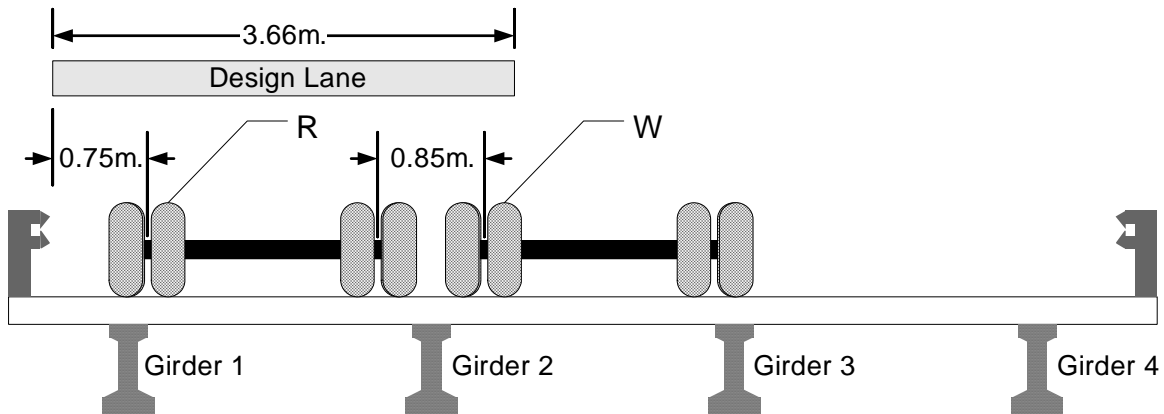
Figure 64: Worst Case – Two Design Lanes Using Truck Positions R and W

Table 28: Summary of Saco Bridge Girder Distribution Factors

Girder	Bridge	AASHTO GDF EQUATION	WORST CASE (R-W)
Interior Girder	Conventional	65%	61%
	Empirical	66%	59%
	HPC	65%	57%
Exterior Girder	Conventional	64%	65%
	Empirical	65%	59%
	HPC	64%	61%

Referring to Table 28,

1. the GDFs are similar for all three bridges, and
2. the GDFs determined from the 2003 test data are similar but generally lower in magnitude than the AASHTO GDFs.

The AASHTO factors were developed to conservatively produce design demands approximately 5 percent greater than the actual expected demands, and the difference in the measured and calculated GDFs for all three decks generally ranges from 5 to 10 percent. The maximum difference in the AASHTO and experimentally determined GDFs was approximately 10 percent for the case of an interior girder in the Conventional and Empirical decks, and an exterior girder in the Empirical deck. Further, the experimentally determined GDFs for the Conventional bridge are the closest in magnitude to the AASHTO calculated values. For the interior girder case, the smallest test-based GDF (most uniform load sharing) was for the HPC deck (57%) and the greatest GDF (least uniform sharing) was for the Conventional deck (61%). The smallest and largest test-based GDFs for the exterior girder were for the Empirical (59%) and Conventional decks (65%), respectively.

The apparent similarities in load flow through all three bridges revealed by this analysis means that any differences in the magnitudes of the strains in the bridges may be due to the differences in their absolute stiffnesses (albeit these differences are small in magnitude). Despite this possibility, and referring back to Figure 43, the strains measured in the longitudinal direction in all three decks are grouped fairly closely together, and no one deck consistently exhibits either the largest or the smallest strains across all gage locations. The situation is similar in the transverse direction (see Figure 51), with the response grouped fairly closely together for all decks, with no one deck overwhelmingly exhibiting either the largest or smallest strains across all gage locations. Recall that in the transverse direction the mean strains measured in the bottom of the decks were 2.0, 1.6, and 1.7 microstrain, respectively, for the Conventional, Empirical, and HPC decks. Taken at face value, these results are contrary to expectations based

on relative stiffness. That is, the softest deck (the Empirical deck) also has the lowest mean strain. Also recall, however, that statistically the mean strains in the three decks were not found to be significantly different (p-values of 0.7 and greater for all comparisons).

7.1.5 Superposition

The Principle of Superposition was used to determine whether the Saco bridge decks behave in a linear elastic manner. This principle, which has been used in scientific and engineering applications ranging from heat transfer to simple beam theory, essentially states that in a linear system, the effects caused by combined loadings may be predicted by the summation of individual effects due to each load in the combination. Therefore, validation of superposition should verify that the bridge decks are behaving linear elastically.

During live load testing, the three Saco bridges were tested using two heavily loaded three-axle dump trucks, traveling side-by-side along the length of the bridge, namely two-truck tests TT-WR and TT-XT (refer to Figure 40-b). Using superposition, strains measured during individual single-truck tests (ST-X and ST-T) were added together and the results compared to the strains measured during two-truck test (TT-XT) for the Conventional bridge deck at two truck positions, 40 m and 42 m. (Single truck test ST-W was not run, so superposition could not be directly evaluated for two truck test TT-WR.) Figures 65 and 66 compare the summed response from the separate single truck tests to the measured two-truck test response along Gage Line D for the Conventional deck at the 40 m and 42 m truck positions, respectively. With regard to shape and magnitude, the two transverse profiles look very similar overall, indicating superposition is valid. The greatest differences in strain magnitudes are observed at Gage Location D-2, but even these differences are nominal. It is unclear why differences at this location are larger than the other gage locations. Gage Location D-2 may be near the point of curvature reversal in the deck, and therefore be more sensitive to minor variations in the specific locations of the tires and/or the presence of an additional truck.
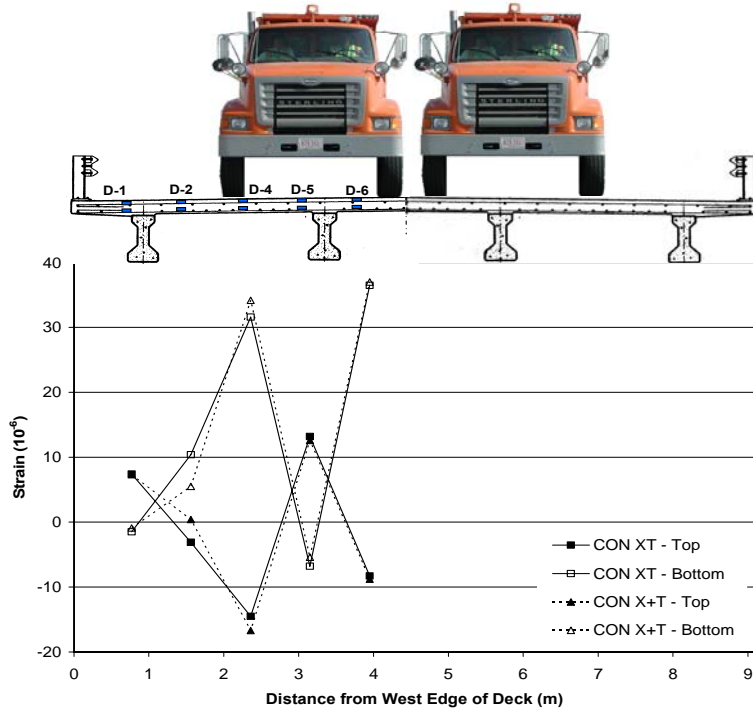
Figure 65: Transverse Strain Profile Showing Superposition in the Conventional Deck from Gage Line D at the 40 m Truck Position
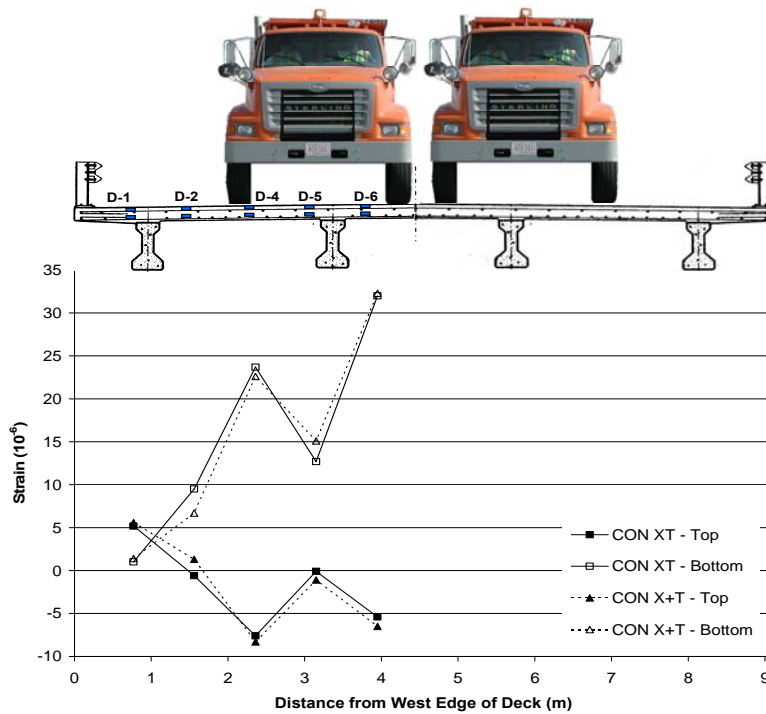
Figure 66: Transverse Strain Profile Showing Superposition in the Conventional Deck from Gage Line D at the 42 m Truck Position

7.1.6 High Speed Live Load Tests

Typical longitudinal strains measured at the same location for the same test vehicle traveling at low and high speeds on the same longitudinal path are presented in Figure 67 (results for the Conventional deck are shown). For this vehicle path and in this span, the maximum strain reported in the high speed event was only 90 percent of the maximum strain reported in the low speed event. Generally, the dynamic load allowance used for design is greater than one (1.33). This allowance is significantly influenced by surface and approach roughness. With new, smooth bridge decks and approaches, a value for this factor approaching unity seems reasonable. In this case, the further apparent reduction in strain in the high speed test relative to the low speed test speed may possibly be explained by vehicle positioning error. Vehicle position was more difficult to control in the high speed tests relative to the low speed tests. Thus, the longitudinal path of the vehicle may not have been identical in the two tests. Therefore, until further review of the data is completed, care should be exercised in attaching too much significance to the difference in strain response commented on above.
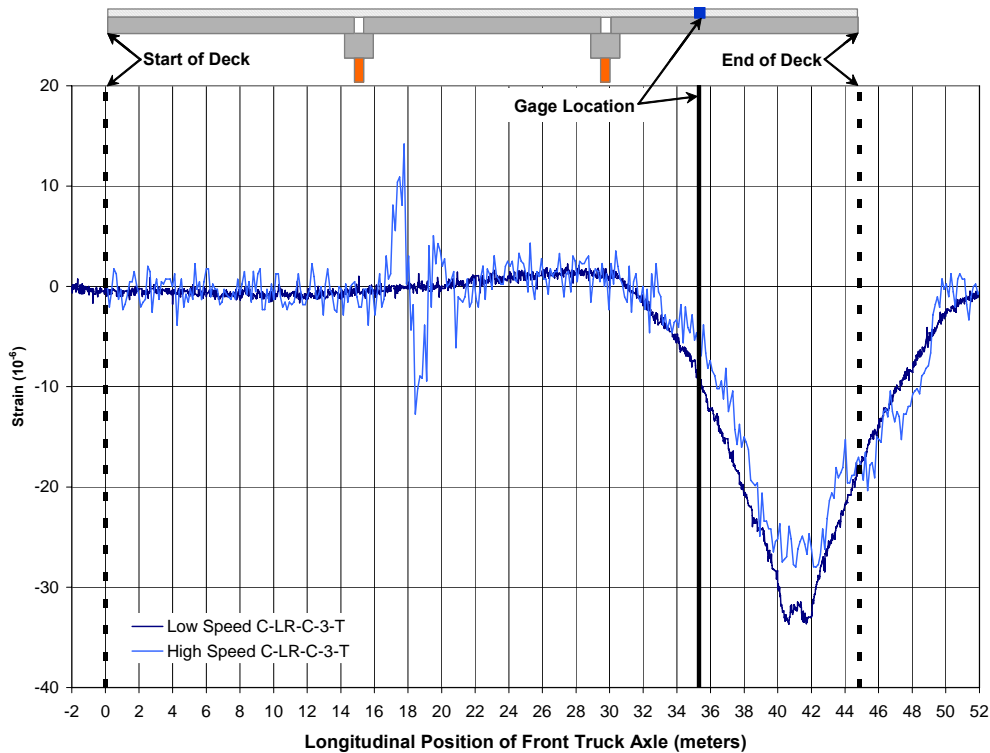
Figure 67: Comparison of the Longitudinal Strain Response in Low and High Speed Tests for the Conventional Deck

7.1.7 Review of Analysis Observations – 2003

Throughout the preceding analyses of the live load test data, several conclusions were reached, namely:

- All three decks exhibit similar global longitudinal behaviors, and these behaviors are in agreement with expected behaviors.

- No longitudinal cracking of the underside of the concrete decks is evident from strain data collected in the positive moment regions of any of the decks.

- The presence of in-plane axial forces is inferred from the strain data from each of the decks. Most of the reported axial strains are tensile and of relatively small magnitude (less than 10 microstrain). Finite element analysis also confirmed the presence of axial tension in an uncracked deck.

- No internal arching is evident in any of the decks because none of the decks is cracked and little evidence of in-plane compression exists.

- No longitudinal cracking of the topside of the concrete is evident from the strain data in the negative moment regions over the top of the girders of any of the decks, nor is such cracking imminent.

- Negative bending over the girders is not critical under live load demands.

- The GDFs determined from strain data are similar for all three bridges, and consistently less than the GDFs calculated by AASHTO equation.

- Linear superposition works well for all three bridge decks, indicating that all three decks are behaving linear-elastically.

- For the parameters analyzed in this research (i.e., mean strain levels, neutral axis position under load, mean in-plane axial strain), no consistent difference in behavior was observed between the three bridge decks.

7.2 Results of Second Live Load Tests – 2005

7.2.1 General Behaviors

The response of the bridge decks during the 2005 live load tests was very similar to that observed during the 2003 tests. This result is not necessarily surprising, as the decks are still relatively young (only two years old), and at least visually they experienced only minor distress between 2003 and 2005 (see Section 8.3 of this report). This distress, consisting of cracking adjacent to the bents at each end of each bridge, and cracking over the bents, was of limited extent and severity, and would not be expected to substantially affect load transfer mechanisms in the bridges. Thus, the theoretical bridge and deck behaviors that were predicted during the live load tests in 2003 are also generally appropriate for the 2005 tests, and rather than speaking in detail once again to these behaviors, the discussion below is focused on the comparison of responses between decks and over time. With the exception of the longitudinal strains over the bents, all strains measured in the 2005 live load tests were below the values expected to cause any permanent distress in the decks.

Note that the same vehicles were used in the 2003 and 2005 load tests, operating at slightly different (lighter) weights. In particular, as reported in Section 6.1, the vehicle used in the single truck (ST) tests was 2 percent lighter in the 2005 tests compared to the 2003 tests, which was expected to have a proportionally small/negligible impact on the comparison of the live load response between years. The second vehicle, used in the two truck tests, was 8 percent lighter in the 2005 tests compared to the 2003 tests. The primary purpose of the two truck tests was to investigate load flow through the decks (using GDFs) and the linearity of their response (using superposition). Relative to these parameters, an analysis is first done independently for each set of tests (2003 and 2005), the results of which are largely dependent only on the order of magnitude of the weights of the vehicles being used, rather than their specific values. Thus, once again, the difference in weight of the second truck between 2003 and 2005 was not expected to effect response comparisons between the two test years.

The general conclusion in qualitatively reviewing the data from the 2005 live load tests is that the three decks are behaving very similar to each other, as was observed in 2003. Additionally, the behavior of the three decks changed little over time, as the data collected in the 2005 tests closely matches that collected in the 2003 tests. Once again, in an effort to reveal possible subtle differences in response between bridges, and over time, additional quantitative review of the data was performed (i.e., calculation and comparison of mean response levels, neutral axis positions, in-plane axial stresses, and general load flow and linearity of response).

7.2.1.1   Longitudinal Response

Typical strains measured in the longitudinal direction at the same location between the girders in the interior of all three decks during the 2005 live load tests are presented in Figure 68 (gage location D-3, ST-T test). As previously discussed, some of the instrumentation failed between the 2003 and 2005 live load tests. In this case, for example, while top and bottom deck measurements were available at this location for all three bridges in 2003, only bottom strains were available for all three decks in 2005. Referring to the bottom strains in Figure 68, the response is similar in character and magnitude in all three decks, as was seen at all of the interior longitudinal gage locations remote from the bents and abutments (i.e., locations B-3, C-3, and D-3). In this instance, the response of the Empirical deck, with peak compressive and tensile strains of approximately -16 and 18 microstrain, respectively, may be marginally greater in magnitude than that of the Conventional deck, which is in turn nominally greater than that of the HPC deck. This specific ordering of the response, however, was not consistent across all interior gage locations.
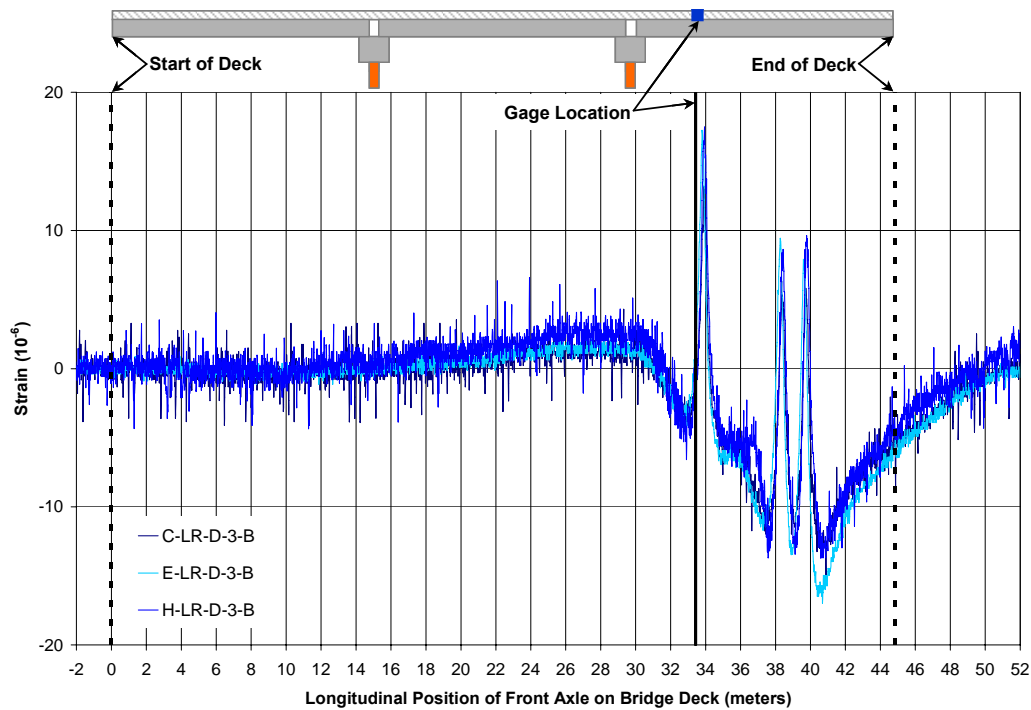
Figure 68: Strain History – 2005, All Three Decks Longitudinal Gage Location D-3 (ST-T)

Statistical comparison of the mean longitudinal strains in the bottom of the decks also indicated no clear, strong trend in the relative magnitudes of the strains based on deck configuration. The mean strains in the Conventional and Empirical decks were the most similar (p-value of 0.84); followed by the mean strains for the Empirical and HPC decks (p-value of 0.69).

A comparison of the longitudinal strains measured in 2003 and 2005 at this same location (D-3, ST-T test) is presented in Figure 69. Referring to Figure 69, the response is very similar between 2003 and 2005 for each bridge. Statistically, comparing the mean longitudinal strains of all the bottom gages in the interior of the decks following the procedures outlined in Appendix F, the response of the HPC and Empirical decks was particularly similar between 2003 and 2005 (p-values of 0.95 and 0.94, respectively). The similarity in the mean response of the Conventional deck between test years was less pronounced (p-value of 0.64).
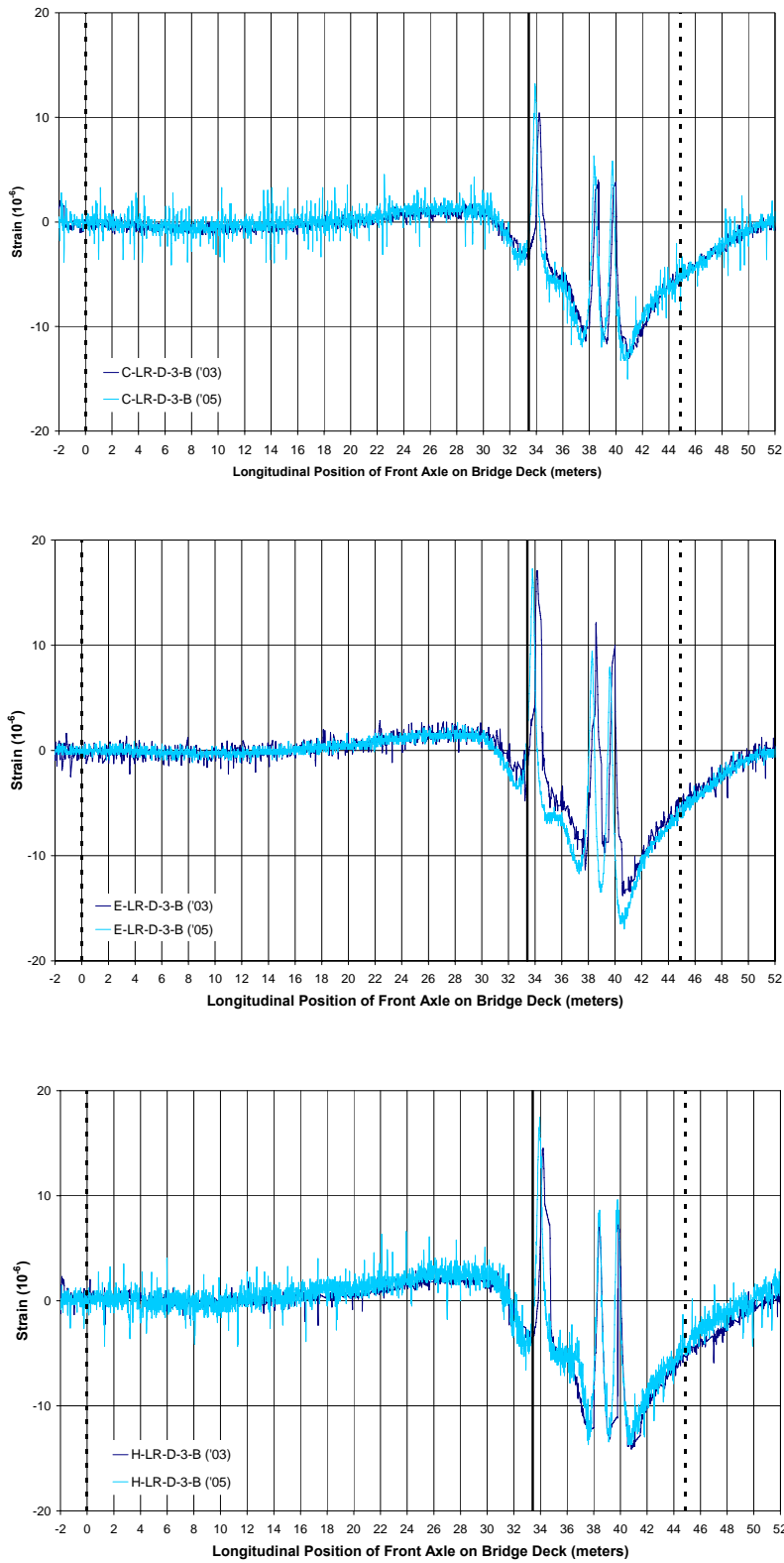
Figure 69: Strain History – 2003 vs. 2005, All Three Decks, Longitudinal Gage Location D-3 (ST-T)

Notable differences were seen in the strain response between bridges and between years at locations where the bridges experienced visible distress, that is, in the cracked zones near the abutments, and over the bents (corresponding to gage lines A and F). Typical longitudinal strains measured in the bottom of the decks in the 2005 live load tests near the abutment end of the span (location A-3, ST-T test) are presented in Figure 70. Unlike the strains reported in Figure 69 for the interior of the span (location D-3), the strains measured in the three decks at this location varied significantly in magnitude. The greatest strains were observed in the Conventional deck, with peak values of approximately -28 and 32 microstrain in compression and tension, respectively. Conversely, the peak compressive strains in the Empirical and Conventional decks were approximately 11 and 7 microstrain, respectively. This ordering of the strain magnitudes is consistent with the degree of local distress visually observed in each deck in 2005. That is, the Conventional deck had a pronounced diagonal crack in the top surface at gage location A-3 (see Figure 104a). The Empirical deck experienced less severe but more numerous cracks then the Conventional deck at gage location A-3 (see Figure 104b). Finally, the HPC deck was uncracked in and around location A-3 (see Figure 104c).
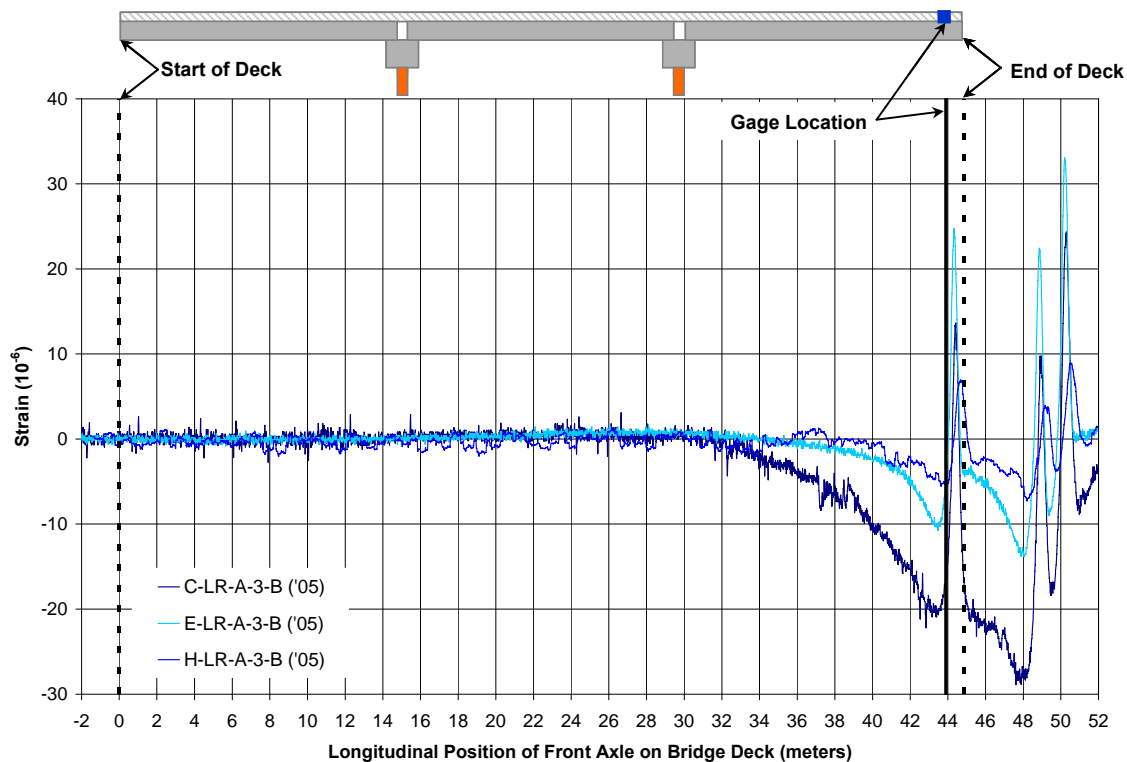
Figure 70: Strain History – 2005, All Three Decks Longitudinal Gage Location A-3 (ST-T)

The correlation of the magnitudes of the longitudinal strains at location A-3 with the occurrence of visible distress in the decks is generally supported by the change in the strain response at this location in each deck between the live load tests in 2003 and 2005. The longitudinal strains measured in the bottom of the decks at location A-3 in 2003 are compared

with the 2005 values Figure 71. In the case of the Conventional deck, the compressive strains increased in magnitude by over a factor of two between 2003 and 2005, coincident with the appearance of the crack at the gage location. The peak tensile strains, on-the-other-hand, were similar in magnitude in both years. The exact mechanism by which this crack may be effecting the compressive behavior at this location is unclear, but it appears to be more than a coincidence that this behavior change occurred at the crack location. In the case of the Empirical deck, the peak tensile strains increased in magnitude by a factor of 1.5 between 2003 and 2005, while the peak compression strains were almost identical both years. Finally, the compressive strains measured in the live load tests in 2003 and 2005 in the HPC deck, which exhibited no cracking in the gage area, were very similar (note that no data was available from the top gage at this location in the HPC deck).

Typical longitudinal strains measured over the bent at Gage Line F during the 2005 live load tests are reported in Figure 72 (Location F-3, ST-T test). The strains measured at this location in 2005 varied significantly in magnitude between the Empirical and HPC bridges, as was observed in 2003 (note that no data was available from the bottom gage at this location in the Conventional deck). Referring to Figure 72, tensile strains were observed once again in the bottom of the Empirical deck, consistent with the presence of a negative bending moment over the bent in this bridge being carried through the mechanism of a tensile resultant in the deck and a compression resultant at the girder support (see Figure 48). In the HPC deck, the negative moment response over the bent under the live load appeared once again to be superimposed on a compression across the depth of deck, which was attributed to arching action from the camber in the girders on this bridge.
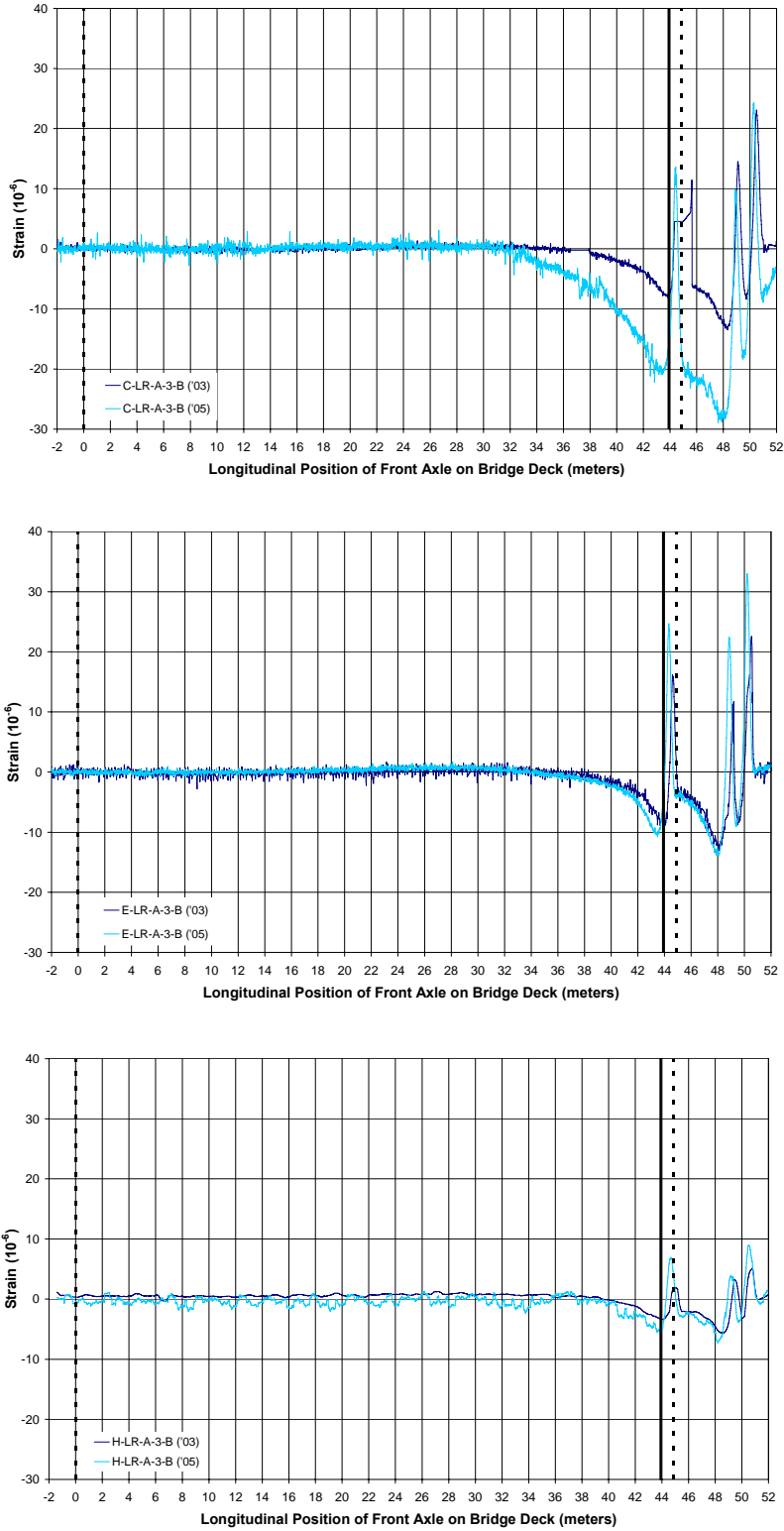
Figure 71: Strain History – 2003 vs. 2005, All Three Decks Longitudinal Gage Location A-3 (ST-T)
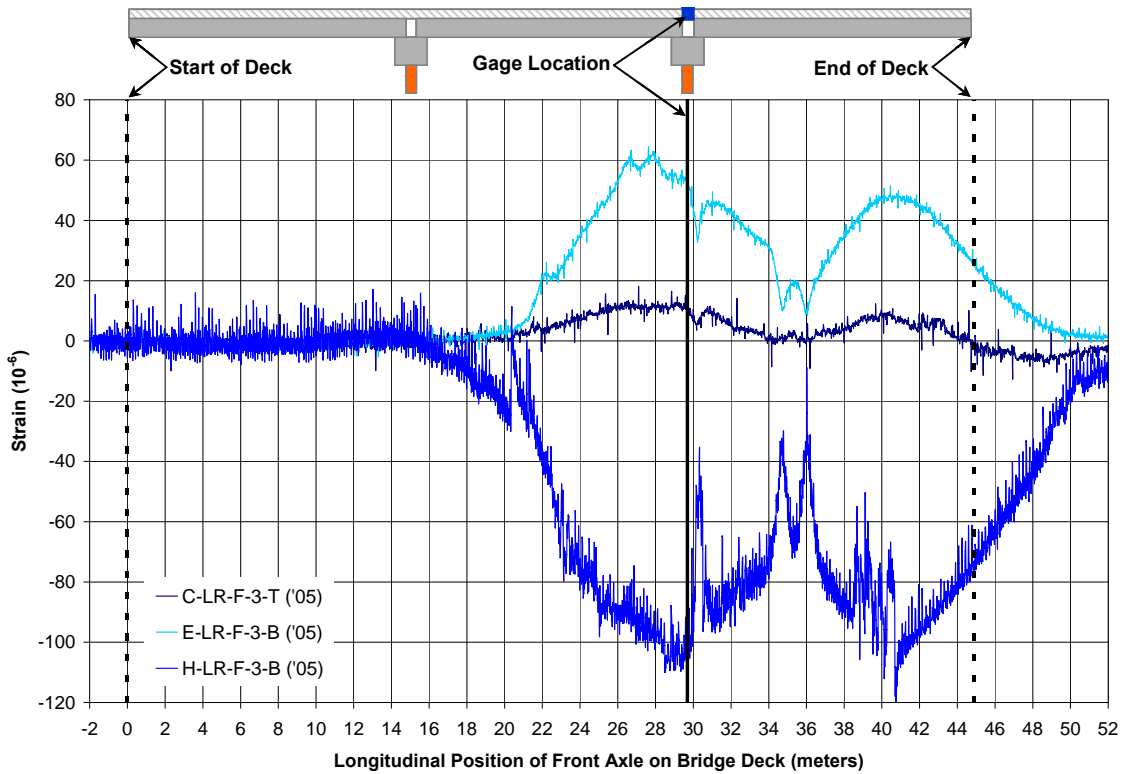
Figure 72: Strain History – 2005, All Three Decks Longitudinal Gage Location F-3 (ST-T)

As in 2003, the absolute greatest strains observed during the live load tests were seen over the bents at Gage Line F, where peak measured strains in all three decks were between 100 and 150 microstrain.

The local behavior of the Conventional and Empirical decks over the bent appears to have changed through time, while it has been relatively stable in the HPC deck. A typical comparison of the longitudinal strains observed at this location in the 2003 and 2005 live load tests is presented in Figure 73. The difference in the longitudinal strains in the Conventional and Empirical decks between 2003 and 2005 is dramatic, while the strains in the HPC deck were relatively unchanged between the 2 years (note: due to gage loss in the Conventional deck, top gages were used in this comparison, while bottom gages were used for the Empirical and HPC decks). While admittedly the useable data for this comparison is limited due to gage losses between 2003 and 2005, the data that is available indicates that conditions at this crack may have stabilized relatively early in the HPC deck (hence the similarity in strains in 2003 and 2005), while they changed between the 2003 and 2005 tests in the Conventional and Empirical decks.
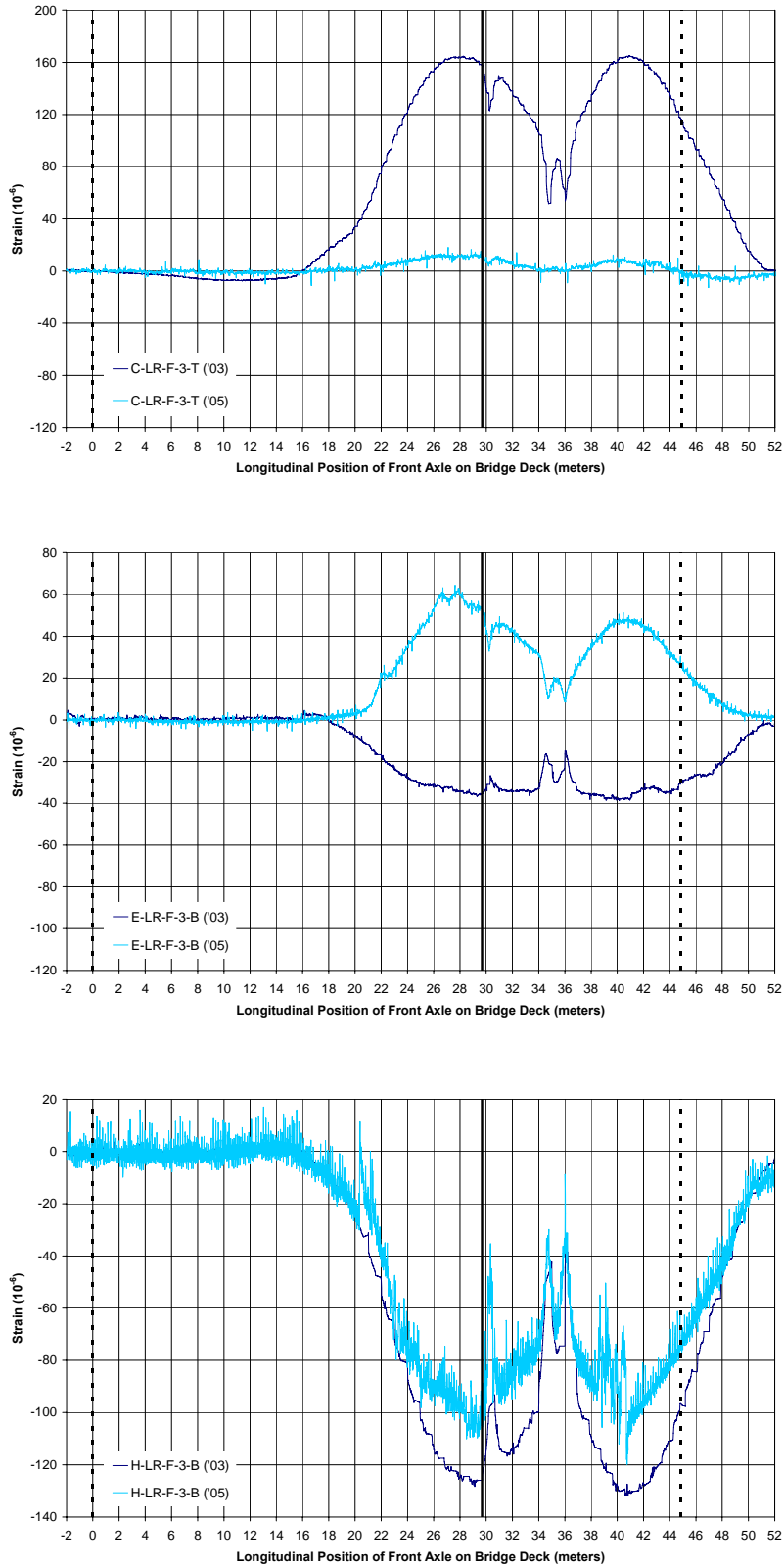
Figure 73: Strain History – 2003 vs. 2005, All Three Decks Longitudinal Gage Location F-3 (ST-T)

7.2.2 Transverse Response

Typical transverse strains measured at the same location between the girders in the interior of all three decks during the 2005 live load tests are presented in Figure 74 (specifically for gage location D-4, ST-T test). Once again, due to gage failures between the 2003 and 2005 live load tests, information could only be presented in this figure for the bottom gages in the decks. Referring to Figure 74, the response of all three decks is very similar in both waveform and magnitude, as was seen for all transverse gages located between girders (e.g., locations D-2, D-4, D-6). For the specific location presented in Figure 74, the maximum response of approximately 50 microstrain (tension) was seen in the Empirical deck, followed closely by the response in the HPC and Conventional decks. The ordering of this response, however, was not consistent at all locations and across all truck runs. Viewed at the face of the stringers (as opposed to between stringers), the transverse strain response did diverge more between bridges, as can be seen in Figure 75 (Gage Location D-5, ST-T test). In this case, the magnitude of the peak tensile and compressive responses ranged from approximately 12 to 18 and -10 to -12 microstrain, respectively, across all three decks.
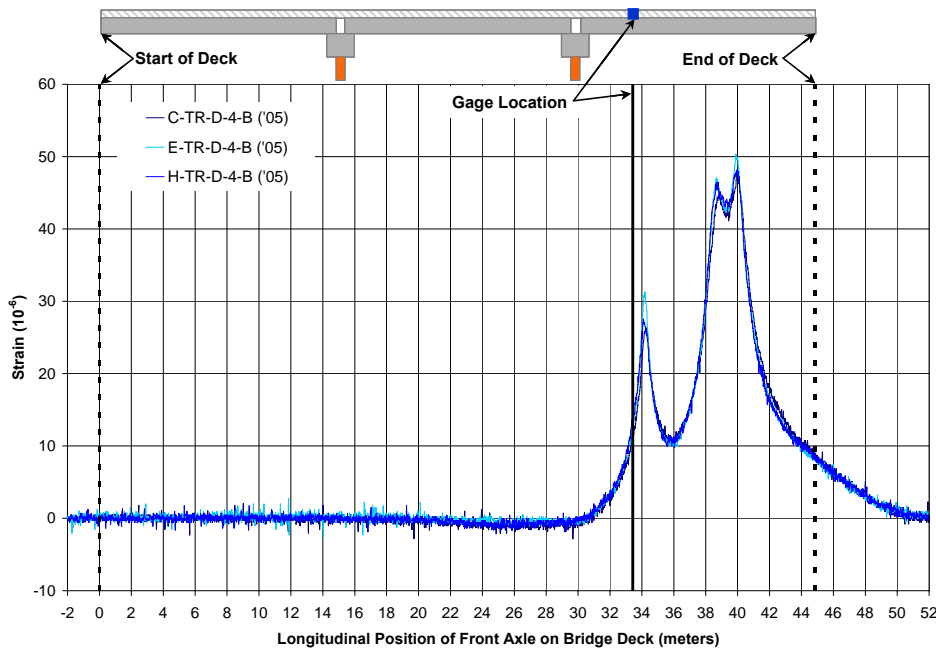
Figure 74: Strain History – 2005 – All Three Decks Transverse Gage Location D-4 (ST-U)
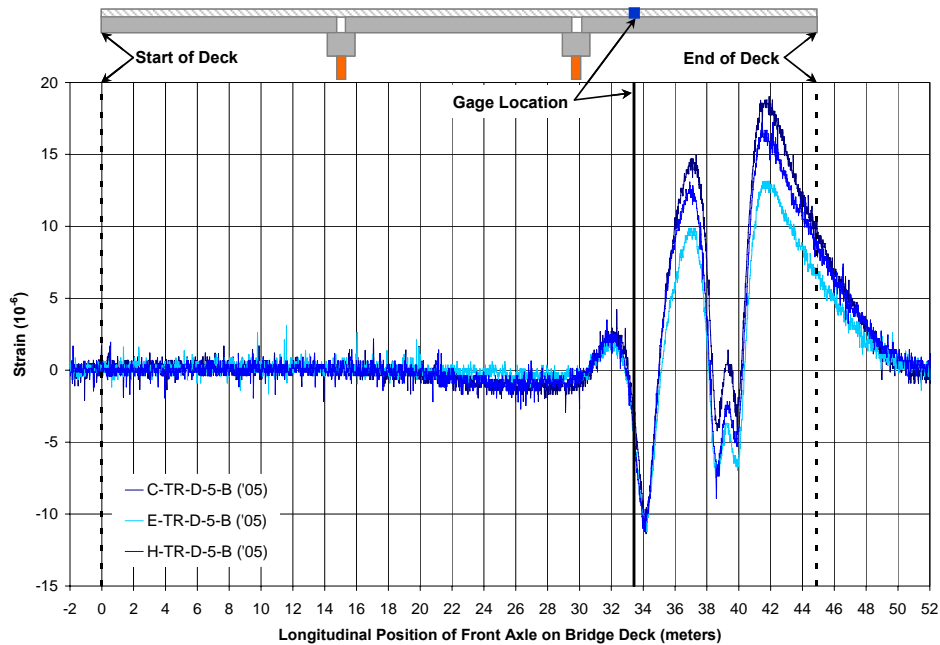
Figure 75: Strain History – 2005 – All Three Decks Transverse Gage Location D-5 (ST-U)

Statistical comparison of the mean transverse strains measured in the bottom of the decks once again is useful in more closely evaluating the relative magnitude of the transverse strain in all three decks and in formulating conclusions on whether they are performing the same. These mean transverse strains in 2005 were 1.6, 1.5, and 2.6 microstrain, respectively, in the Conventional, Empirical, and HPC decks. As was the case for the longitudinal response, the greatest similarity in mean transverse response in the bottom of the decks was observed between the Conventional and Empirical decks (p-value of 0.94); the greatest difference, between the HPC and Empirical decks (p-value of 0.67).

The transverse response during the 2003 and 2005 live load tests are compared in Figure 76 at a location between girders in each bridge (Gage Location D-4, ST-T test). The response in 2005 for all the decks is very similar to that observed in 2003. While for the specific data presented in Figure 76 the response in 2005 appears to be consistently greater in magnitude than that in 2003, this situation was not universally observed at all gage locations and across all test runs. At this same location, for example, the strains recorded in 2003 and 2005 in test run ST-S are compared in Figure 77. In this case, the response in the HPC and Empirical decks is almost identical between years, while in the Conventional deck the strains in 2005 are once again nominally greater than the strains in 2003.
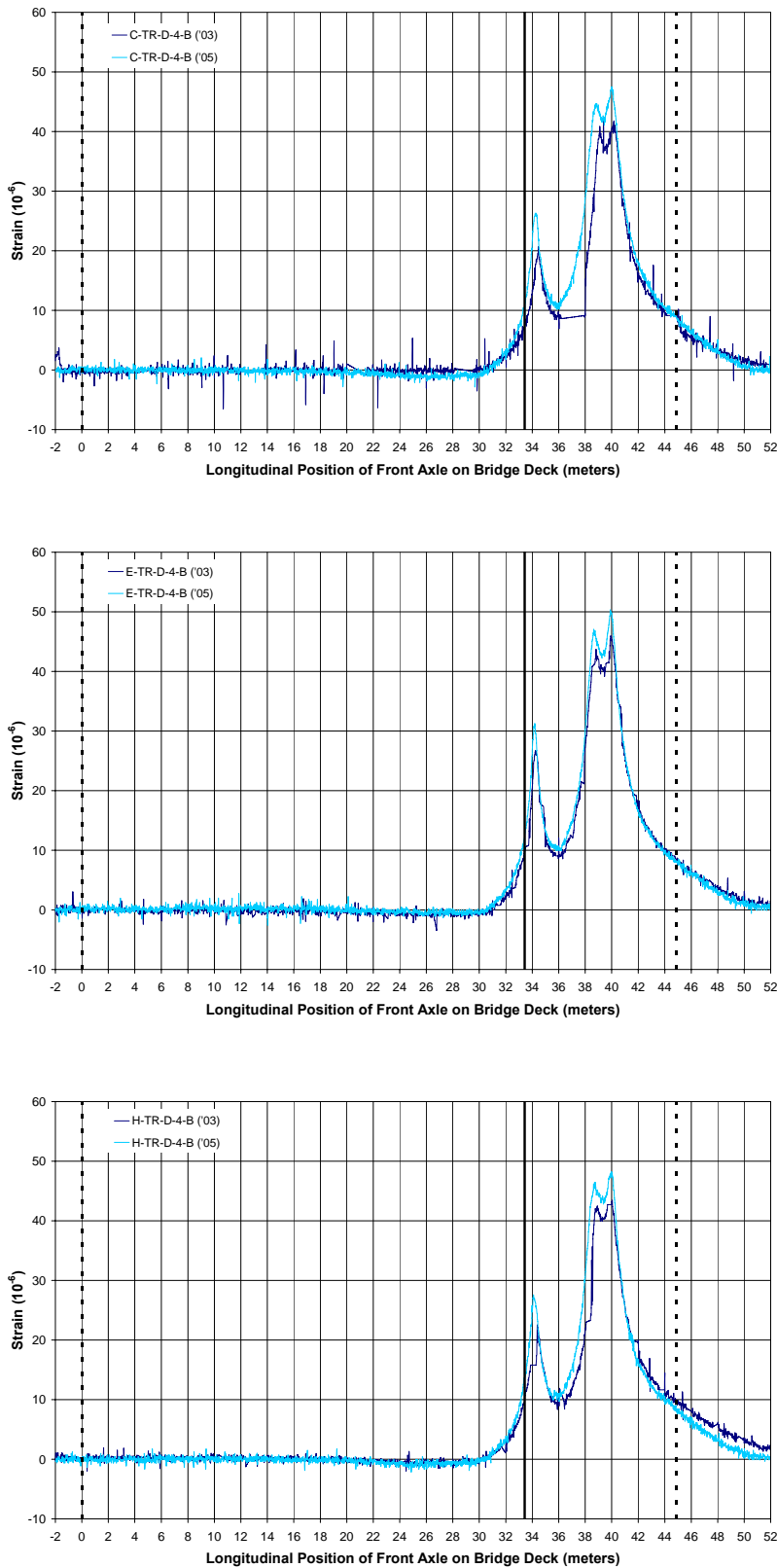
Figure 76: Strain History – 2003 vs. 2005, All Three Decks Transverse Gage Location D-4 (ST-U)
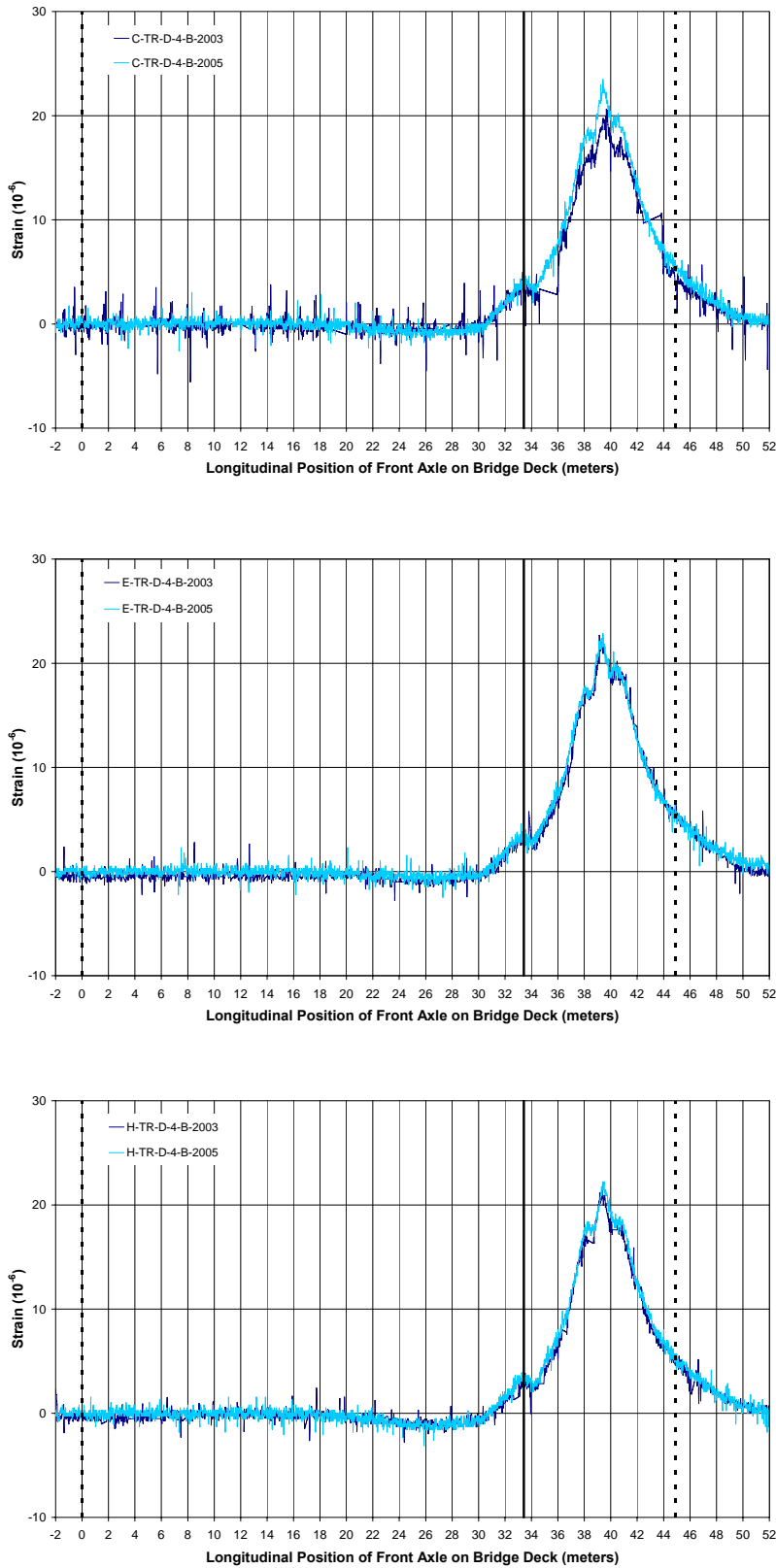
Figure 77: Strain History – 2003 vs. 2005, All Three Decks Transverse Gage Location D-4 (ST-S)

Statistical comparisons of the mean strain response were performed for each bridge in an effort to more rigorously conclude if the response over time was as similar as indicated by qualitative comparison of the strain traces. Based on the mean transverse strains in the bottom of the decks, the greatest similarity in response between 2003 and 2005 was seen for the Empirical deck (p-value of 0.93); the greatest difference in response, for the HPC deck (p-value of 0.70), with the Conventional deck in between (p-value of 0.74). Thus, it may be concluded that, overall, the mean strains generally have not changed from year to year, regardless of bridge deck type, where changes were less in the Empirical deck and more in the Conventional and HPC decks.

7.2.3 Position of the Neutral Axis

As was done with the results of the 2003 live load tests, the transverse strain data collected during the 2005 live load tests was used to estimate the location of the neutral axis in the decks during the tests. Also as before, the intention of this analysis was to possibly reveal subtle differences in deck performance not obvious in a qualitative comparison of the deck response. Further, if any such subtle differences in neutral axis position were detected, causes for these differences (e.g., deterioration) were to be investigated. Estimation of the neutral axis depth requires data from two depths (e.g., top and bottom) within the deck at a given location. In light of the failure of many of the top gages in the HPC deck prior to the 2005 live load tests, insufficient data on the HPC deck was available for this analysis. Thus, the discussion below is confined to the behavior of the Conventional and Empirical decks.

The results of the neutral axis position analysis on the 2005 live load test data is summarized in Tables 29, 30, and 31. As was observed in the 2003 data:

1. For positive moment response, the neutral axis position as determined from the test data tended to be higher in the deck cross-section than the theoretical location of the pure bending neutral axis for the uncracked case, which was approximately 104 mm.
2. For negative moment response, the neutral axis position determined from the test data tended to be lower in the deck cross-section then the theoretical location of the pure bending neutral axis for the uncracked case. Further, the neutral axis positions calculated for negative moment response were considerably more variable in magnitude than those calculated for positive moment response.

Table 29: Actual Neutral Axis Positions for the Conventional Bridge Deck – 2005

Truck Position	Strain Gage Location	Single-Truck Tests * (mm)									Two-Truck Tests * (mm)	
		ST-R	ST-S	ST-T	ST-U	ST-V	ST-W	ST-X	ST-Y	ST-Z	TT-XT	TT-WR
40 m	D-1	---	129.9	---	---	---	---	34.5	---	---	---	---
	D-2	---	---	---	---	---	---	---	---	---	---	---
	D-4	---	105.5	108.6	106.2	122.6	---	92.3	103.3	109.6	108.1	122.2
	D-5	244.2	124.1	66.3	37.8	113.4	147.6	95.2	101.8	102.3	81.3	173.2
	D-6	---	95.7	118.9	120.4	116.9	116.7	130.7	127.5	115.7	117.6	115.5
42 m	D-1	---	68.2	---	---	---	---	8.0	---	---	---	---
	D-2	---	---	---	---	---	---	---	---	---	---	---
	D-4	---	110.5	112.7	108.1	139.2	---	80.1	90.2	103.5	119.1	128.1
	D-5	149.3	110.7	105.0	109.0	109.6	111.7	74.7	92.9	96.5	119.2	117.0
	D-6	---	100.8	117.8	116.6	119.2	122.0	137.6	119.8	112.7	123.8	118.4

* shading indicates negative moment
--- no data

Table 30: Actual Neutral Axis Positions for the Empirical Bridge Deck – 2005

Truck Position	Strain Gage Location	Single-Truck Tests * (mm)									Two-Truck Tests * (mm)	
		ST-R	ST-S	ST-T	ST-U	ST-V	ST-W	ST-X	ST-Y	ST-Z	TT-XT	TT-WR
40 m	D-1	-420.1	-284.7	45.5	52.7	-13.0	---	65.7	150.0	161.9	43.2	-237.7
	D-2	---	125.3	67.8	55.2	---	---	---	---	128.3	35.9	113.2
	D-4	126.0	116.9	138.2	140.8	-372.2	---	106.7	141.2	129.2	143.2	138.4
	D-5	188.5	227.2	86.9	78.3	147.8	-34.3	93.1	103.1	101.0	96.5	-215.6
	D-6	---	†	127.9	123.3	---	---	---	137.1	123.2	124.8	125.0
42 m	D-1	651.8	316.2	-335.3	-32.0	-188.0	---	57.6	203.8	99.3	-103.0	441.0
	D-2	---	127.3	97.2	99.1	---	---	---	---	109.3	108.4	132.8
	D-4	127.8	137.8	145.4	144.5	502.6	---	98.1	130.9	126.8	154.0	161.4
	D-5	113.0	152.1	135.3	127.9	122.1	146.7	67.0	93.5	89.7	148.5	138.4
	D-6	---	239.3	132.6	128.2	---	---	---	133.2	126.3	141.8	139.0

† values are very large due to small strains
* shading indicates negative moment
--- no data

Table 31: Actual Neutral Axis Positions for the HPC Bridge Deck – 2005

Truck Position	Strain Gage Location	Single-Truck Tests * (mm)									Two-Truck Tests * (mm)	
		ST-R	ST-S	ST-T	ST-U	ST-V	ST-W	ST-X	ST-Y	ST-Z	TT-XT	TT-WR
40 m	D-1	---	---	---	---	---	---	---	---	---	46.8	---
	D-2	---	---	---	---	---	---	---	---	---	---	---
	D-4	---	---	---	---	---	---	---	---	---	---	---
	D-5	---	---	---	---	---	---	---	---	---	---	---
	D-6	118.2	---	---	---	---	---	---	---	---	---	---
42 m	D-1	---	---	---	---	---	---	---	---	---	-267.2	---
	D-2	---	---	---	---	---	---	---	---	---	---	---
	D-4	---	---	---	---	---	---	---	---	---	---	---
	D-5	---	---	---	---	---	---	---	---	---	---	---
	D-6	193.5	---	---	---	---	---	---	---	---	---	---

* shading indicates negative moment
--- no data

Considering the location of the neutral axis in positive moment (which appears to be less erratic than the results for negative moment), the mean neutral axis position in the Conventional and Empirical decks was calculated from the 2005 test data to be 121 mm and 163 mm, respectively. The apparent disparity in these mean values for 2005 is statistically shown to be different (p-value of 0.02). Some differences were observed in the mean position of the neutral axis between the 2003 and 2005 live load tests. Notably, in the Empirical deck the mean neutral axis position shifted up from 158 mm in 2003 to 163 mm in 2005, and the similarities in these mean values is statistically verified (p-value 0.82). This slight shift is consistent with the occurrence of some cracking in the bottom of the deck, and certainly the Empirical deck experienced an increase in cracking distress between 2003 and 2005 (see Section 8.3). In the case of the Conventional deck, the mean neutral axis position actually moved down in the deck from 139 mm in 2003 to 121 mm in 2005, even though cracking was also observed in this deck between 2003 and 2005, although the cracking was not as extensive as in the Empirical deck. In the case of the Conventional deck, this shift in the neutral axis position once again has some significance (p-value of 0.24). Thus, the correlation between the shift in the neutral axis position and the occurrence of distress in the deck appears strong in the case of the Empirical deck while it is counter to expectations in the case of the Conventional deck. The level of distress seen in both decks thus far is relatively light, specifically at the gage locations (where only hairline longitudinal cracks at most have occurred to-date). Therefore, as further physical damage occurs in the decks in the future, the change in the neutral axis position may yet emerge as a possible active instrumentation indicator of the occurrence of such damage.

The mean neutral axis positions calculated in both the Empirical and HPC decks in 2005 exceeded the theoretical pure bending neutral axis position of 104 mm, which, as previously

discussed, could result from either cracking in the bottom of the deck and/or the presence of in-plane axial tension forces in the decks. As only hairline longitudinal cracking has been observed immediately at the gage locations in the decks, the shift in neutral axis position from the theoretical bending position seen in 2005 was believed to still primarily result from the presence of in-plane axial forces in the decks, as was surmised in 2003. If the effects of the hairline cracks are ignored, the in-plane axial stresses inferred to be present in the decks from the difference between the actual and theoretical bending positions of the neutral axis are summarized in Tables 32, 33, and 34. In general, the in-plane axial stresses are tensile in nature when the test vehicle is on the same side of the bridge as the instrumented span (i.e., in test runs R, S, T, U, and V), while they are more frequently compressive in nature when the vehicle is on the opposite side of the bridge (i.e., in test runs Y and Z). The tensile strains are believed to be related to secondary membrane stresses that develop in the decks as they deflect down between the girders under the transverse vehicle loads. Considering positive moment cases, the maximum mean in-plane axial strains in the Conventional and Empirical decks in the 2005 tests were 2.9 and 4.1 microstrain (in tension), respectively. In this case, these mean values were statistically found to be different (p-value of 0.10). The significance of this observation is still under investigation.

Table 32: Back-Calculated Axial Strains for the Conventional Deck – 2005

Truck Position	Strain Gage Location	Single-Truck Tests * (µε)									Two-Truck Tests * (µε)	
		ST-R	ST-S	ST-T	ST-U	ST-V	ST-W	ST-X	ST-Y	ST-Z	TT-XT	TT-WR
40 m	D-1	---	-0.2	---	---	---	---	1.4	---	---	---	---
	D-2	---	---	---	---	---	---	---	---	---	---	---
	D-4	---	0.4	2.7	1.2	1.2	---	1.4	0.1	-0.4	1.8	4.3
	D-5	6.1	2.3	2.9	4.0	1.5	1.8	1.0	0.2	0.2	4.4	5.3
	D-6	---	-0.6	5.4	5.4	4.5	5.6	1.3	-2.3	-1.5	5.4	5.1
42 m	D-1	---	-0.7	---	---	---	---	1.5	---	---	---	---
	D-2	---	---	---	---	---	---	---	---	---	---	---
	D-4	---	1.4	2.8	1.3	2.6	---	1.8	1.0	0.1	3.9	5.4
	D-5	4.6	1.1	0.2	1.1	1.1	1.1	0.8	0.8	0.6	2.7	3.2
	D-6	---	-0.3	3.8	3.5	4.4	5.2	2.3	-1.3	-1.0	6.0	4.0

* shading indicates negative moment; positive values = axial tension; negative values = axial compression
--- no data

Table 33: Back-Calculated Axial Strains for the Empirical Deck – 2005

Truck Position	Strain Gage Location	Single-Truck Tests * (µε)									Two-Truck Tests * (µε)	
		ST-R	ST-S	ST-T	ST-U	ST-V	ST-W	ST-X	ST-Y	ST-Z	TT-XT	TT-WR
40 m	D-1	4.7	5.6	3.3	2.6	1.3	---	0.9	-0.7	-0.3	3.0	6.2
	D-2	---	5.5	-6.5	-7.7	---	---	---	---	-0.6	-7.0	1.4
	D-4	5.7	3.3	14.6	14.9	3.9	---	-0.2	-1.6	-1.2	12.4	7.4
	D-5	2.1	3.7	2.6	2.8	3.0	2.9	1.1	0.1	0.1	1.7	5.8
	D-6	---	3.6	7.7	5.8	---	---	---	-2.5	-1.9	6.7	8.0
42 m	D-1	2.5	3.1	2.4	2.1	0.5	---	1.1	-1.0	0.0	2.4	4.0
	D-2	---	3.0	-0.8	-0.5	---	---	---	---	-0.2	0.2	2.4
	D-4	3.6	5.3	8.7	7.7	4.3	---	0.4	-1.1	-1.1	7.6	8.0
	D-5	0.6	2.8	3.4	3.0	1.9	2.7	1.3	0.4	0.5	4.4	4.0
	D-6	---	3.7	5.7	4.7	---	---	---	-2.0	-1.8	6.7	6.2

* shading indicates negative moment; positive values = axial tension; negative values = axial compression
--- no data

Table 34: Back-Calculated Axial Strains for the HPC Deck – 2005

Truck Position	Strain Gage Location	Single-Truck Tests * (µε)									Two-Truck Tests * (µε)	
		ST-R	ST-S	ST-T	ST-U	ST-V	ST-W	ST-X	ST-Y	ST-Z	TT-XT	TT-WR
40 m	D-1	---	---	---	---	---	---	---	---	---	4.7	---
	D-2	---	---	---	---	---	---	---	---	---	---	---
	D-4	---	---	---	---	---	---	---	---	---	---	---
	D-5	---	---	---	---	---	---	---	---	---	---	---
	D-6	2.0	---	---	---	---	---	---	---	---	---	---
42 m	D-1	---	---	---	---	---	---	---	---	---	4.6	---
	D-2	---	---	---	---	---	---	---	---	---	---	---
	D-4	---	---	---	---	---	---	---	---	---	---	---
	D-5	---	---	---	---	---	---	---	---	---	---	---
	D-6	3.4	---	---	---	---	---	---	---	---	---	---

* shading indicates negative moment; positive values = axial tension; negative values = axial compression
--- no data

Comparing the in-plane axial tensile strains in each deck between the 2003 and 2005 live load tests (positive moment case), in the case of the Conventional deck, the mean axial in-plane tensile strain decreased from 2.99 to 2.89 microstrain; in the case of the Empirical deck, the mean strain decreased from 4.42 to 4.13 microstrain. In both cases, however, it could not be concluded that these changes in the mean response were overly significant (p-values of 0.82 and 0.68 for the Conventional and Empirical decks, respectively). Once again, however, the possible similarity of the response between 2003 and 2005 was greater for the Conventional deck than the

Empirical deck, which was consistent with the relative change in general physical distress in the decks between 2003 and 2005.

7.2.4 Deck Stiffness

Relative to deck stiffness, the decision was made in 2005 to simply quantify the stiffness condition of the deck/girder systems of each bridge using the GDFs determined from the test data. The 2005 GDFs for each bridge, reported in Table 35, were determined following the same analysis approach that was used in 2003, but this analysis was executed using displacement rather than strain data from the girders (note that girder displacement measurements were not made in the 2003 tests).

Referring to Table 35, the GDFs calculated from data collected in 2005 very closely match the GDFs calculated using the AASHTO equations. The maximum difference was approximately 2 percent for the exterior girder for the Conventional deck. The 2005 GDFs are very similar between bridges, with potentially a nominal pattern in which the lowest GDF values were calculated for the Conventional deck in both the interior and exterior cases. In the case of the interior girder, the GDFs calculated for all the decks were between 5 and 15 percent higher in 2005 compared to 2003. This behavior indicates less load sharing occurred transversely between the girders in 2005 relative to 2003, which would be consistent with a "softening" of the deck behaviors in the transverse direction over time. Such softening further would be consistent with the occurrence of longitudinal cracking in the decks. Noticeable longitudinal cracking of this type was observed by the abutments of all the bridges, and hairline crazing and cracking was observed at other locations throughout the decks. The correlation of the change in the GDFs and the extent of distress in the decks was not, however, completely as would be expected. In a global sense, the HPC deck experienced the least significant visual cracking between 2003 and 2005, but it experienced the greatest increase in interior girder GDFs (15 percent). This situation may imply that the HPC deck has experienced broader but less severe, and thus less evident, cracking damage than the other two decks.

Table 35: Summary of Saco Bridge Girder Distribution Factors

Girder	Bridge	AASHTO GDF Equation	Worst Case (R-W)	
			2003	2005
Interior Girder	Conventional	65%	61%	64%
	Empirical	66%	59%	65%
	HPC	65%	57%	66%
Exterior Girder	Conventional	64%	65%	62%
	Empirical	65%	59%	65%
	HPC	64%	61%	65%

7.2.5 Superposition

Live load data from 2005 was analyzed to validate whether superposition within the decks still holds, thus verifying that the bridge decks continue to behave linear elastically. As during live load testing in 2003, the three Saco bridges were tested in 2005 using two heavily loaded three-axle dump trucks, traveling side-by-side along the length of the bridge, namely two-truck tests TT-WR and TT-XT (refer to Figure 40-b). Strains measured during selected single-truck tests (ST-X and ST-T, and ST-W and ST-R) were added together and the results compared to the strains measured during the corresponding two-truck tests (TT-XT and TT-WR, respectively). If superposition was valid (i.e., the behavior was linear elastic), the sum of the strains from the single truck tests should equal the strain in the two truck test. As was observed in 2003, the summed single truck strains from 2005 live load tests (evaluated at positions of 40 m and 42 m) were typically within 10 percent of the two truck test strains in all three bridges, confirming their linear elastic behavior. Figures 78 and 79 show typical comparisons of the summed response from the separate single truck tests ST-X and ST-T to the measured two-truck test response (Gage Line D, Conventional deck). Similarly, Figures 80 and 81 show typical comparisons of the summed response from the separate single truck tests ST-W and ST-R to the measured two-truck test response (Gage Line D, Conventional deck).
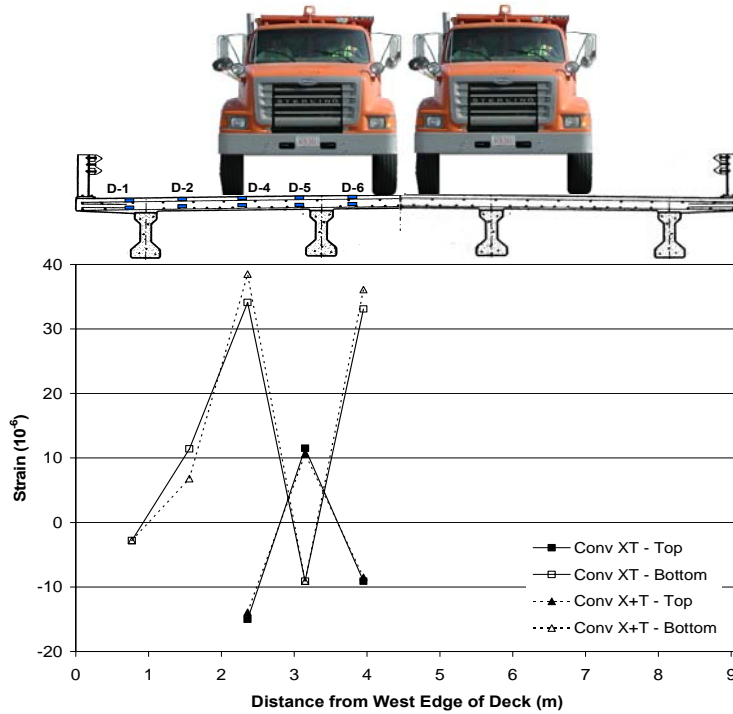
Figure 78: Transverse Strain Profile Showing Superposition in the Conventional Deck from Gage Line D at the 40 m Truck Position for the X and T Truck Runs – 2005
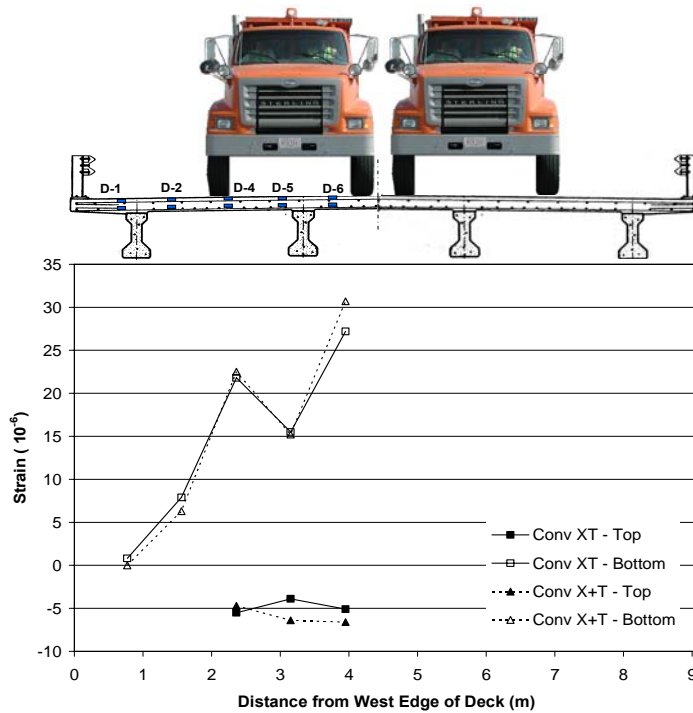
Figure 79: Transverse Strain Profile Showing Superposition in the Conventional Deck from Gage Line D at the 42 m Truck Position for the X and T Truck Runs – 2005
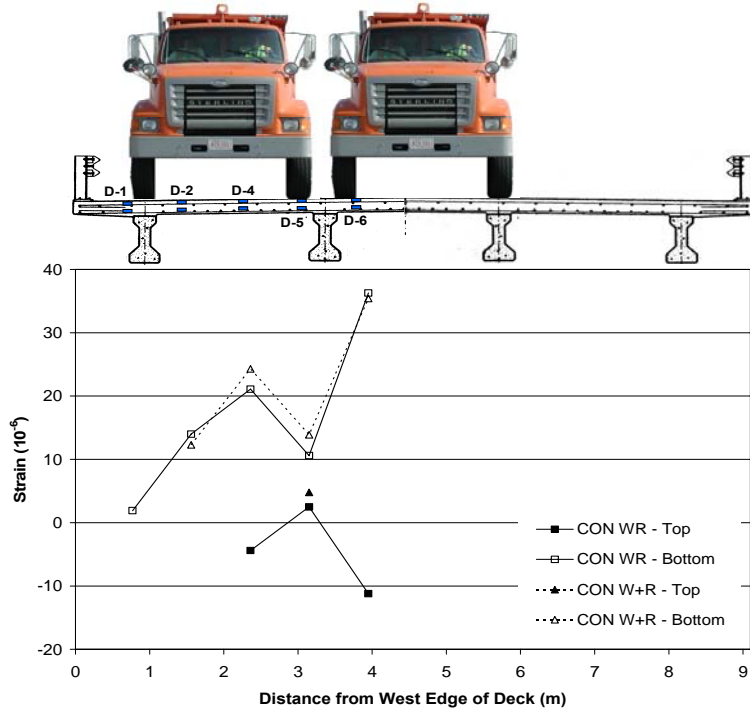
Figure 80: Transverse Strain Profile Showing Superposition in the Conventional Deck from Gage Line D at the 40 m Truck Position for the W and R Truck Runs – 2005
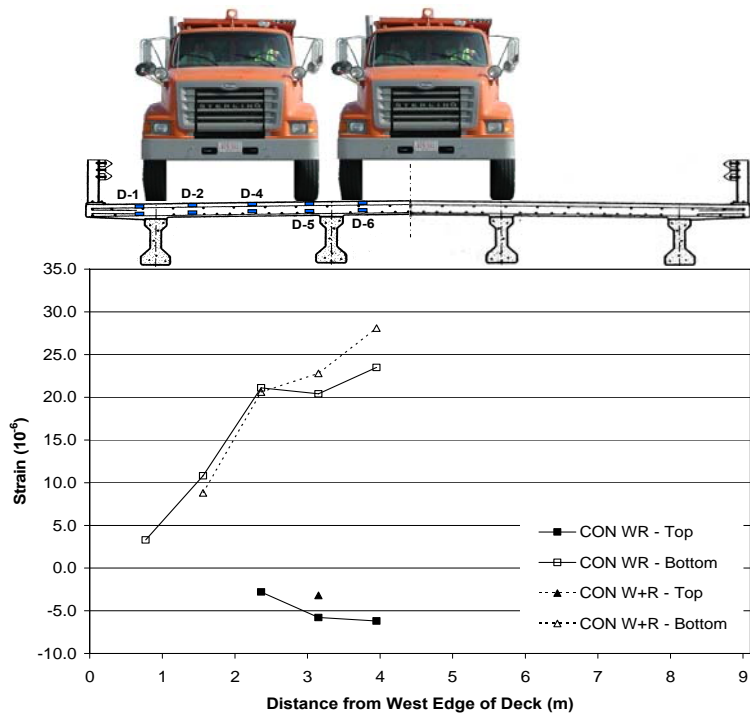
Figure 81: Transverse Strain Profile Showing Superposition in the Conventional Deck from Gage Line D at the 42 m Truck Position for the W and R Truck Runs – 2005

7.2.6 High Speed Live Load Tests

High speed live load test results were compared to corresponding slow speed or crawl test results to determine whether dynamic loading affected the strains within each of the decks. Comparisons between multiple gages and truck runs generally revealed that maximum responses were the same in the slow and fast live load tests. When discrepancies did exist, the slow speed tests had slightly higher maximum strain values. This result is similar to those found from comparisons made using the 2003 data. These differences were less noticeable in truck runs that were further from the instrumented portion of the deck (i.e., truck-runs V, X and Y), and truck run U contained the greatest differences between the slow speed and high speed tests. Nevertheless, it can be concluded from this analysis that there are generally no differences in maximum response between any of the decks when high speed tests are compared to their corresponding slow speed test.

7.2.7 Review of Analysis Observations – 2005

Based on the preceding analyses of the results of the 2005 live load tests, and the attendant comparisons between the results of the 2003 and 2005 tests, several conclusions were reached. The broad conclusions from the 2005 live load tests are that:

- all three decks continued to behave in a similar fashion, relative to each other; and
- the behavior of each deck changed very little over time (2003 versus 2005).

Differences in deck behavior by type and over time could not be discerned based simply on qualitative comparisons of the data collected from each bridge. Comparisons of the various quantitative measures of deck performance being considered in this analysis generally confirmed the similarity in deck response. Some success was realized in correlating changes in these quantitative parameters for each deck over time with the attendant changes in the physical distresses in the decks. Notably, smaller changes in the quantitative response parameters between 2003 and 2005 generally corresponded to smaller changes in the physical damage experienced by the decks during this same interval. In making this observation, it is important to note that a) the observed changes in the quantitative response parameters were small in magnitude, and b) that only limited cracking has been seen in the decks to date. In the future as additional cracking occurs, the correlation between these quantitative parameters and physical distress may become more apparent. Based on changes in the internal strains experienced in the decks in the 2003 and 2005 live load tests, the behavior of the HPC deck was the most stable (unchanged) over this time interval, while the behavior of the Empirical deck was the least stable (most changed) over this interval. Additional observations and conclusions include:

- All measured tension strains were significantly below those levels that would be expected to cause cracking in the decks (average peak value of approximately 40 microstrain).

- The presence of in-plane axial forces in the decks in the transverse direction was inferred from the strain data from the Conventional and Empirical decks (this analysis could not be completed for the HPC deck due to instrumentation losses). These strains were below 10 microstrain in magnitude, with a greater mean strain occurring in the Empirical relative to the Conventional deck.

- All three decks exhibited similar stiffnesses and load flow behaviors, based on the GDFs experimentally determined for each bridge.

- Linear superposition worked well for all three bridge decks, indicating that all three decks were still behaving linear-elastically.

- Changes in the neutral axis position and GDFs for the Empirical bridge were consistent with a visual assessment of the change in its physical condition between 2003 and 2005. This same correlation between these quantitative behavior parameters and physical deck condition, however, was not as consistently seen for the Conventional and HPC decks. This situation may imply that physical changes have occurred in the HPC and Conventional decks, but that these changes are simply less apparent by visual examination of the decks.

- All three decks responded similarly regardless of the speed at which the live load was applied.

8   LONG TERM MONITORING

Long term monitoring at the bridges consisted of measuring internal deck strains and temperatures, assessing corrosion potential, mapping cracks, and detecting global movement of the bridge structures from survey data. The data acquisition system was programmed to collect strain and temperature information from all of the embedded sensors on an hourly basis. All other effects were monitored through periodic visits to the bridge site spaced at three to six month intervals immediately following construction, transitioning to annual surveys thereafter.

8.1   Internal Monitoring

Long-term data has been continuously collected from embedded sensors in each of the bridge decks since the time of their construction. All the active long term sensors were set up to provide measurements once every hour. This data acquisition schedule was been interrupted on occasion due to maintenance and other activities.   These interruptions were considered inconsequential in terms of the entire length of the project and are noticed as gaps in the graphs of the long term data.

The data available from the long term monitoring was studied with the goal of correlating changes in deck performance with the vehicle and environmental loads they experienced, and then further evaluating the relative performance of the three types of decks. Presented herein are the observations to-date in this regard, based on the data obtained from the vibrating wire gages cast in the deck during their construction. The primary "environmental" behaviors experienced by the decks are related to the dimensional changes that they have experienced due to changes in relative humidity (shrinkage of the concrete) and temperature (shrinkage and expansion of both the concrete and the reinforcing steel). An inherent assumption throughout this investigation was that due to their close proximity, all three bridges have experienced the same environment. Thus, before looking at the strain response of the decks, some information is presented on the temperatures and relative humidity experienced at the bridges. This information is followed by a discussion of the strain data, and an analysis of the associated deformations of the decks in response to temperature changes that was performed using this data.

8.1.1 Temperature and Relative Humidity

Over the past two years, the air temperatures recorded at 15 minute intervals at the weather station at the Saco School have ranged from approximately -37 to 41 ^{o}C. More precise geographically, temperatures have also been recorded hourly in the instrumentation box located under each bridge, coincident with the strain readings taken for the long term monitoring program. These temperatures have ranged from -34° to 41 ^{o}C, with an average value of approximately 12 ^{o}C. The temperatures at each bridge, as represented by these instrumentation box values, have been remarkably consistent between bridges throughout the project, as shown

in Figure 82. The significance of this observation is that any differences in the recorded strain response between bridges should not be caused by differences in temperature between the bridges, as the temperature environment at each bridge is essentially the same. This conclusion can be even further strengthened by comparing the hourly temperatures measured inside each deck at each instrumentation location, as while the air temperature at each deck could be the same, the decks themselves could be at different temperatures if they have different thermal radiation, reflectance, or other properties. Such temperature measurements were available, as temperature is measured automatically at each gage location as part of the vibrating wire measurement process. Typical graphs of the temperature measurements at common locations in all three decks are presented in Figures 83 and 84 at sensors embedded toward the bottom and top of the deck, respectively (specifically, for gage location TV-D-3). Once again, referring to these figures, the temperatures are very similar in all three decks at both locations.
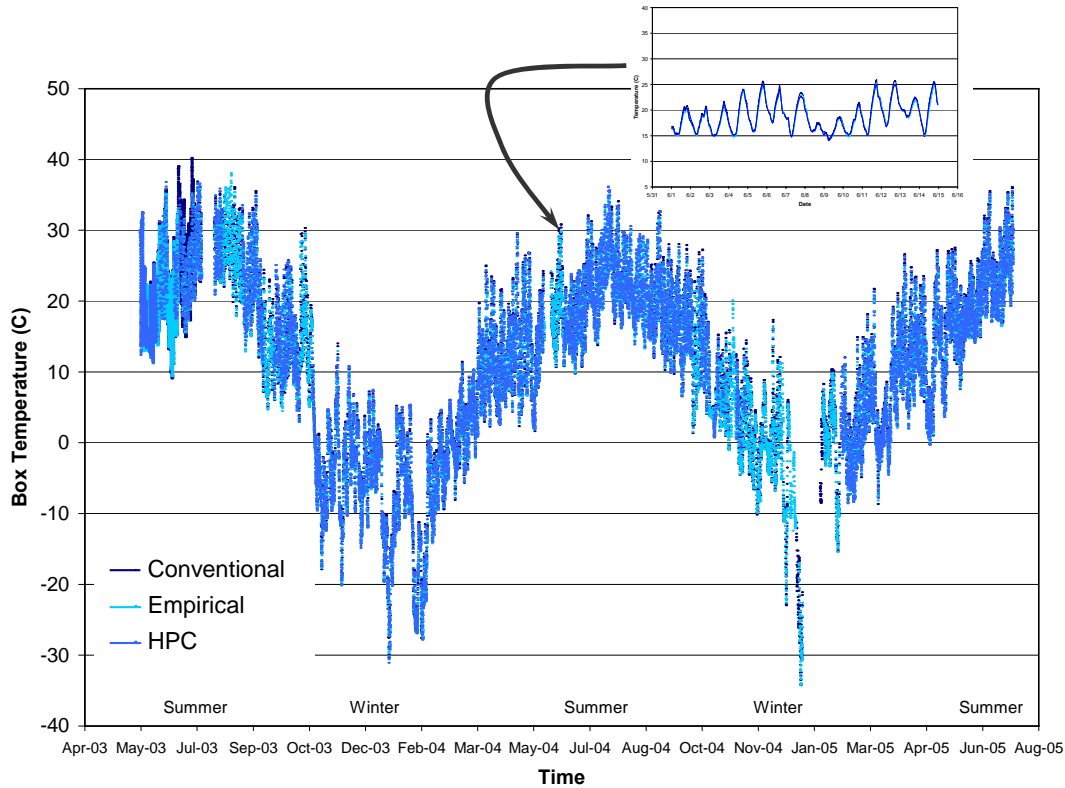
Figure 82: Temperature History – All Three Decks – Instrumentation Box
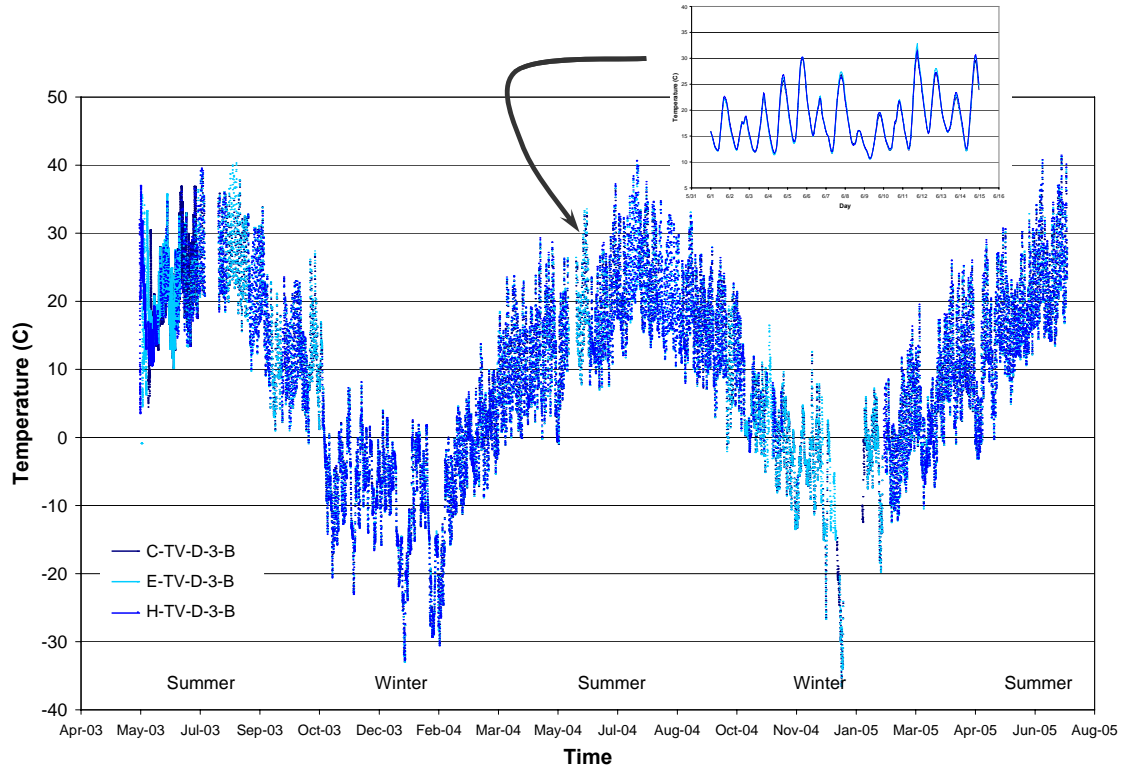
Figure 83: Temperature History – All Three Decks Transverse Gage Location TV-D-3-B (Bottom)
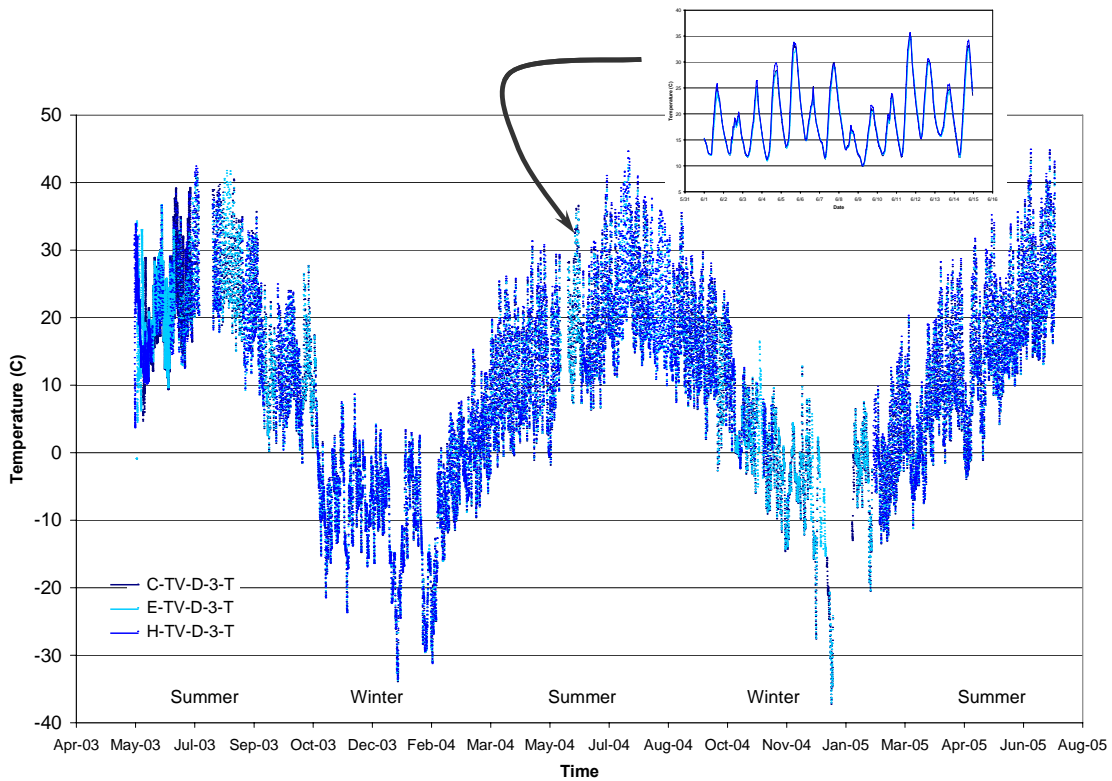
Figure 84: Temperature History – All Three Decks Transverse Gage Location TV-D-3-T (Top)

Naturally, the temperatures toward the top and bottom of the decks at any given location often were different, as temperature gradients developed across the deck thickness in response to uneven heating and cooling of the top and bottom surfaces. Typical temperature gradients measured through the depth of the cross-section (with a negative gradient representing increasing temperature from the bottom of the deck towards the top) and average temperatures of the cross-section calculated at the centroid are shown in Figure 85 for approximately a year and one-half period. The extreme gradient temperatures are approximately 2 °C (seen in the winter) and -6 °C (seen in the summer). These gradients are much less then the approximate 20 °C temperature gradient proposed by AASHTO. However, AASHTO's recommendation of multiplying their recommended temperature gradient by -0.3 for the inverse temperature gradient is supported by the measured temperatures. This inverse gradient, with greater temperatures at the bottom surface of the bridge deck relative to the top surface, seems to occur regularly throughout the year. The temperature gradients are largest during the summer months, probably in response to larger amounts of solar radiation received at the bridge site during the summer months relative to the winter months.
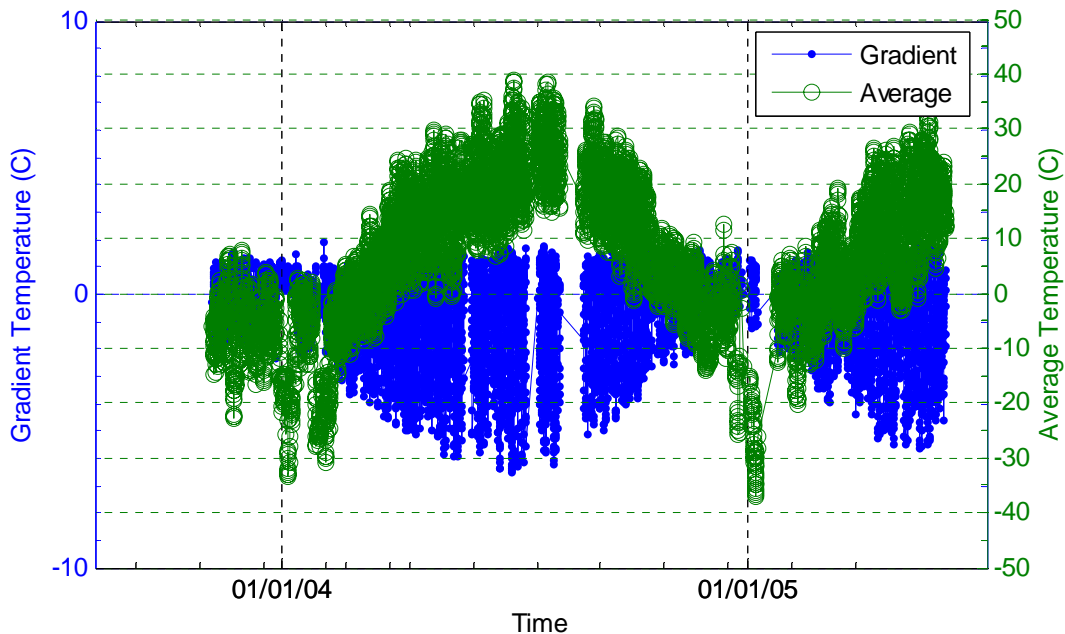
Figure 85: Temperatures and Temperature Gradients Conventional Deck Gage Location TV-D-3

The measured minimum and maximum average temperatures in the decks were approximately -38 °C and 40 °C, respectively, which exceed the proposed AASHTO recommendations of -18 to 27 °C. AASHTO's recommended values do encompass the majority of the temperature measurements, excluding rare extreme events. Thus, AASHTO's values may represent only the most probable and persistent temperatures for design stresses, and they may rely on inherent safety factors to keep stresses within reason for extreme thermal events.

Early data collected from the bridges showed that internal temperatures were elevated during curing of the concrete. Cyclic behavior has been seen in most of the strain gages that obviously correlates with diurnal temperature fluctuations. Figure 86 shows the temperature near the bottom of the three bridge decks as a function of time since they were cast. Variations in the hydration temperatures between the decks are obvious at early times after their construction. Temperatures were measured at Gage Location F-3. Note that the peak temperature in the HPC deck occurred later than the peaks for the Empirical and Conventional decks. This behavior is most likely attributable to the retardant used in the HPC mix design. Also note that even though the Conventional and Empirical decks utilized the same concrete mix design, their peak temperatures are quite different. Ambient conditions for these two decks during the pour were similar. At this point, there is no certain explanation as to why these differences occurred or if they are truly significant. Temperatures measured at different locations in one deck have been seen to vary by up to ten degrees during curing. Cyclic behavior of the deck temperature is a result of diurnal temperature fluctuations. These effects are more noticeable once the curing cycle was complete. Straight-line portions of the graph correspond to intervals when the data logger was not operating.
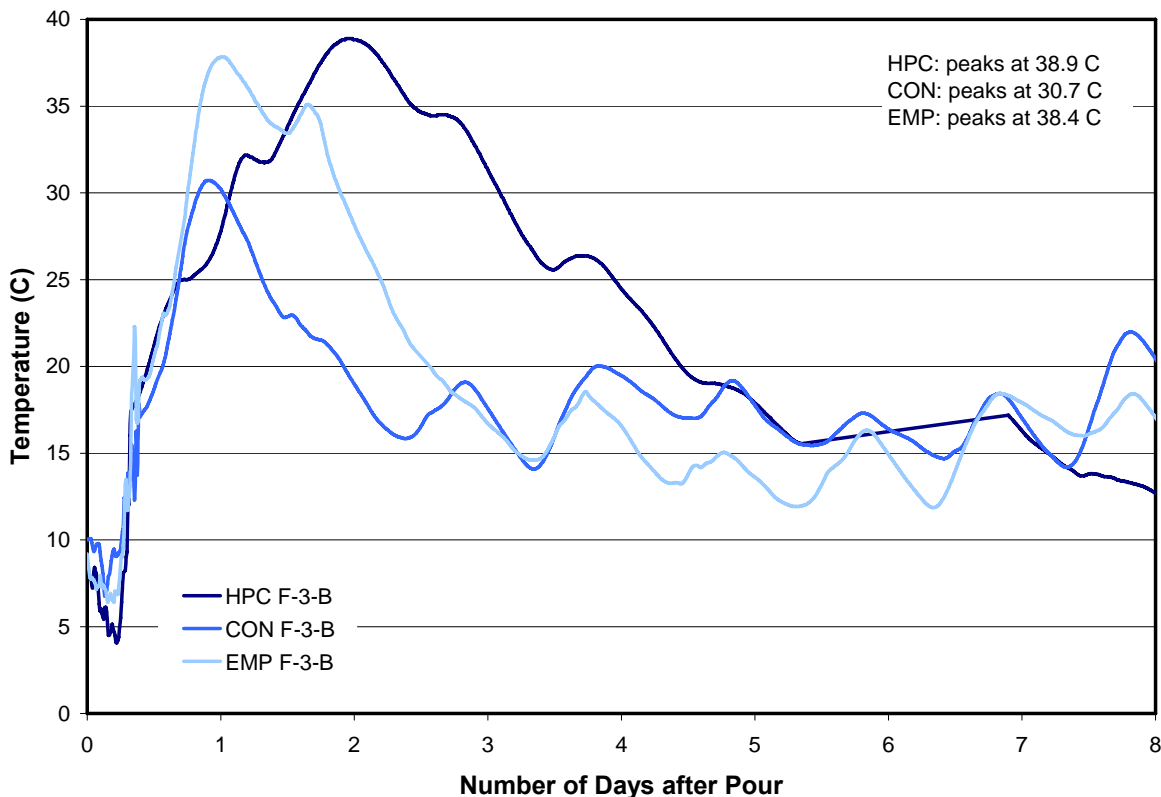
Figure 86: Comparison of Bottom Deck Temperatures during the Cure Cycle.

The relative humidity measured at the Saco School ranged from approximately 10 percent to 100 percent, with an average value of approximately 63 percent. Relative humidities measured over the life of the project are presented in Figure 87.
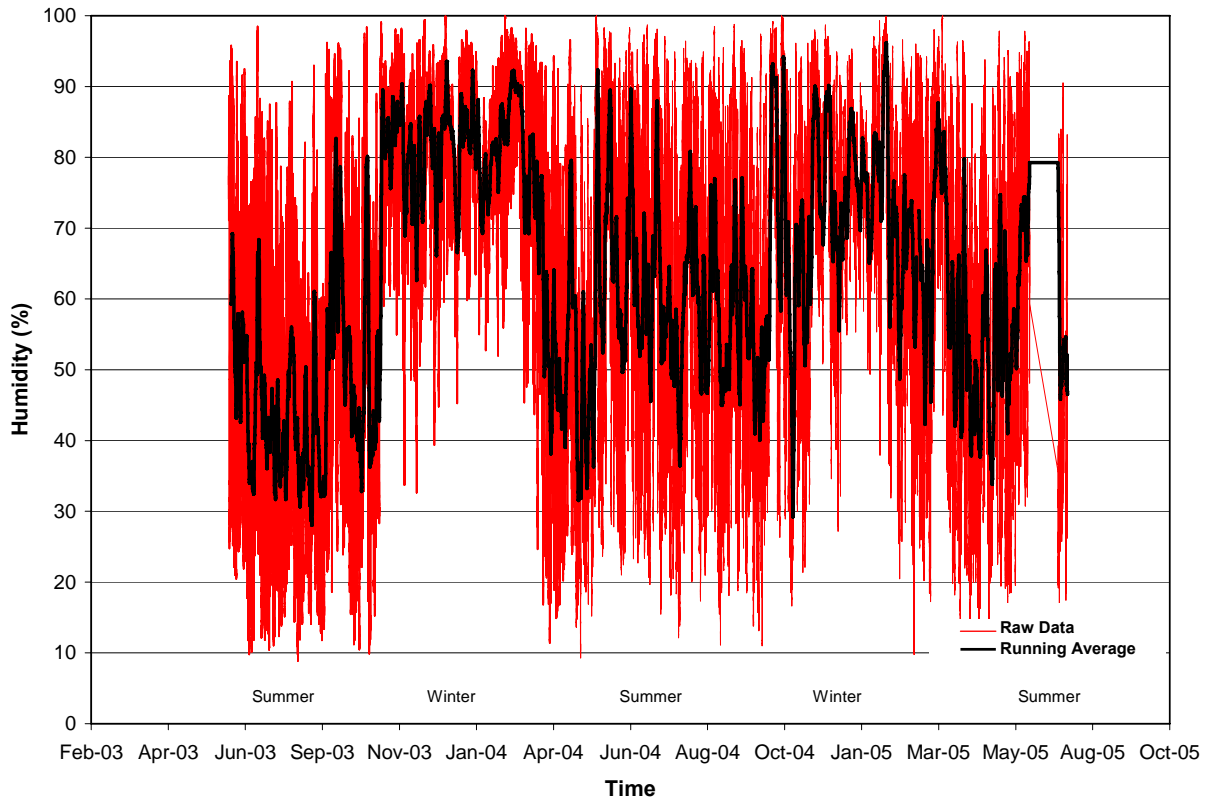
Figure 87: Relative Humidity History – Weather Station

8.1.2 Strain Response

At any instant in time, the total strains experienced by the bridge decks are the net combination of four effects, namely, load, temperature, shrinkage, and creep effects. Often, attention is focused on load related strains, as such strains can be directly related to the stress in an element using the principles of mechanics. In this case, the decision was made to initially investigate total strain, and to focus on the deformed shape of the bridges under temperature, shrinkage, and creep effects. The response recorded for the vibrating wire strain gages included load, shrinkage, and creep effects, but it was automatically compensated for temperature effects, and thus the data had to be processed to restore the temperature contribution to the total strain. This processing consisted of modifying the recorded response by the differential between the coefficient of thermal expansion of the deck concrete and the reinforcing steel, multiplied by the change in temperature. Thus, to affect this adjustment, values of the coefficient of thermal expansion of each deck concrete were required. Often, and as was previously discussed, the coefficient of thermal expansion of concrete is simply assumed to be approximately the same as

that of steel. In this case, differences in the fundamental behavior of the two deck concretes being studied could be important to the objectives of the project, so the decision was made to experimentally determine the coefficients of thermal expansion for each concrete.

A laboratory investigation was conducted to determine the CTEs of the concretes used in the bridge decks (Johnson, 2005). This investigation was conducted by cycling instrumented specimens of the deck concretes (which were cast at the time of deck construction) between -45°C and 45°C, and measuring their strain response. The values of CTE at various temperatures for all three deck concretes are shown graphically in Figure 88, during a typical heating cycle. The CTE values were found to vary significantly with temperature (ranging by as much as 6 $\mu\varepsilon$/°C at -10°C to 13 $\mu\varepsilon$/°C at 40 °C), which was attributed primarily to the behavior and interaction of the water in the paste with the pore structure. The CTEs for the concretes were also found to be less than that of steel at lower temperatures (below approximately 15 °C). In addition, the CTEs for the high performance and Conventional concretes were found to be different, particularly at lower temperatures (see Figure 88). These differences in CTE behavior may be related, among other things, to the structure of the paste of the high performance concrete, which affects the behavior of the water within it pores. Similarities in the Conventional and Empirical deck concrete specimens are evident, as expected, since they utilized the same concrete mix design.
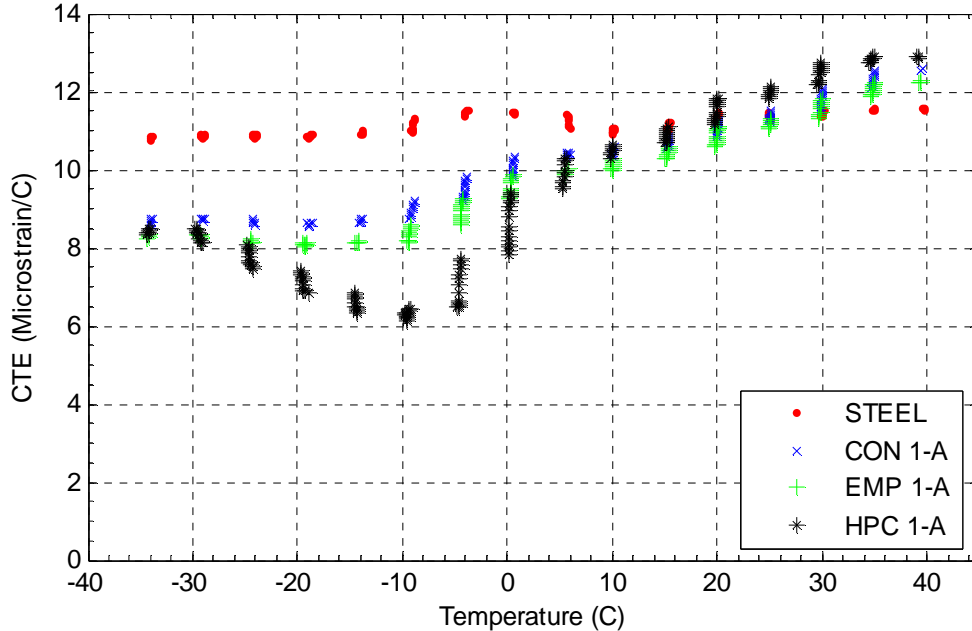
Figure 88: Coefficients of Thermal Expansion for the Bridge Deck Concrete as It Is Heated

Once the CTEs were determined, the strain data collected from the vibrating wire gages was processed to obtain the total strains experienced by each deck since their construction as a function of time. A typical transverse strain response toward the top of the decks between the

girders is presented in Figure 89 for all three decks (specifically, Gage Location TV-D-3-T). The transverse as opposed to the longitudinal response is being discussed first, as strain conditions in the longitudinal direction are complicated by the composite action of the deck with the prestressed girders, as well as by the potentially complex boundary conditions at the integral abutments at each end and at the intermediate bents.

Referring to Figure 89, the diurnal strain changes in response to daily temperature cycles are clearly evident in the data, and to a certain extent they interfere with formulating comparisons of the average values and seasonal fluctuations in the strain response between bridges. In Figure 90, these diurnal cycles have been smoothed out of the primary traces using a one-week moving average. The diurnal cycles have then been detailed at a larger scale in the inset included in the Figure. As is evident in Figure 90, the transverse strain response for the all three decks was similar in character, consisting of contraction in the winter and expansion in the summer, superimposed on an overall, in-plane shrinkage of the deck concretes that primarily occurred within a few months of their completion. The average long term strain in all three decks is approximately 320 microstrain, which is less than

1) the shrinkage strain predicted for the decks using the concrete shrinkage equation proposed by AASHTO, which gave a shrinkage strain of approximately 400 microstrain at two years of age; and

2) the shrinkage strain directly measured at two years of age on concrete specimens cast with the deck, which gave shrinkage strains of 500, 530, and 360 microstrain, respectively, for the Conventional, Empirical, and HPC specimens (note that these specimens were exposed for an extended period to a relative humidity of approximately 30 percent, which is one-half the average relative humidity at the test site).

This difference in the actual deck strains and the expected strains based on shrinkage could result from restraint provided by the girders to transverse deformations in the decks. The overall long term contraction of the HPC deck appears to be approximately 20 percent lower in magnitude than that of the other two decks, which is of the same order of magnitude as the difference in shrinkage strains in the HPC and conventional concretes, as determined from the shrinkage test specimens. By absolute magnitude, the maximum long term compression and tension strains observed at this location in the decks were approximately -600 to -700 and 90 to 110 microstrain, respectively.

The changes in strain during typical diurnal cycles were compared with the corresponding changes in temperature during these cycles. These changes were generally similar to those that would be expected based on the coefficients of thermal expansion of the different deck concretes.
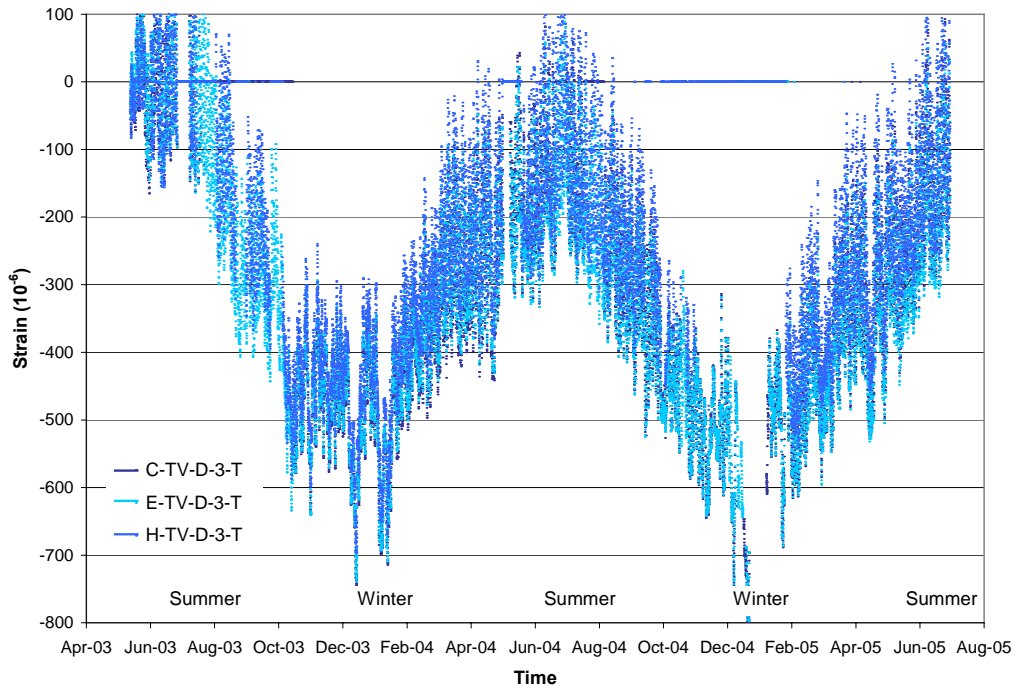
Figure 89: Strain History All Three Decks Transverse Gage Location TV-D-3-T (Raw)
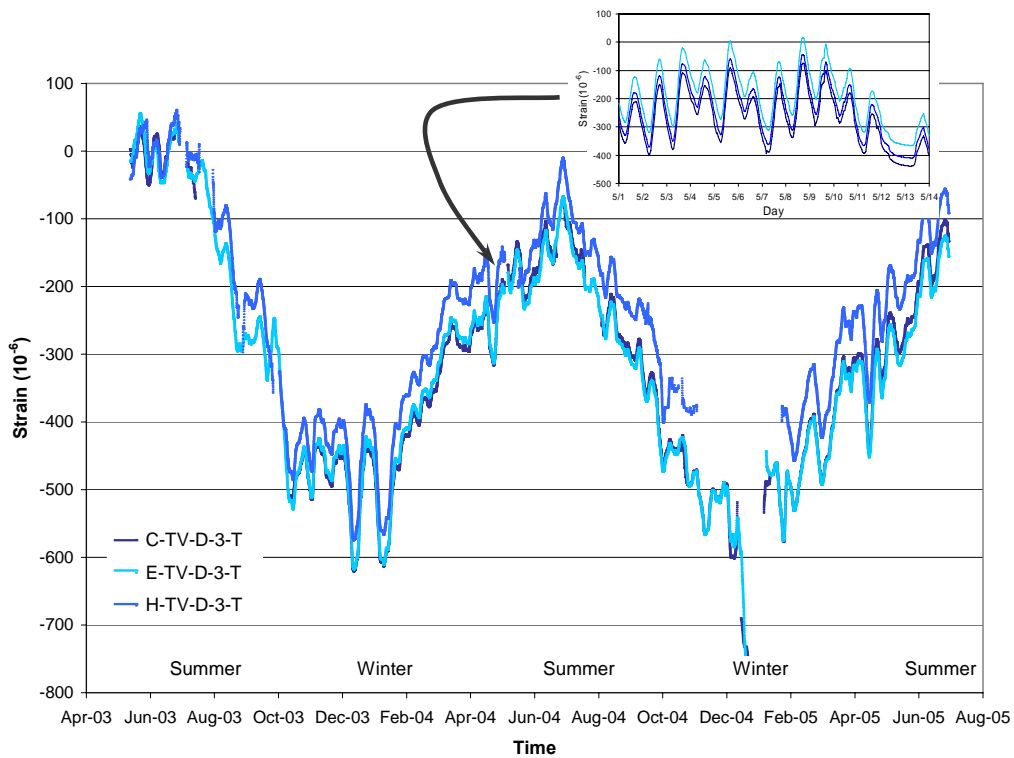
Figure 90: Strain History All Three Decks Transverse Gage Location TV-D-3-T (Smoothed)

The typical longitudinal strain response in the interior of the decks between the girders (specifically, at Gage Location LV-D-3-B) is shown in Figure 91. Once again, the diurnal cycles have been filtered out of the primary traces, so that the average response of the three decks is more readily apparent. As mentioned above, thermal movements in the decks in the longitudinal direction were expected to be influenced by their composite connection to the girders, the constraint offered by the integral abutments, and the conditions at the transverse cracks over the bents. These factors could easily vary between the decks, which would affect their relative strain response. In this case, referring to Figure 91, the overall response of all three bridges is very similar to that seen in the transverse direction (see Figure 90), consisting of diurnal temperature cycles superimposed on the strain changes associated with broader seasonal temperature changes, which are further superimposed on the fundamental drying shrinkage in the concrete. In this case, however, the lowest mean strains are observed in the Conventional deck (recall that in the transverse direction, the lowest mean strains were seen in the HPC deck). The mean strains in the Conventional deck furthermore were noticeably lower in magnitude than the longitudinal strains seen in this deck in the transverse direction. This reduction in strain level could result from a difference in the longitudinal restraint in this deck relative to situation in the Empirical and Conventional decks. Additional information presented below on the longitudinal response of the decks indicates that the transverse crack over the bents is structurally more severe in the Conventional deck relative to the HPC and Empirical decks. Thus, the presence of this crack could also be influencing the longitudinal response at this location in the Conventional deck.
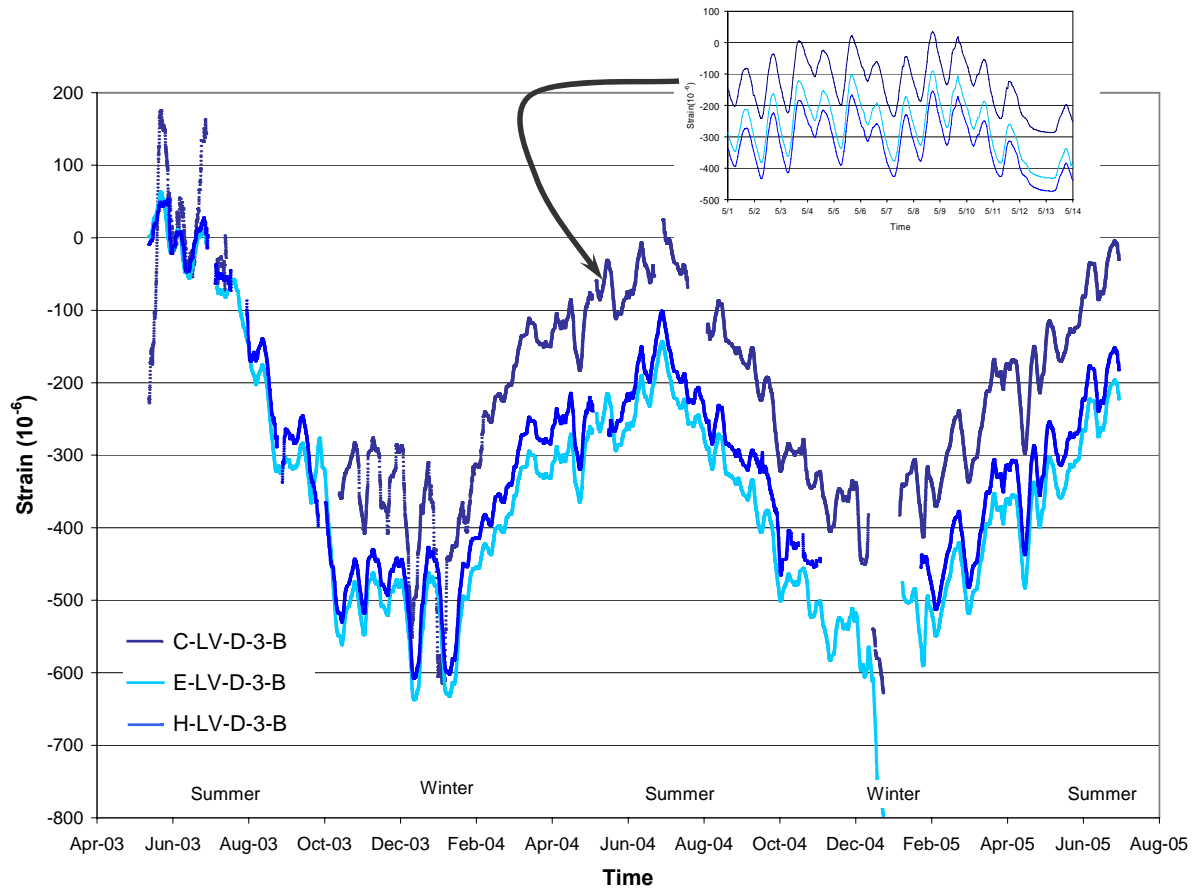
Figure 91: Strain History All Three Decks Longitudinal Gage Location LV-D-3-B (Smoothed)

Reported in Figure 92 is the longitudinal strain response at Gage Location LV-F-3-B. These gages are in the immediate area of the cracks in the decks over the bents, and as expected, their behavior is somewhat difficult to understand due the abrupt interruption in the structure that these cracks create. Despite the presence of the cracks, the decks generally shrank in the winter and expanded in the summer at this location. While early in the record the seasonal temperature variations were superimposed on an overall shrinkage in the decks, the magnitude of the mean shrinkage slowly decreased with time. In the case of the HPC deck, the mean response actually became expansive (tensile) in nature in the second year of the record. This gradual shift could be related to crack growth, and increasingly independent action of the two now separate deck slabs on either side of the bent. The diurnal strain response at the bents also differs between the bridges, as is evident in the inset in Figure 92. The strain cycles in the Conventional deck are out of phase with the cycles in the HPC and Empirical decks, which in turn are in phase with the temperature cycles. This behavior is consistent with the crack over the bent in the Conventional deck being more fully formed than those in the HPC and Empirical decks. The crack in the Conventional deck is functioning at a diurnal level as a joint, allowing the deck to expand and contract as two separate pieces on either side of the crack. While the diurnal cycles in the

Empirical and HPC decks are in phase (and in phase with the temperature cycles), the magnitude of the diurnal cycles in the Empirical deck are much smaller than in the HPC deck, which is indicative that the crack in the Empirical deck is more fully formed than that in the HPC deck.
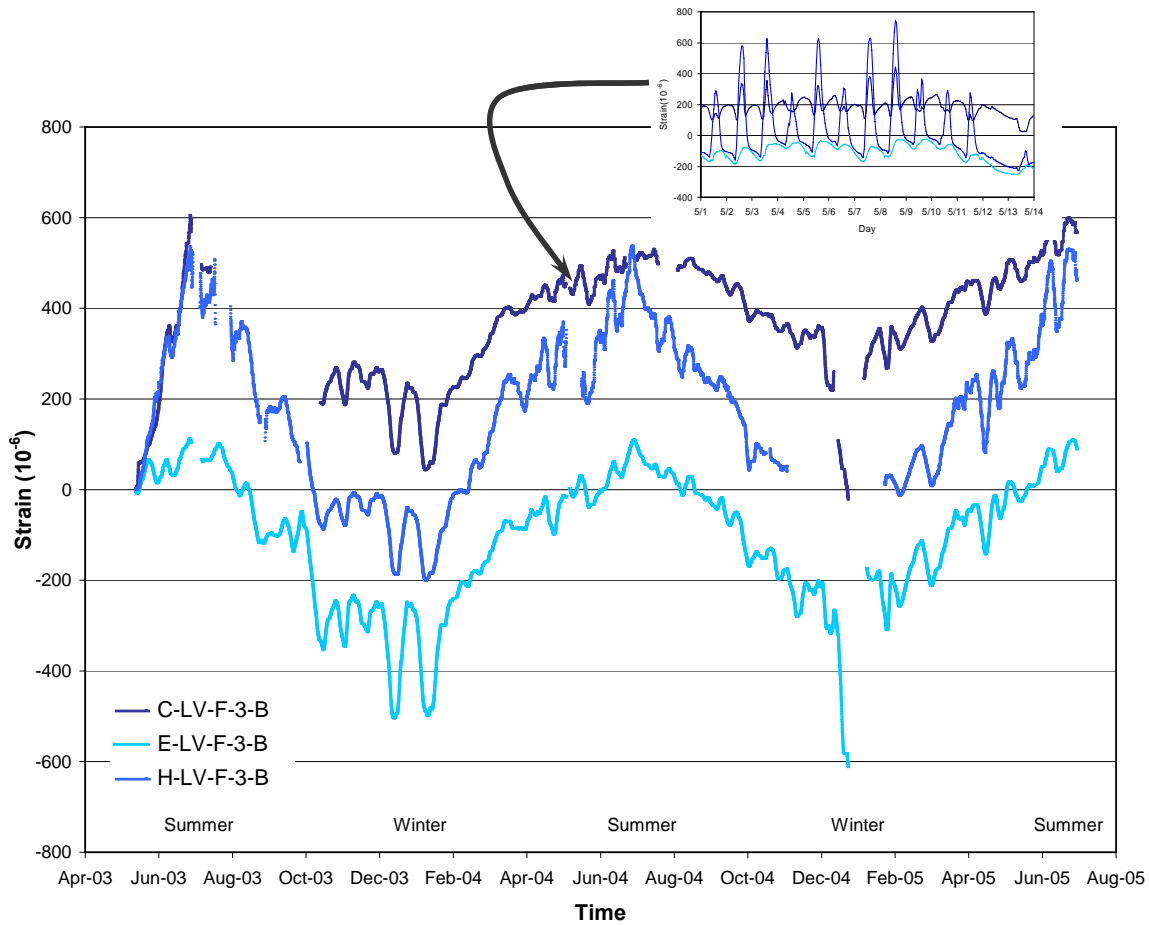
Figure 92: Strain History All Three Decks Longitudinal Gage Location LV-F-3-B (Smoothed)

Looking more closely at the early strain response at Gage Line F, the occurrence of the anticipated transverse cracks over the bents was captured by the instrumentation. Physical cracks have been observed over all the interior bents, and the data collected from the vibrating wire strain gages spanning Gage Line F reflect the occurrence of these cracks. In general, cracking that intercepts the vibrating wire gage will increase cyclic strain levels due to daily and seasonal temperature fluctuations. The gage length of the vibrating wire strain gages is 153 mm, so prior to the formation of a crack anywhere along its length, measured strains would indicate tensile or compressive strains only in this region. After a crack forms, strains will also include differential movements of the separate concrete segments, made up of the three bridge deck panels. Figure 93 illustrates this phenomenon using strain data from vibrating wires on Gage Line F for all three decks. Recall that the HPC bridge deck was poured on May 28, the Empirical deck on June 2 and the Conventional deck on June 5. Both the HPC and Conventional

decks showed small daily strain fluctuations (~10-20 με) prior to cracking. Once the crack formed, daily fluctuations greatly increased to approximately 250 με. The empirical deck behaved slightly differently in that the data indicated the presence of a hairline crack in the deck shortly after the pour and a more fully developed crack occurring later. Notably, all cracks seem to have either formed or fully formed near June 19th. Further investigation into this matter may reveal the reason for this concurrent behavior.
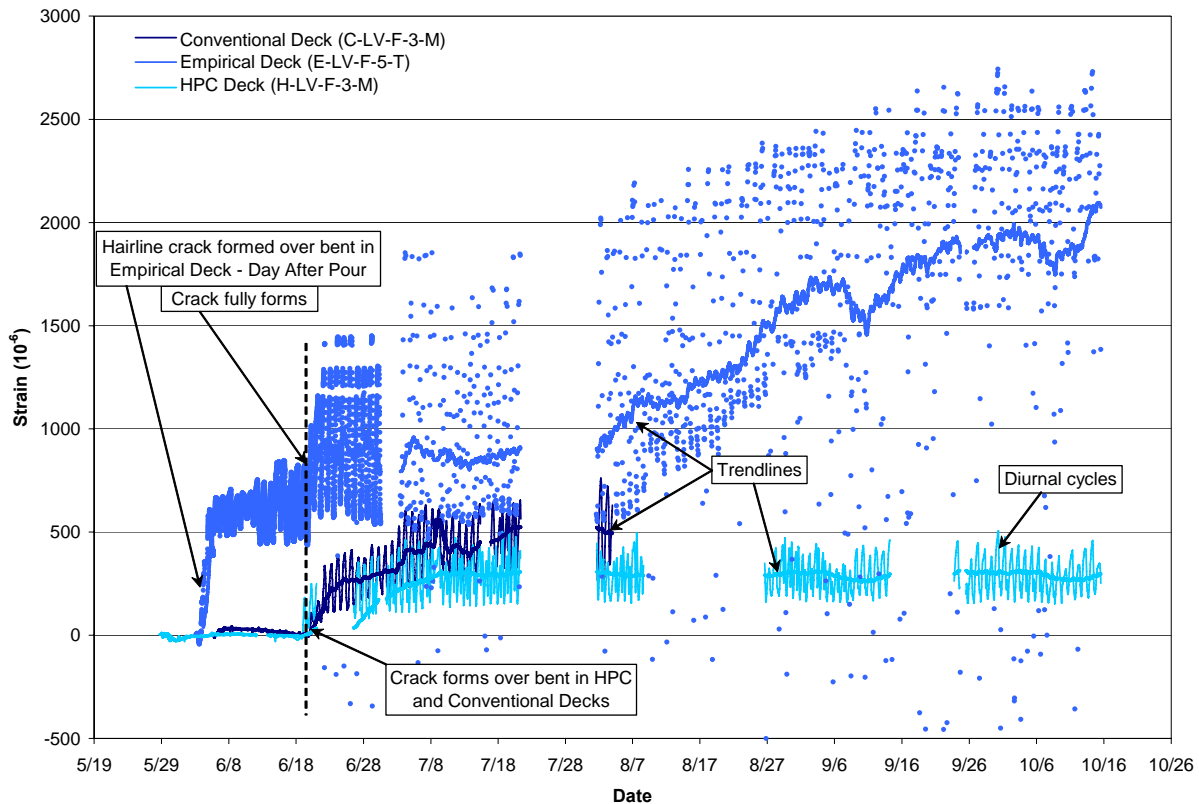
Figure 93: Long Term Data Showing the Formation of Cracks in All Three Decks.

Unlike sensors spanning the bents, longitudinal sensors installed away from the bents (i.e., position D-3, halfway between the bents and the diaphragms and halfway between two girders) did not show that cracking had occurred. Figure 94 shows the response from vibrating wire strain gages near the top of the deck in each of the decks at this position. Diurnal strain fluctuations are small (approximately 20 to 70 με), indicating contraction due to temperature changes and not cracks in the concrete.
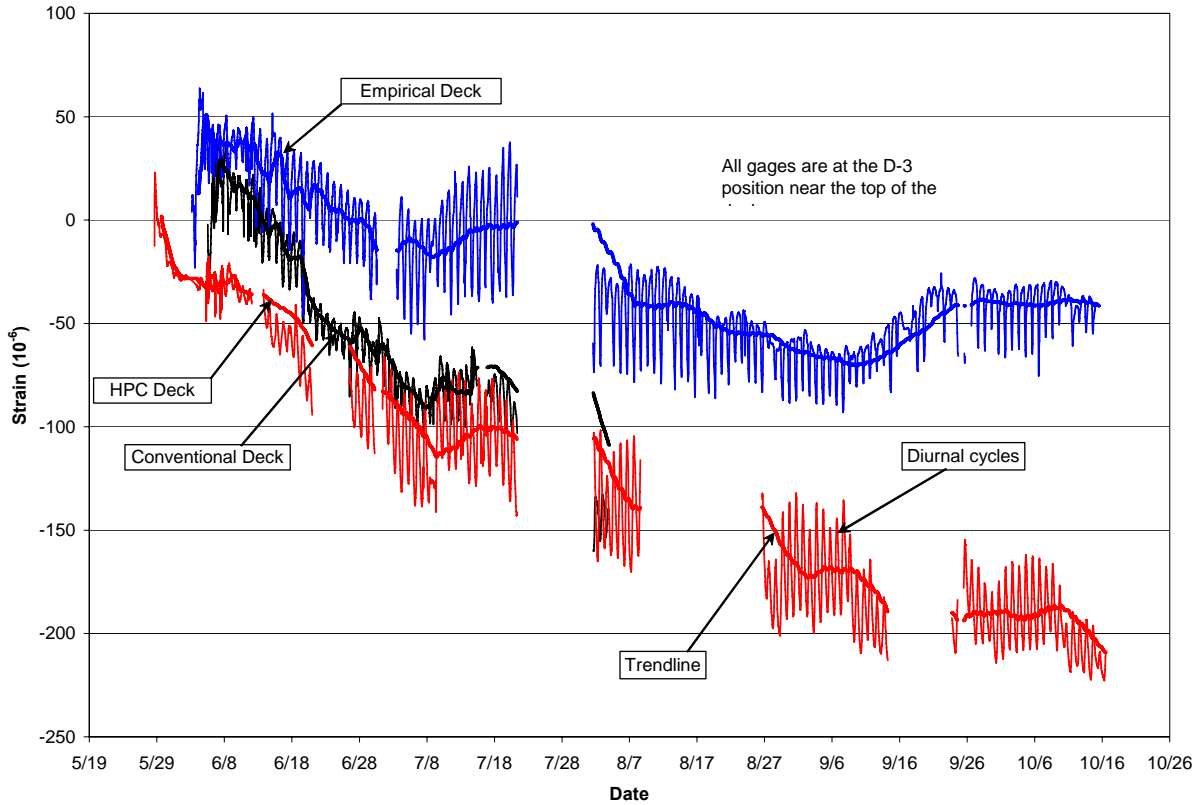
Figure 94: Long Term Data Illustrating Non-Cracked Portion of the Deck.

The formation and presence of a crack can clearly be seen in the data from the Conventional deck presented in Figure 95. In this case, longitudinal strains collected over the interior bent (Gage Location F-3) and over the intermediate diaphragm (Gage Location B-3) are compared. Prior to cracking, strains in these two locations are almost identical, simultaneously fluctuating based on daily temperature oscillations. Notably, prior to crack formation, lower temperatures caused decreases in strain indicating thermal compression. Conversely, higher temperatures produced increases in strain (Line A, Figure 95).
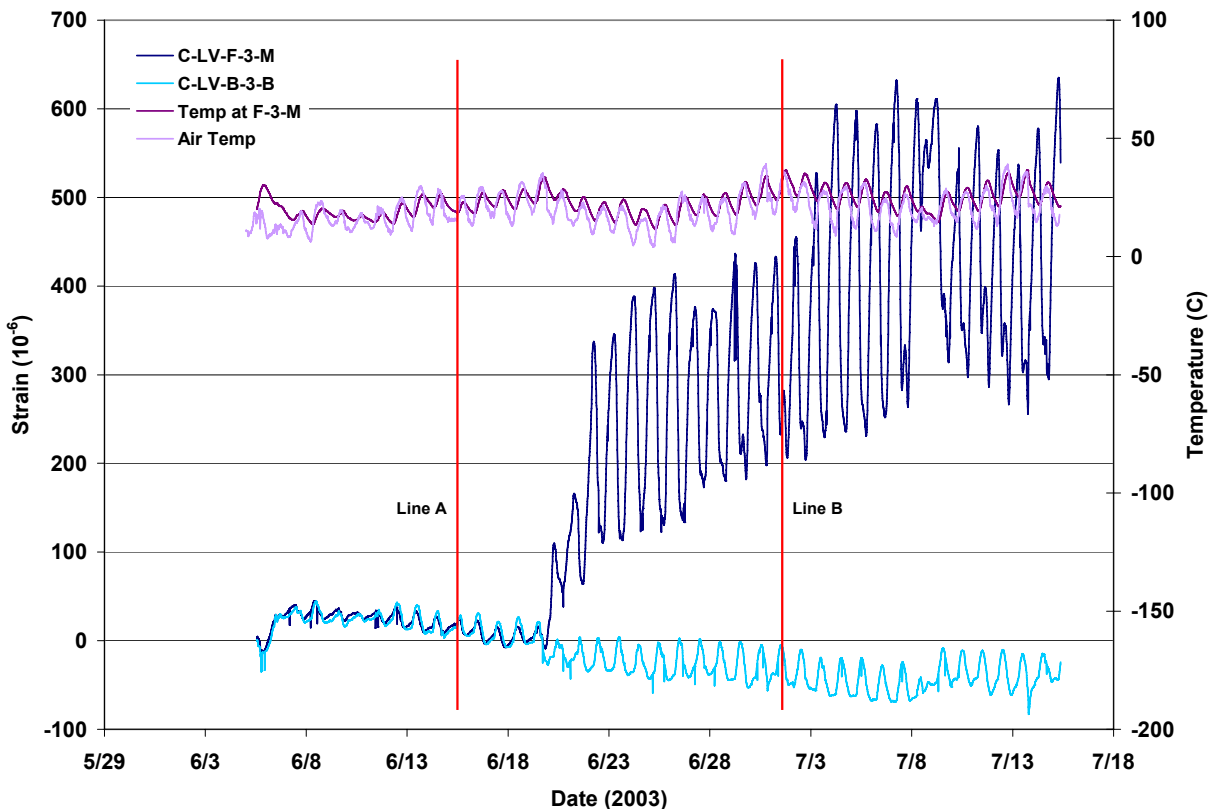
Figure 95: Comparison of Cracked and Non-cracked Position in the Conventional Deck.

On the evening of June 19th, strains over Bent #2 (Gage Location F-3) noticeably began to deviate from those at Gage Location B-3. This deviation is most certainly because a crack formed over the bent and intercepted the vibrating wire gage installed at that location. Following the formation of the crack at position F-3, two effects can be observed, 1) diurnal strain fluctuations increased in magnitude at the crack location, and 2) the mean level of strain at the crack location increased in magnitude and became tensile in nature due to deck concrete shrinkage on either side of the crack. First, daily changes in temperature produced higher strain values over the bent since the bridge deck concrete was essentially separated at that point. This separation caused contractive strains from each section of deck to be realized as increased strains across the crack. Therefore, what used to be decreasing strains over the bents before the crack occurred now became increasing strains. Moreover, the lowest temperatures during the day now produced the highest strains over the bents (Line B, Figure 95). Strains at Gage Location B-3, however, retained their original cyclic behavior.

Shrinkage of the deck concrete can also be observed using these same two locations. Average strain at both positions is decreasing slightly over time until the crack forms over the bent. At that time, the average strain at position B-3 continued to decrease, but average strain at position F-3 began to increase. In the body of the deck (B-3), the concrete shrank, placing the

gage in compression. Conversely, as the "slabs" on either side of the crack shrank, they drew away from the crack, placing the gage at the crack in tension. Possible reasons for the higher rate of increase of the mean strains at the bents (F-3) relative to the body of the slab (B-3) are that 1) strains across the crack represent a concentration of the shrinkage strain effects that are distributed across the adjacent "slabs", and/or 2) ratcheting of the crack is occurring as small concrete particles hold it increasing open after each cycle of expansion.

8.1.3 Analysis of Long Term Deck Deformations

Another way to view the effects of environmental conditions on the Saco bridge decks is to more globally consider their bending and in-plane axial deformations. Curvatures can be conveniently used to look at the bending deformations of the decks, because they are easily visualized and can be readily calculated from the strains directly measured in the field. Curvatures and in-plane axial strains were calculated from the long term strain data following a similar procedure to that used with the live load test data (see Section 7.1.2). That is, the strains measured in the top and the bottom of the deck were used to establish a strain profile across the depth of the deck, from which curvature and axial in-plane strain were calculated. In this process, the transverse response of the decks under different thermal conditions was viewed in terms of two components:

1. The net change in average temperature across the depth of the decks was assumed to predominantly generate in-plane deformations.
2. The temperature gradient across the depth of the deck was assumed to primarily result in bending curvature of the decks, with a negative gradient (greater temperature at the top of the deck relative to the soffit) generating negative curvature.

Following this approach, typical bending and axial deformations of the bridge decks during diurnal temperature cycles were determined using the strain data from July 3, 2004 to July 5, 2004. These days were chosen for this analysis because of their even heating and cooling cycles which are generally representative of the bridge decks' daily behavior. These deformations are plotted from midnight on July 2 to midnight on July 4 in Figures 96, 97, and 98 for the conventional, empirical and high performance decks, respectively. The response shown is for a location in the decks three-quarters along the span, and midway between the girders (Location D 3 in Figure 14). Also shown in Figures 96, 97, and 98 are the average temperatures across the depth of the decks, as well as the temperature gradients, as a function of time. Note once again that deformations in the transverse direction were analyzed in this investigation due to the relatively simpler boundary conditions in the transverse compared to the longitudinal direction of the decks.
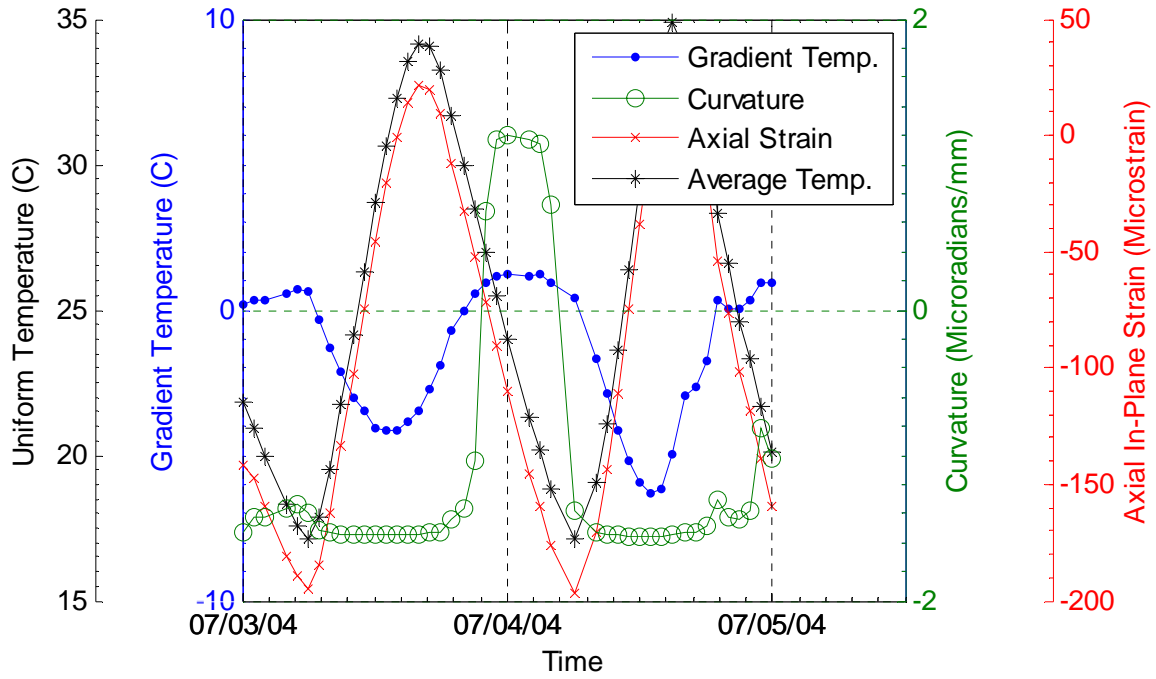
Figure 96: Conventional Deck Behavior at Location TV-D-3 (Total Response)
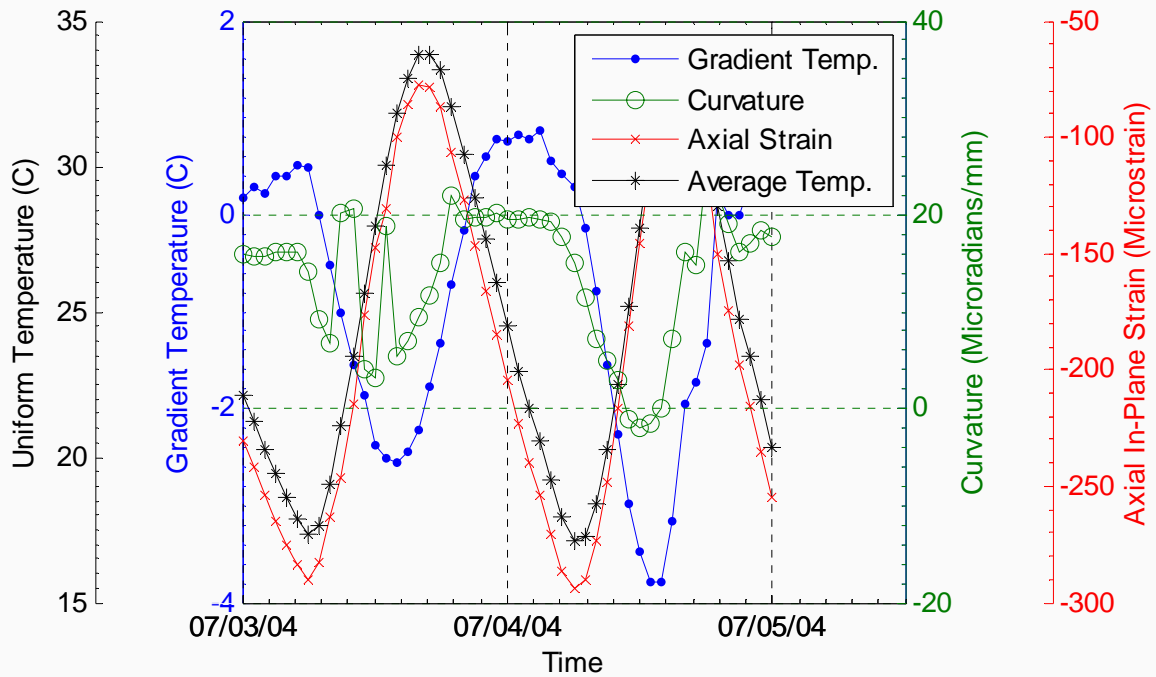
Figure 97: Empirical Deck Behavior at Location TV-D-3 (Total Response)
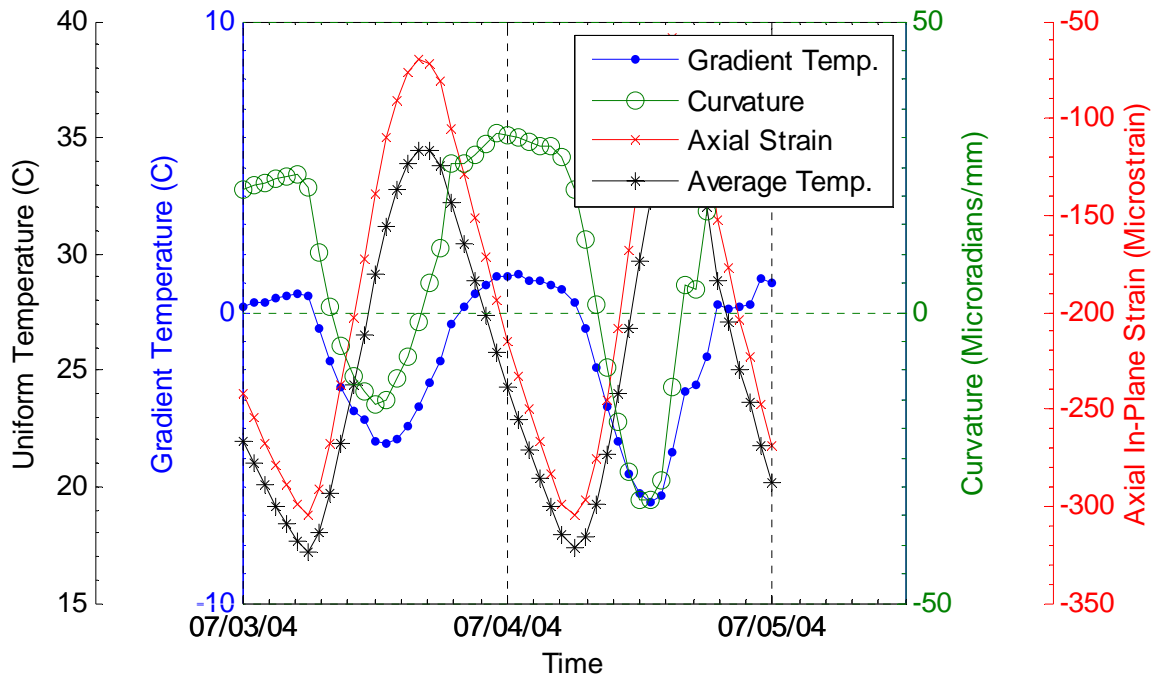
Figure 98: High Performance Deck Behavior at Location TV-D-3 (Total Response)

Referring to Figures 96 to 98, the deformations are remarkably similar in all three decks; therefore, the behavior of only one of the decks, specifically the Conventional deck (Figure Figure 96), will be discussed in detail below. Further, note that a more comprehensive view of the deck behavior in the transverse direction can be obtained by simultaneously looking at the data available at the face of a girder, as well as midway between the girders. The deformations of the conventional deck in the transverse direction at the face of a girder (location D-5 in Figure 15) are shown in Figure 99.
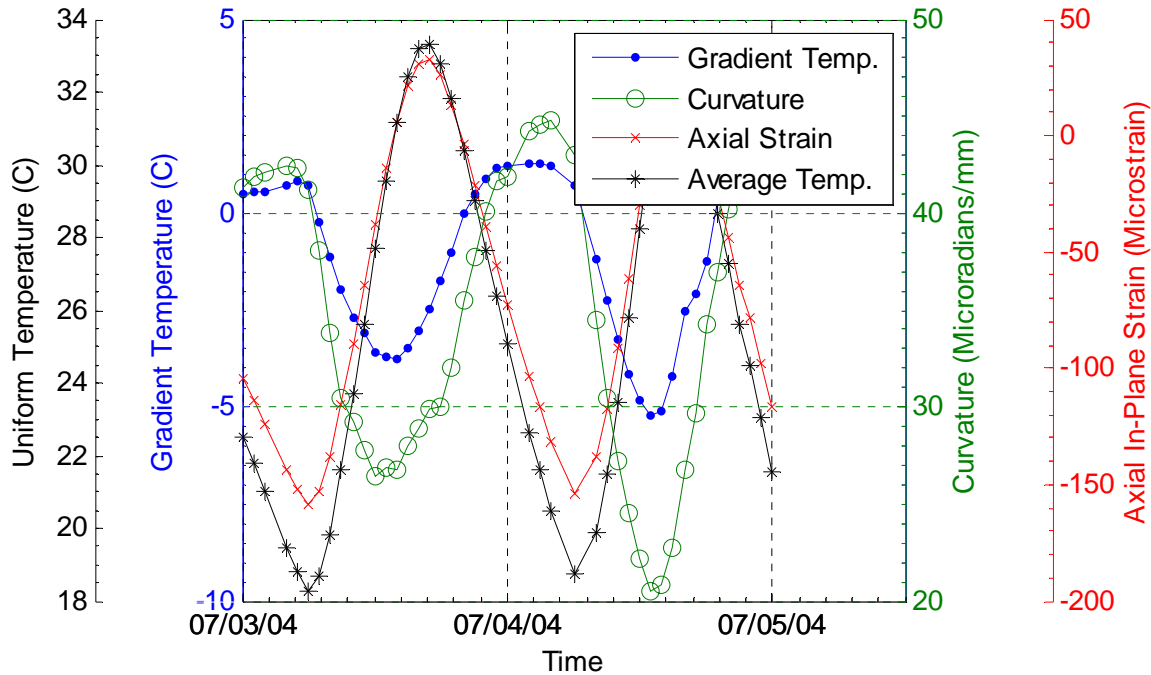
Figure 99: Conventional Deck Behavior at Location TV-D-5 (Total Response)

Referring to Figures 96 and 99, the average temperature in the deck is lowest in the early morning (approximately 5:00 AM), with a value of approximately 18 °C; it climbs during the day to a peak of approximately 34 °C in the late afternoon (approximately 4:00 PM). Note that the temperatures at the strain gage located in the middle of the span between the girders (Figure 96) are approximately one degree cooler at the low point and one degree higher at the high point than the temperatures at the face of the girder (Figure 99). This behavior results from the thermal mass of the girder nominally moderating the temperature extremes in the deck immediately adjacent to it.

The temperature gradient experienced by the deck also varies throughout the day. The gradient, less than 1 °C at 5:00 AM, becomes increasingly negative throughout the morning, as the top surface of the deck heats up more rapidly than the bottom surface. The peak negative gradient occurs around noon and is approximately -6 °C for the location within the deck span and is -4 °C at the face of the girder. The peak positive gradient temperature occurs near midnight, as the top surface of the deck cools more rapidly then the bottom surface, possibly because the girders and the ground below the bridge act as a heat sink, storing the day's heat and radiating it to the bottom of the deck in the evening.

Relative to the coincident deformations experienced by the deck under these thermal conditions, the total in-plane axial transverse strains are positive as the temperature increases, which is consistent with the deck expanding as the temperature increases. The magnitude of the

change in the strain as the temperature moves between its extreme values is approximately 215 µε for the location between the girders and 190 µε for the location at the face of the girder. This difference of 25 µε is due to the difference in the extreme temperatures at the two locations. The two degree difference in the extreme temperatures corresponds to a strain difference of 25 µε using a CTE of 12.5 µε/°C. Therefore, the in-plane response at the two locations under the thermal change is nearly identical.

The significance of the absolute magnitudes of the in-plane strains reported in Figures 96 through 99 is somewhat uncertain, as it is possible that some baseline shifts may have inadvertently occurred in the data as a result of some rewiring that had to be done for the data acquisition system. Nonetheless, the absolute strain magnitudes are uniformly negative, which is consistent with the expected unrestrained shrinkage of the deck concrete over time. Furthermore, the general level of the absolute strains is consistent with the magnitude of the shrinkage strain estimated by the AASHTO shrinkage equation.

The curvature deformations of the decks are consistent with the thermal gradients that they experienced. A negative temperature gradient in the middle of the day, for example, during which the top of the deck expands more than the bottom, corresponds with a negative curvature (see Figure 100). Correspondingly a positive temperature gradient in the evening during which the soffit of the deck expands more than the top, corresponds with a positive curvature (see Figure 101).
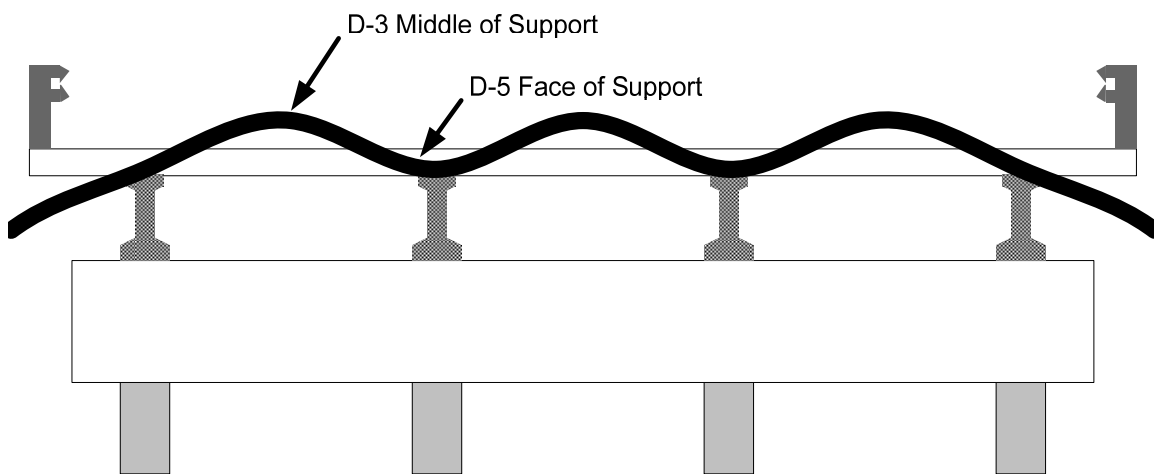
Figure 100: Expected Physical Bridge Deck Deformations (for a Negative Temperature Gradient)
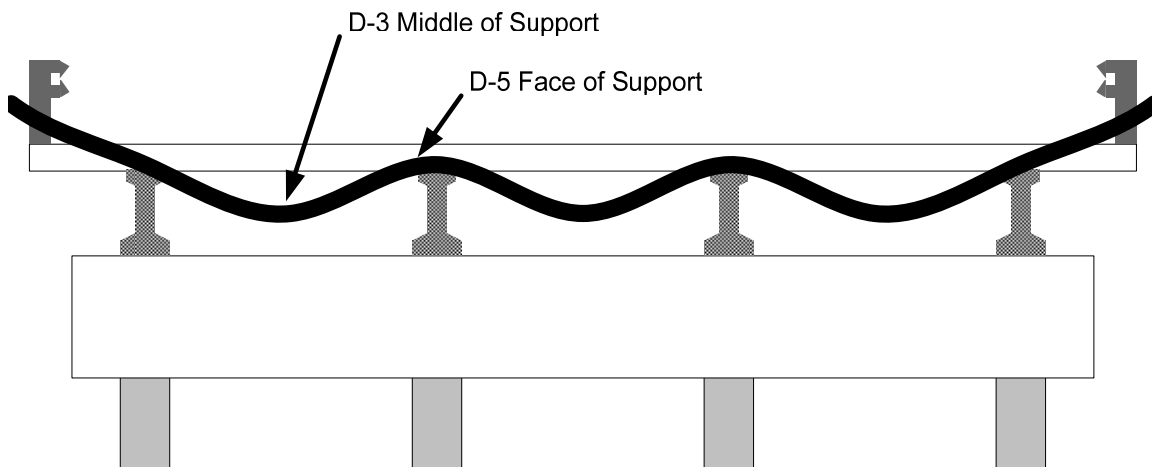
Figure 101: Expected Physical Bridge Deck Deformations (for a Positive Temperature Gradient)

One anomaly in this response is that the changes in curvature observed in the interior of the spans (between the girders) are in the same direction as the changes in curvature at the face of the girders. The deck was expected to act in the transverse direction somewhat like a continuous beam over several supports, with opposite curvatures in the interior of the spans relative to the curvatures at the supports (i.e., at the girders). One explanation for the observed response is that the expected point of contraflexure in the curvature occurs closer to the girders than the location of the strain gage at the face of the girders. In this case, the strain gages in the middle of the span and at the face of the girder would indicate the same direction of curvature. Relative to the absolute magnitudes of the reported curvatures, their significance is uncertain due to possible baseline shifts in the strain data. Nonetheless, the magnitude of the curvatures calculated at the location between the girders in the Conventional deck (see Figure 96) are dramatically smaller than those of the other curvatures (2.5 μκ/mm compared with an average value of 19 μκ/mm at other locations). One explanation for this apparent anomaly is that the deck has experienced some physical damage at this location, possibly cracking, that has interrupted the continuity of the structure. It may be possible that changes in curvature of this kind can be developed as an indicator of the occurrence of physical distress in the decks.

Close examination of Figures 96 and 99 reveals that the extreme deformation response occurs slightly ahead of the extreme temperatures in time. One possible explanation for this behavior is that the strain compatibility and strain boundary conditions are driven primarily by in-plane conditions in the longitudinal and transverse directions; while the thermal compatibility and thermal boundary conditions are primarily in the out-of-plane direction. Thus, the local bridge deformations are influenced by what is happening over a much larger area of the bridge, compared to the local absolute temperatures experienced in the decks. The significance of one occurring before the other is uncertain.

8.1.4 Summary of Long Term Strain Monitoring Observations

The three decks have experienced very similar temperature histories since they were cast two years ago. Therefore, differences seen in the internal strains measured in the decks as part of the long term monitoring program would be expected to result from the differences in their construction, rather than temperature differentials. The dimensional changes that the three bridge decks have experienced in response to the relative humidity (which results in drying shrinkage of the concrete) and changes in temperature (expansion and contraction of the concrete and the reinforcing steel) are well characterized in the long term strain data. In general, the decks are all responding the same, where this response consists of temperature related diurnal strain cycles superimposed on broader seasonal temperature related strain cycles, all of which are superimposed on basic long term shrinkage strains. The long term shrinkage strain in the decks ranged from 300 to 350 microstrain, with the lowest shrinkage strains occurring in the HPC deck. The shrinkage strains in the decks are generally consistent with the shrinkage strains observed in concrete samples cast at the time of deck construction. Changes in strain associated with temperature are as would be expected based on the coefficients of thermal expansion of the deck concretes. Deck curvatures and net in-plane strains generated from the strain data were useful in picturing the behavior of the decks under different temperature conditions, and they produced deflected deck shapes that were consistent with those expected.

With the exception of the behavior of the decks over the bents (where major transverse cracks occurred), no obviously significant differences in behavior between the decks were observed in the long term strain data. Such differences may develop with time, as the decks experience more distress. The ability of the instrumentation in the decks to reflect the presence of such distress in the decks was demonstrated using the changes in the longitudinal strain data in the Conventional deck when it cracked in the transverse direction over the bent. The occurrence of this crack was directly captured by the gage at his location, and it may further have influenced the longitudinal response recorded at other locations in this deck.

8.2 Corrosion Testing

Corrosion of reinforcing steel is a major concern with respect to the long-term durability of bridge decks. This corrosion is often associated with the migration of chloride ions from deicers into the deck concrete. However, the Saco bridge decks are expected to experience only nominal exposure to deicers over their service life. Chloride content and half-cell potential tests were conducted to provide benchmark data on these parameters. Half-cell potential tests were conducted on selected bars (and will only be valid for these bars, as epoxy coated reinforcement is being used in the bridges). Similar to the situation with corrosion of the reinforcing steel, carbonation is a possible deterioration mechanism of the concrete, but it is believed that this distress will not likely manifest itself until well into the future. Nonetheless, benchmark

carbonation tests were conducted throughout this research project in the event that unusual deterioration of the concrete was observed over the life of the decks.

8.2.1 Half-Cell Potential Tests

Half-cell tests measure the potential for corrosion in the embedded reinforcement within the bridge decks. This test is used to estimate the likelihood of corrosion activity at the time of the measurement, but does not provide any information on the rate of corrosion of the reinforcement. Corrosion of steel is an electrochemical process involving anodic (corroding) and cathodic (passive) areas of the metal. By measuring the electrical potential between the surface of the concrete and a standard reference electrode (the reinforcement), the presence and location of corrosion and its probable future development may be assessed. Corrosion probability determined from half-cell resistance measurements fall into one of three categories, as described in Table 36.

Table 36: Categories of Corrosion Probability for the Half-Cell Test

Category	Corrosion Probability
I	90% probability of no corrosion
II	an increasing probability of corrosion
III	90% probability of corrosion

ASTM C876 the "Standard Test Method for Half-Cell Potentials of Uncoated Reinforcing Steel in Concrete" (referenced in Appendix B) is intended to be used for uncoated rebar only, however, prior to pouring the bridge deck concrete, copper wire leads were connected to two transverse and two longitudinal bars in each deck to facilitate a direct connection with the epoxy-coated reinforcement (see Figure 102). The lead wires exit the concrete on the west side of the bridge decks. Normally, one of the wire leads can be connected to the guardrail or other metal object that is in contact with the embedded reinforcing mat, however, the epoxy coating insulates the reinforcing bars from one another, making it necessary to connect individual leads to each bar.
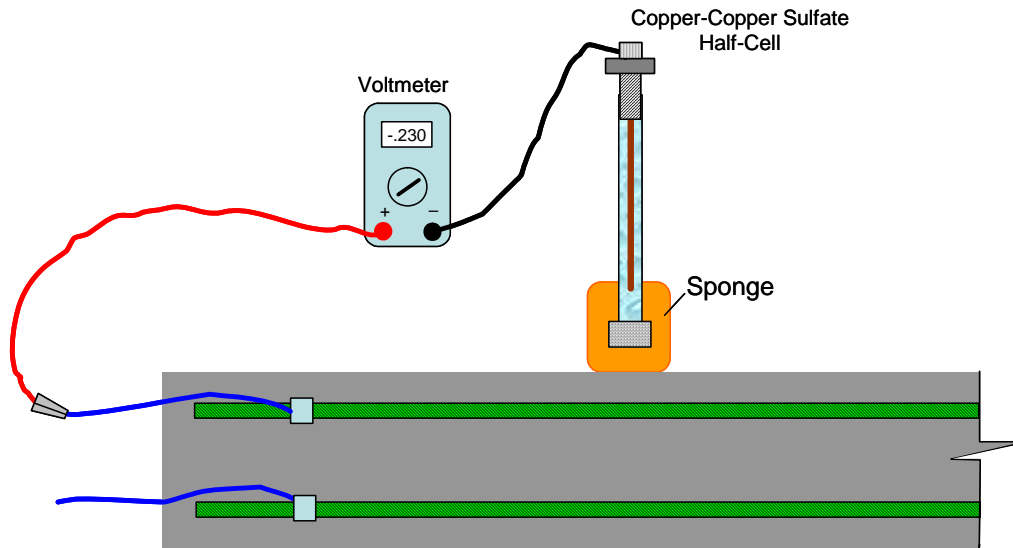
Figure 102: Illustration of Half-Cell Test on Saco Bridges

Half-cell potential readings were taken approximately one month after the decks were cast (July 2003) and at yearly intervals after that (July 2004 and July 2005). Tabulated results from these tests for each bridge are summarized in Appendix G. Results from the initial tests conducted in 2003 showed more corrosion potential than subsequent tests run in 2004 and 2005. This may be due to two factors: concrete hydration and deck sealant. Because the initial half-cell tests were run approximately one month after the decks were cast, the decks were hydrating at a higher rate then in the future. This meant that there was more free water available in the concrete to help make the electrical connection. In addition, the chemistry of the concrete during this higher hydration period may have affected the readings. Sealant applied to the deck surface may also have affected readings since the water solution used in the half-cell testing was not able to penetrate the surface to make the electrical connection. Nevertheless, very little potential for corrosion was measured using the half-cell test method.

8.2.2 Carbonation Tests

A solution of phenolphthalein ($Ca(OH)_2$), a colorless acid/base indicator that turns purple when the pH is above 9, was used to detect the presence of carbonation. When this solution is blotted on a sample of concrete and it turns purple (or a shade thereof), carbonation has not occurred. A concrete's resistance to carbonation is an indicator of its ability to protect embedded reinforcement from being penetrated by carbon dioxide which fuels corrosion. The pore microstructure of the concrete is how carbon dioxide penetration is facilitated.

Carbonation tests were conducted on the surface of all three bridge decks approximately one month after the decks were cast (July 2003) and at yearly intervals after that (July 2004 and July 2005). To conduct these tests, two areas of the deck were first cleaned using an abrasive pad to remove the outer layer of applied sealer. On each deck, one test was done in the wheel path and

one was done out of the wheel path. Once the area was blown free of dust, a dropper-full of phenolphthalein was blotted on the surface and allowed to absorb into the surface. In all cases, and at all times, the phenolphthalein turned purple which indicated that no significant carbonation had occurred at any of the locations on all three deck surfaces.

8.3   Visual Distress Surveys

The development of cracks, irregularities and delaminations in the bridge decks were monitored through periodic visual surveys of the surface and selected undersides of each bridge deck. Visual distress surveys of the top surface of the deck were comprehensive, but since access to the entire underside was impossible without the use of special equipment, only the north and south ends of the deck were examined (approximately one-third of each end span). Soundings, via a chain drag, were conducted to detect the presence of delaminations. During the site visit in July 2005, the bridge approaches were also examined. A schedule of the visual distress surveys conducted during the course of this project is provided in Table 37. Visual distress data were organized into the following categories: controlled transverse cracking over the bents, top-surface and full-depth cracking near the abutments, full-depth cracking in the cantilevered edges, hairline cracks on the underside, crazing and delaminations, and bridge approaches. Figures 103 and 104 show the results of the distress surveys for each of the bridges for 2004 and 2005, respectively. The subsections that follow describe these distresses in more detail. Additional detail (including additional photographic documentation) is provided in Appendix H.

Table 37: Date of Distress Surveys

Date of Crack Survey	Approximate Age of Bridge Decks (months)
July 2003	2
November 2003	5
March 2004	9
June 2004	12
July 2004[†]	13
July 2005[†]	25

[†]delamination survey also conducted using chain drag

Top Surface Crack
Through Thickness Crack
Bottom Hairline Cracks

a) Conventional Bridge – 2004

Evidence of crazing and
surface cracking

b) Empirical Bridge – 2004

Transverse Cracking in
Cantilevered Edge: Intermittent,
mostly on the southern end
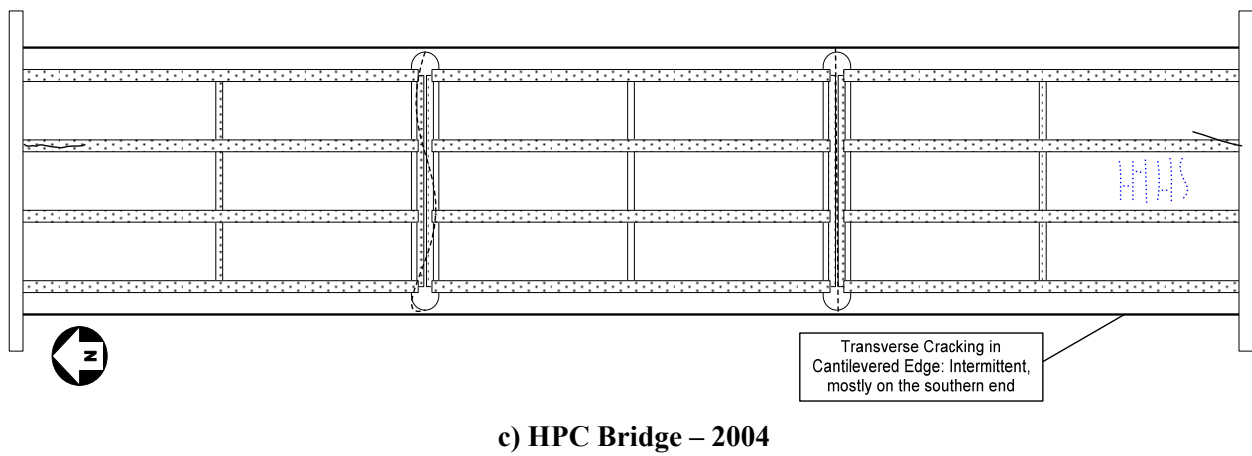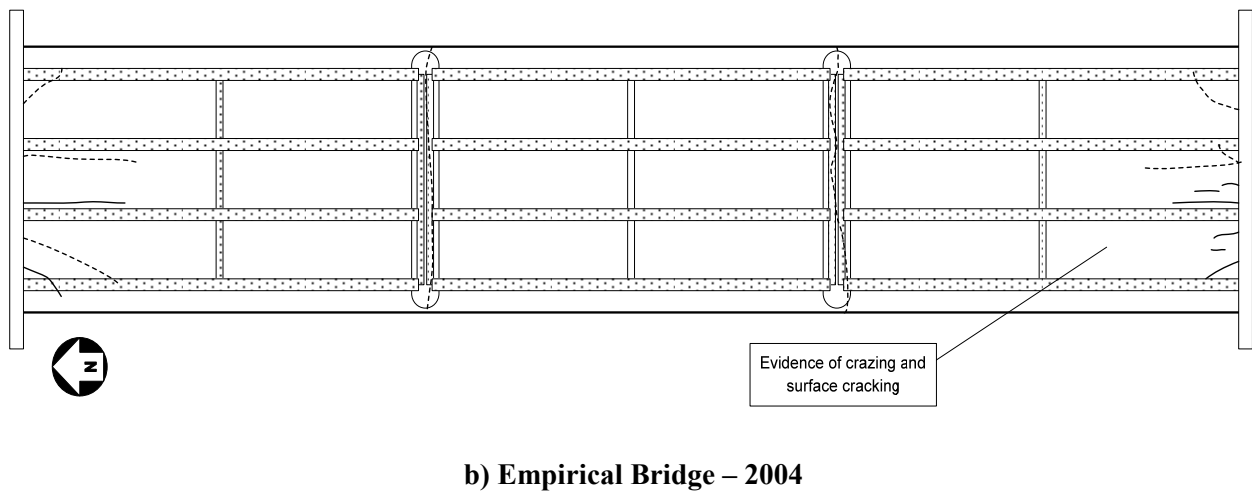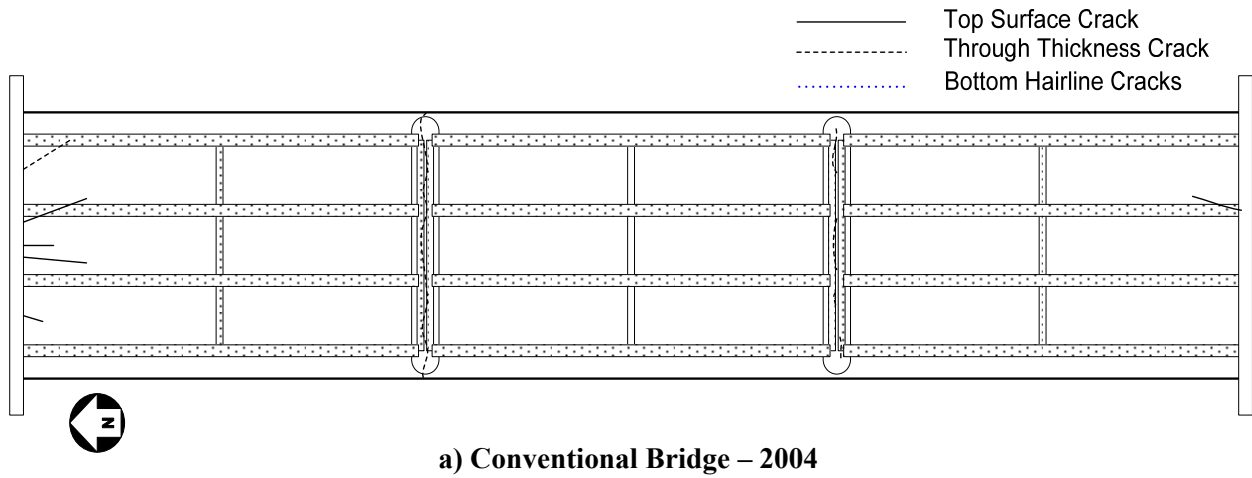
c) HPC Bridge – 2004

Figure 103: Distress Survey Maps of the Saco Bridges – 2004
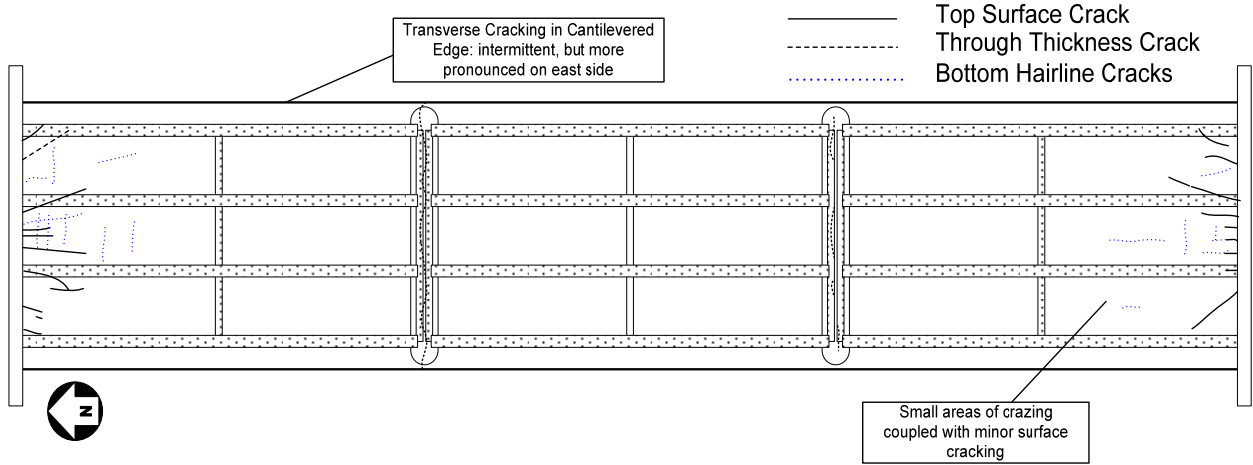
a) Conventional Bridge – 2005
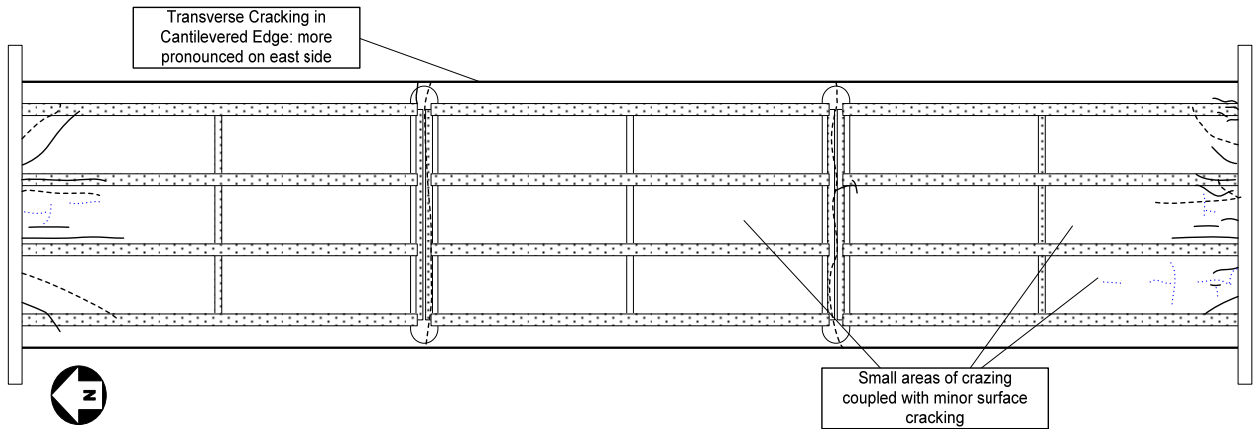
b) Empirical Bridge – 2005
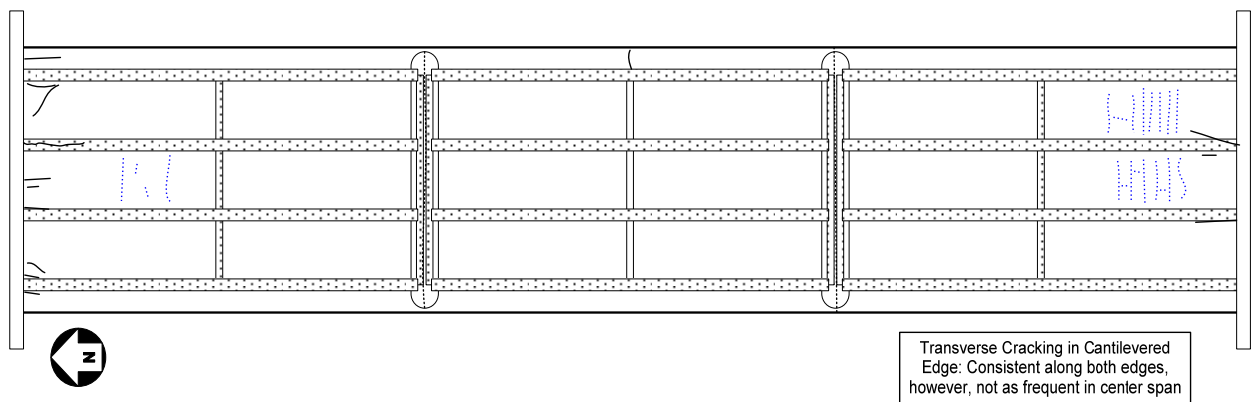
c) HPC Bridge – 2005

Figure 104: Distress Survey Maps of the Saco Bridges – 2005

8.3.1 Controlled Transverse Cracking over the Bents

The monolithic or continuous bridge decks are used to minimize problems that typically occur at the joints between adjacent deck slabs. By making the deck continuous across the bents or piers (where the girders are discontinuous), the need for frequent maintenance should be reduced. However, since transverse cracking in this region is expected, the area is saw-cut and sealed to control the location of the crack and to seal the crack from water migration. As expected, transverse cracks formed directly over the bents early in the life of all of the decks. Bent #2 (the southern-most interior bent) on each of the bridges was saw-cut to control the position of the anticipated crack over the bent. Bent #3 (the northern-most interior bent) was not saw-cut. This was done to study differences in performance between saw-cutting and letting the crack form naturally. However, the transverse cracks formed over Bent #2 in the Empirical and Conventional decks prior to saw-cutting, making the saw-cut and sealant ineffectual. Site visits soon after construction showed that these cracks were noticeably larger in the Empirical and Conventional decks than in the HPC deck. Portions of the cracks over Bent #3 (the unsawed bent) for each of the decks are shown in Figures 105, 106 and 107. Saw-cutting of Bent #2 on the HPC deck was done prior to crack formation, and the crack followed this channel. Even so, it is believed that Bent #2 on the HPC deck cracked at approximately the same time as the other bridges but went unnoticed due to the saw-cut and crack sealant. Two new sizeable cracks were detected near the bents in the Empirical deck during the 2005, and are likely a product of the high stresses experienced at that location.

Figure 105: Full-Depth Transverse Crack at Northern-Most Interior Bent – Conventional Deck

Figure 106: Full-Depth Transverse Crack at Northern-Most Interior Bent – Empirical Deck

Figure 107: Full-Depth Transverse Crack at Northern-Most Interior Bent – East HPC Deck

8.3.2 Top-Surface and Full-Depth Cracking Near the Abutments

Extensive surveys of the decks during site visits in July of 2004 and 2005 revealed top-surface and full-depth cracking near the bridge abutments. Top-surface cracks are those which are detectable from the top surface of the deck only, while full-depth cracks were detected and extended from both the top and bottom surfaces. In some cases, white precipitate had formed around cracks on the underside of the deck indicating that they were full-depth.   The Conventional deck had three sizable cracks on the north end, one of which was a full-depth crack. Only one top surface crack was detected near the south end. Many more top surface cracks were revealed during the visual distress survey conducted on the Conventional deck in 2005, most of which were small or hairline in nature. Throughout this evaluation the Empirical deck performed well, but showed more distress than the Conventional and HPC bridges. There were six sizeable, full-depth cracks and several smaller surface cracks on both ends of the Empirical deck in 2004. Fewer new cracks were revealed during the 2005 survey of the Empirical deck than in the Conventional and HPC decks. The HPC deck showed the least distress near the ends of the deck, having only one small crack on each end in 2004. Cracking near the north abutment had somewhat increased by summer 2005. Examples of top surface cracking near the northwest corners of each of the bridges are shown in Figures 108, 109 and 110. Note – cracks in most of the photographs were highlighted with a black marker to make them more visible.

Many of the cracks near the abutment radiate diagonally from the centerline of the bridges. This phenomenon is most prevalent in the Conventional and Empirical bridges, and was noticed early-on (March 2004) in the Empirical deck. Several of these diagonal cracks extend through the full depth of the concrete and, at times, into the abutment itself (Figures 111 and 112 for the Conventional and Empirical decks, respectively). A study conducted by Schmitt and Darwin (1995) concluded that bridges with integral abutments were approximately two to three times more likely to have these types of cracks near the abutment when compared to pin-end girders. This type of cracking often indicates inadequate design near the abutments which instigates flexural and drying shrinkage cracking.

8.3.3 Full-Depth Transverse Cracking in the Cantilevered Edges

Full-depth transverse cracking of the cantilevered edges (i.e., east and west overhangs) was first noticed in the HPC deck during the July 2004 site visit. These randomly spaced cracks were concentrated mostly on the southern end of the bridge and did not extend beyond the outer edge of the outside stringers. Edge cracking was not discovered in the Conventional and Empirical decks in 2004, but by July 2005, edge cracking was common in all three decks. The HPC and Conventional decks exhibited this type of cracking along both edges, while the Empirical deck only had a few cracks on the west edge and showed less edge cracking overall. Spacing of these cracks in the HPC deck is approximately 60 to 100 cm. Interestingly, edge cracking in all three decks was generally more pronounced on the east side of the deck when compared to the west. This phenomenon could be caused by differential solar heating effects in the two sides of the deck as the sun traverses the sky in the east-west direction relative to the north-south orientation of the decks.

Figure 108: Top-Surface Cracking at West Side of North Abutment – Conventional Deck

Figure 109: Top-Surface Cracking at West Side of North Abutment – Empirical Deck

Figure 110: Top-Surface Cracking at West Side of North Abutment – HPC Deck

Figure 111: Full-Depth Crack at Northeast Corner (shown from underside) – Conventional Deck

Figure 112: Full-Depth Crack at Northwest Corner (shown from underside) – Empirical Deck

8.3.4 Hairline Cracks on the Underside of Deck

A comprehensive survey of the underside of the bridge decks was not possible without special equipment. Approximately one-third of the length of the end spans was accessible from below the bridges. An effort was made to survey more of the undersides of each deck using binoculars, but this approach proved to be ineffective due to the poor light conditions and the flat angle of the observation relative to the deck surface. Nevertheless, hairline cracks were seen in the ends spans of each of the decks. The HPC deck was the first to show this distress in July 2004. Hairline cracks at that time were randomly spaced and less extensive than in 2005. Neither the Empirical nor the Conventional decks showed evidence of hairline cracking of the underside in 2004, although surface scaling on the bottom of these decks made detecting them difficult. Later evaluations revealed the presence of hairline cracks on each of these decks. Hairline cracking is most extensive in the HPC deck (Figure 113), followed by the Conventional

and Empirical decks, respectively. In general, these hairline cracks seemed to follow reinforcing bars in the bottom mat of reinforcement.

Figure 113: Hairline Cracking near South Abutment (shown from underside) – HPC Deck

8.3.5 Crazing and Delaminations

Mild crazing was first spotted in the Empirical deck during the July 2004 site visit. Crazing had become more evident when this deck was scrutinized in 2005. It appears that surface crazing is leading to hairline cracks in the deck surface. Crazing was detected in the Conventional deck in 2005, some of which also seem to be leading to hairline cracks. Crazing has not been detected in the surface of the HPC bridge deck. Soundings conducted using the chain drag revealed only one delamination in the Empirical deck in 2005. A small area adjacent to the crack near the southern-most interior bent is beginning to spall.

8.3.6 Bridge Approaches

Differential settlement of bridge approaches is a common problem. Excessive settlement can cause increased forces on the bridge as vehicle suspensions are dynamically excited by the resulting bump at the edge of the deck, although, little evidence of increased strains were detected from the high speed live load tests. During the final visit to the bridge site in July 2005, photos were taken of the bridge approaches to qualitatively assess their roughness (Figures 114, 115 and 116 for the Conventional, Empirical and HPC decks, respectively). A straight board was placed on the bridge deck and extended out over the paved approach adjacent to the bridge. Photos were taken from the side to illustrate the gap formed from the settlement of the paved approach. In general, these photos revealed that the HPC bridge had the least differential settlement in the north approach's wheel path, and that the Empirical bridge had the most differential settlement. The wheel path of the south approaches of the Conventional and Empirical bridges had settled less than the HPC bridge.

Figure 114: Paved Approaches of the Conventional Deck (NW-left, SE-right)

Figure 115: Paved Approaches of the Empirical Deck (NW-left, SE-right)

Figure 116: Paved Approaches of the HPC Deck (NW-left, SE-right)

8.3.7 Summary

Cracking in bridge decks is affected by a complex combination of numerous factors generally related to design, materials and construction. Visual distress monitoring of the Saco bridges over their short life has already revealed various types of cracking distresses, as discussed above. Overall, cracking behaviors are similar between the three bridges, yet show subtle differences. Comparison between the three decks generally indicates that cracking near the abutments and over the bents is most pronounced in the Empirical deck. The Conventional deck is performing similar to the Empirical deck, but the cracking is less acute. The HPC deck has not exhibited as much cracking near the abutments, however, edge cracking and underside hairline cracking are more pronounced on this deck. From the data collected thus far, it is anticipated that each of the decks will experience similar types of distresses and that differences between them will become more apparent as the bridge decks age.

8.4 Surveying

Global bridge movements were monitored by measuring relative changes in the elevation and the horizontal position of various points on the surface of each deck. Initial elevation and position measurements were made just prior to conducting the first set of live load tests, and were referenced from permanent points installed at the west side of the north abutments of each bridge during construction. Subsequent measurements were made during summer 2004 and 2005. Elevation measurements were made at 50 locations on each deck, namely, over the abutments, interior bents, and diaphragms of each bridge at the location of each stringer and between stringers in the instrumented areas of the decks. In the horizontal plane, 18 position measurements were made over the abutments, interior bents, and diaphragms of each bridge at the location of the exterior stringers. Elevation and position measurements also were made at the east and west ends of each abutment. Figure 117 shows where each of these measurements was made. Elevations were measured with an accuracy of approximately 1 millimeter, whereas the horizontal locations were measured with an accuracy of approximately 3 millimeters.
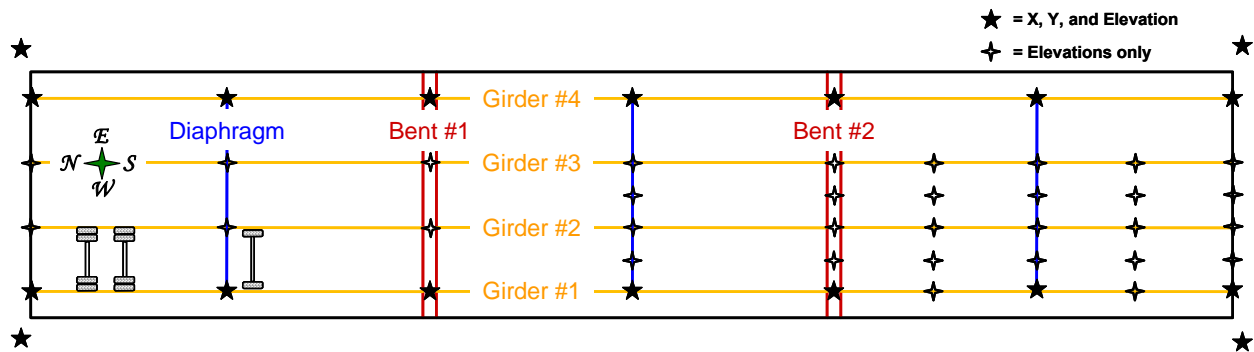
Figure 117: Survey Points Shown on Plan View of Bridge Deck

   Three-dimensional plots were created using the elevation and position data from all three bridges and all three years (Figures 118, 119 and 120 for the Conventional, Empirical and HPC decks, respectively). These plots show an exaggerated view of the surface elevation of the decks. Different colors are used for each year to highlight areas that potentially have changed. The crown of the deck is noticeable in each of these plots, and generally matches what was specified in the construction plans. Overall, the elevations of the three decks were very similar and did not exhibit significant changes over time. Of particular interest, however, are the longitudinal arches near the instrumented portion of the HPC bridge deck (southwest corner), which are presumed to correspond to the camber in the bridge girders. As discussed in Section 7.1.1.1, knowing this deck shape has helped explain unusual strain responses across the southernmost bent in the HPC deck.
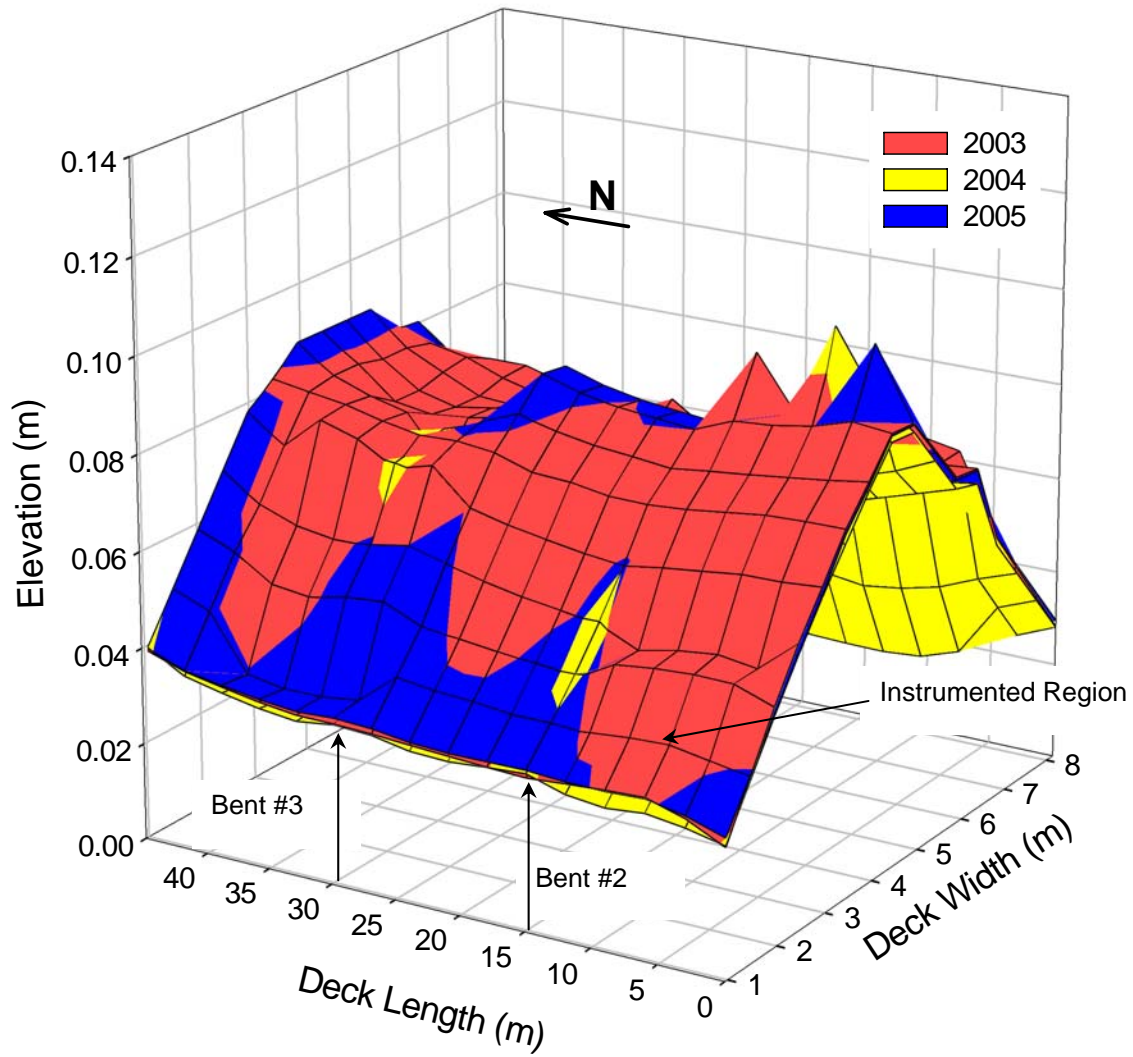
Figure 118: Topographic Map of Conventional Bridge Deck Surface
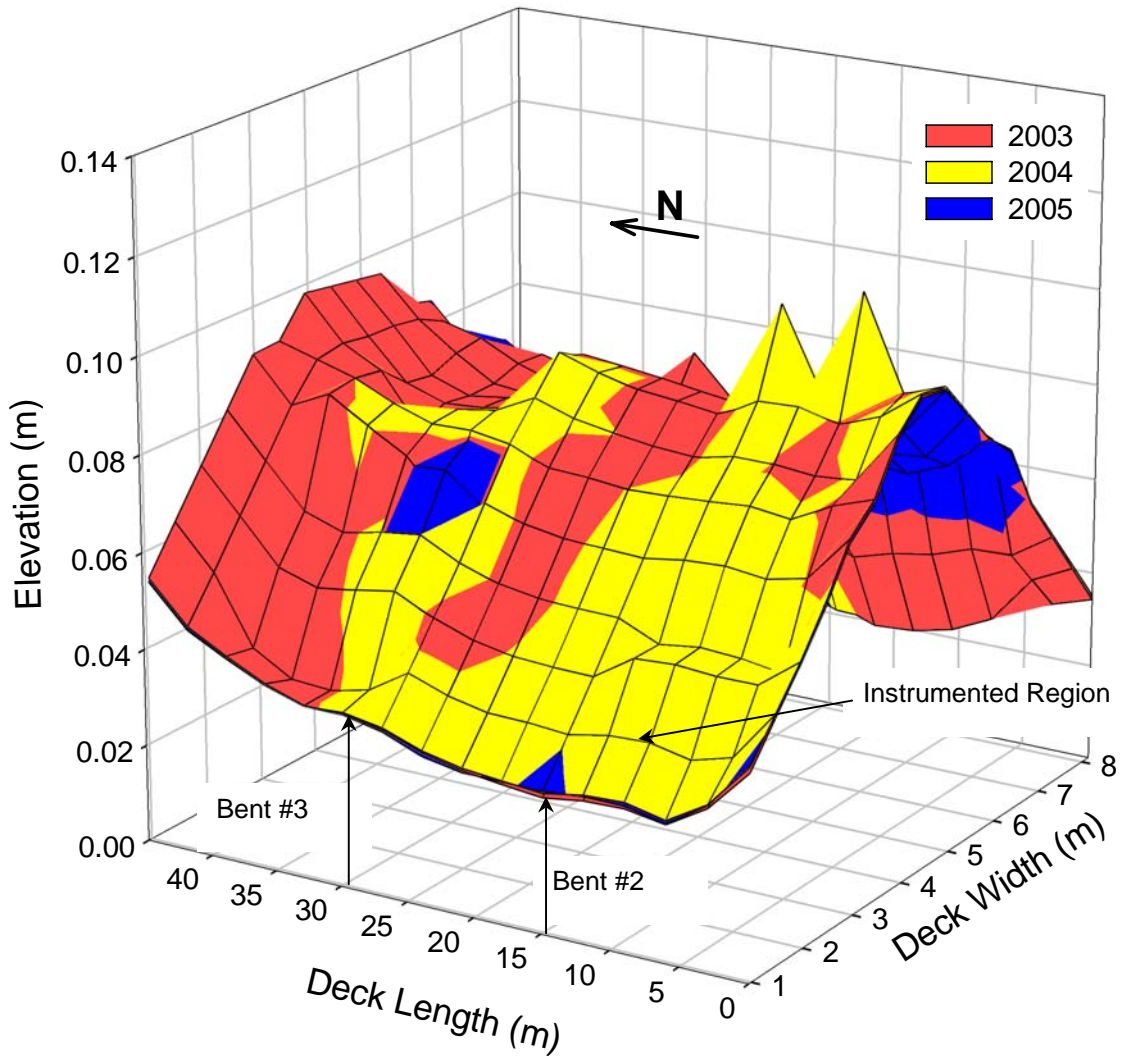
Figure 119: Topographic Map of Empirical Bridge Deck Surface
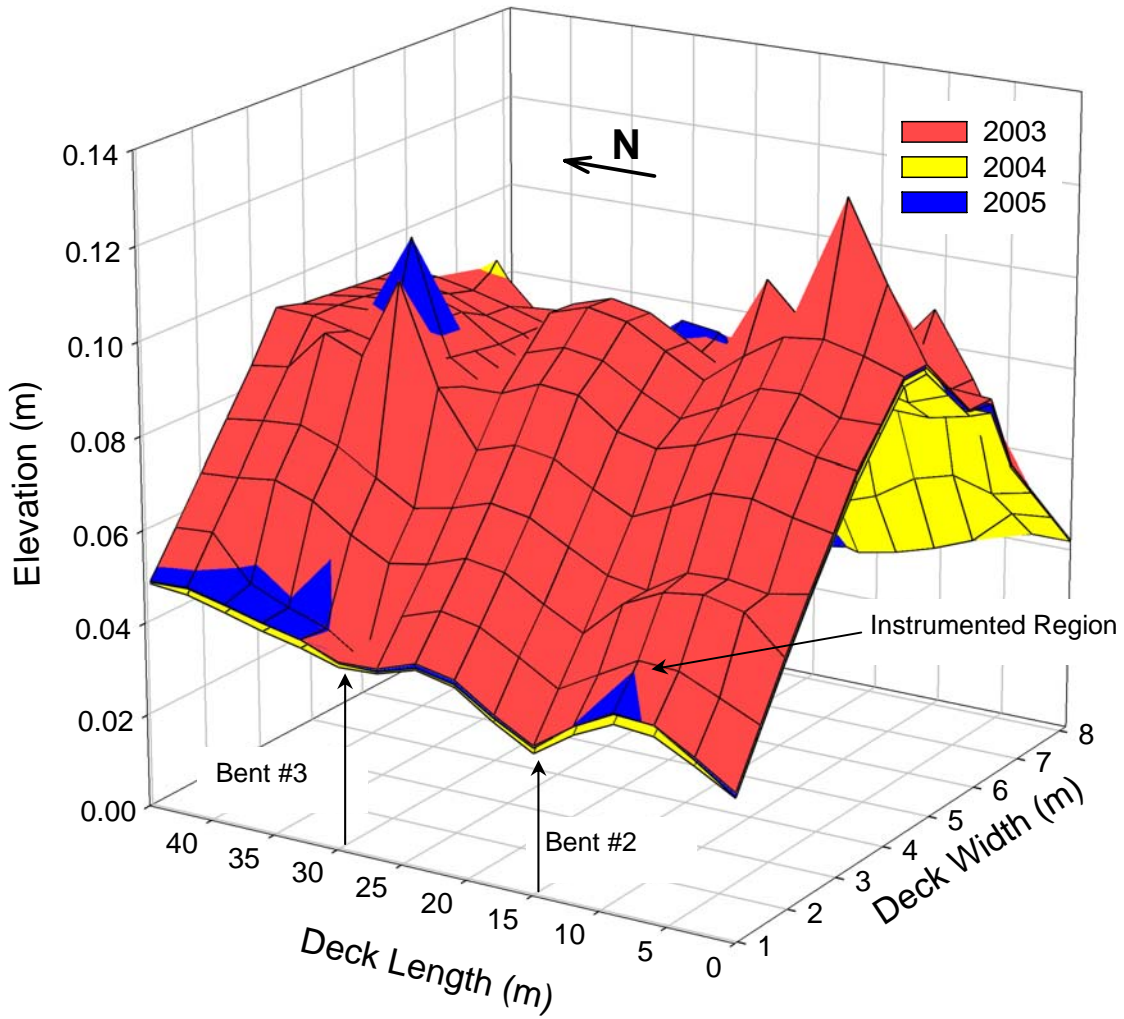
Figure 120: Topographic Map of HPC Bridge Deck Surface

9   COST ANALYSIS

To conduct a meaningful life-cycle cost analysis, construction, maintenance, repair and rehabilitation cost data are necessary. Unfortunately, many agencies have only just begun to track this information. Preliminary cost and performance information has been documented for the Saco bridge decks, and is discussed below.

As stated in the analysis section, data collected from the three bridges have revealed that each of the deck types is performing similarly; consequently, predicting disparities between life span or maintenance needs is purely speculative. Not surprisingly, all behaviors pertinent to long-term performance have not yet manifested themselves during the two-year monitoring period. Nevertheless, construction cost data was collected in the event that future distresses reveal distinct and quantifiable differences that would allow life-cycle costs to be determined. Costs were determined only for placement and materials (i.e., concrete and steel reinforcement) associated with the concrete bridge decks. No significant maintenance activities have been performed on the bridges since their construction. The construction costs shown in Table 38 are only slightly different between the bridges. The concrete for each of the bridges was bid at the same price ($450/m^3). The Empirical deck, however, used less reinforcement in its design, and thus resulted in a lower overall cost when compared to the Conventional and HPC decks.

Table 38: Construction and Maintenance Costs for the Saco Bridge Decks

Deck	Concrete	Steel	Maint.	Total
CON	$39,915	$17,757	$0	$57,672
EMP	$39,915	$12,257	$0	$52,172
HPC	$39,915	$17,757	$0	$57,672

The engineer's estimates for the cost of the bridge concretes (standard versus HPC) were not the same. These estimates were $625 and $725/m^3 for standard and high-performance concrete, respectively. Nationally, engineer's estimates for HPC, based on 2002 prices, typically range between approximately $450 and $700/m^3, respectively (FHWA, 2005). FHWA (2005) also provides examples that show clear differences in price between conventional and HPC concrete mixes. The first example was of a cast-in-place concrete wall that required 770 yd^3 of concrete. Cost estimates revealed that conventional concrete cost $57.30/yd^3 and HPC cost $60.76/yd^3. In-place costs for this type of project were actually lower for the HPC design, even though the cost of the concrete was higher, mainly because it was more efficient to construct. Another example was from a prestressed concrete plant. In this case, the HPC mix was more expensive than the traditional concrete ($78.38/yd^3 versus $55.53/yd^3). FHWA states that, overall, the cost of HPC concrete is approximately 20 percent higher than that of conventional concrete, however, many states justify the increased costs based on improvements in quality. Cost differences are influenced by numerous factors, and in some cases, fly-ash and slag components are equal or less

expensive than traditional cement, thereby making HPC mixes similarly priced to conventional mixes.

A national survey of state departments of transportation was conducted by the former AASHTO/SHRP Lead State Team in 1997. Results from this survey are reproduced in Table 39 to show how much HPC concretes cost when used in bridge decks.

Table 39: Cost Data of HPC Bridge Decks (adapted from FHWA, 2005)

State	Bridge Dimensions			Deck Concrete Cost	
	Length (ft.)	Main Span (ft.)	Width (ft.)	English units	Metric units
DE	81-120	81-120	49-56	$10/ft^2	$108/m^2
GA	---	---	---	$427/yd^3	$558/m^3
KY	301-400	81-120	49-56	$363/yd^3	$475/m^3
NE	181-240	80	>77	$511/yd^3	$668/m^3
NH	80	80	57-68	$545/yd^3	$713/m^3
NY	80-600	80-180	26-77	$21/ft^2	$226/m^2
TX	---	---	---	$9/ft^2	$97/m^2

In conclusion, the lack of cost and performance differences between the three Saco bridge decks makes a life-cycle cost analysis ineffectual. Future monitoring of the bridge decks, as well as costs and timing of costs associated with maintenance, repair and rehabilitation should be recorded to determine cost-benefit of each design type.

10 SUMMARY, CONCLUSIONS & RECOMMENDATIONS

The deterioration of bridge decks in Montana prompted the Montana Department of Transportation (MDT) to investigate possible solutions to mitigate this problem. Specifically, MDT was interested in evaluating procedures that reduce concrete cracking and corresponding steel corrosion resulting from corrosive agents accessing the steel via those cracks. Three new bridges with identical geometries being constructed near Saco, Montana within one mile of each other along the same roadway afforded an excellent opportunity for such an evaluation. The bridges were built by the same contractor and the decks were poured within two weeks of each other. The only difference between the three bridges was in the construction of the reinforced concrete deck. One bridge followed a conventional deck design, which is the typical design used by MDT, consisting of a standard concrete mix and reinforcement layout. The second bridge deck was designed according to the AASHTO empirical design methodology, which allows the volume of the steel to be reduced throughout the deck, but utilizes a standard concrete mix like the Conventional bridge deck. The third bridge deck was built using High Performance Concrete (HPC) coupled with the conventional reinforcement layout.

10.1 Summary

Prior to pouring the deck concrete on each bridge, a suite of strain and temperature sensors was installed in the decks to monitor their response under vehicle and environmental loads. This monitoring has been active for the past two years, during which two series of controlled live load tests have also been performed. The first set of live load tests were conducted in 2003, prior to opening the bridges to regular traffic. A series of eight low speed single-truck tests, five high speed single-truck tests, and two low speed two-truck tests was performed on each bridge. A second set of live load tests were conducted when the decks reached two years of age using the same test protocols as the first live load tests.

Strains recorded during the live load testing were analyzed to evaluate structural behaviors for each deck. Strain data recorded from longitudinally-oriented gages during these tests was analyzed to establish the validity of the measured response relative to expected direction and magnitude. Strains from transversely-oriented reinforcement gages were subsequently used to investigate deck behaviors unique to each deck design. This analysis investigated several aspects of the deck behavior, including longitudinal cracking, in-plane axial forces, deck integrity, relative deck stiffness, and general non-linear behaviors.

Long term monitoring at the bridges consisted of measuring internal deck strains and temperatures, assessing corrosion potential, conducting visual distress surveys, and detecting global movement of the bridge structures from topographic surveys. The data acquisition system was programmed to collect strain and temperature information from all of the embedded sensors on an hourly basis. All other effects were monitored through periodic visits to the bridge site.

The data available from the long term monitoring was studied in an effort to correlate changes in deck performance with the vehicle and environmental loads they experienced, and then further to evaluate the relative performance of the three types of decks. The primary "environmental" behaviors experienced by the decks are related to the dimensional changes that they have experienced due to changes in relative humidity (shrinkage of the concrete) and temperature (shrinkage and expansion of both the concrete and the reinforcing steel). A review and analysis of the strain data was performed, including an analysis of the associated deformations of the decks due to temperature changes.

10.2 Conclusions

The primary conclusion from the analysis of the live load data and long term monitoring is that all three bridge decks are behaving in a similar fashion. This conclusion was drawn from live load tests, long term monitoring, visual distress surveys, corrosion testing and other qualitative assessments of each of the bridge decks. Additional monitoring is needed to capture and explain differences if and when they arise.

The analysis of the live load test data revealed that the shape and magnitude of the strain response under vehicle loads matches expected behavior and is similar in the three decks. No evidence of concrete cracking in the deck was found from the analysis of the live load data. Particularly, there was no indication of cracking of the top of the decks over the girders, nor was there any indication that cracking will occur in the future over the girders due to vehicle loads. Neither was there any evidence that cracking had occurred in the bottom of the deck at the time of live load testing. Moreover, there was no evidence of non-linear behavior in any of the three decks, as determined by examining strains via superposition, implying that the decks are behaving linear-elastically.

Although the behavior of all three decks was similar in nearly all respects, a few nominal differences were observed between them. These differences are merely behavioral differences noted during the analysis, which do not necessarily reveal differences in the performance of each deck relative to long-term durability, cracking or corrosion. Longitudinal behavior over the bent was different between the three bridges, indicating differences between the three decks in the in-plane axial forces at this location.

Based on the analyses of the results of the live load tests, and the attendant comparisons between the results of the 2003 and 2005 tests, several conclusions can and were reached. The broad conclusions from the live load tests are that 1) all three decks continued to behave in a similar fashion, relative to each other, and 2) the behavior of each deck changed very little over time (2003 versus 2005). Differences in deck behavior by type and over time could not be discerned based simply on qualitative comparisons of the data collected from each bridge. Comparisons of the various quantitative measures of deck performance being considered in this

analysis generally confirmed the similarity in deck response. Some success was realized in correlating changes in these quantitative parameters for each deck over time with the attendant changes in the physical distresses in the decks. Notably, smaller changes in the quantitative response parameters between 2003 and 2005 generally corresponded to smaller changes in the physical damage experienced by the decks during this same interval. In making this observation, it is important to note that a) the observed changes in the quantitative response parameters were small in magnitude, and that b) only limited cracking has been seen in the decks to date. In the future as additional cracking occurs, the correlation between these quantitative parameters and physical distress may become more apparent. Based on changes in the internal strains experienced in the decks in the 2003 and 2005 live load tests, the behavior of the HPC deck was the most stable (unchanged) over this time interval, while the behavior of the Empirical deck was the least stable (most changed) over this interval. Additional observations and conclusions include:

- All measured tension strains were significantly below those levels that would be expected to cause cracking in the decks (average peak value of approximately 40 microstrain).

- The presence of in-plane axial forces in the decks in the transverse direction was inferred from the strain data from the Conventional and Empirical decks (this analysis could not be completed for the HPC deck due to instrumentation losses). These strains were below 10 microstrain in magnitude, with a greater mean strain occurring in the Empirical relative to the Conventional deck.

- All three decks exhibited similar stiffnesses and load flow behaviors, based on the GDFs experimentally determined for each bridge.

- Linear superposition worked well for all three bridge decks, indicating that all three decks were still behaving linear-elastically.

- Changes in the neutral axis position and GDFs for the Empirical bridge were consistent with a visual assessment of the change in its physical condition between 2003 and 2005. This same correlation between these quantitative behavior parameters and physical deck condition, however, was not as consistently seen for the Conventional and HPC decks. This situation may imply that physical changes have occurred in the HPC and Conventional decks, but that these changes are simply less apparent by visual examination of the decks.

- All three decks responded similarly regardless of the speed at which the live load was applied.

The long term strain data indicated that the decks were behaving as expected in the transverse direction with regard to curvature and strain while undergoing thermal loads. The only significant difference in the strain response between the Conventional, Empirical, and HPC bridge decks may be in the magnitude of the long term transverse contraction that they have experienced, which is believed to be shrinkage and/or restraint related. The contraction of the HPC deck in the transverse direction is approximately 80 percent of that observed in the

Conventional and Empirical decks (both being cast with the same conventional mix design), which is generally consistent with the underlying differences in the shrinkage behaviors of the HPC and standard concretes from which they were cast.

A laboratory investigation did show significant variations in the CTEs of deck concretes as a function of temperature. In general, CTE decreases as temperature decreases. This variation is believed to be related to behavior of the water in the concrete's nanostructure. Small differences were observed in the CTEs for the HPC and the standard deck concretes, particularly at lower temperatures.

Based on the long term strain analysis, the decks generally are all responding the same, where this response consists of temperature related diurnal strain cycles superimposed on broader seasonal temperature related strain cycles, all of which are superimposed on basic long term shrinkage strains. The long term shrinkage strain in the decks ranged from 300 to 350 microstrain, with the lowest shrinkage strains occurring in the HPC deck. The shrinkage strains in the decks are generally consistent with the shrinkage strains observed in concrete samples cast at the time of deck construction. Changes in strain associated with temperature are as would be expected based on the coefficients of thermal expansion of the deck concretes. Deck curvatures and net in-plane strains generated from the strain data were useful in picturing the behavior of the decks under different temperature conditions, and they produced deflected deck shapes that were consistent with those expected.

With the exception of the behavior of the decks over the bents (where major transverse cracks occurred), no obviously significant differences in behavior between the decks were observed in the long term strain data. Such differences may develop with time, as the decks experience more distress. The ability of the instrumentation in the decks to reflect the presence of such distress in the decks was demonstrated using the changes in the longitudinal strain data in the Conventional deck when it cracked in the transverse direction over the bent. The occurrence of this crack was directly captured by the gage at this location, and it may further have influenced the longitudinal response recorded at other locations in this deck.

Visual distress surveys of the Saco bridges over their relatively short life revealed various types of cracking distresses. Overall, cracking behaviors are similar between the three bridges, yet show subtle differences. Comparison between the three decks generally indicated that cracking near the abutments and over the bents is most pronounced in the Empirical deck, and that the cracking in the Conventional deck is similar but not as acute as that in the Empirical deck. The HPC deck has not exhibited as much cracking near the abutments as the other two decks, however, edge cracking and underside hairline cracking are more pronounced on this deck. From the data collected thus far, it is anticipated that each of the decks will experience similar types of distresses and that differences between them will become more apparent as the bridge decks age.

Corrosion monitoring using half-cell and carbonation tests, and topographic surveys were also used to evaluate differences in performance between the three bridge decks. Periodic corrosion monitoring indicated that the deck reinforcement and concrete had not shown potential for corrosion, nor did it reveal any differences between the decks. Based on topographic surveys of each of the bridge decks, the elevations of the three decks were very similar and did not exhibit significant changes over time.

The analysis presented herein generally serves as a baseline to establish the condition of the three bridges before prolonged demands from traffic and the environment. Should a follow-on project be initiated, data obtained from continued long-term monitoring and live load testing will likely provide a more complete body of evidence from which to make judgments about which deck design offers superior performance. Based on all of the information obtained to-date, the HPC deck potentially will offer the most cost effective performance of the three deck configurations, followed closely by the Conventional deck, and more distantly by the Empirical deck. This conclusion is primarily based on the relative visual distresses observed in the decks and on the relative stability of their behavior over time, as inferred from the live load strain data. In making this statement, it is important to recognize that, as is emphasized above; a) the differences in performance between the decks were small; b) the various pieces of evidence of their relative performance sometimes tell a conflicting story; and c) presently subtle differences in their performance could become significant in the future. Thus, this conclusion must be considered as "preliminary" in nature, until it can be confirmed (or refuted) based on additional study of the decks' performance over time.

10.3 Recommendations for Future Work

The extensive monitoring program carried out on the Saco bridges has resulted in the objectives of this project being attained. However, because the three bridges are relatively young, significant behavioral and performance differences between the decks are not clearly evident. Therefore, continued monitoring of these structures is recommended so that if and when these distresses appear, their cause and effect are well documented and understood. Four main activities are recommended to further study these structures: long-term monitoring, live load testing, finite element analysis and laboratory exploration. Each of these efforts is developed in greater detail below.

10.3.1 Long Term Monitoring

Long term monitoring is crucial to understand and quantify potential differences in the behavior of these three structures over time. Much more can be learned in the future by capitalizing on the instrumentation infrastructure and analytical methodologies already established. Equipment installed at the beginning of this project continues to work well, and continued maintenance of this equipment should ensure its longevity well into the future. Data

from these sensors can be analyzed in the same manner as previously outlined to determine behavioral differences over time. Other items that should be monitored over time are:

- visual distresses – to document the formation of cracks, delaminations, and settlement of the bridge approaches;
- half-cell and carbonation levels – to detect possible deterioration of the reinforcement and concrete;
- deck elevations – to monitor global movements of the structures;
- shrinkage (using samples cast with the deck) – to establish shrinkage strains within the decks; and
- maintenance costs – to evaluate the cost effectiveness of each deck type.

10.3.2 Live Load Tests

Live load tests are also vital to evaluate the performance and behavior of the decks under vehicle loading with the ultimate goal of quantifying crack potential, deck stiffness, and verifying superposition. It is recommended that live load tests be conducted in the future when the decks reach a certain age (say, 7 years old) or when there are significant changes in the deterioration or strain levels within the decks based on long term monitoring. By continuing to collect this information over time, even subtle changes in condition will be captured and documented. When more significant distress occurs, this data will help determine the cause of more significant distresses, if and when they occur.

10.3.3 Finite Element Modeling

This project has established baseline data of the behavior of the three decks. There are still many unknowns regarding the behavior of certain components of these bridges (e.g., the concentration of cracking near the integral abutments). Finite element analysis will help verify particular behaviors and/or measured responses thought to affect the overall performance of each bridge deck type.

10.3.4 Laboratory Studies

During the course of this research project, four other laboratory studies were conducted to evaluate certain aspects of material and deck performance in a controlled environment. In one laboratory study, a scale model of a transverse section of the bridge deck was built and instrumented with the same sensors as were used in the three bridges in Saco. This model was then subjected to static loads while each of the sensors was monitored. In addition, it was stored outside to experience daily and seasonal temperature cycles – similar to the Saco bridges. Further testing of this beam is necessary to evaluate transverse behaviors of the bridge decks in Saco, sensor drift and the effects of temperature on sensor function. A new climate controlled laboratory soon to be built at Montana State University will also allow this type of physical model to be tested at a variety of environments and temperatures.

Two other laboratory studies were conducted to evaluate the performance of the embedded instrumentation under cyclic temperature loads. Understanding the behavior of the sensors within various climates was necessary so that the data from the Saco bridges could be properly interpreted. Additional work is needed in this area to evaluate the long term performance of the instrumentation. This will verify the accuracy of future readings taken from sensors embedded in the bridge decks in Saco.

Lastly, an extensive laboratory study was conducted to determine the coefficients of thermal expansion of the three deck concretes. Additional work is needed to verify these results and to investigate other material properties that are relevant with respect to the overall performance of the Saco bridge decks.

10.3.5 Other Projects

Additional monitoring is needed to determine the cause of the cracking near the integral abutments of the Saco bridges. Additional sensors can be mounted on the deck near the abutments or attached to the abutments to measure strain and inclination. Ideally, a new project could be planned and executed to specifically look at integral abutment effects relative to traditional abutments. For such a project, a bridge could possibly be built with an integral abutment on one end, and a traditional abutment on the other end, so that traffic and environmental loads experienced by two different abutments would be the same. As may be obvious, an even better situation would be to identify and capitalize on another multiple bridge replacement project as was done for this study.

11 REFERENCES

AASHTO (1989), AASHTO Guide Specifications: Thermal Effects in Concrete Bridge Superstructures, American Association of State Highway and Transportation Officials, Washington D.C.

AASHTO (2000), LRFD Bridge Design Specifications, 2nd ed., American Association of State Highway and Transportation Officials, Washington D.C.

Amer, A., Arockiasamy, M., Shahawy, M. (1999). "Load Distribution of Existing solid Slab Bridges Based on Field Tests", Journal of Bridge Engineering, ASCE, Vol. 4, No. 3, August, 1999, pp. 189-193.

Bakht, B., Al-Bazi, G., Banthia, N., Cheung, M., Erki, M., Faoro, M., Machida, A.; Mufti, A.; Neale, K. And Tadros, G. (2000). "Canadian Bridge Design code Provisions for Fiber-Reinforced Concrete Bridges", Journal of Composites for Construction, ASCE, Vol. 4, No. 1, February, 2000, pp. 3-15.

Bakht, B. and Lam, C. (2000). "Behavior of Transverse confining Systems for Steel-Free Deck Slabs", Journal of Bridge Engineering, ASCE, Vol. 5, No. 2, May, 2000, pp. 139-147.

Bakht, B. and Mufti, A. A. (1998). "Five Steel-Free Bridge Deck Slabs in Canada", Structural Engineering International, March 1998, pp. 196-200.

Berwanger, Carl. (1971). The Modulus of Concrete and the Coefficient of Expansion of Concrete and Reinforced Concrete at Below Normal Temperatures. Temperature and Concrete SP 25-8. Detroit, Michigan: American Concrete Institute.

Buckler, J.; Barton, F.; Gomez, J.; Massarelli, P.; and McKeel Jr., W. "Effect of Girder Spacing on Bridge Deck Response," Virginia Transportation Research Council, 2001.

Cao, L., Allen, J.H., Shing, P.B. and Woodham, D; "A Case Study of Concrete Deck Behavior in a Four-Span Prestressed Girder Bridge: Correlation of Field Tests and Numerical Results," Report No. CDOT-CU-R-94-8, Colorado Department of Transportation, April 1994.

Cao, L. (1996). "Analysis and Design of Slab-on-Girder Highway Bridge Decks", PhD Dissertation. University of Colorado, August, 1996.

Carrier, R.E. and Cady, P.D. (1973), "Deterioration of 249 Bridge Decks", HRR 423, Transportation Research Board, National Research Council, Washington, D.C.

Csagoly, P. F. and Lybas J. M. (1989). "Advanced Design Method for Concrete Bridge Deck Slabs", Concrete International, May, 1989, pp. 53-63.

Darwin, D. (2002), "Proposal for: Construction of Crack Free Concrete Bridge Decks", TPF-5(051), Transportation Pooled Fund Program, Federal Highway Administration, Washington, D.C.

Fang, I. K., Worley, J., Burns, N. H., and Klingner, R. E. (1990). "Behavior of Isotropic R/C Bridge Decks on Steel Girders", Journal of Structural Engineering, ASCE, Vol. 116, No. 3, March 1990, pp. 659-678.

Federal Highway Administration (2005), "High Performance Concrete Structural Designers' Guide", FHWA Publication No. FHWA-ERC-02-006, March 2005.

Fenwick, R. C. and Dickson, A. R. (1989). "Slabs Subjected to Concentrated Loading", ACI Structural Journal, V. 86, No. 6, Nov-Dec 1989, pp. 673-678.

Gopalaratnam, V. S. and Shah, S. P. (1985). "Softening Response of Plain Concrete in Direct Tension", ACI Journal, May-June, 1985, pp. 310-323.

Hammer, T.A. and E. J. Sellevold. (1990). Frost Resistance of High-Strength Concrete. High-Strength Concrete, Second International Symposium, 1990, Stavanger, Norway; Ed. by W.T. Hester; American Concrete Institute, Detroit, MI, pp 457-487. (ACI SP-121)

Hughes, G., Smith, J. S. C., and Kanagasundaram, S. (2000). "Remote Monitoring of Bridge Decks", Concrete Engineering International, May 2000, pp. 46-49.

Imbsen, R.A.; D.E. Vandershaf; R.A. Schamber and R.V. Nutt. (1985). National Cooperative Highway Research Program Report 276: Thermal Effects in Concrete Bridge Superstructures, Washington, D.C. Transportation Research Board, 1985.

James, R.; Zimmerman, R.; and McCreary, C. (1987), "Effects of Overloads on Deterioration of Concrete Bridges", TRR 1118, Transportation Research Board, National Research Council, Washington, D.C.

Johnson, J. (2005), "Concrete Bridge Deck Behavior under Thermal Loads", Thesis submitted to Montana State University for the fulfillment of a Master's degree in Civil Engineering, Bozeman, Montana.

Kosmatka, S. H.; B. Kerkoff; and W. C. Panarese. (2002). Design and Control of Concrete Mixtures. 14th ed. United States: Portland Cement Association.

Lenett, M. S., Hunt, V. J., Helmicki, A. J., and Aktan, A. E. (2001). "Instrumentation, Testing, and Monitoring of a Newly Constructed Reinforced Concrete Deck-on-Steel Girder Bridge – Phase III", Report # UC-CII 01/1, Cincinnati Infrastructure Institute, May 2001.

Lindquist, W.; Darwin, D.; and Browning, J. (2005), "Cracking and Chloride Contents in Reinforced Concrete Bridge Decks", SM Report No. 78, University of Kansas Center for Research, Inc., Lawrence, KS.

Mehta, K. P. (1986). Concrete: Structure, Properties, and Materials. United States: Prentice-Hall.

Mourad, S. and Tabsh, S. W. (1999). "Deck Slab Stresses in Integral Abutment Bridges", Journal of Bridge Engineering, ASCE, Vol. 4, No. 2, May, 1999, pp. 125-130.

Nassif, H., Suksawang, N., Gindy, M., Abu-Amra, T., and Davis, J. (2003). "Instrumentation and Field Testing of the Doremus Avenue Bridge", Compendium of Papers CD-ROM of the 82nd Annual Meeting of the Transportation Research Board, January 12-18, 2003, Washington, D. C.

Powers, T. C. and T. L. Brownyard. (1947). *Studies of the Physical Properties of Hardened Portland Cement Paste.* Journal American Concrete Institute. (October 1946 – April 1947)

Pyć, W., Weyers, R. E., Weyers, R. M., Mokarem, D., Zemajtis, J., Sprinkel, M., and Dillard, J. (2000), "Field Performance of Epoxy-Coated Reinforcing Steel in Virginia Bridge Decks", VTRC 00-R16, Virginia Transportation Research Council, Charlottesville, VA.

Ramakrishnan, V. and Sigl, A. (2001), "Evaluation of High Performance Concrete in Four Bridge Decks as well as Prestressed Girders for Two Bridges", Study SD98-06, South Dakota Department of Transportation, Pierre, SD.

Russell, H. (2004), "Concrete Bridge Deck Performance", NCHRP Synthesis of Highway Practice, Report 333, Transportation Research Board, National Research Council, Washington, D.C.

Sargent, D. D., Ventura, C. E., Mufti, A. A., and Bakht, B. (1999). "Testing of Steel-Free Bridge Decks", Concrete International, August, 1999, pp. 55-61.

Schmitt, T.R., and Darwin, D. (1995). "Cracking in Concrete Bridge Decks," SM Report Number 39, The University of Kansas Center for Research, Inc., Lawrence, Kansas, 151 pp.

Shah, S. P. and S. H. Ahmad. (1994). "High Performance Concrete: Properties and Applications." New York: McGraw-Hill.

Stallings, J. M. and Porter, P. (2002), "Live Load Tests of Alabama's HPC Bridge", TE-036 Report, ALDOT Research Project 930-373, Auburn University Highway Research Center.

Tabsh, S. W. and Tabatabai, M. (2001). "Live Load Distribution in Girder Bridges Subject to Oversized Trucks", Journal of Bridge Engineering, ASCE, Vol. 6, No. 1, January/February, 2001, pp. 9-16.

Wang, C. K. and Salmon, C. G. (1985). Reinforced Concrete Design (4th Ed.). New York: Harper and Row.

Yang, Y. and Myers, J. J. (2003). "Live Load Test results of Missouri's First High Performance Concrete Superstructure Bridge", Paper No. 03-3717, Compendium of Papers CD-ROM of the 82nd Annual Meeting of the Transportation Research Board, January 12-18, 2003, Washington, D. C.

Zia, P.; S. Ahmad, and M. Leming. (1997) "High-Performance Concretes: A State-of-the-Art Report (1989-1994)." Turner Fairbanks Highway Research Center Report: FHWA-RD-97-030. http://tfhrc.gov/structur/hpc/hpc2/contnt.htm.

Zokaie, T., T.A. Osterkamp, R.A. Imbsen. (1991) "Distribution of Wheel Loads on Highway Bridges," NCHRP Report 12-2611, TRB, National Research Council, Washington, D.C.

Appendix A – Deck Concrete Material Properties

Table A-1: Concrete Summary Data for All Decks from MDT

Sample #	Bridge Location	Sample Location	Date Cast	Cement Brand	Cement Type	Bin & Grind No.	Air Content (%)	Slump (in.)	Date Tested	Age (days)	Strength (psi)	Load (lbs)
1HPC11	11+57.24	11+44	5/28/2003	Holnam	HPC-GU	T-476	5.0	5.5	6/5/2003	8	5947	168,147
2HPC11	11+57.24	11+44	5/28/2003	Holnam	HPC-GU	T-476	5.0	5.5	6/25/2003	28	8267	233,744
3HPC11	11+57.24	11+44	5/28/2003	Holnam	HPC-GU	T-476	5.0	5.5	6/25/2003	28	8267	233,744
4HPC11	11+57.24	11+72	5/28/2003	Holnam	HPC-GU	T-476	5.2	7.75	6/5/2003	8	5221	147,620
5HPC11	11+57.24	11+72	5/28/2003	Holnam	HPC-GU	T-476	5.2	7.75	6/25/2003	28	7542	213,245
6HPC11	11+57.24	11+72	5/28/2003	Holnam	HPC-GU	T-476	5.2	7.75	6/25/2003	28	7252	205,045
1SD16	16+81.74	16+72	6/2/2003	Holnam	1-2	T-524	6.5	3.25	6/11/2003	9	3481	98,423
2SD16	16+81.74	16+72	6/2/2003	Holnam	1-2	T-524	6.5	3.25	6/30/2003	28	4641	131,221
3SD16	16+81.74	16+72	6/2/2003	Holnam	1-2	T-524	6.5	3.25	6/30/2003	28	4641	131,221
4SD16	16+81.74	16+95	6/2/2003	Holnam	1-2	T-524	6.5	4.0	6/11/2003	9	3626	102,523
5SD16	16+81.74	16+95	6/2/2003	Holnam	1-2	T-524	6.5	4.0	6/30/2003	28	4931	139,421
6SD16	16+81.74	16+95	6/2/2003	Holnam	1-2	T-524	6.5	4.0	6/30/2003	28	4931	139,421
7SD19	19+23.24	19+19	6/5/2003	Holnam	1-2	T-524	6.4	3.0	6/12/2003	7	3626	102,523
8SD19	19+23.24	19+19	6/5/2003	Holnam	1-2	T-524	6.4	3.0	7/3/2003	28	5221	147,620
9SD19	19+23.24	19+19	6/5/2003	Holnam	1-2	T-524	6.4	3.0	7/3/2003	28	5076	143,521
10SD10	19+23.24	19+39	6/5/2003	Holnam	1-2	T-524	6.1	3.25	6/12/2003	7	4351	123,022
11SD19	19+23.24	19+39	6/5/2003	Holnam	1-2	T-524	6.1	3.25	7/3/2003	28	5802	164,048
12SD19	19+23.24	19+39	6/5/2003	Holnam	1-2	T-524	6.1	3.25	7/3/2003	28	5802	164,048

Table A-2: Concrete Cylinder Summary Data for Conventional Deck from WTI

Truck	Specimen Number	Specimen Type	Size (in)	Curing	Test Type	Time to Test	Age (days)	Stress (psi)	Stress (Mpa)	Notes:
C-4	1C	cylinder	6x12	moist	compression	28 days	28	4,910	33.9	
	2C	cylinder	6x12	moist	compression	28 days	28	4,853	33.5	See Figure A-1
	3C	cylinder	6x12	moist	compression	28 days	28	4,743	32.7	See Figure A-1
	4C	cylinder	6x12	with deck	compression	live load 1	61	5,711	39.4	
	5C	cylinder	6x12	with deck	compression	live load 1	61	5,929	40.9	See Figure A-2
	6C	cylinder	6x12	with deck	compression	live load 1	61	6,210	42.8	See Figure A-2
	7C	cylinder	6x12	with deck	compression	live load 2	806	6,020	41.5	
	8C	cylinder	6x12	with deck	compression	live load 2	847	6,412	44.2	See Figure A-3
	9C	cylinder	6x12	with deck	compression	Remaining				
C-5	1C	cylinder	6x12	with deck	compression	live load 1	61	4,750	32.8	
	2C	cylinder	6x12	with deck	compression	live load 1	61	5,293	36.5	See Figure A-2
	3C	cylinder	6x12	with deck	compression	live load 2	806	5,390	37.2	
	4C	cylinder	6x12	with deck	compression	live load 2	847	5,071	35.0	See Figure A-3
C-6	1C	cylinder	6x12	moist	compression	28 days	28	4,757	32.8	
	2C	cylinder	6x12	moist	compression	28 days	28	4,661	32.1	See Figure A-1
	3C	cylinder	6x12	moist	compression	28 days	28	4,569	31.5	See Figure A-1
	4C	cylinder	6x12	with deck	compression	live load 1	61	5,332	36.8	
	5C	cylinder	6x12	with deck	compression	live load 1	61	5,622	38.8	See Figure A-2
	6C	cylinder	6x12	with deck	compression	live load 1	61	5,362	37.0	See Figure A-2
	7C	cylinder	6x12	with deck	split cylinder	live load 1	61	796	5.5	
	8C	cylinder	6x12	with deck	split cylinder	live load 1	61	817	5.6	See Figure A-2
	9C	cylinder	6x12	with deck	split cylinder	live load 1	61	882	6.1	See Figure A-2
	10C	cylinder	6x12	with deck	compression	live load 2	806	5,965	41.1	
	11C	cylinder	6x12	with deck	compression	live load 2	806	5,793	39.9	
	12C	cylinder	6x12	with deck	compression	live load 2	847	5,855	40.4	See Figure A-3
	13C	cylinder	6x12	with deck	split cylinder	live load 2	806	848	5.8	
	14C	cylinder	6x12	with deck	split cylinder	live load 2	806	734	5.1	
	15C	cylinder	6x12	with deck	split cylinder	Remaining				
C-7	1C	cylinder	6x12	moist	compression	28 days	28	4,655	32.1	
	2C	cylinder	6x12	moist	compression	28 days	28	3,967	27.4	See Figure A-1
	3C	cylinder	6x12	moist	compression	28 days	28	4,184	28.8	See Figure A-1
	4C	cylinder	6x12	with deck	split cylinder	live load 1	61	706	4.9	
	5C	cylinder	6x12	with deck	split cylinder	live load 1	61	845	5.8	
	6C	cylinder	6x12	with deck	split cylinder	live load 1	61	868	6.0	
	7C	cylinder	6x12	with deck	compression	live load 2	806	6,265	43.2	
	8C	cylinder	6x12	with deck	compression	live load 2	847	6,047	41.7	See Figure A-3
	9C	cylinder	6x12	with deck	compression	Remaining				
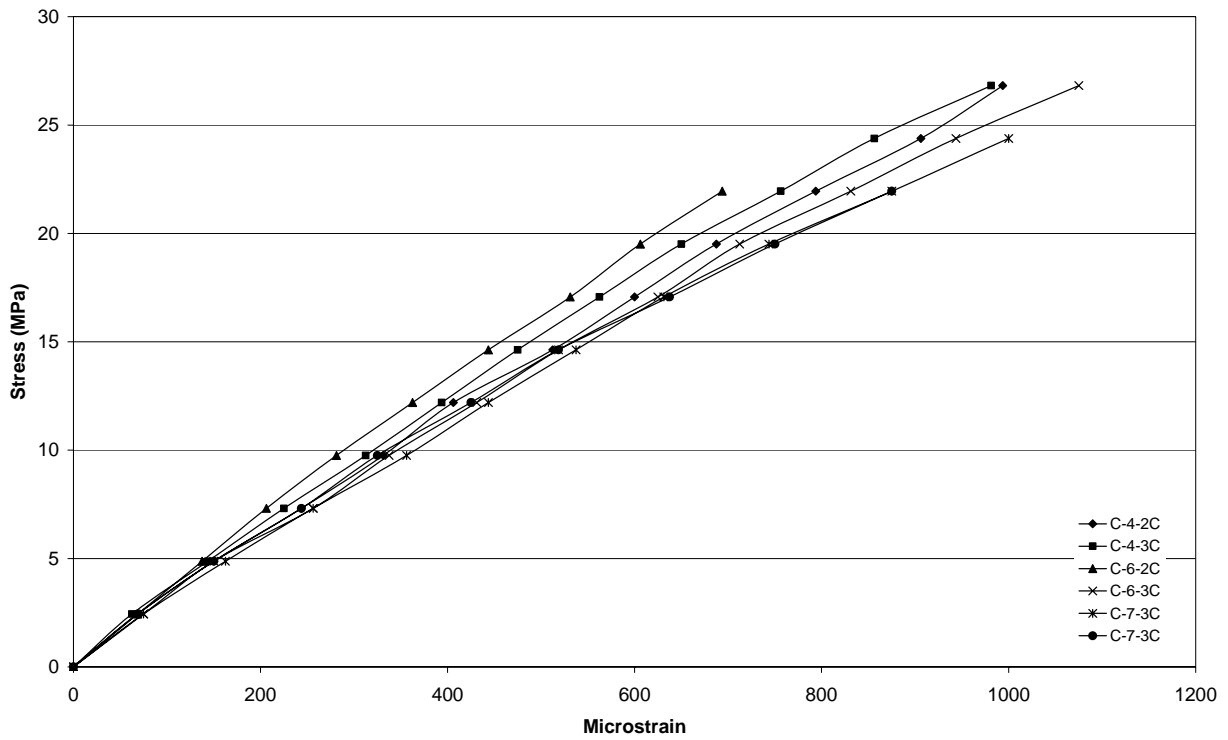
Figure A-1: Concrete Stress/Strain Plots for the Conventional Bridge Deck (28-Day)
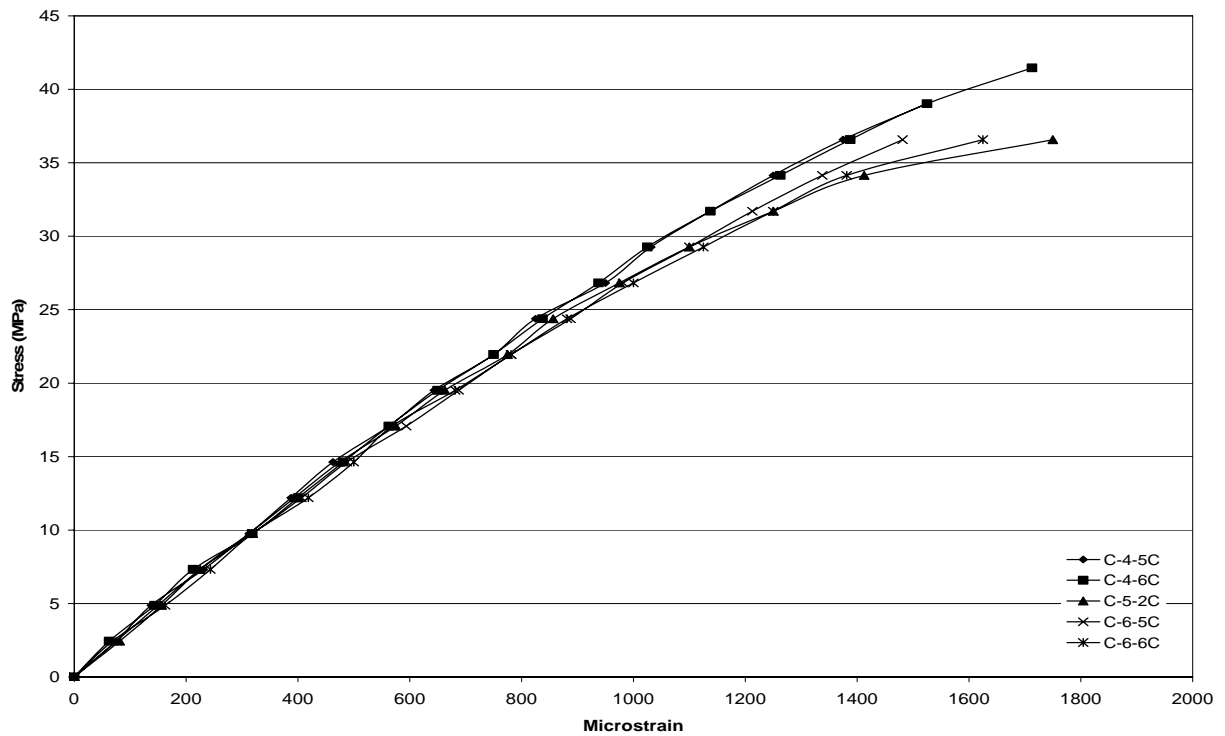
Figure A-2: Concrete Stress/Strain Plots for the Conventional Bridge Deck (Live-Load 1)
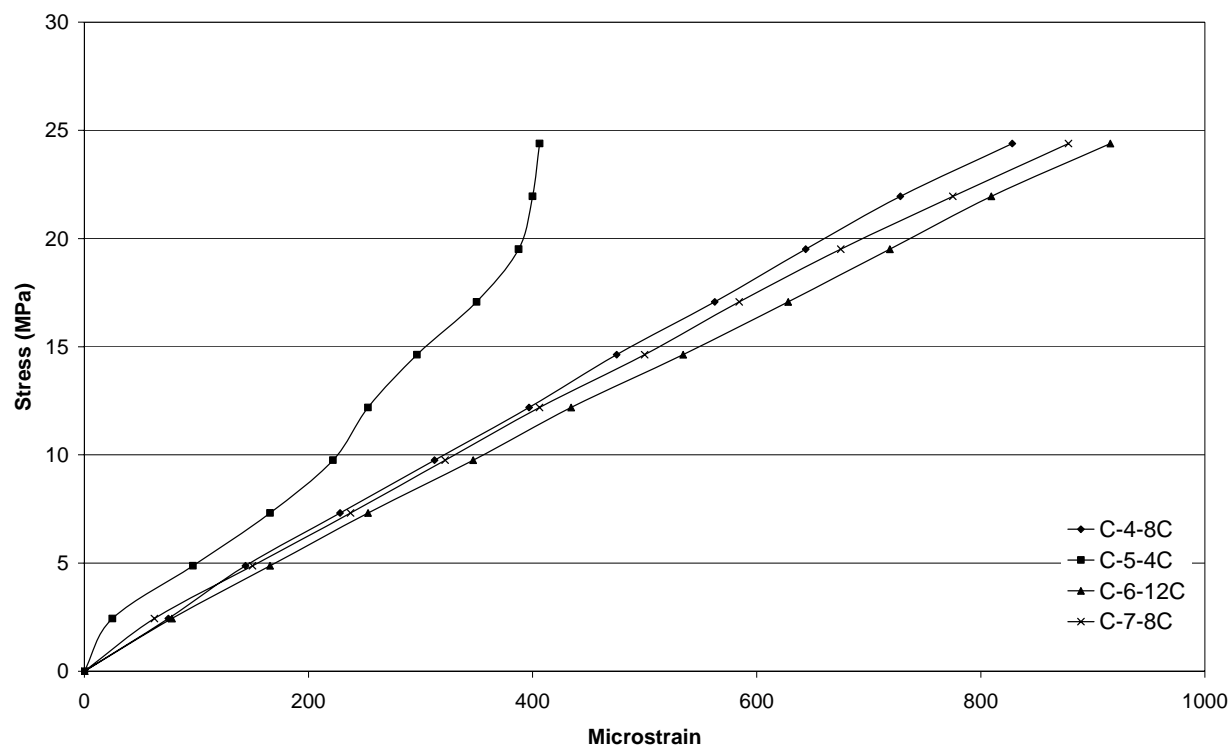
Figure A-3: Concrete Stress/Strain Plots for the Conventional Bridge Deck (Live-Load 2)

Table A-3: Concrete Rupture Beam Summary Data for the Conventional Deck from WTI

Truck	Specimen Number	Specimen Type	Size (in)	Curing	Test Type	Time to Test	Age (days)	Stress (psi)	Stress (Mpa)
C-4	1R	rupture beam	6x6x20	with deck	bending	live load 1	60	522	3.6
	2R	rupture beam	6x6x20	with deck	bending	live load 1	60	439	3.0
C-6	1R	rupture beam	6x6x20	with deck	bending	live load 1	60	540	3.7
	2R	rupture beam	6x6x20	with deck	bending	live load 1	60	546	3.8
	3R	rupture beam	6x6x20	with deck	bending	live load 2	806	708	4.9
	4R	rupture beam	6x6x20	with deck	bending	live load 2	806	789	5.4
	5R	rupture beam	6x6x20	with deck	bending	Remaining			
C-7	1R	rupture beam	6x6x20	with deck	bending	live load 2	806	722	5.0
	2R	rupture beam	6x6x20	with deck	bending	live load 2	806	628	4.3

Table A-4: Concrete Cylinder Summary Data for the Empirical Deck from WTI

Truck	Specimen Number	Specimen Type	Size (in)	Curing	Test Type	Time to Test	Age (days)	Stress (psi)	Stress (Mpa)	Notes:
E-5	1C	cylinder	6x12	moist	compression	28 days	28	4,089	28.2	
	2C	cylinder	6x12	moist	compression	28 days	28	4,055	28.0	See Figure A-4
	3C	cylinder	6x12	moist	compression	28 days	28	3,926	27.1	See Figure A-4
	4C	cylinder	6x12	with deck	compression	live load 1	63	5,021	34.6	
	5C	cylinder	6x12	with deck	compression	live load 1	63	4,677	32.2	See Figure A-5
	6C	cylinder	6x12	with deck	compression	live load 1	63	4,496	31.0	See Figure A-5
	7C	cylinder	6x12	with deck	compression	live load 2	809	4,846	33.4	
	8C	cylinder	6x12	with deck	compression	live load 2	850	4,902	33.8	See Figure A-6
	9C	cylinder	6x12	with deck	compression	Remaining				
E-7	1C	cylinder	6x12	moist	compression	28 days	28	3,728	25.7	
	2C	cylinder	6x12	moist	compression	28 days	28	4,103	28.3	See Figure A-4
	3C	cylinder	6x12	moist	compression	28 days	28	4,154	28.6	See Figure A-4
	4C	cylinder	6x12	with deck	compression	live load 1	63	4,736	32.7	
	5C	cylinder	6x12	with deck	compression	live load 1	63	4,823	33.3	
	6C	cylinder	6x12	with deck	compression	live load 1	63	4,330	29.9	See Figure A-5
	7C	cylinder	6x12	with deck	split cylinder	live load 1	64	415	2.9	
	8C	cylinder	6x12	with deck	split cylinder	live load 1	64	415	2.9	
	9C	cylinder	6x12	with deck	split cylinder	live load 1	64	484	3.3	
	10C	cylinder	6x12	with deck	compression	live load 2	809	4,706	32.4	
	11C	cylinder	6x12	with deck	compression	live load 2	850	4,736	32.7	See Figure A-6
	12C	cylinder	6x12	with deck	compression	Remaining				
	13C	cylinder	6x12	with deck	split cylinder	live load 2	809	444	3.1	
	14C	cylinder	6x12	with deck	split cylinder	live load 2	809	438	3.0	
	15C	cylinder	6x12	with deck	split cylinder	Remaining				
E-9	1C	cylinder	6x12	moist	compression	28 days	28	4,276	29.5	
	2C	cylinder	6x12	moist	compression	28 days	28	3,583	24.7	See Figure A-4
	3C	cylinder	6x12	moist	compression	28 days	28	3,872	26.7	See Figure A-4
	4C	cylinder	6x12	with deck	compression	live load 1	63	5,054	34.8	
	5C	cylinder	6x12	with deck	compression	live load 1	63	5,119	35.3	See Figure A-5
	6C	cylinder	6x12	with deck	compression	live load 1	63	4,658	32.1	See Figure A-5
	7C	cylinder	6x12	with deck	compression	live load 2	809	5,530	38.1	
	8C	cylinder	6x12	with deck	compression	live load 2	850	5,152	35.5	See Figure A-6
	9C	cylinder	6x12	with deck	compression	Remaining				
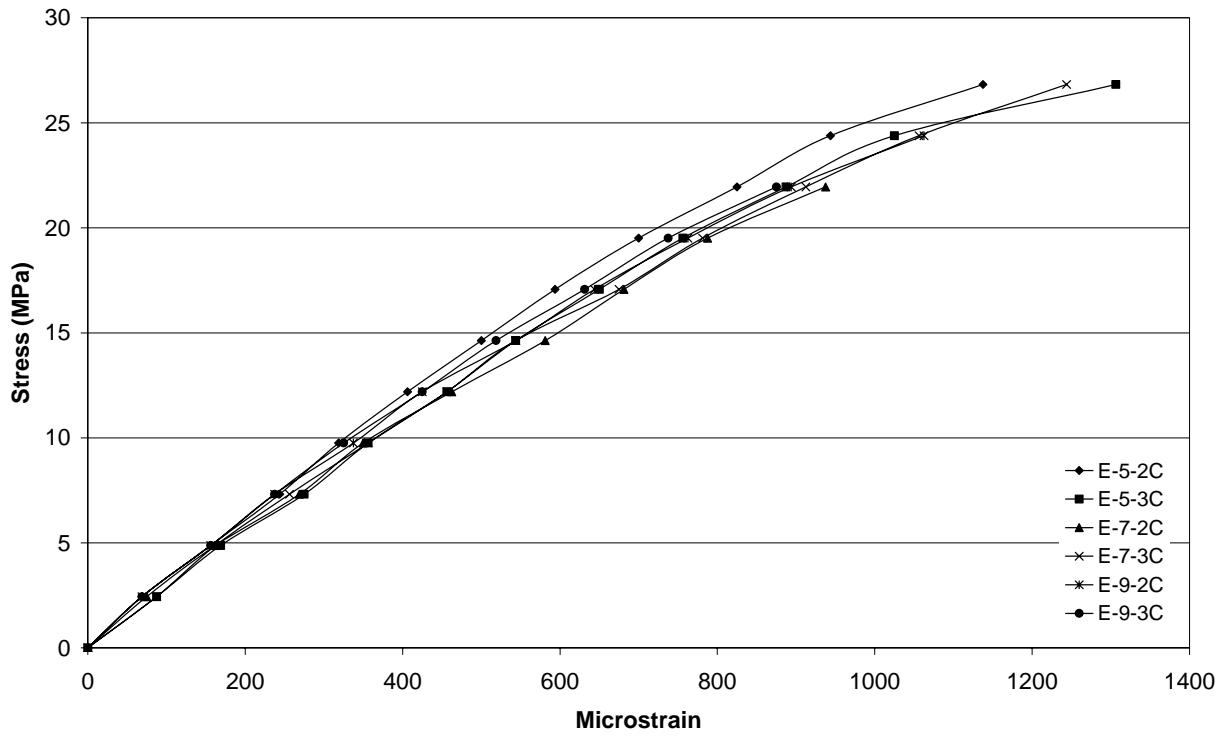
Figure A-4: Concrete Stress/Strain Plots for the Empirical Bridge Deck (28-Day)
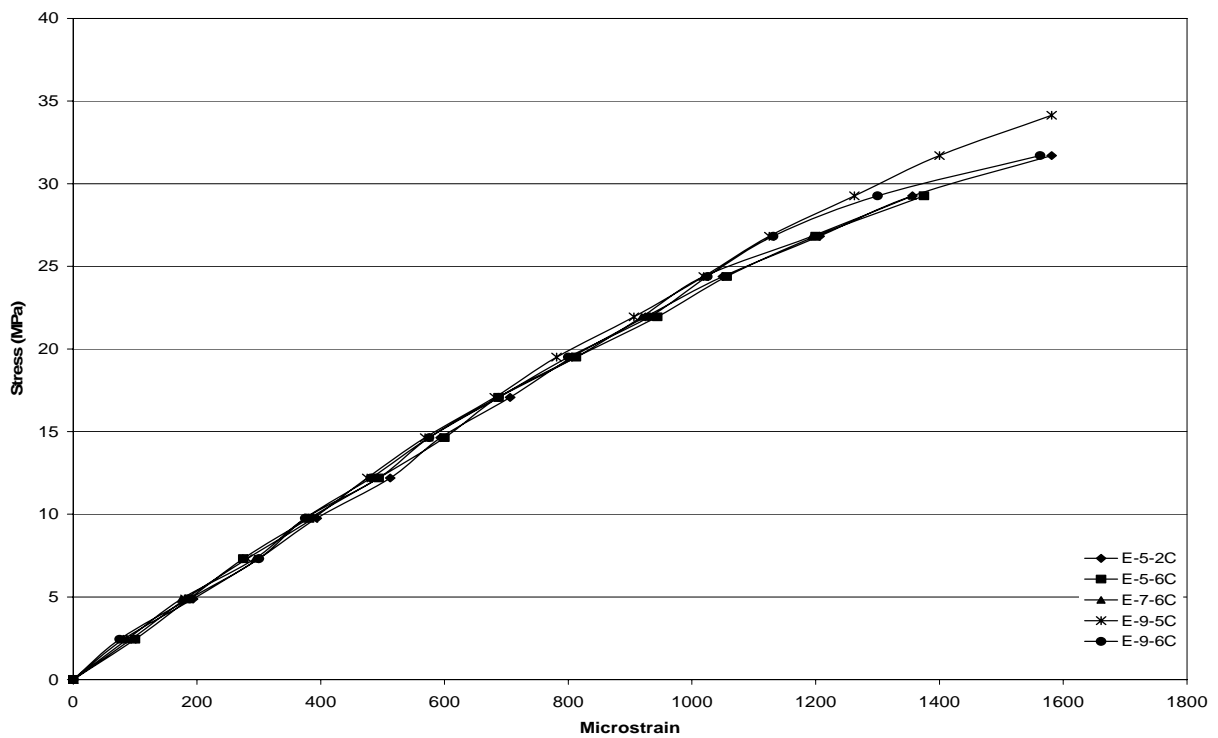
Figure A-5: Concrete Stress/Strain Plots for the Empirical Bridge Deck (Live-Load 1)
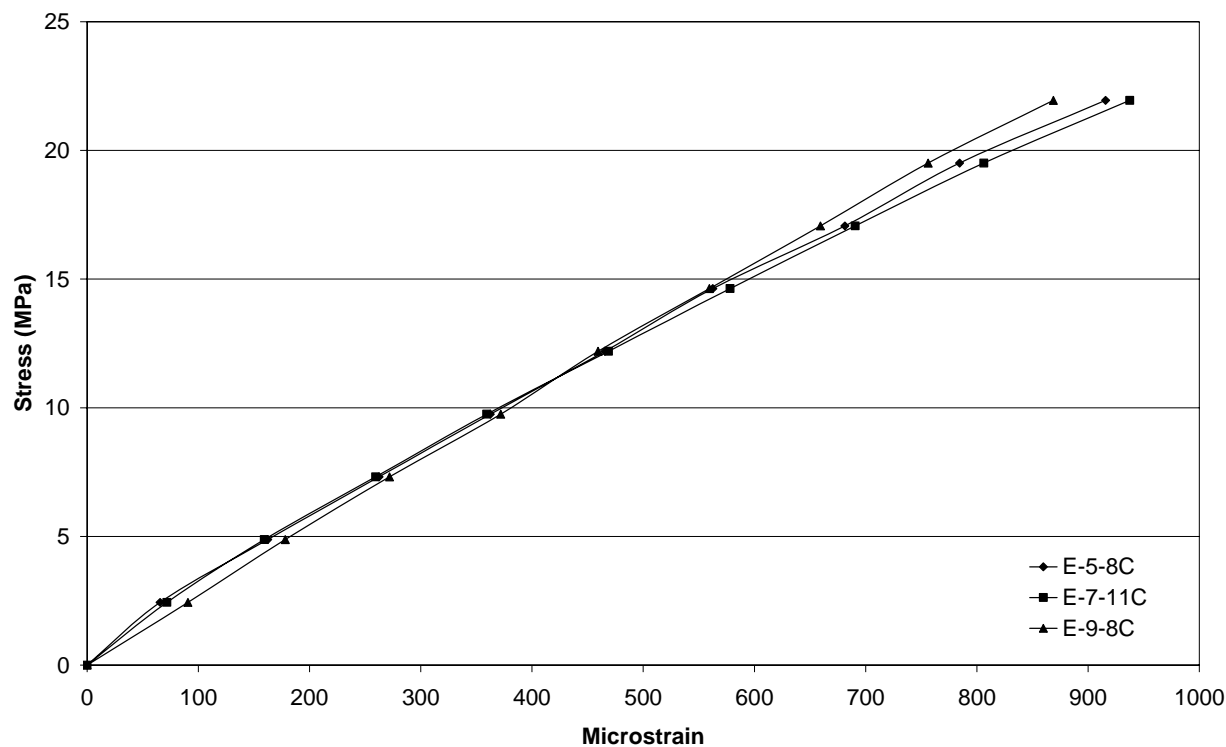
Figure A-6: Concrete Stress/Strain Plots for the Empirical Bridge Deck (Live-Load 2)

Table A-5: Concrete Rupture Beam Summary Data for the Empirical Deck from WTI

Truck	Specimen Number	Specimen Type	Size (in)	Curing	Test Type	Time to Test	Age (days)	Stress (psi)	Stress (Mpa)
E-5	1R	rupture beam	6x6x20	with deck	bending	live load 1	63	484	3.3
	2R	rupture beam	6x6x20	with deck	bending	live load 1	63	484	3.3
E-7	1R	rupture beam	6x6x20	with deck	bending	live load 1	63	487	3.4
	2R	rupture beam	6x6x20	with deck	bending	live load 1	63	484	3.3
	3R	rupture beam	6x6x20	with deck	bending	live load 2	809	714	4.9
	4R	rupture beam	6x6x20	with deck	bending	live load 2	809	669	4.6
	5R	rupture beam	6x6x20	with deck	bending	Remaining			
E-9	1R	rupture beam	6x6x20	with deck	bending	live load 2	809	610	4.2
	2R	rupture beam	6x6x20	with deck	bending	live load 2	809	559	3.9

Table A-6: Concrete Cylinder Summary Data for the HPC Deck from WTI

Truck	Specimen Number	Specimen Type	Size (in)	Curing	Test Type	Time to Test	Age (days)	Stress (psi)	Stress (Mpa)	Notes:
H-4	1C	cylinder	6x12	moist	compression	28 days	28	7,236	49.9	See Figure A-7
	2C	cylinder	6x12	with deck	compression	live load 1	69	7,748	53.4	See Figure A-8
	3C	cylinder	6x12	with deck	compression	live load 1	69	8,079	55.7	See Figure A-8
	4C	cylinder	6x12	with deck	split cylinder	live load 1	69	577	4.0	
	5C	cylinder	6x12	with deck	split cylinder	live load 1	69	589	4.1	
	6C	cylinder	6x12	with deck	compression	live load 2	814	8,517	58.7	
	7C	cylinder	6x12	with deck	compression	live load 2	855	7,833	54.0	See Figure A-9
	8C	cylinder	6x12	with deck	split cylinder	Remaining				
	9C	cylinder	6x12	with deck	split cylinder	Remaining				
H-6	1C	cylinder	6x12	moist	compression	28 days	28	6,420	44.3	See Figure A-7
	2C	cylinder	6x12	moist	compression	28 days	28	6,813	47.0	See Figure A-7
	3C	cylinder	6x12	with deck	compression	live load 1	69	6,404	44.2	See Figure A-8
	4C	cylinder	6x12	with deck	compression	live load 1	69	6,979	48.1	See Figure A-8
	5C	cylinder	6x12	with deck	compression	live load 2	814	7,213	49.7	
	6C	cylinder	6x12	with deck	compression	live load 2	855	6,834	47.1	See Figure A-9
H-8	1C	cylinder	6x12	moist	compression	28 days	28	6,238	43.0	See Figure A-7
	2C	cylinder	6x12	with deck	compression	live load 1	69	6,785	46.8	See Figure A-8
	3C	cylinder	6x12	with deck	compression	live load 1	69	6,819	47.0	See Figure A-8
	4C	cylinder	6x12	with deck	compression	live load 2	855	6,787	46.8	See Figure A-9
	5C	cylinder	6x12	with deck	compression	Remaining				
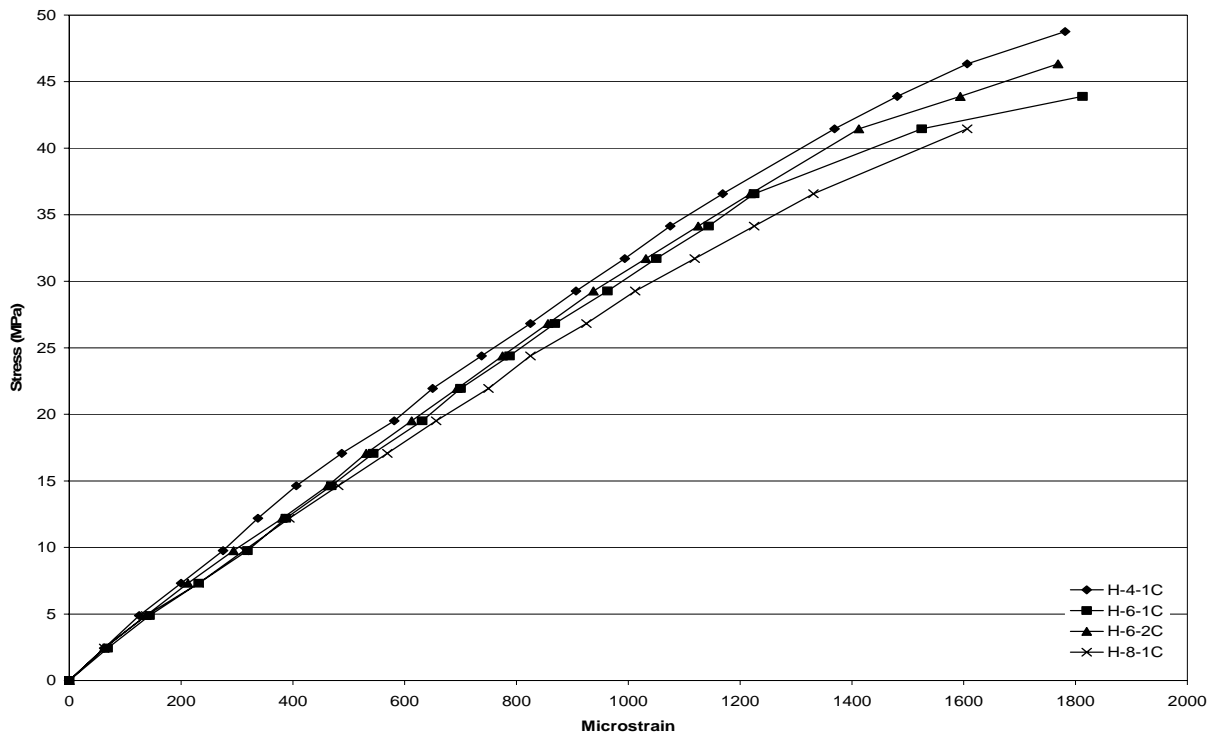
Figure A-7: Concrete Stress/Strain Plots for the HPC Bridge Deck (28-Day)
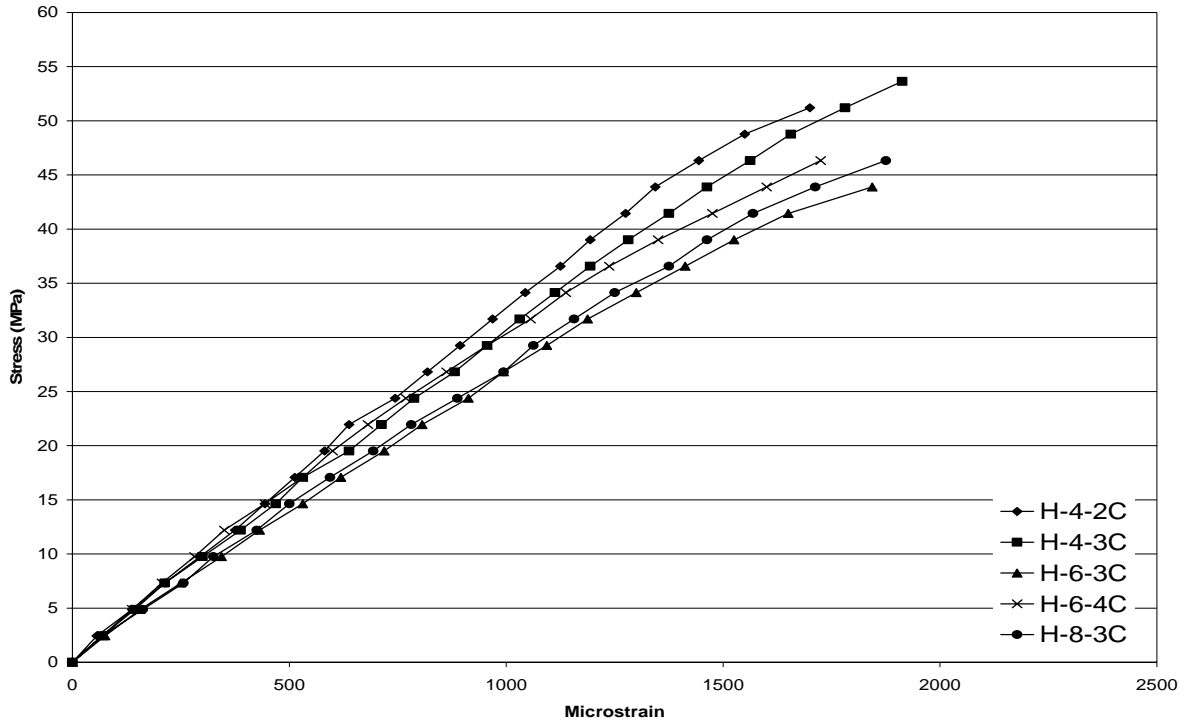
Figure A-8: Concrete Stress/Strain Plots for the HPC Bridge Deck (Live-Load 1)
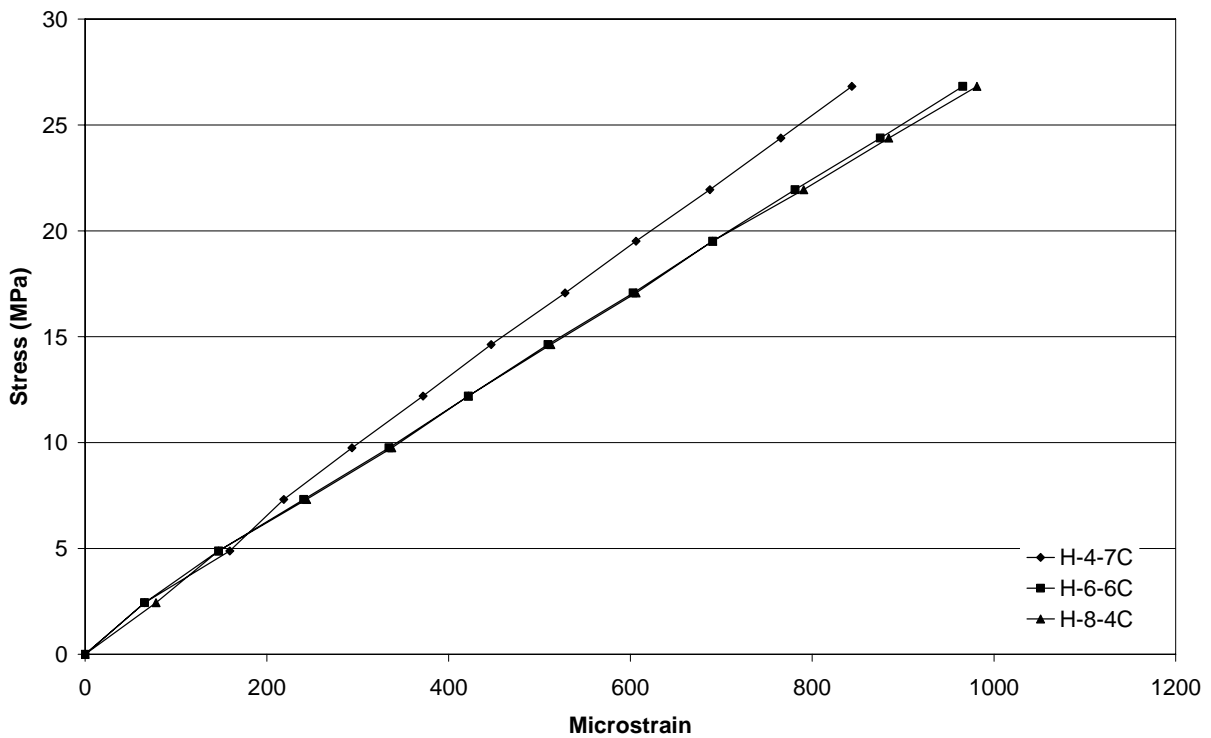
Figure A-9: Concrete Stress/Strain Plots for the HPC Bridge Deck (Live-Load 2)

Table A-7: Concrete Rupture Beam Summary Data for the HPC Deck from WTI

Truck	Specimen Number	Specimen Type	Size (in)	Curing	Test Type	Time to Test	Age (days)	Stress (psi)	Stress (Mpa)
H-4	1R	rupture beam	6x6x20	with deck	bending	live load 1	68	561	3.9
	2R	rupture beam	6x6x20	with deck	bending	live load 1	68	633	4.4
	3R	rupture beam	6x6x20	with deck	bending	damaged	---	---	---
H-6	1R	rupture beam	6x6x20	with deck	bending	live load 1	68	610	4.2
	2R	rupture beam	6x6x20	with deck	bending	live load 1	68	603	4.2
	3R	rupture beam	6x6x20	with deck	bending	remaining			
H-8	1R	rupture beam	6x6x20	with deck	bending	live load 1	68	565	3.9
	2R	rupture beam	6x6x20	with deck	bending	live load 2	814	702	4.8
	3R	rupture beam	6x6x20	with deck	bending	live load 2	814	624	4.3

Appendix B – ASTM Specification References

1. ASTM C 31-00: "Standard Practice for Making and Curing Concrete Test Specimens in the Field."

2. ASTM C 39-01: "Standard Test Method for Compressive Strengths of Cylindrical Concrete Specimens."

3. ASTM C 78-00: "Standard Test Method for Flexural Strength of Concrete (Using Simple Beam with Third Point Loading)."

4. ASTM C 172-99: "Standard Practice for Sampling Freshly Mixed Concrete."

5. ASTM C 173-01: "Standard Test Method for Air content of Freshly Mixed Concrete by the Volumetric Method."

6. ASTM C 192-00: "Standard Practice for Making and Curing Concrete Test Specimens in the Laboratory."

7. ASTM C 231-97: "Standard Test Method for Air Content of Freshly Mixed Concrete by the Pressure Method."

8. ASTM C 452-95: "Standard Test Method for Static Modulus of Elasticity and Poisson's Ratio of Concrete in Compression."

9. ASTM C 496-96: "Standard Test Method for Splitting Tensile Strength of Cylindrical Concrete Specimens."

10. ASTM C 876-91 (1999): "Standard Test Method for Half-Cell Potentials of Uncoated Reinforcing of Steel in Concrete."

11. ASTM C 4580-86 (1997): "Standard Test Method for Measuring Delaminations in Concrete Bridge Decks by Sounding."

Appendix C – Deck Rebar Material Properties

Table C-1: Mill Test Data for Deck Reinforcing Steel

North Star Steel

Certificate #	Sales Order	Purchase Order	Product	Size (mm)	Grade	Heat #	Yield (Mpa)	Yield (ksi)	Tensile (Mpa)	Tensile (ksi)	% Elongation
31124	Z030421	1205-A	Rebar	13	60	50719603	477.7	69.28	731.88	105.15	14.40
31374	Z031693	115-B	Rebar	16	60	11565270	494.1	71.66	747.94	108.46	14.75
31404	Z031174	102-B	Rebar	13	60	420224396	475.5	68.96	742.57	107.70	13.70
SMI - Texas			Product	Size (mm)	Grade	Heat #	Yield (Mpa)	Yield (ksi)	Tensile (Mpa)	Tensile (ksi)	% Elongation
			Rebar	19	60	225533	466.8	67.7	738.2	105.9	15

Table C-2: Other Test Data for Deck Reinforcing Steel

Date Sampled	Date Checked & Approved	Quantity (kg)	Name of Material	Grade	Manufacturer	Paint	Thickness	Holidays	Bend Test
3/10/2003	3/26/2003	17,992	Epoxy Reinforcing Steel, # 13 bar	60	North Star & SMI	7 / 8 / 9	10 / 9 / 12	OK	OK
3/10/2003	3/26/2003	13,850	Epoxy Reinforcing Steel, #19 bar	60	North Star & SMI	11 / 8 / 8	8 / 10 / 10	OK	OK

Table C-3: Coating Properties as Reported by Manufacturers

ABC Coating Co., Inc. of Colorado

Job #	Work Order #	Invoice #	Size	Weight (lbs)	Heat(s)	Powder Lot(s)
029-MT	3330	3330	#4 / 13M	2,858	420224396	3141901809
			#5 / 16M	1,858	11565270	3141901809
			#6 / 19M	25,818	225533	3141901809
029-MT	3332	3332	#4 / 13M	20,602	50719603	2T41901527
			#5 / 16M	5,030	11565270	3141901809
			#6 / 19M	14,034	225533	3141901993

Valspar Corporation

Date	Specification	Valspar Product Code	Batch Number	Production Date	Batch Size (lbs)
12/5/2003	ASTM A775 & ASHTO M284	720A009 Greenbar Fusion Bond Epoxy Powder Coating	2T41901527	10/18/2002	41,400
1/27/2003	ASTM A775 & ASHTO M284	720A009 Greenbar Fusion Bond Epoxy Powder Coating	3141901809	1/13/2003	41,540
2/25/2003	ASTM A775 & ASHTO M284	720A009 Greenbar Fusion Bond Epoxy Powder Coating	3141901993	1/23/2003	41,400

Appendix D – Prestressed Girder Material Properties

Table D-1: Concrete Cylinder Summary Data for Conventional Deck Girders

Beam Numbers			Lab No.	Date Cast	Age	Load	Individual Cylinders		3 Cylinder Avg		Spread	% Spread
							psi	MPa	psi	MPa		
25	29	33	824267	10/9/2002	28	84320	**6710**	**46.3**	8302	57.2	2737	**33.0%**
			824268	10/9/2002	28	109940	8749	60.3				
			824269	10/9/2002	28	118720	9447	65.1				
26	30	34	824270	10/11/2002	28	120680	9603	66.2	9659	66.6	94	1.0%
			824271	10/11/2002	28	121600	9677	66.7				
			824272	10/11/2002	28	121860	9697	66.9				
27	31	35	824273	10/14/2002	28	105960	8432	58.1	9047	62.4	1261	**13.9%**
			824274	10/14/2002	28	121800	9693	66.8				
			824275	10/14/2002	28	113320	9018	62.2				
28	32	36	824300	10/15/2002	28	122740	9767	67.3	9572	66.0	404	4.2%
			824301	10/15/2002	28	117660	9363	64.6				
			824302	10/15/2002	28	120440	9584	66.1				

Table D-2: Concrete Cylinder Summary Data for Empirical Deck Girders

Beam Numbers			Lab No.	Date Cast	Age	Load	Individual Cylinders		3 Cylinder Avg		Spread	% Spread
							psi	MPa	psi	MPa		
13	17	21	823985	10/3/2002	28	108860	8663	59.7	9079	62.6	766	8.4%
			823986	10/3/2002	28	114920	9145	63.1				
			823987	10/3/2002	28	118480	9428	65.0				
14	18	22	823988	10/4/2002	28	100320	7983	55.0	8428	58.1	711	8.4%
			823989	10/4/2002	28	109260	8695	59.9				
			823990	10/4/2002	28	108160	8607	59.3				
15	19	23	824092	10/7/2002	28	113520	9034	62.3	8577	59.1	780	9.1%
			824093	10/7/2002	28	106100	8443	58.2				
			824094	10/7/2002	28	103720	8254	56.9				
16	20	24	824095	10/8/2003	28	115260	9172	63.2	9283	64.0	294	3.2%
			824096	10/8/2003	28	118960	9467	65.3				
			824097	10/8/2003	28	115740	9210	63.5				

Table D-3: Concrete Cylinder Summary Data for HPC Deck Girders

Beam Numbers			Lab No.	Date Cast	Age	Load	Individual Cylinders		3 Cylinder Avg		Spread	% Spread
							psi	MPa	psi	MPa		
2	6	10	823636	9/27/2002	28	115000	9151	63.1	9314	64.2	902	**9.7%**
			823637	9/27/2002	28	123740	9847	67.9				
			823638	9/27/2002	28	112400	8945	61.7				
3	7	11	823639	9/30/2002	28	121500	9669	66.7	8990	62.0	1049	**11.7%**
			823640	9/30/2002	28	108320	8620	59.4				
			823641	9/30/2002	28	109100	8682	59.9				
1	5	9	823780	10/1/2002	28	125780	10009	69.0	9791	67.5	729	7.4%
			823781	10/1/2002	28	126240	10046	69.3				
			823782	10/1/2002	28	117080	9317	64.2				
4	8	12	823783	10/2/2002	28	118580	9436	65.1	9123	62.9	673	7.4%
			823784	10/2/2002	28	110120	8763	60.4				
			823785	10/2/2002	28	115240	9171	63.2				

Table D-4: Saco Bridge Girder Layout

Conventional	36	32	28
	35	31	27
	34	30	26
	33	29	25
Empirical	24	20	16
	23	19	15
	22	18	14
	21	17	13
HPC	12	8	4
	11	7	3
	10	6	2
	9	5	1

Note: North is to the left of the Table

Appendix E: Instrumentation Plan

Table of Contents

Introduction

This instrumentation plan is for the Saco bridges located at station 11+57.24, 16+81.74 and 19+23.24, which correspond to the HPC, Empirical and Conventional bridges, respectively. The instrumentation for each bridge deck includes 35 reinforcing strain gages, 9 embedded strain gages, and 20 vibrating wire gages.

The position referencing nomenclature described in Section 3.2 of the body of the report was used throughout this instrumentation plan. This plan details the following information for each bridge:

Section A: General bridge deck layout
Section B: Detailed rebar layout
Section C: Plan view of gage locations
Section D: Cable-exiting plan
Section E: Detailed instrumentation list
Section F: Detailed drawings of reinforcing bars instrumented with bonded strain gages

Part 1: HPC Deck @11+57.24

The series of numbers along the bottom of the bridge correspond to the longitudinal gage positions used in the reference number system described above. Likewise, the numbers along the right edge correspond to the transverse position of the gages used in the reference number system. The arrows on the left side show the direction of travel across the bridge of a typical truck.

The S200E bars numbered 1 through 8 are the S200E ~ # 13 bars called out in the bridge plans for the top longitudinal reinforcement. The S300E bars numbered 2,4,5, and 7 are the S300E ~ #13 bars called out in the plans for the Bottom longitudinal reinforcement. Each of the longitudinal bars is 12.19 meters in length. The S100E bars numbered 1 through 3 are the S100E ~ # 19 bars called out in the plans as the top and bottom transverse reinforcement. Each transverse bar is 8.95 meters long.

Section C-1: Plan View of Gage Locations

High Performance Concrete Deck at 11+57.24

Bonded Strain Gage Layout

6 transverse bars   (16 gage locations)
12 longitudinal bars (19 gage locations)

■ Transverse gage, top and bottom mat

▬ Longitudinal gage, top and bottom mat

▬ Longitudinal gage, top mat only

⬭ Longitudinal gage, bottom of stringer

H-TR-D-4-B
H-TR-D-4-T

H-TR-D-6-B
H-TR-D-6-T

H-LR-F-7-B
H-LR-F-7-T

H-LR-D-5-T
H-TR-D-5-B
H-TR-D-5-T

H-TR-E-5-B
H-TR-E-5-T

H-LR-G-5-T

H-LR-B-5-T

H-LR-F-5-T

H-LR-D-3-B
H-LR-D-3-T

H-LR-C-3-B
H-LR-C-3-T

H-LR-B-3-B
H-LR-B-3-T

H-LR-A-3-B
H-LR-A-3-T

H-LR-F-3-B
H-LR-F-3-T

H-TR-E-2-B
H-TR-E-2-T

H-TR-D-2-B
H-TR-D-2-T

H-TR-B-2-B
H-TR-B-2-T

H-LR-F-1-B
H-LR-F-1-T

H-LR-B-1-T

H-TR-D-1-B
H-TR-D-1-T

7
7
6
5
5
4
3
3
2
1
1

G   F   E   D   C   B   A

Embedded Strain Gage Layout

9 locations

■ Transverse gage, mid and near surface

▬ Longitudinal gage, mid and near surface

▬ Longitudinal gage, bottom, mid, and near surface

H-LE-F-7-M
H-LE-F-7-T

H-TE-D-5-M
H-TE-D-5-T

H-LE-F-5-B
H-LE-F-5-M
H-LE-F-5-T

H-TE-D-2-M
H-TE-D-2-T

7
6
5
4
3
2
1

G   F   E   D   C   B   A

Vibrating Wire Gage Layout

20 locations

Transverse gage, top, mid, and bottom

Transverse gage, top and bottom

Longitudinal gage, top and bottom

Longitudinal gage, top, mid and bottom

H-LV-F-7-B
H-LV-F-7-T

H-TV-D-5-B
H-TV-D-5-M
H-TV-D-5-T

H-TV-C-3-B
H-TV-C-3-T

H-LV-F-5-B
H-LV-F-5-T

H-LV-B-3-B
H-LV-B-3-T

H-LV-F-3-B
H-LV-F-3-M
H-LV-F-3-T

H-LV-A-3-B
H-LV-A-3-T

H-LV-D-3-B
H-LV-D-3-T

H-TV-D-3-B
H-TV-D-3-T

7
6
5
4
3
2
1

G   F   E   D   C   B   A

Cable Exit Layout Showing Gage Clusters

Gage Cluster

Exit Location
Each exit is 1½" in diameter

Longitudinal Reinforcement Strain Gages

Table 1-1: Detailed list of strain gages bonded to longitudinal reinforcement in bridge @ 11+57.24 (HPC)

Reference No.	General Position			Expected Response (με)	Cable Exit Port	Approx. Lead Wire Length (m)	Bar Number	Purpose
	X	Y	Z					
H-LR-G-5-T	Over 2nd bent	Over stringer B	Top mat	-53.8	A1	25	S200E-1	Effect of saw cut
H-LR-F-5-T	Over 3rd bent	Over Stringer B	Top mat	-53.8	B2	4	S200E-3	String-Bent interaction
H-LR-F-1-T	Over 3rd bent	Over Stringer A	Top mat	-86.9	C2	7	S200E-5	String-Bent interaction
H-LR-F-1-B	Over 3rd bent	Over Stringer A	Bot mat	-86.9	C2	7	S300E-5	String-Bent interaction
H-LR-F-3-T	Over 3rd bent	Btwn stringer A&B	Top mat	-10.3	C1	7	S200E-4	Bending across bent
H-LR-F-3-B	Over 3rd bent	Btwn stringer A&B	Bot mat	-10.3	C1	7	S300E-4	Bending across bent
H-LR-F-7-T	Over 3rd bent	Btwn stringer B&C	Top mat	-6.21	B1	7	S200E-2	Bending across bent
H-LR-F-7-B	Over 3rd bent	Btwn stringer B&C	Bot mat	-6.21	B1	7	S300E-2	Bending across bent
H-LR-D-3-T	Btwn bent &dia	Btwn stringer A&B	Top mat	6.21	C6	9	S200E-7	Local deck behavior
H-LR-D-3-B	Btwn bent &dia	Btwn stringer A&B	Bot mat	6.21	C6	9	S300E-7	Local deck behavior
H-LR-C-3-T	Btwn bent &dia	Btwn stringer A&B	Top mat	5.86	D3	11	S200E-7	Local deck behavior
H-LR-C-3-B	Btwn bent &dia	Btwn stringer A&B	Bot mat	5.86	D3	11	S300E-7	Local deck behavior
H-LR-B-3-T	Over dia 3 to 4	Btwn stringer A&B	Top mat	4.83	E1	12.5	S200E-7	Effect of diaphragm
H-LR-B-3-B	Over dia 3 to 4	Btwn stringer A&B	Bot mat	4.83	E1	12.5	S300E-7	Effect of diaphragm
H-LR-A-3-T	Over 4th bent	Btwn stringer A&B	Top mat	-1.03	E4	20	S200E-7	Continuity effects
H-LR-A-3-B	Over 4th bent	Btwn stringer A&B	Bot mat	-1.03	E4	20	S300E-7	Continuity effects
H-LR-B-1-T	Over dia 3 to 4	Over Stringer A	Top mat	-12.1	E3	12.5	S200E-8	Global bending
H-LR-D-5-T	Btwn bent &dia	Over stringer B	Top mat	4.14	D1	12	S200E-6	Global bending
H-LR-B-5-T	Over dia 3 to 4	Over Stringer B	Top mat	-0.345	D4	12	S200E-6	Global bending

Transverse Reinforcement Strain Gages

Table 1-2: Detailed list of strain gages bonded to transverse reinforcement in bridge @ 11+57.24 (HPC)

Reference No.	General Position			Expected Response (με)	Cable Exit Port	Approx. Lead Wire Length (m)	Bar Number	Purpose
	X	Y	Z					
H-TR-D-1-T	Btwn bent & dia	Over stringer A	Top mat	6.21	C4	9	S100E-2	Stringer effects
H-TR-D-1-B	Btwn bent & dia	Over stringer A	Bot mat	6.21	C4	9	S100E-2	Stringer effects
H-TR-E-2-T	Btwn bent & dia	Btwn stringers A&B	Top mat	7.93	C3	7	S100E-1	Local deck behavior
H-TR-E-2-B	Btwn bent & dia	Btwn stringers A&B	Bot mat	7.93	C3	7	S100E-1	Local deck behavior
H-TR-D-2-T	Btwn bent & dia	Btwn stringers A&B	Top mat	6.9	C5	9	S100E-2	Local deck behavior
H-TR-D-2-B	Btwn bent & dia	Btwn stringers A&B	Bot mat	6.9	C5	9	S100E-2	Local deck behavior
H-TR-B-2-T	Over diaphragm	Btwn stringers A&B	Top mat	-2.07	E2	11	S100E-3	Effect of diaphragm
H-TR-B-2-B	Over diaphragm	Btwn stringers A&B	Bot mat	-2.07	E2	11	S100E-3	Effect of diaphragm
H-TR-D-4-T	Btwn bent & dia	Btwn stringers A&B	Top mat	7.24	D2	10.5	S100E-2	Local deck behavior
H-TR-D-4-B	Btwn bent & dia	Btwn stringers A&B	Bot mat	7.24	D2	10.5	S100E-2	Local deck behavior
H-TR-E-5-T	Btwn bent & dia	Over stringer B	Top mat	5.86	B3	5	S100E-1	Stringer effects
H-TR-E-5-B	Btwn bent & dia	Over stringer B	Bot mat	5.86	B3	5	S100E-1	Stringer effects
H-TR-D-5-T	Btwn bent & dia	Over stringer B	Top mat	4.83	D1	12	S100E-2	Stinger effects
H-TR-D-5-B	Btwn bent & dia	Over stringer B	Bot mat	4.83	D1	12	S100E-2	Stringer effects
H-TR-D-6-T	Btwn bent & dia	Btwn stringers B&C	Top mat	6.9	B4	10.5	S100E-2	Local deck behavior
H-TR-D-6-B	Btwn bent & dia	Btwn stringers B&C	Bot mat	6.9	B4	10.5	S100E-2	Local deck behavior

Embedded Strain Gages

Table 1-3: Detailed list of embedded strain gages in bridge @ 11+57.24 (HPC)

Reference No.	Orientation	General Position			Expected Response ($\mu\varepsilon$)	Cable Exit Port	Approx. Lead Wire Length (m)	Purpose
		X	Y	Z				
H-LE-F-5-B	Longitudinal	Over 2nd bent	Over stringer B	Bot	-15.6	B2	4	Stringer – Bent interaction
H-LE-F-5-M	Longitudinal	Over 2nd bent	Over stringer B	Mid	-15.6	B2	4	Stringer – Bent interaction
H-LE-F-5-T	Longitudinal	Over 2nd bent	Over stringer B	Top	-15.6	B2	4	Stringer – Bent interaction
H-TE-D-5-M	Transverse	Btwn bent & dia	Over stringer B	Mid	-1.8	D1	12	Stringer effects
H-TE-D-5-T	Transverse	Btwn bent & dia	Over stringer B	Top	-1.8	D1	12	Stringer effects
H-LE-F-7-M	Longitudinal	Over 2nd bent	Btwn stringers B & C	Mid	-1.8	B1	7	Bending across bent
H-LE-F-7-T	Longitudinal	Over 2nd bent	Btwn stringers B & C	Top	-1.2	B1	7	Bending across bent
H-TE-D-2-M	Transverse	Btwn bent & dia	Btwn stringers A & B	Mid		C5	9	Local bending effects
H-TE-D-2-T	Transverse	Btwn bent & dia	Btwn stringers A & B	Top		C5	9	Local bending effects

Vibrating Wire Strain Gages

Table 1-4: Detailed list of vibrating wire strain gages in bridge @ 11+57.24 (HPC)

Reference No.	Orientation	General Position			Expected Response (µε)	Cable Exit Port	Approx Lead Wire Length (m)	Purpose
		X	Y	Z				
H-LV-F-3-B	Longitudinal	Over bent	Btwn stringers A & B	Bot	-3.0	C1	7	Bending across bent
H-LV-F-3-M	Longitudinal	Over bent	Btwn stringers A & B	Mid	-3.0	C1	7	Bending across bent
H-LV-F-3-T	Longitudinal	Over bent	Btwn stringers A & B	Top	-3.0	C1	7	Bending across bent
H-LV-F-5-B	Longitudinal	Over bent	Over stringer B	Bot	-15.6	B2	4	Stringer – bent interaction
H-LV-F-5-T	Longitudinal	Over bent	Over stringer B	Top	-15.6	B2	4	Stringer – bent interaction
H-LV-F-7-B	Longitudinal	Over bent	Btwn stringers B & C	Bot	-1.8	B1	7	Bending across bent
H-LV-F-7-T	Longitudinal	Over bent	Btwn stringers B & C	Top	-1.8	B1	7	Bending across bent
H-LV-D-3-B	Longitudinal	Btwn bent & dia	Btwn stringers A & B	Bot	1.8	C6	9	Local deck behavior
H-LV-D-3-T	Longitudinal	Btwn bent & dia	Btwn stringers A & B	Top	1.8	C6	9	Local deck behavior
H-LV-B-3-B	Longitudinal	Over dia	Btwn stringers A & B	Bot	-1.4	E1	12.5	Diaphragm effects
H-LV-B-3-T	Longitudinal	Over dia	Btwn stringers A & B	Top	-1.4	E1	12.5	Diaphragm effects
H-LV-A-3-B	Longitudinal	Over 4th bent	Btwn stringers A & B	Bot	-0.3	E4	20	Effects of end Bent
H-LV-A-3-T	Longitudinal	Over 4th bent	Btwn stringers A & B	Top	-0.3	E4	20	Effects of end bent
H-TV-D-3-B	Transverse	Btwn bent & dia	Btwn stringers A & B	Bot	2.3	C6	9	Local deck behavior
H-TV-D-3-T	Transverse	Btwn bent & dia	Btwn stringers A & B	Top	2.3	C6	9	Local deck behavior
H-TV-C-3-B	Transverse	Btwn dia & bent	Btwn stringers A & B	Bot	2.7	D3	11	Local deck behavior
H-TV-C-3-T	Transverse	Btwn dia & bent	Btwn stringers A & B	Top	2.7	D3	11	Local deck behavior
H-TV-D-5-B	Transverse	Btwn bent & dia	Over stringer B	Bot	1.4	D1	12	Stringer effects
H-TV-D-5-M	Transverse	Btwn bent & dia	Over stringer B	Mid	1.4	D1	12	Stringer effects
H-TV-D-5-T	Transverse	Btwn bent & dia	Over stringer B	Top	1.4	D1	12	Stringer effects

Longitudinal Bars – Top Mat

H-LR-G-5-T

5380

S200E-1-H

9370   21560

H-LR-F-7-T

8800

S200E-2-H

20950   33140

H-LR-F-5-T

8800

S200E-3-H

20950   33140

H-LR-F-3-T

8800

S200E-4-H

20950   33140

H-LR-F-1-T

8800

S200E-5-H

20950   33140

*Numbers at either end of the bar represent the longitudinal beginning and ending positions (in mm) with respect to the bridge deck.

Longitudinal Bars – Top Mat (continued)

4720

970

H-LR-B-5-T

S200E-6-H

32530

44720

H-LR-D-5-T

11470

4720

2845

970

S200E-7-H

44720

32530

H-LR-D-3-T

H-LR-C-3-T

H-LR-B-3-T

H-LR-A-3-T

720

4720

H-LR-B-1-T

S200E-8-H

44720

32530

*Numbers at either end of the bar represent the longitudinal beginning and ending positions (in mm) with respect to the bridge deck.

**A total of 8 S200E ~ #13 bars of length 12.19 m are needed for instrumentation from the top mat.

Longitudinal Bars – Bottom Mat

*Numbers at either end of the bar represent the longitudinal beginning and ending positions (in mm) with respect to the bridge deck.

**A total of 4 S300E ~ # 19 bars of length 12.19 m are needed for instrumentation from the bottom mat.

Transverse Bars – Top Mat

S100E-1-H   S100E-2-H   S100E-3-H

transverse centerline of bridge deck

H-TR-D-6-T

H-TR-E-5-T   H-TR-D-5-T

H-TR-D-4-T

H-TR-E-2-T   H-TR-D-2-T   H-TR-B-2-T

H-TR-D-1-T

* A total of 3 S100E ~ # 19 bars of length 8.95 m are needed for instrumentation from the top mat

Transverse Bars – Bottom Mat

S100E-1-H   S100E-2-H   S100E-3-H

transverse centerline of bridge deck

1200
2800

H-TR-E-5-B

H-TR-E-2-B

400
2000
3600
1200
2800

H-TR-D-6-B

H-TR-D-5-B

H-TR-D-4-B

H-TR-D-2-B

H-TR-D-1-B

2800

H-TR-B-2-B

* A total of 3 S100E ~ # 19 bars of length 8.95 m are needed for instrumentation from the bottom mat

Part 2: Empirical Deck @16+81.74

The series of numbers along the bottom of the bridge correspond to the longitudinal gage positions used in the reference number system described above. Likewise, the numbers along the right edge correspond to the transverse position of the gages used in the reference number system. The arrows on the left side show the direction of travel across the bridge of a typical truck.

The S200E bars numbered 1 through 8 are the S200E ~ # 13 bars called out in the bridge plans for the top longitudinal reinforcement. The S300E bars numbered 2,4,5, and 7 are the S300E ~ #13 bars called out in the plans for the Bottom longitudinal reinforcement. Each of the longitudinal bars is 12.19 meters in length. The S100E bars numbered 1 through 3 are the S100E ~ # 19 bars called out in the plans as the top and bottom transverse reinforcement. Each transverse bar is 8.95 meters long.

Not to scale

Empirical Top

26-S200E-#13 (3 per line) top
longitudinal bars lap with S201E-#13
(See Transverse Section for spacing)

S200E-2-E

S200E-1-E   S200E-3-E   S200E-6-E

S200E-4-E   S200E-7-E

S200E-5-E   S200E-8-E

Empirical Bottom

26-S200E-#13 (3 per line) top
longitudinal bars lap with S201E-#13
(See Transverse Section for spacing)

S300E-2-E

S300E-4-E   S300E-7-E

S300E-5-E

Empirical (Top)

Empirical (Bottom)

Bonded Strain Gage Layout

6 transverse bars   (16 gage locations)
12 longitudinal bars (19 gage locations)

Transverse gage, top and bottom mat

Longitudinal gage, top and bottom mat

Longitudinal gage, top mat only

Longitudinal gage, bottom of stringer

E-TR-D-4-B
E-TR-D-4-T

E-TR-D-6-B
E-TR-D-6-T

E-LR-F-7-B
E-LR-F-7-T

E-LR-D-5-T
E-TR-D-5-B
E-TR-D-5-T

E-TR-E-5-B
E-TR-E-5-T

E-LR-G-5-T

E-LR-B-5-T

E-LR-F-5-T

E-LR-D-3-B
E-LR-D-3-T

E-LR-C-3-B
E-LR-C-3-T

E-LR-B-3-B
E-LR-B-3-T

E-LR-A-3-B
E-LR-A-3-T

E-LR-F-3-B
E-LR-F-3-T

E-TR-E-2-B
E-TR-E-2-T

E-TR-D-2-B
E-TR-D-2-T

E-TR-B-2-B
E-TR-B-2-T

E-LR-F-1-B
E-LR-F-1-T

E-LR-B-1-T

E-TR-D-1-B
E-TR-D-1-T

7
7
6
5
5
4
4
3
3
2
2
1
1

G   F E D C B   A

Embedded Strain Gage Layout

9 locations

■ Transverse gage, mid and near surface

■ Longitudinal gage, mid and near surface

■ Longitudinal gage, bottom, mid, and near surface

E-LE-F-7-M
E-LE-F-7-T

E-TE-D-5-M
E-TE-D-5-T

E-LE-F-5-B
E-LE-F-5-M
E-LE-F-5-T

E-TE-D-2-M
E-TE-D-2-T

G   F   E   D   C   B   A

7
6
5
4
3
2
1

Vibrating Wire Gage Layout

20 locations

Transverse gage, top, mid, and bottom

Transverse gage, top and bottom

Longitudinal gage, top and bottom

Longitudinal gage, top, mid and bottom

E-LV-F-7-B
E-LV-F-7-T

E-TV-D-5-B
E-TV-D-5-M
E-TV-D-5-T

E-TV-C-3-B
E-TV-C-3-T

E-LV-F-5-B
E-LV-F-5-T

E-LV-B-3-B
E-LV-B-3-T

E-LV-F-3-B
E-LV-F-3-M
E-LV-F-3-T

E-LV-A-3-B
E-LV-A-3-T

E-LV-D-3-B
E-LV-D-3-T

E-TV-D-3-B
E-TV-D-3-T

7
6
5
4
3
2
1

G   F   E   D   C   B   A

Cable Exit Layout Showing Gage Clusters

□ Gage Cluster

● Exit Location
Each exit is 1½" in diameter

Section E-2: Detailed Instrumentation List

Empirical Deck at 16+81.74

Longitudinal Reinforcement Strain Gages

Table 2-1: Detailed list of strain gages bonded to longitudinal reinforcement in bridge @ 16+81.74 (empirical deck)

Reference No.	General Position			Expected Response (με)	Cable Exit Port	Approx. Lead Wire Length (m)	Bar Number	Purpose
	X	Y	Z					
E-LR-G-5-T	Over 2nd bent	Over stringer B	Top mat	-53.8	A1	25	S200E-1	Effect of saw cut
E-LR-F-5-T	Over 3rd bent	Over Stringer B	Top mat	-53.8	B2	4	S200E-3	String-Bent interaction
E-LR-F-1-T	Over 3rd bent	Over Stringer A	Top mat	-86.9	C2	7	S200E-5	String-Bent interaction
E-LR-F-1-B	Over 3rd bent	Over Stringer A	Bot mat	-86.9	C2	7	S300E-5	String-Bent interaction
E-LR-F-3-T	Over 3rd bent	Btwn stringer A&B	Top mat	-10.3	C1	7	S200E-4	Bending across bent
E-LR-F-3-B	Over 3rd bent	Btwn stringer A&B	Bot mat	-10.3	C1	7	S300E-4	Bending across bent
E-LR-F-7-T	Over 3rd bent	Btwn stringer B&C	Top mat	-6.21	B1	7	S200E-2	Bending across bent
E-LR-F-7-B	Over 3rd bent	Btwn stringer B&C	Bot mat	-6.21	B1	7	S300E-2	Bending across bent
E-LR-D-3-T	Btwn bent &dia	Btwn stringer A&B	Top mat	6.21	C6	9	S200E-7	Local deck behavior
E-LR-D-3-B	Btwn bent &dia	Btwn stringer A&B	Bot mat	6.21	C6	9	S300E-7	Local deck behavior
E-LR-C-3-T	Btwn bent &dia	Btwn stringer A&B	Top mat	5.86	D3	11	S200E-7	Local deck behavior
E-LR-C-3-B	Btwn bent &dia	Btwn stringer A&B	Bot mat	5.86	D3	11	S300E-7	Local deck behavior
E-LR-B-3-T	Over dia 3 to 4	Btwn stringer A&B	Top mat	4.83	E1	12.5	S200E-7	Effect of diaphragm
E-LR-B-3-B	Over dia 3 to 4	Btwn stringer A&B	Bot mat	4.83	E1	12.5	S300E-7	Effect of diaphragm
E-LR-A-3-T	Over 4th bent	Btwn stringer A&B	Top mat	-1.03	E4	20	S200E-7	Continuity effects
E-LR-A-3-B	Over 4th bent	Btwn stringer A&B	Bot mat	-1.03	E4	20	S300E-7	Continuity effects
E-LR-B-1-T	Over dia 3 to 4	Over Stringer A	Top mat	-12.1	E3	12.5	S200E-8	Global bending
E-LR-D-5-T	Btwn bent &dia	Over stringer B	Top mat	4.14	D1	12	S200E-6	Global bending
E-LR-B-5-T	Over dia 3 to 4	Over Stringer B	Top mat	-0.345	D4	12	S200E-6	Global bending

Transverse Reinforcement Strain Gages

Table 2-2: Detailed list of strain gages bonded to transverse reinforcement in bridge @ 16+81.74 (empirical deck)

Reference No.	General Position			Expected Response (με)	Cable Exit Port	Approx. Lead Wire Length (m)	Bar Number	Purpose
	X	Y	Z					
E-TR-D-1-T	Btwn bent & dia	Over stringer A	Top mat	6.21	C4	9	S100E-2	Stringer effects
E-TR-D-1-B	Btwn bent & dia	Over stringer A	Bot mat	6.21	C4	9	S100E-2	Stringer effects
E-TR-E-2-T	Btwn bent & dia	Btwn stringers A&B	Top mat	7.93	C3	7	S100E-1	Local deck behavior
E-TR-E-2-B	Btwn bent & dia	Btwn stringers A&B	Bot mat	7.93	C3	7	S100E-1	Local deck behavior
E-TR-D-2-T	Btwn bent & dia	Btwn stringers A&B	Top mat	6.9	C5	9	S100E-2	Local deck behavior
E-TR-D-2-B	Btwn bent & dia	Btwn stringers A&B	Bot mat	6.9	C5	9	S100E-2	Local deck behavior
E-TR-B-2-T	Over diaphragm	Btwn stringers A&B	Top mat	-2.07	E2	11	S100E-3	Effect of diaphragm
E-TR-B-2-B	Over diaphragm	Btwn stringers A&B	Bot mat	-2.07	E2	11	S100E-3	Effect of diaphragm
E-TR-D-4-T	Btwn bent & dia	Btwn stringers A&B	Top mat	7.24	D2	10.5	S100E-2	Local deck behavior
E-TR-D-4-B	Btwn bent & dia	Btwn stringers A&B	Bot mat	7.24	D2	10.5	S100E-2	Local deck behavior
E-TR-E-5-T	Btwn bent & dia	Over stringer B	Top mat	5.86	B3	5	S100E-1	Stringer effects
E-TR-E-5-B	Btwn bent & dia	Over stringer B	Bot mat	5.86	B3	5	S100E-1	Stringer effects
E-TR-D-5-T	Btwn bent & dia	Over stringer B	Top mat	4.83	D1	12	S100E-2	Stinger effects
E-TR-D-5-B	Btwn bent & dia	Over stringer B	Bot mat	4.83	D1	12	S100E-2	Stringer effects
E-TR-D-6-T	Btwn bent & dia	Btwn stringers B&C	Top mat	6.9	B4	10.5	S100E-2	Local deck behavior
E-TR-D-6-B	Btwn bent & dia	Btwn stringers B&C	Bot mat	6.9	B4	10.5	S100E-2	Local deck behavior

Embedded Strain Gages

Table 2-3: Detailed list of embedded strain gages in bridge @ 16+81.74 (empirical deck)

Reference No.	Orientation	General Position			Expected Response ($\mu\varepsilon$)	Cable Exit Port	Approx. Lead Wire Length (m)	Purpose
		X	Y	Z				
E-LE-F-5-B	Longitudinal	Over 2nd bent	Over stringer B	Bot	-15.6	B2	4	Stringer – Bent interaction
E-LE-F-5-M	Longitudinal	Over 2nd bent	Over stringer B	Mid	-15.6	B2	4	Stringer – Bent interaction
E-LE-F-5-T	Longitudinal	Over 2nd bent	Over stringer B	Top	-15.6	B2	4	Stringer – Bent interaction
E-TE-D-5-M	Transverse	Btwn bent & dia	Over stringer B	Mid	-1.8	D1	12	Stringer effects
E-TE-D-5-T	Transverse	Btwn bent & dia	Over stringer B	Top	-1.8	D1	12	Stringer effects
E-LE-F-7-M	Longitudinal	Over 2nd bent	Btwn stringers B & C	Mid	-1.8	B1	7	Bending across bent
E-LE-F-7-T	Longitudinal	Over 2nd bent	Btwn stringers B & C	Top	-1.2	B1	7	Bending across bent
E-TE-D-2-M	Transverse	Btwn bent & dia	Btwn stringers A & B	Mid		C5	9	Local bending effects
E-TE-D-2-T	Transverse	Btwn bent & dia	Btwn stringers A & B	Top		C5	9	Local bending effects

Vibrating Wire Strain Gages

Table2- 4: Detailed list of vibrating wire strain gages in bridge @ 19+23.24 (conventional deck)

Reference No.	Orientation	General Position			Expected Response (με)	Cable Exit Port	Approx Lead Wire Length (m)	Purpose
		X	Y	Z				
E-LV-F-3-B	Longitudinal	Over bent	Btwn stringers A & B	Bot	-3.0	C1	7	Bending across bent
E-LV-F-3-M	Longitudinal	Over bent	Btwn stringers A & B	Mid	-3.0	C1	7	Bending across bent
E-LV-F-3-T	Longitudinal	Over bent	Btwn stringers A & B	Top	-3.0	C1	7	Bending across bent
E-LV-F-5-B	Longitudinal	Over bent	Over stringer B	Bot	-15.6	B2	4	Stringer – bent interaction
E-LV-F-5-T	Longitudinal	Over bent	Over stringer B	Top	-15.6	B2	4	Stringer – bent interaction
E-LV-F-7-B	Longitudinal	Over bent	Btwn stringers B & C	Bot	-1.8	B1	7	Bending across bent
E-LV-F-7-T	Longitudinal	Over bent	Btwn stringers B & C	Top	-1.8	B1	7	Bending across bent
E-LV-D-3-B	Longitudinal	Btwn bent & dia	Btwn stringers A & B	Bot	1.8	C6	9	Local deck behavior
E-LV-D-3-T	Longitudinal	Btwn bent & dia	Btwn stringers A & B	Top	1.8	C6	9	Local deck behavior
E-LV-B-3-B	Longitudinal	Over dia	Btwn stringers A & B	Bot	-1.4	E1	12.5	Diaphragm effects
E-LV-B-3-T	Longitudinal	Over dia	Btwn stringers A & B	Top	-1.4	E1	12.5	Diaphragm effects
E-LV-A-3-B	Longitudinal	Over 4th bent	Btwn stringers A & B	Bot	-0.3	E4	20	Effects of end Bent
E-LV-A-3-T	Longitudinal	Over 4th bent	Btwn stringers A & B	Top	-0.3	E4	20	Effects of end bent
E-TV-D-3-B	Transverse	Btwn bent & dia	Btwn stringers A & B	Bot	2.3	C6	9	Local deck behavior
E-TV-D-3-T	Transverse	Btwn bent & dia	Btwn stringers A & B	Top	2.3	C6	9	Local deck behavior
E-TV-C-3-B	Transverse	Btwn dia & bent	Btwn stringers A & B	Bot	2.7	D3	11	Local deck behavior
E-TV-C-3-T	Transverse	Btwn dia & bent	Btwn stringers A & B	Top	2.7	D3	11	Local deck behavior
E-TV-D-5-B	Transverse	Btwn bent & dia	Over stringer B	Bot	1.4	D1	12	Stringer effects
E-TV-D-5-M	Transverse	Btwn bent & dia	Over stringer B	Mid	1.4	D1	12	Stringer effects
E-TV-D-5-T	Transverse	Btwn bent & dia	Over stringer B	Top	1.4	D1	12	Stringer effects

Section F-2: Detailed Drawings of Reinforcement with Bonded Strain Gages *Empirical Deck at 16+81.74*

Longitudinal Bars – Top Mat

E-LR-G-5-T

5380

S200E-1-E

9370

21560

E-LR-F-7-T

8800

S200E-2-E

20950

33140

E-LR-F-5-T

8800

S200E-3-E

20950

33140

E-LR-F-3-T

8800

S200E-4-E

20950

33140

E-LR-F-1-T

8800

S200E-5-E

20950

33140
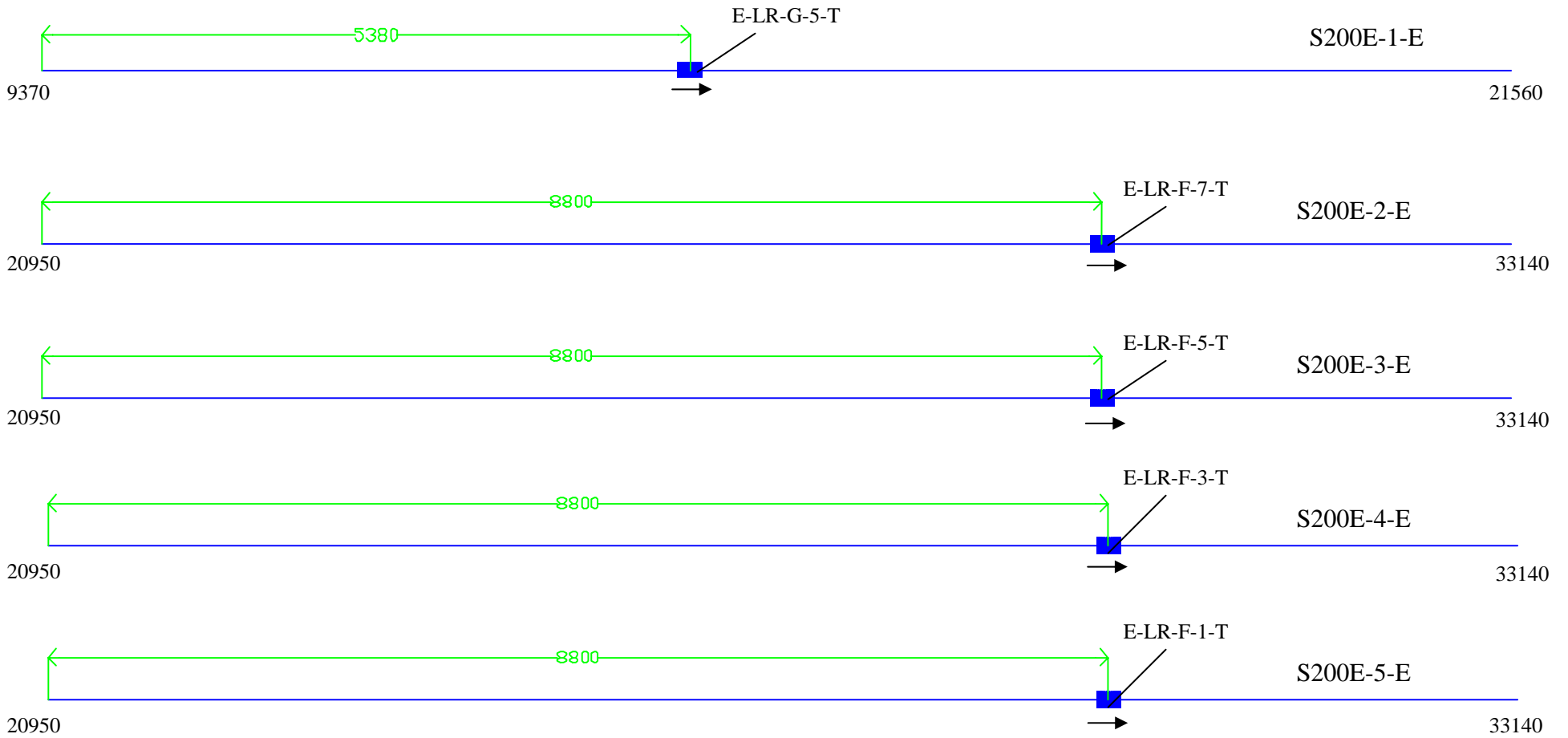
*Numbers at either end of the bar represent the longitudinal beginning and ending positions (in mm) with respect to the bridge deck.

Longitudinal Bars – Top Mat (continued)

*Numbers at either end of the bar represent the longitudinal beginning and ending positions (in mm) with respect to the bridge deck.

**A total of 8 S200E ~ #13 bars of length 12.19 m are needed for instrumentation from the top mat.

<u>Longitudinal Bars – Bottom Mat</u>

*Numbers at either end of the bar represent the longitudinal beginning and ending positions (in mm) with respect to the bridge deck.

**A total of 4 S300E ~ # 19 bars of length 12.19 m are needed for instrumentation from the bottom mat.

Section F-2: Detailed Drawings of Reinforcement with Bonded Strain Gages *Empirical Deck at 16+81.74*

Transverse Bars – Top Mat

S100E-1-E   S100E-2-E   S100E-3-E

transverse centerline of bridge deck

E-TR-D-6-T

1200

E-TR-E-5-T   E-TR-D-5-T

2000

E-TR-D-4-T

2800   3600   2800   2800

C-TR-E-2-T   E-TR-D-2-T   E-TR-B-2-T

E-TR-D-1-T

400
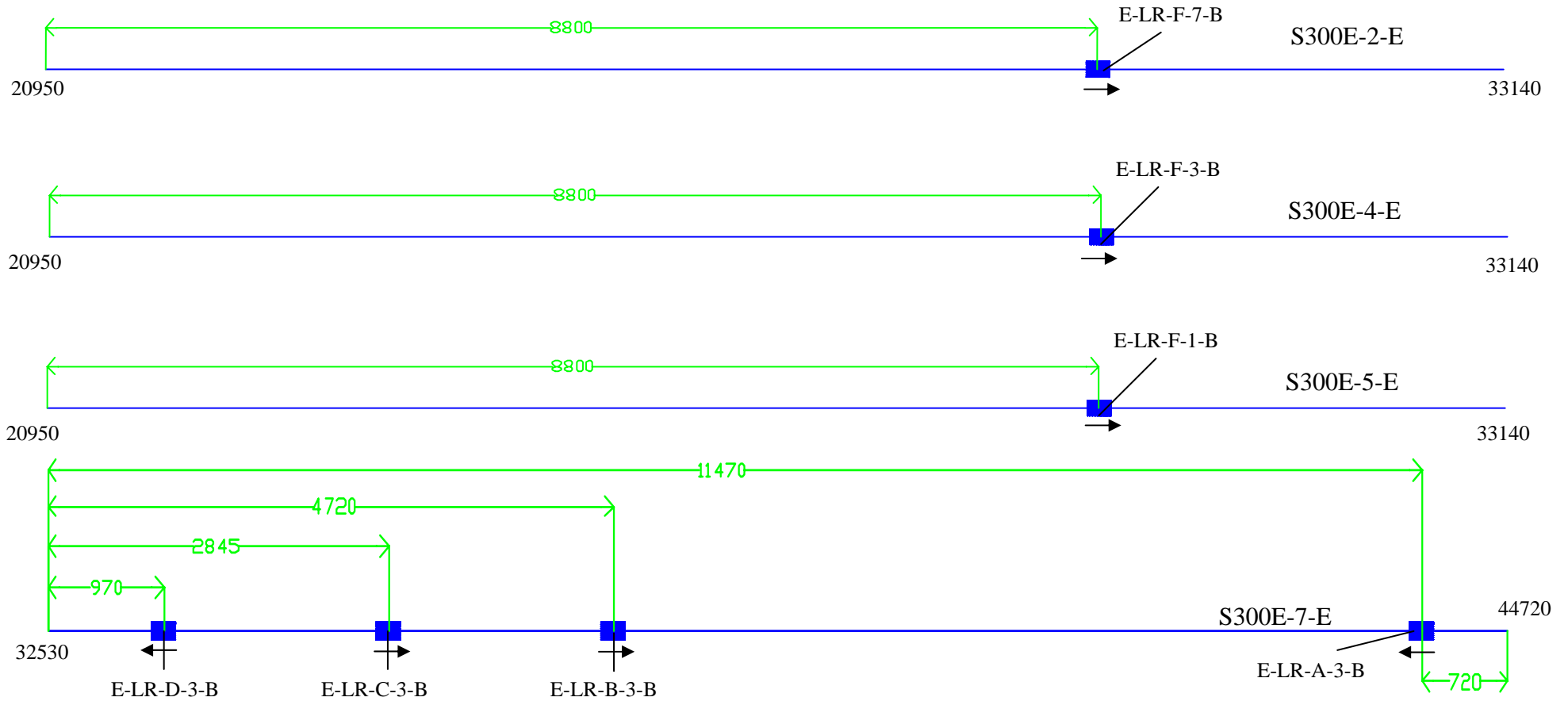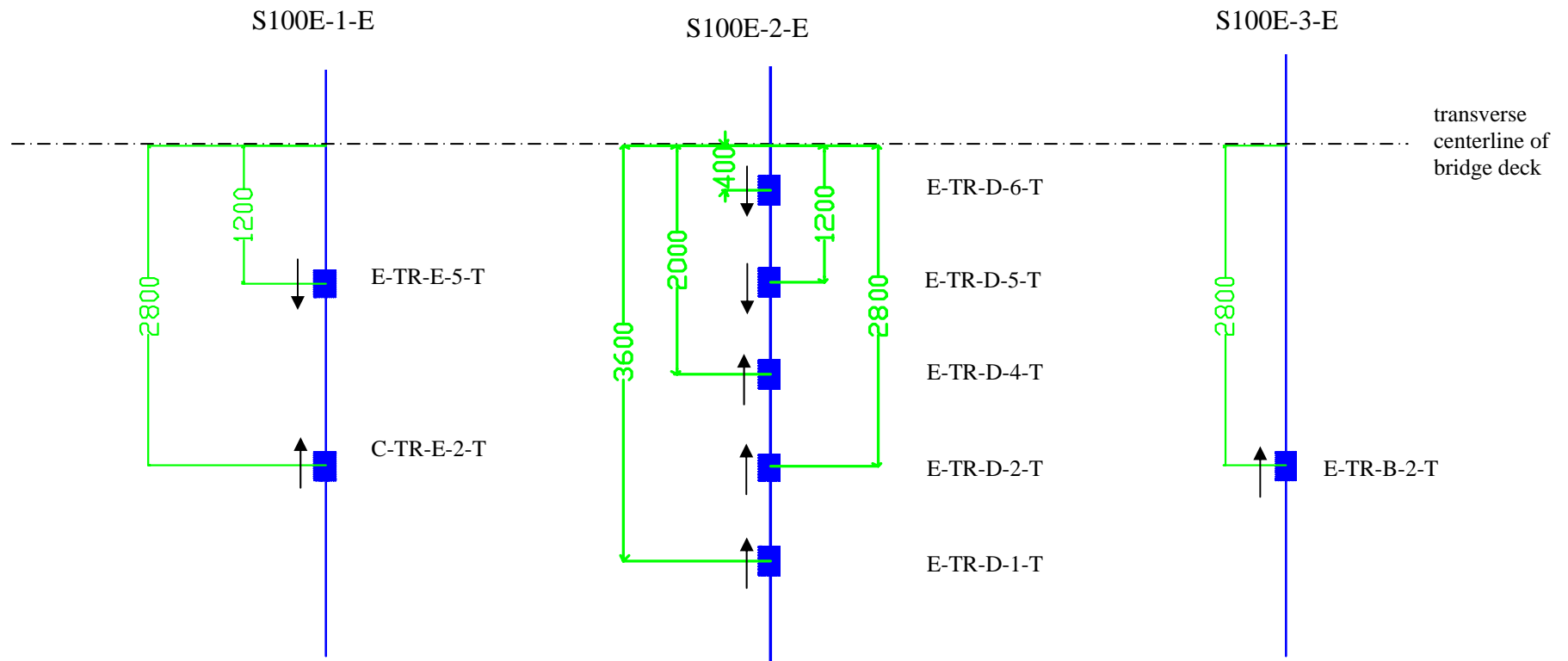
* A total of 3 S100E ~ # 13 bars of length 7.64 m are needed for instrumentation from the top mat

Transverse Bars – Bottom Mat
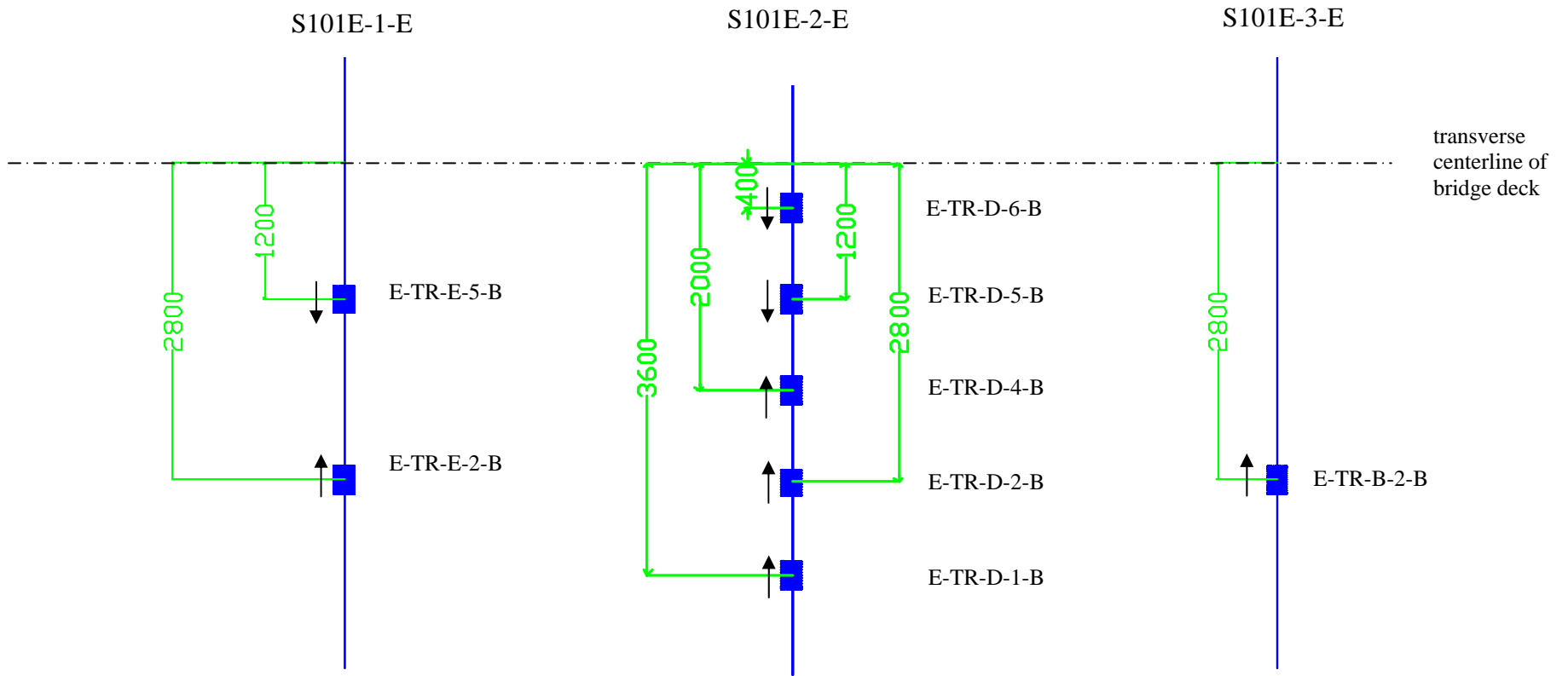
* A total of 3 S101E ~ # 16 bars of length 7.82 m are needed for instrumentation from the bottom mat

Part 3: Conventional Deck @19+23.24

The series of numbers along the bottom of the bridge correspond to the longitudinal gage positions used in the reference number system described above. Likewise, the numbers along the right edge correspond to the transverse position of the gages used in the reference number system. The arrows on the left side show the direction of travel across the bridge of a typical truck.

The S200E bars numbered 1 through 8 are the S200E ~ # 13 bars called out in the bridge plans for the top longitudinal reinforcement. The S300E bars numbered 2,4,5, and 7 are the S300E ~ #13 bars called out in the plans for the Bottom longitudinal reinforcement. Each of the longitudinal bars is 12.19 meters in length. The S100E bars numbered 1 through 3 are the S100E ~ # 19 bars called out in the plans as the top and bottom transverse reinforcement. Each transverse bar is 8.95 meters long.

Section B-3: Specific Rebar Layout

Top Longitudinal

26~S200E~#13 (3 per line) top
longitudinal bars lap with S201E~#13
(See Transverse Section for spacing)

S200E-1-C
S200E-2-C
S200E-3-C
S200E-6-C
S200E-7-C
S200E-4-C
S200E-5-C
S200E-8-C

Bottom Longitudinal

26~S200E~#13 (3 per line) top
longitudinal bars lap with S201E~#13
(See Transverse Section for spacing)

S300E-2-C
S300E-4-C
S300E-7-C
S300E-5-C

Top and Bottom Transverse

26-S200-E #13 (3 per line) top
Longitudinal bars top with S201F #13
(See Transverse Section for spacing)

Section C-3: Plan View of Gage Locations

Conventional Deck at 19+23.24

Bonded Strain Gage Layout

6 transverse bars   (16 gage locations)
12 longitudinal bars (19 gage locations)

■ Transverse gage, top and bottom mat

▬ Longitudinal gage, top and bottom mat

▬ Longitudinal gage, top mat only

⬤ Longitudinal gage, bottom of stringer

C-TR-D-4-B
C-TR-D-4-T
C-TR-D-6-B
C-TR-D-6-T
C-LR-F-7-B
C-LR-F-7-T
C-LR-D-5-T
C-TR-D-5-B
C-TR-D-5-T
C-TR-E-5-B
C-TR-E-5-T
C-LR-G-5-T
C-LR-B-5-T
C-LR-F-5-T
C-LR-D-3-B
C-LR-D-3-T
C-LR-C-3-B
C-LR-C-3-T
C-LR-B-3-B
C-LR-B-3-T
C-LR-A-3-B
C-LR-A-3-T
C-LR-F-3-B
C-LR-F-3-T
C-TR-E-2-B
C-TR-E-2-T
C-TR-D-2-B
C-TR-D-2-T
C-TR-B-2-B
C-TR-B-2-T
C-LR-F-1-B
C-LR-F-1-T
C-LR-B-1-T
C-TR-D-1-B
C-TR-D-1-T

7
6
5
4
3
2
1

G   F E D C B   A

Section C-3: Plan View of Gage Locations

Embedded Strain Gage Layout

9 locations

▮	Transverse gage, mid and near surface
▭ (magenta)	Longitudinal gage, mid and near surface
▭ (red)	Longitudinal gage, bottom, mid, and near surface

C-LE-F-7-M
C-LE-F-7-T

C-TE-D-5-M
C-TE-D-5-T

C-LE-F-5-B
C-LE-F-5-M
C-LE-F-5-T

C-TE-D-2-M
C-TE-D-2-T

7
6
5
4
3
2
1

G   F   E   D   C   B   A

Section C-3: Plan View of Gage Locations

Vibrating Wire Gage Layout

20 locations

■ Transverse gage, top, mid, and bottom

■ Transverse gage, top and bottom

■ Longitudinal gage, top and bottom

■ Longitudinal gage, top, mid and bottom

C-LV-F-7-B
C-LV-F-7-T

C-TV-D-5-B
C-TV-D-5-M
C-TV-D-5-T

C-TV-C-3-B
C-TV-C-3-T

C-LV-F-5-B
C-LV-F-5-T

C-LV-B-3-B
C-LV-B-3-T

C-LV-F-3-B
C-LV-F-3-M
C-LV-F-3-T

C-LV-A-3-B
C-LV-A-3-T

C-LV-D-3-B
C-LV-D-3-T

C-TV-D-3-B
C-TV-D-3-T

7
6
5
4
3
2
1

G   F E D C B   A

Cable Exit Layout Showing Gage Clusters

Longitudinal Reinforcement Strain Gages

Table 3-1: Detailed list of strain gages bonded to longitudinal reinforcement in bridge @ 19+23.24 (conventional deck)

Reference No.	General Position			Expected Response ($\mu\varepsilon$)	Cable Exit Port	Approx. Lead Wire Length (m)	Bar Number	Purpose
	X	Y	Z					
C-LR-G-5-T	Over 2nd bent	Over stringer B	Top mat	-53.8	A1	25	S200E-1	Effect of saw cut
C-LR-F-5-T	Over 3rd bent	Over Stringer B	Top mat	-53.8	B2	4	S200E-3	String-Bent interaction
C-LR-F-1-T	Over 3rd bent	Over Stringer A	Top mat	-86.9	C2	7	S200E-5	String-Bent interaction
C-LR-F-1-B	Over 3rd bent	Over Stringer A	Bot mat	-86.9	C2	7	S300E-5	String-Bent interaction
C-LR-F-3-T	Over 3rd bent	Btwn stringer A&B	Top mat	-10.3	C1	7	S200E-4	Bending across bent
C-LR-F-3-B	Over 3rd bent	Btwn stringer A&B	Bot mat	-10.3	C1	7	S300E-4	Bending across bent
C-LR-F-7-T	Over 3rd bent	Btwn stringer B&C	Top mat	-6.21	B1	7	S200E-2	Bending across bent
C-LR-F-7-B	Over 3rd bent	Btwn stringer B&C	Bot mat	-6.21	B1	7	S300E-2	Bending across bent
C-LR-D-3-T	Btwn bent &dia	Btwn stringer A&B	Top mat	6.21	C6	9	S200E-7	Local deck behavior
C-LR-D-3-B	Btwn bent &dia	Btwn stringer A&B	Bot mat	6.21	C6	9	S300E-7	Local deck behavior
C-LR-C-3-T	Btwn bent &dia	Btwn stringer A&B	Top mat	5.86	D3	11	S200E-7	Local deck behavior
C-LR-C-3-B	Btwn bent &dia	Btwn stringer A&B	Bot mat	5.86	D3	11	S300E-7	Local deck behavior
C-LR-B-3-T	Over dia 3 to 4	Btwn stringer A&B	Top mat	4.83	E1	12.5	S200E-7	Effect of diaphragm
C-LR-B-3-B	Over dia 3 to 4	Btwn stringer A&B	Bot mat	4.83	E1	12.5	S300E-7	Effect of diaphragm
C-LR-A-3-T	Over 4th bent	Btwn stringer A&B	Top mat	-1.03	E4	20	S200E-7	Continuity effects
C-LR-A-3-B	Over 4th bent	Btwn stringer A&B	Bot mat	-1.03	E4	20	S300E-7	Continuity effects
C-LR-B-1-T	Over dia 3 to 4	Over Stringer A	Top mat	-12.1	E3	12.5	S200E-8	Global bending
C-LR-D-5-T	Btwn bent &dia	Over stringer B	Top mat	4.14	D1	12	S200E-6	Global bending
C-LR-B-5-T	Over dia 3 to 4	Over Stringer B	Top mat	-0.345	D4	12	S200E-6	Global bending

Transverse Reinforcement Strain Gages

Table 3-2: Detailed list of strain gages bonded to transverse reinforcement in bridge @ 19+23.24 (conventional deck)

Reference No.	General Position			Expected Response (µε)	Cable Exit Port	Approx. Lead Wire Length (m)	Bar Number	Purpose
	X	Y	Z					
C-TR-D-1-T	Btwn bent & dia	Over stringer A	Top mat	6.21	C4	9	S100E-2	Stringer effects
C-TR-D-1-B	Btwn bent & dia	Over stringer A	Bot mat	6.21	C4	9	S100E-2	Stringer effects
C-TR-E-2-T	Btwn bent & dia	Btwn stringers A&B	Top mat	7.93	C3	7	S100E-1	Local deck behavior
C-TR-E-2-B	Btwn bent & dia	Btwn stringers A&B	Bot mat	7.93	C3	7	S100E-1	Local deck behavior
C-TR-D-2-T	Btwn bent & dia	Btwn stringers A&B	Top mat	6.9	C5	9	S100E-2	Local deck behavior
C-TR-D-2-B	Btwn bent & dia	Btwn stringers A&B	Bot mat	6.9	C5	9	S100E-2	Local deck behavior
C-TR-B-2-T	Over diaphragm	Btwn stringers A&B	Top mat	-2.07	E2	11	S100E-3	Effect of diaphragm
C-TR-B-2-B	Over diaphragm	Btwn stringers A&B	Bot mat	-2.07	E2	11	S100E-3	Effect of diaphragm
C-TR-D-4-T	Btwn bent & dia	Btwn stringers A&B	Top mat	7.24	D2	10.5	S100E-2	Local deck behavior
C-TR-D-4-B	Btwn bent & dia	Btwn stringers A&B	Bot mat	7.24	D2	10.5	S100E-2	Local deck behavior
C-TR-E-5-T	Btwn bent & dia	Over stringer B	Top mat	5.86	B3	5	S100E-1	Stringer effects
C-TR-E-5-B	Btwn bent & dia	Over stringer B	Bot mat	5.86	B3	5	S100E-1	Stringer effects
C-TR-D-5-T	Btwn bent & dia	Over stringer B	Top mat	4.83	D1	12	S100E-2	Stinger effects
C-TR-D-5-B	Btwn bent & dia	Over stringer B	Bot mat	4.83	D1	12	S100E-2	Stringer effects
C-TR-D-6-T	Btwn bent & dia	Btwn stringers B&C	Top mat	6.9	B4	10.5	S100E-2	Local deck behavior
C-TR-D-6-B	Btwn bent & dia	Btwn stringers B&C	Bot mat	6.9	B4	10.5	S100E-2	Local deck behavior

Embedded Strain Gages

Table 3-3: Detailed list of embedded strain gages in bridge @ 19+23.24 (conventional deck)

Reference No.	Orientation	General Position			Expected Response (μɛ)	Cable Exit Port	Approx. Lead Wire Length (m)	Purpose
		X	Y	Z				
C-LE-F-5-B	Longitudinal	Over 2nd bent	Over stringer B	Bot	-15.6	B2	4	Stringer – Bent interaction
C-LE-F-5-M	Longitudinal	Over 2nd bent	Over stringer B	Mid	-15.6	B2	4	Stringer – Bent interaction
C-LE-F-5-T	Longitudinal	Over 2nd bent	Over stringer B	Top	-15.6	B2	4	Stringer – Bent interaction
C-TE-D-5-M	Transverse	Btwn bent & dia	Over stringer B	Mid	-1.8	D1	12	Stringer effects
C-TE-D-5-T	Transverse	Btwn bent & dia	Over stringer B	Top	-1.8	D1	12	Stringer effects
C-LE-F-7-M	Longitudinal	Over 2nd bent	Btwn stringers B & C	Mid	-1.8	B1	7	Bending across bent
C-LE-F-7-T	Longitudinal	Over 2nd bent	Btwn stringers B & C	Top	-1.2	B1	7	Bending across bent
C-TE-D-2-M	Transverse	Btwn bent & dia	Btwn stringers A & B	Mid		C5	9	Local bending effects
C-TE-D-2-T	Transverse	Btwn bent & dia	Btwn stringers A & B	Top		C5	9	Local bending effects

Vibrating Wire Strain Gages

Table 3-4: Detailed list of vibrating wire strain gages in bridge @ 19+23.24 (conventional deck)

Reference No.	Orientation	General Position			Expected Response (με)	Cable Exit Port	Approx Lead Wire Length (m)	Purpose
		X	Y	Z				
C-LV-F-3-B	Longitudinal	Over bent	Btwn stringers A & B	Bot	-3.0	C1	7	Bending across bent
C-LV-F-3-M	Longitudinal	Over bent	Btwn stringers A & B	Mid	-3.0	C1	7	Bending across bent
C-LV-F-3-T	Longitudinal	Over bent	Btwn stringers A & B	Top	-3.0	C1	7	Bending across bent
C-LV-F-5-B	Longitudinal	Over bent	Over stringer B	Bot	-15.6	B2	4	Stringer – bent interaction
C-LV-F-5-T	Longitudinal	Over bent	Over stringer B	Top	-15.6	B2	4	Stringer – bent interaction
C-LV-F-7-B	Longitudinal	Over bent	Btwn stringers B & C	Bot	-1.8	B1	7	Bending across bent
C-LV-F-7-T	Longitudinal	Over bent	Btwn stringers B & C	Top	-1.8	B1	7	Bending across bent
C-LV-D-3-B	Longitudinal	Btwn bent & dia	Btwn stringers A & B	Bot	1.8	C6	9	Local deck behavior
C-LV-D-3-T	Longitudinal	Btwn bent & dia	Btwn stringers A & B	Top	1.8	C6	9	Local deck behavior
C-LV-B-3-B	Longitudinal	Over dia	Btwn stringers A & B	Bot	-1.4	E1	12.5	Diaphragm effects
C-LV-B-3-T	Longitudinal	Over dia	Btwn stringers A & B	Top	-1.4	E1	12.5	Diaphragm effects
C-LV-A-3-B	Longitudinal	Over 4th bent	Btwn stringers A & B	Bot	-0.3	E4	20	Effects of end Bent
C-LV-A-3-T	Longitudinal	Over 4th bent	Btwn stringers A & B	Top	-0.3	E4	20	Effects of end bent
C-TV-D-3-B	Transverse	Btwn bent & dia	Btwn stringers A & B	Bot	2.3	C6	9	Local deck behavior
C-TV-D-3-T	Transverse	Btwn bent & dia	Btwn stringers A & B	Top	2.3	C6	9	Local deck behavior
C-TV-C-3-B	Transverse	Btwn dia & bent	Btwn stringers A & B	Bot	2.7	D3	11	Local deck behavior
C-TV-C-3-T	Transverse	Btwn dia & bent	Btwn stringers A & B	Top	2.7	D3	11	Local deck behavior
C-TV-D-5-B	Transverse	Btwn bent & dia	Over stringer B	Bot	1.4	D1	12	Stringer effects
C-TV-D-5-M	Transverse	Btwn bent & dia	Over stringer B	Mid	1.4	D1	12	Stringer effects
C-TV-D-5-T	Transverse	Btwn bent & dia	Over stringer B	Top	1.4	D1	12	Stringer effects

Longitudinal Bars – Top Mat

*Numbers at either end of the bar represent the longitudinal beginning and ending positions (in mm) with respect to the bridge deck.

Longitudinal Bars – Top Mat (continued)

C-LR-B-5-T

S200E-6-C

4720

970

32530   44720

C-LR-D-5-T

11470

4720

2845

970

S200E-7-C   44720

32530

C-LR-D-3-T   C-LR-C-3-T   C-LR-B-3-T

C-LR-A-3-T

720

4720

C-LR-B-1-T

S200E-8-C

32530   44720

*Numbers at either end of the bar represent the longitudinal beginning and ending positions (in mm) with respect to the bridge deck.

**A total of 8 S200E ~ #13 bars of length 12.19 m are needed for instrumentation from the top mat.

Longitudinal Bars – Bottom Mat

C-LR-F-7-B

8800

S300E-2-C

20950   33140

C-LR-F-3-B

8800

S300E-4-C

20950   33140

C-LR-F-1-B

8800

S300E-5-C

20950   33140

11470

4720

2845

970

S300E-7-C   44720

32530

C-LR-D-3-B   C-LR-C-3-B   C-LR-B-3-B   C-LR-A-3-B   720

*Numbers at either end of the bar represent the longitudinal beginning and ending positions (in mm) with respect to the bridge deck.

**A total of 4 S300E ~ # 19 bars of length 12.19 m are needed for instrumentation from the bottom mat.

Transverse Bars – Top Mat

S100E-1-C

S100E-2-C

S100E-3-C

transverse centerline of bridge deck

C-TR-D-6-T

C-TR-E-5-T

C-TR-D-5-T

C-TR-D-4-T

C-TR-E-2-T

C-TR-D-2-T

C-TR-B-2-T

C-TR-D-1-T

1200

2800

400

2000

1200

3600

2800

2800

* A total of 3 S100E ~ # 19 bars of length 8.95 m are needed for instrumentation from the top mat

Transverse Bars – Bottom Mat

S100E-1-C   S100E-2-C   S100E-3-C

C-TR-E-5-B

C-TR-E-2-B

C-TR-D-6-B

C-TR-D-5-B

C-TR-D-4-B

C-TR-D-2-B

C-TR-D-1-B

C-TR-B-2-B

transverse centerline of bridge deck

* A total of 3 S100E ~ # 19 bars of length 8.95 m are needed for instrumentation from the bottom mat

Addendum: List of Failed Gages over Time

Legend:
As of May 2004
As of July 2005

Conventional Deck		
Resistance	Embedded	Vibrating
C-LR-B-5-T	C-LE-F-5-M	C-TV-D-5-M
C-LR-F-3-T	C-LE-F-5-T	C-LV-F-5-M
C-LR-F-5-T	C-LE-F-7-M	C-LV-F-5-T
C-LR-G-5-T	C-LE-F-7-T	
C-LR-B-3-B	C-TE-D-2-T	
C-LR-B-1-T		
C-LR-D-3-T		
C-LR-B-3-T		
C-TR-D-1-B		
C-TR-D-5-T		
C-TR-D-1-T		
C-TR-D-4-T		
C-LR-D-5-T		
C-TR-D-6-T		
C-TR-E-5-T		
C-LR-F-7-T		
C-LR-F-1-B		

HPC Deck		
Resistance	Embedded	Vibrating
H-LR-F-7-T	H-LE-F-5-T	
H-LR-B-3-T	H-LE-F-7-M	
H-LR-F-5-T	H-LE-F-5-B	
H-TR-D-5-B	H-LE-F-7-T	
H-LR-A-3-T	H-LE-F-5-M	
H-LR-B-1-T		
H-LR-B-5-T		
H-TR-B-2-T		
H-TR-B-2-B		
H-LR-B-3-B		
H-LR-C-3-T		
H-TR-D-5-T		
H-TR-D-2-T		
H-TR-D-6-T		
H-TR-D-1-B		
H-LR-D-3-B		
H-TR-D-4-T		
H-TR-D-1-T		
H-LR-D-5-T		
H-TR-D-6-B		
H-TR-E-5-T		
H-TR-E-2-T		
H-LR-F-3-T		
H-LR-G-5-T		

Empirical Deck		
Resistance	Embedded	Vibrating
E-LR-F-1-B	E-LE-F-5-M	E-LV-F-5-T
E-TR-D-1-T	E-LE-F-5-T	E-LV-F-5-B
E-LR-F-3-T	E-LE-F-7-T	E-LV-F-7-B
E-LR-C-3-T		
E-TR-D-6-T		

**Appendix F – Methodology for Statistical Comparisons of Deck
Responses under Live Load Testing**

Statistical analyses of live load data were used to reveal or verify any differences in behavior between the three bridge decks or over time. The first of two separate analyses was conducted using the results of the neutral axis and axial strain analysis (detailed in Sections 7.1.2 and 7.1.3 of the report). These parameters were determined using strain responses from transverse sensors attached to the reinforcement; namely, the D-Line. The second analysis used raw strains from all embedded instrumentation that were active during the live load tests. The methodologies and results of these analyses are elaborated on in more detail below. However, the implications of these results are discussed within the body of the report – not in this appendix.

Statistical Analysis of Neutral Axes and Axial Strains

Statistical methods are used to determine the probability that true differences exist. Dissimilarities in the bending neutral axis height or the axial strain may reveal differences in behavior between the three decks or between decks over time. The four variables thought to affect the height of the bending neutral axis or the axial strains were: the direction of the bending moment (negative or positive), position of the truck along the bridge (40 m or 42 m), year the live load test was conducted (2003 or 2005) and type of bridge (Conventional, Empirical or HPC). Each of the variables was used in various combinations to determine a single combined mean value that can be compared between bridges or over time. For example, to determine whether there was any difference between the neutral axis height of the Conventional and Empirical bridges in 2003, all neutral axis heights determined using 2003 live load data were averaged, whether positive or negative moment, 40 m or 42 m position for the Conventional bridge and compared to a similarly derived value for the Empirical bridge. Mean values from each of the bridges was statistically compared to the other using standard deviations, coefficients of variation (COV), and the number of samples, *N*. Tables F-1 through F-5 show the combined means of the bending neutral axes, and Tables F-6 through F-10 show the combined means of the axial strains for each of the bridges and each year.

Table F-1: Mean Neutral Axis Height – All Years, All Moments, All Truck Positions

Bridge	Mean	St. Dev.	COV	N
CON	98.9	103.9	105.1	164
EMP	97.8	152.8	156.3	187
HPC	107.0	129.9	121.4	103

Table F-2: Mean Neutral Axis Height – All Moments, All Truck Positions

Year	Bridge	Mean	St. Dev.	COV	N
2003	**CON**	91.5	130.5	142.5	100
	EMP	98.7	154.5	156.6	100
	HPC	110.4	126.6	114.6	99
2005	**CON**	110.3	30.8	27.9	64
	EMP	96.8	151.7	156.8	87
	HPC	22.8	202.4	886.6	4

Table F-3: Mean Neutral Axis Height – All Truck Positions

Moment	Year	Bridge	Mean	St. Dev.	COV	N
Negative	**2003**	**CON**	35.9	133.2	370.9	46
		EMP	34.2	187.7	548.9	48
		HPC	60.5	120.6	199.3	46
	2005	**CON**	89.8	30.6	34.1	22
		EMP	23.0	159.2	691.8	41
		HPC	-110.2	222.0	-201.5	2
Positive	**2003**	**CON**	138.9	108.4	78.1	54
		EMP	158.2	79.6	50.3	52
		HPC	153.7	116.1	75.6	53
	2005	**CON**	121.0	25.2	20.8	42
		EMP	162.6	110.0	67.7	46
		HPC	155.8	53.3	34.2	2

Table F-4: Mean Neutral Axis Height – All Moments

Position	Year	Bridge	Mean	St. Dev.	COV	N
40 m	**2003**	**CON**	103.6	128.7	124.2	50
		EMP	108.4	86.6	79.9	50
		HPC	98.3	98.0	99.7	49
	2005	**CON**	112.7	35.8	31.8	32
		EMP	58.9	144.7	245.8	43
		HPC	82.5	50.5	61.2	2
42 m	**2003**	**CON**	79.5	132.4	166.6	50
		EMP	88.9	201.3	226.5	50
		HPC	122.3	149.4	122.2	50
	2005	**CON**	107.9	25.1	23.3	32
		EMP	133.9	150.8	112.7	44
		HPC	-36.8	325.8	-884.1	2

Table F-5: Mean Neutral Axis Height

Moment	Position	Year	Bridge	Mean	St. Dev.	COV	N
Negative	40 m	2003	CON	57.2	76.7	134.0	25
			EMP	70.7	67.0	94.8	27
			HPC	66.7	121.1	181.5	26
		2005	CON	92.1	30.2	32.8	13
			EMP	10.6	171.8	1613.9	25
			HPC	46.8	---	---	1
	42 m	2003	CON	10.5	177.8	1687.9	21
			EMP	-12.7	269.9	-2121.4	21
			HPC	52.5	122.7	233.8	20
		2005	CON	86.5	32.8	37.9	9
			EMP	42.3	140.3	331.5	16
			HPC	-267.2	---	---	1
Positive	40 m	2003	CON	150.0	153.1	102.1	25
			EMP	152.7	87.2	57.1	23
			HPC	134.0	42.4	31.7	23
		2005	CON	126.7	33.0	26.1	19
			EMP	125.9	43.5	34.6	18
			HPC	118.2	---	---	1
	42 m	2003	CON	129.4	44.3	34.2	29
			EMP	162.5	74.4	45.8	29
			HPC	168.8	149.3	88.4	30
		2005	CON	116.2	15.5	13.3	23
			EMP	186.2	132.3	71.1	28
			HPC	193.5	---	---	1

Table F-6: Mean Axial Strain – All Years, All Moments, All Truck Positions

Bridge	Mean	St. Dev.	COV	N
CON	2.3	2.3	97.1	164
EMP	2.8	3.3	116.4	188
HPC	2.4	2.4	100.2	104

Table F-7: Mean Axial Strain – All Moments, All Truck Positions

Year	Bridge	Mean	St. Dev.	COV	N
2003	CON	2.4	2.3	95.4	100
	EMP	2.9	2.6	90.3	100
	HPC	2.3	2.4	103.4	100
2005	CON	2.1	2.1	100.1	64
	EMP	2.7	3.9	143.9	88
	HPC	3.6	1.3	34.5	4

Table F-8: Mean Axial Strains– All Truck Positions

Moment	Year	Bridge	Mean	St. Dev.	COV	N
Negative	2003	CON	1.8	2.3	128.3	46
		EMP	1.2	2.2	179.9	48
		HPC	1.1	2.2	204.0	46
	2005	CON	0.7	1.6	237.5	22
		EMP	1.1	2.2	197.5	42
		HPC	4.6	0.1	1.7	2
Positive	2003	CON	3.0	2.2	74.4	54
		EMP	4.4	1.9	43.6	52
		HPC	3.4	2.0	57.0	53
	2005	CON	2.9	2.0	68.6	42
		EMP	4.1	4.5	108.9	46
		HPC	2.7	1.0	36.5	2

Table F-9: Mean Axial Strains – All Moments

Position	Year	Bridge	Mean	St. Dev.	COV	N
40 m	2003	CON	2.5	2.6	105.5	50
		EMP	2.9	2.8	98.5	50
		HPC	2.4	2.8	116.2	50
	2005	CON	2.2	2.4	104.8	32
		EMP	2.8	4.8	169.1	44
		HPC	3.3	1.9	57.2	2
42 m	2003	CON	2.4	2.1	84.9	50
		EMP	2.9	2.4	82.6	50
		HPC	2.2	1.8	84.9	50
	2005	CON	2.0	1.9	95.3	32
		EMP	2.6	2.8	107.9	44
		HPC	4.0	0.8	21.4	2

Table F-10: Mean Axial Strains

Moment	Position	Year	Bridge	Mean	St. Dev.	COV	N
Negative	40 m	2003	CON	2.1	2.6	124.5	25
			EMP	1.6	2.6	164.5	27
			HPC	1.6	2.7	175.1	26
		2005	CON	0.8	2.0	235.2	13
			EMP	1.7	2.5	149.8	26
			HPC	4.7	---	---	1
	42 m	2003	CON	1.4	1.8	129.4	21
			EMP	0.8	1.7	202.6	21
			HPC	0.5	1.0	218.1	20
		2005	CON	0.5	1.0	220.7	9
			EMP	0.3	1.4	534.4	16
			HPC	4.6	---	---	1
Positive	40 m	2003	CON	2.8	2.6	91.4	25
			EMP	4.4	2.3	52.8	23
			HPC	3.6	2.6	72.3	23
		2005	CON	3.2	2.1	66.4	19
			EMP	4.5	6.6	146.4	18
			HPC	2.0	---	---	1
	42 m	2003	CON	3.1	1.9	61.0	29
			EMP	4.4	1.6	35.7	29
			HPC	3.3	1.3	39.5	30
		2005	CON	2.6	1.9	70.9	23
			EMP	3.9	2.5	64.0	28
			HPC	3.4	---	---	1

These combined mean values were compared with one another using a two-sample, two-sided t-test. This statistical method utilizes the means, standard deviations, coefficients of variation, and sample size from each combination. The results from this test can be used to determine the p-value, which is an indicator that the means are similar. P-values range between zero and one, with p-values closer to zero indicating that the means are statistically less similar to one another and p-values closer to one indicating that the means are statistically more similar to one another. The results from these statistical tests are provided in Tables F-11 and F-12 for the bending neutral axis analysis and Tables F-13 and F-14 for the axial strain analysis. Tables 11 and 13 provide the statistical p-values for cross bridge examinations regardless of the year they were tested. Tables F-12 and F-14 take into considerations the year they were tested. The columns on the left side of the table indicate which variables were used to determine the composite mean values being compared. Italicized values are for 2005 and non-italicized values are for 2003. For example, the p-value to determine whether the mean bending neutral axis is the same between the Empirical and HPC deck in 2005, considering all truck positions but only negative moments, is 0.56. This essentially indicates that when values of the bending neutral axis are randomly sampled from the entire data set, the means are equal 56 percent of the time. As previously mentioned, the implications of these results are elaborated on in further detail within the body of the report.

Table F-11: P-Values for Bridge to Bridge Comparisons of Neutral Axis Regardless of Year Tested

Comparisons	P-Value
CON/EMP	0.94
CON/HPC	0.59
EMP/HPC	0.59

Table F- 12: P-Values Indicating Whether the Mean Neutral Axes are Similar

Moment Positive	Moment Negative	Position 40 m	Position 42 m			2005 CON	2005 EMP	2005 HPC
▨	▨	▨	▨	2003	CON	0.17	0.42	0.45
					EMP	0.73	0.93	0.52
					HPC	0.30	0.56	0.45
	▨	▨	▨	2003	CON	0.01	0.01	0.42
					EMP	0.96	0.76	0.56
					HPC	0.36	0.42	0.48
▨		▨	▨	2003	CON	0.24	0.02	0.53
					EMP	0.30	0.82	0.90
					HPC	0.50	0.82	0.97
▨	▨	▨		2003	CON	0.64	0.02	0.56
					EMP	0.83	0.05	0.67
					HPC	0.82	0.59	0.75
▨	▨		▨	2003	CON	0.15	0.27	0.64
					EMP	0.78	0.22	0.60
					HPC	0.13	0.35	0.62
	▨	▨		2003	CON	0.05	0.03	---
					EMP	0.50	0.11	---
					HPC	0.74	0.88	---
	▨		▨	2003	CON	0.07	0.25	---
					EMP	0.74	0.43	---
					HPC	0.38	0.32	---
▨		▨		2003	CON	0.47	0.95	---
					EMP	0.94	0.21	---
					HPC	0.62	0.36	---
▨			▨	2003	CON	0.14	0.01	---
					EMP	0.05	0.41	---
					HPC	0.18	0.84	---

Table F-13: P-Values for Bridge to Bridge Comparisons of Axial Strains Regardless of Year Tested

Comparisons	P-Value
CON/EMP	0.11
CON/HPC	0.91
EMP/HPC	0.18

Table F- 14: P-Values Indicating Whether the Mean Axial Strains are Similar

Moment		Position				*2005*		
Positive	Negative	40 m	42 m			CON	EMP	HPC
▨	▨	▨	▨	2003	CON	0.39	*0.26*	*0.09*
					EMP	0.20	0.68	*0.25*
					HPC	0.68	0.10	0.14
	▨	▨	▨	2003	CON	0.03	*0.38*	0.00
					EMP	0.23	0.81	*0.00*
					HPC	0.13	0.73	0.00
▨		▨	▨	2003	CON	0.82	*0.10*	0.82
					EMP	0.00	0.68	*0.23*
					HPC	0.28	0.01	0.49
▨	▨	▨		2003	CON	0.69	*0.49*	0.58
					EMP	0.45	0.95	*0.80*
					HPC	0.97	0.45	0.64
▨	▨		▨	2003	CON	0.38	*0.32*	*0.22*
					EMP	0.28	0.52	*0.20*
					HPC	0.51	0.08	0.22
	▨	▨		2003	CON	0.10	*0.28*	---
					EMP	0.44	0.89	---
					HPC	0.45	1.00	---
	▨		▨	2003	CON	0.09	*0.67*	---
					EMP	0.28	0.27	---
					HPC	0.04	0.40	---
▨		▨		2003	CON	0.58	*0.44*	---
					EMP	0.03	0.96	---
					HPC	0.30	0.26	---
▨			▨	2003	CON	0.34	*0.05*	---
					EMP	0.01	0.34	---
					HPC	0.71	0.00	---

Raw Strain Statistical Analysis

Characterizing overall response of the instrumented portions of the bridge decks was accomplished by averaging the strain responses from instrumentation used during the live load testing (specifically, resistance-strain gages bonded to the reinforcement and embedded directly in the concrete). Only gage lines A, B, C, D and E were considered in this analysis. Gage line F was not used since the transverse cracks over the bents intersect the longitudinal gages in that area, thereby causing more sporadic responses under live loads. Like the statistical analysis described earlier, comparisons between the raw strain responses obtained during live loads may also reveal differences in behavior between the three decks or between decks over time. While maximum and minimum strains are often used to characterized deck response, these values are more sensitive to anomalies such as truck position, sensor placement, or deck composition. By calculating a mean response for each sensor as the truck traverses the bridge, these potential inconsistencies will affect the data less, thus making comparisons between them more reliable. This methodology masks true behavioral shapes of individual strain records, and therefore should be used for comparative purposes only, and not to characterize true deck behavior.

Strain traces from truck runs S, T, U and WR were used in this analysis because of their proximity to the instrumented portion of the deck. Variables that were investigated with respect to their influence on strain response were: deck type, year tested, gage orientation and vertical position of the gage within the deck.

The following procedure was used to get the data into a usable form. During the live load tests, each active sensor output strain as a function of time. Raw strain responses were zeroed and adjusted as a function of longitudinal truck position rather than time. Data was recorded at 50 Hz, so each data trace contained thousands of points. The mean (μ_i) and standard deviation (s_i) were calculated using all of the data records for a particular sensor, regardless of longitudinal truck position. The means and standard deviations for these individual sensors were then sorted based on the four criteria established above. Equations F-1 and F-2, were used to calculate a combined mean (μ_T) and standard deviation (S_T) of a sorted group, respectively. In this case, N represents the number of data traces used to calculate the mean and not the number of data points. The combined coefficient of variation, V_T, was calculated using Equation F-3. Tables F-15 through F-19 show the combined means of the raw strains for the various categories for each of the bridges and each year.

$$\mu_T = \frac{\sum n_i \mu_i}{\sum n_i}$$

Equation F- 1

$$S_T^2 = \frac{1}{\sum n_i}\left[\sum\left(n_i s_i^2 + n_i \mu_i^2\right) - \sum n_i \mu_T^2\right]$$

Equation F- 2

$$V_T = \frac{S_T}{\mu_T}$$

Equation F- 3

Table F- 15: Mean Raw Strains – All Years, All Vertical Positions, All Orientations

Bridge	Mean	St. Dev.	COV	N
CON	0.6	17.6	3030.5	232
EMP	0.1	12.5	13501.1	248
HPC	0.0	31.8	-85111.5	216

Table F- 16: Mean Raw Strains – All Vertical Positions, All Orientations

Year	Bridge	Mean	St. Dev.	COV	N
2003	CON	2.4	24.5	1003.8	120
	EMP	-0.3	8.3	-2742.2	124
	HPC	-1.2	42.7	-3473.6	120
2005	CON	-1.0	6.7	-685.6	113
	EMP	0.4	15.2	3466.2	124
	HPC	1.2	11.5	921.9	96

Table F- 17: Mean Raw Strains – All Vertical Positions

Orient.	Year	Bridge	Mean	St. Dev.	COV	N
Long.	2003	CON	5.0	40.0	804.4	44
		EMP	-2.0	12.4	-627.5	48
		HPC	-5.2	73.6	-1412.1	40
	2005	CON	-3.6	8.7	-239.9	40
		EMP	0.0	24.0	88896.6	48
		HPC	-1.8	9.2	-520.6	28
Trans.	2003	CON	1.0	3.7	379.4	76
		EMP	0.8	3.5	469.5	76
		HPC	0.8	3.4	450.3	80
	2005	CON	0.3	4.4	1387.3	72
		EMP	0.7	3.6	514.7	76
		HPC	2.5	12.1	486.4	68

Table F- 18: Mean Raw Strains – All Orientations

Vertical	Year	Bridge	Mean	St. Dev.	COV	N
Bottom	2003	CON	0.6	5.4	828.4	48
		EMP	0.3	5.7	2128.5	48
		HPC	0.5	4.9	912.2	48
	2005	CON	0.0	6.0	13867.9	48
		EMP	0.1	6.0	4452.9	48
		HPC	1.2	12.3	987.6	48
Top	2003	CON	3.9	33.1	842.3	64
		EMP	-0.8	9.8	-1285.8	72
		HPC	-2.8	58.2	-2056.8	64
	2005	CON	-2.3	7.2	-305.3	56
		EMP	0.6	19.3	3135.4	72
		HPC	1.4	11.7	863.0	40

Table F- 19: Mean Raw Strains

Vertical	Orient.	Year	Bridge	Mean	St. Dev.	COV	N
Bottom	Long.	2003	CON	-2.1	5.3	-249.2	16
			EMP	-2.4	6.3	-258.2	16
			HPC	-1.7	4.5	-267.9	16
		2005	CON	-3.1	6.1	-197.1	16
			EMP	-2.6	7.0	-264.8	16
			HPC	-1.6	7.9	-510.4	16
	Trans.	2003	CON	2.0	4.8	235.7	32
			EMP	1.6	4.9	299.8	32
			HPC	1.7	4.7	285.4	32
		2005	CON	1.6	5.3	326.6	32
			EMP	1.5	4.9	321.5	32
			HPC	2.6	13.7	520.6	32
Top	Long.	2003	CON	9.0	49.5	548.2	28
			EMP	-1.7	14.6	-832.6	32
			HPC	-7.6	94.8	-1255.4	24
		2005	CON	-4.0	10.0	-252.8	24
			EMP	1.4	28.8	2128.6	32
			HPC	-2.1	10.7	-518.8	12
	Trans.	2003	CON	0.0	2.2	-5582.0	36
			EMP	0.0	1.8	8352.0	40
			HPC	0.0	1.9	42810.3	40
		2005	CON	-1.1	3.3	-290.7	32
			EMP	0.0	2.0	8434.7	40
			HPC	2.8	11.8	418.1	28

Individual means were compared to one another using a two-sample, two-sided t-test. As previously discussed, the results from this test can be used to determine the p-value, which is an indicator that the means are similar. P-values range between zero and one, with p-values closer to zero indicating that the means are statistically less similar to one another and p-values closer to one indicating that the means are statistically more similar to one another. Tables F-20 and F-21 show the statistical results (in the form of p-values) from the raw strain analysis. Relevant implications of these results are elaborated on in further detail within the body of the report. The columns on the left side of the table indicate which variables were used to determine the composite mean values being compared between bridges and over time. Italicized values are for 2005 and non-italicized values are for 2003.

Table F-20: P-Values for Bridge to Bridge Comparisons of Raw Strains Regardless of Year Tested

Comparisons	P-Value
CON/EMP	0.73
CON/HPC	0.80
EMP/HPC	0.96

Table F- 21: P-Values Indicating Whether the Mean Raw Strains are Similar

Orientation		Vertical				2005		
Trans.	Long.	Bottom	Top			CON	EMP	HPC
✓	✓	✓	✓	2003	CON	0.14	*0.35*	*0.10*
					EMP	0.25	0.63	*0.65*
					HPC	0.42	0.82	0.54
	✓	✓	✓	2003	CON	0.17	*0.33*	*0.41*
					EMP	0.27	0.61	*0.64*
					HPC	0.44	0.79	0.77
✓		✓	✓	2003	CON	0.33	*0.57*	*0.17*
					EMP	0.72	0.92	*0.24*
					HPC	0.72	0.99	0.26
✓	✓	✓		2003	CON	0.60	*0.94*	*0.55*
					EMP	0.74	0.91	*0.58*
					HPC	0.92	0.80	0.71
✓	✓		✓	2003	CON	0.14	*0.23*	*0.08*
					EMP	0.28	0.59	*0.80*
					HPC	0.42	0.78	0.58
	✓	✓		2003	CON	0.64	*0.84*	*0.54*
					EMP	0.88	0.94	*0.69*
					HPC	0.80	0.70	0.95
✓		✓		2003	CON	0.74	*0.94*	*0.70*
					EMP	0.74	0.93	*0.67*
					HPC	0.75	0.98	0.70
	✓		✓	2003	CON	0.19	*0.34*	*0.61*
					EMP	0.28	0.59	*0.57*
					HPC	0.45	0.77	0.78
✓			✓	2003	CON	0.12	*0.09*	*0.10*
					EMP	0.90	1.00	*0.22*
					HPC	0.93	0.97	0.22

Appendix G – Half-Cell Results

Table G-1: Half-Cell Test Results (July 2003)

Bridge	Reinforcement		Percent of Readings in Each Category		
	Orientation	Position	I	II	III
HPC	Longitudinal	Top	92.9%	7.1%	0.0%
		Bottom	100.0%	0.0%	0.0%
	Transverse	Top	100.0%	0.0%	0.0%
		Bottom	100.0%	0.0%	0.0%
EMP	Longitudinal	Top	82.9%	15.7%	1.4%
		Bottom	94.3%	5.7%	0.0%
	Transverse	Top	70.8%	29.2%	0.0%
		Bottom	100.0%	0.0%	0.0%
CON	Longitudinal	Top	100.0%	0.0%	0.0%
		Bottom	100.0%	0.0%	0.0%
	Transverse	Top	100.0%	0.0%	0.0%
		Bottom	100.0%	0.0%	0.0%

Table G -2: Half-Cell Test Results (July 2004)

Bridge	Reinforcement		Percent of Readings in Each Category		
	Orientation	Position	I	II	III
HPC	Longitudinal	Top	100.0%	0.0%	0.0%
		Bottom	100.0%	0.0%	0.0%
	Transverse	Top	100.0%	0.0%	0.0%
		Bottom	100.0%	0.0%	0.0%
EMP	Longitudinal	Top	100.0%	0.0%	0.0%
		Bottom	100.0%	0.0%	0.0%
	Transverse	Top	100.0%	0.0%	0.0%
		Bottom	95.0%	5.0%	0.0%
CON	Longitudinal	Top	100.0%	0.0%	0.0%
		Bottom	100.0%	0.0%	0.0%
	Transverse	Top	100.0%	0.0%	0.0%
		Bottom	95.0%	5.0%	0.0%

Table G -3: Half-Cell Test Results (July 2005)

Bridge	Reinforcement		Percent of Readings in Each Category		
	Orientation	Position	I	II	III
HPC	Longitudinal	Top	100.0%	0.0%	0.0%
		Bottom	100.0%	0.0%	0.0%
	Transverse	Top	100.0%	0.0%	0.0%
		Bottom	100.0%	0.0%	0.0%
EMP	Longitudinal	Top	100.0%	0.0%	0.0%
		Bottom	100.0%	0.0%	0.0%
	Transverse	Top	100.0%	0.0%	0.0%
		Bottom	100.0%	0.0%	0.0%
CON	Longitudinal	Top	100.0%	0.0%	0.0%
		Bottom	100.0%	0.0%	0.0%
	Transverse	Top	100.0%	0.0%	0.0%
		Bottom	100.0%	0.0%	0.0%

Appendix H – Visual Distress Survey Data
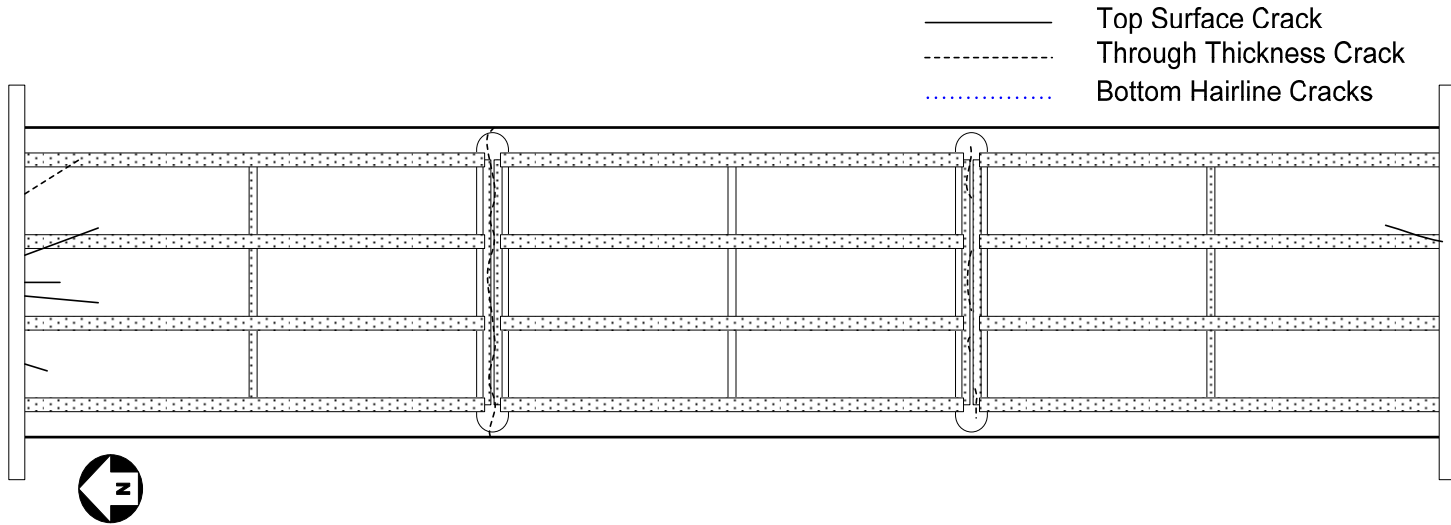
Figure H-1: Distress Survey Map of Conventional Bridge Deck – 2004

Top Surface Crack
Through Thickness Crack
Bottom Hairline Cracks

Edge Cracking: intermittent, but
more pronounced on east side

Figure F-5
Figure F-7
Figure F-4
Figure F-8
Figure F-3
Figure F-6
Figure F-9

Small areas of crazing
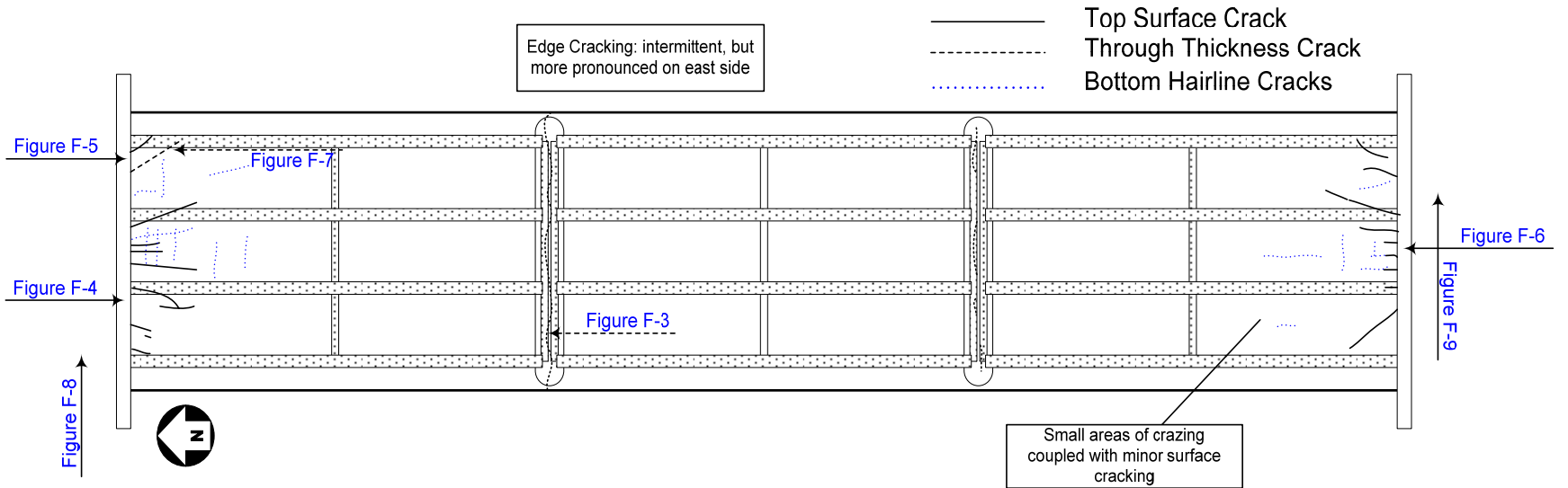coupled with minor surface
cracking

Figure H -2: Distress Survey Map of Conventional Bridge Deck – 2005

Figure H -3: Full-Depth Transverse Crack at Northern-Most Interior Bent – Conventional Deck

Figure H -4: Top-Surface Cracking at West Side of North Abutment – Conventional Deck

Figure H -5: Top-Surface Cracking at East Side of North Abutment – Conventional Deck

Figure H -6: Top-Surface Cracking at South Abutment – Conventional Deck

Figure H -7: Full-Depth Crack at Northeast Corner (shown from underside) – Conventional Deck

Figure H -8: Paved Approach – Northwest End of Conventional Deck

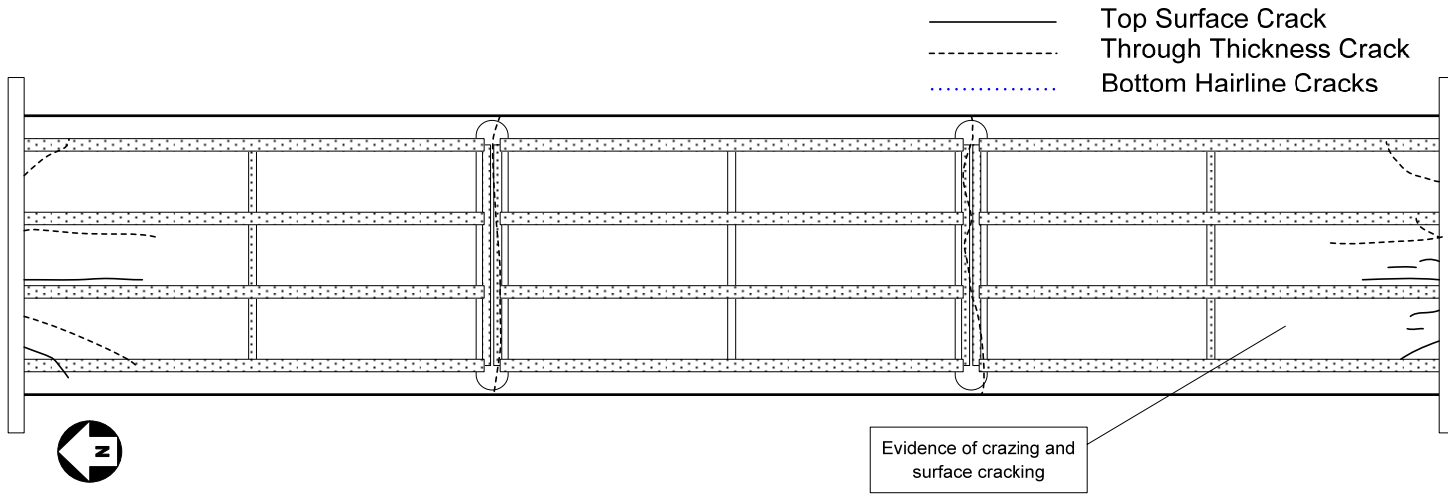**Figure H -9: Paved Approach – Southeast End of Conventional Deck**

Top Surface Crack
Through Thickness Crack
Bottom Hairline Cracks

Evidence of crazing and surface cracking

Figure H -10: Distress Survey Map of Empirical Bridge Deck – 2004

Top Surface Crack
Through Thickness Crack
Bottom Hairline Cracks

Edge Cracking: more pronounced on east side

Figure F-19

Figure F-15

Figure F-16

Figure F-17

Figure F-20

Figure F-22

Figure F-14

Figure F-18

Figure F-12

Figure F-13

Figure F-21

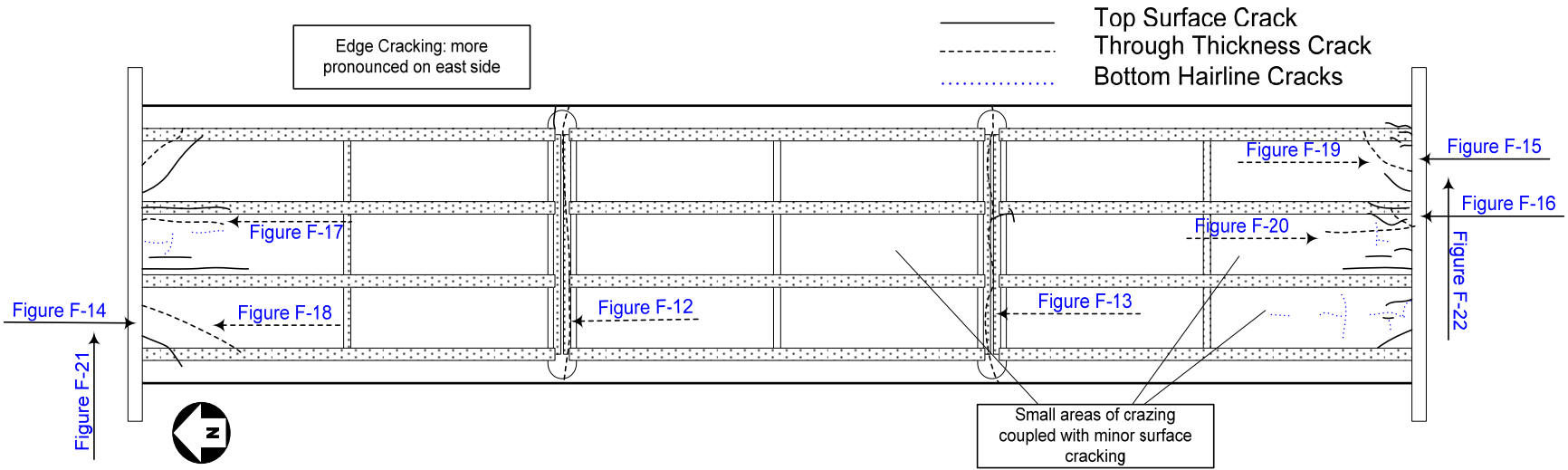Small areas of crazing coupled with minor surface cracking

Figure H -11: Distress Survey Map of Empirical Bridge Deck – 2005

Figure H -12: Full-Depth Transverse Crack at Northern-Most Interior Bent – Empirical Deck

Figure H -13: Full-Depth Transverse Crack at Southern-Most Interior Bent – Empirical Deck

Figure H -14: Top-Surface Cracking at West Side of North Abutment – Empirical Deck

Figure H -15: Top-Surface Cracking at East Side of South Abutment – Empirical Deck

Figure H -16: Top-Surface Cracking at South Abutment – Empirical Deck

Figure H -17: Full-Depth Crack near Center of North End (shown from underside) – Empirical Deck

Figure H -18: Full-Depth Crack at Northwest Corner (shown from underside) – Empirical Deck

Figure H -19: Full-Depth Crack at Southeast Corner (shown from underside) – Empirical Deck

Figure H -20: Full-Depth Crack near Center of South End (shown from underside) – Empirical Deck

Figure H -21: Paved Approach – Northwest End of Empirical Deck

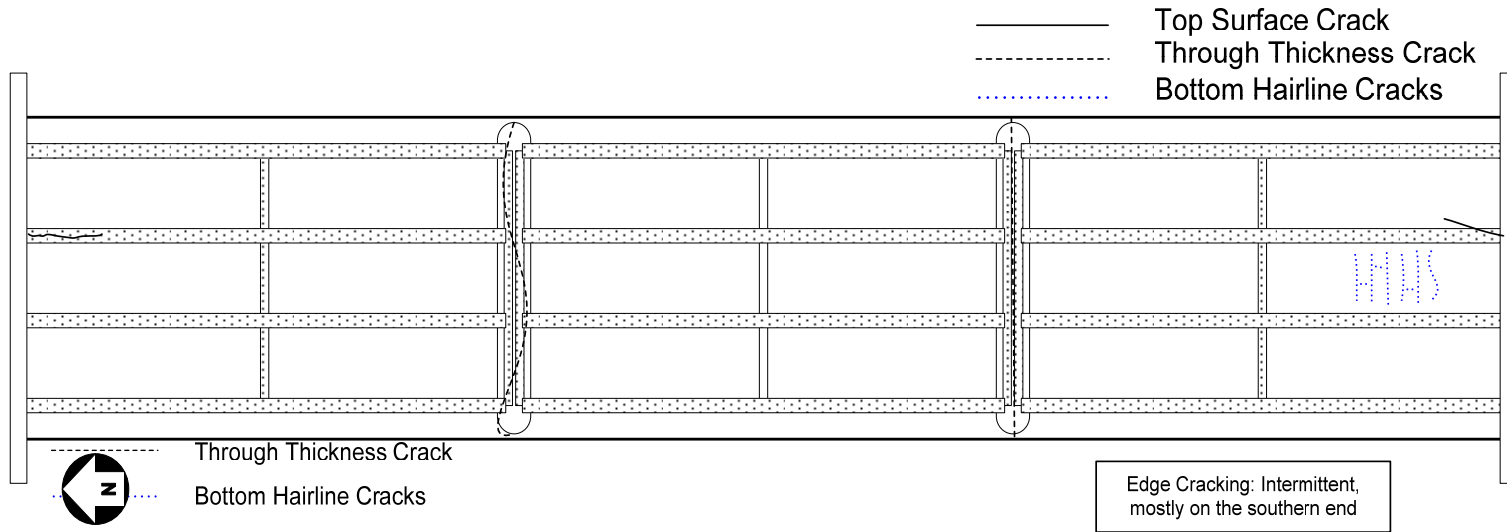**Figure H -22: Paved Approach – Southeast End of Empirical Deck**

Top Surface Crack
Through Thickness Crack
Bottom Hairline Cracks

Through Thickness Crack

Bottom Hairline Cracks

Edge Cracking: Intermittent, mostly on the southern end

Figure H -23: Distress Survey Map of HPC Bridge Deck – 2004

Top Surface Crack
Through Thickness Crack
Bottom Hairline Cracks

Figure F-29

Figure F-26

Figure F-27

Figure F-33

Figure F-28

Figure F-25

Figure F-31

Figure F-32

Figure F-30

Edge Cracking: Consistent along both edges, however, not as frequent in center span
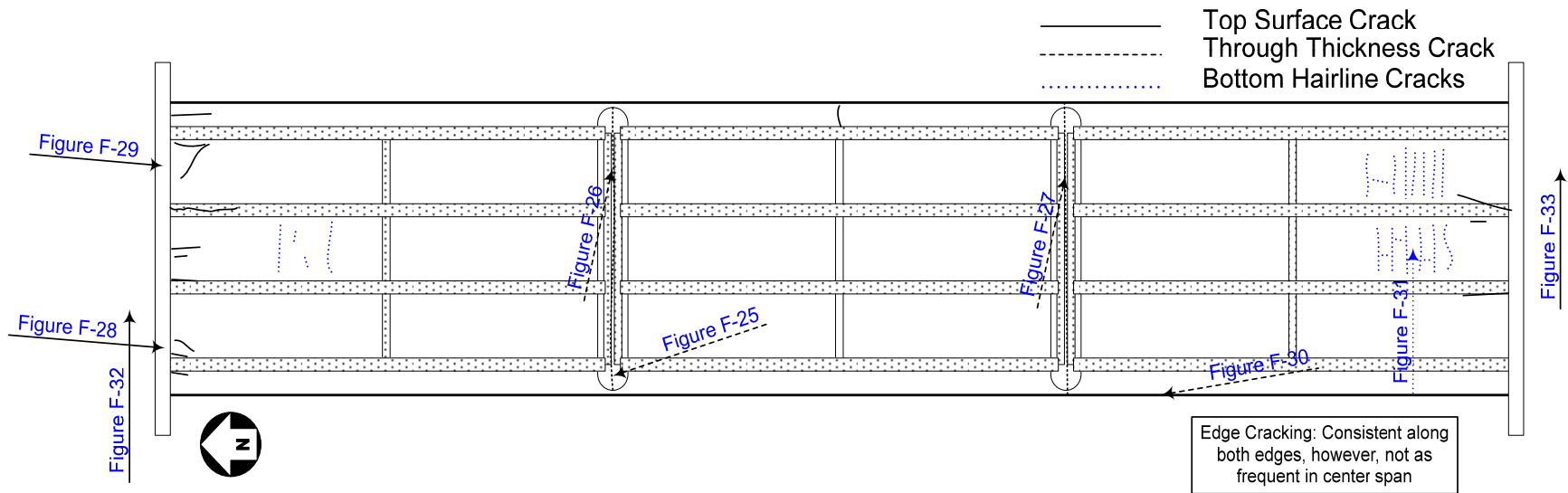
Figure H -24: Distress Survey Map of HPC Bridge Deck – 2005

Figure H -25: Full-Depth Transverse Crack at Northern-Most Interior Bent – West HPC Deck

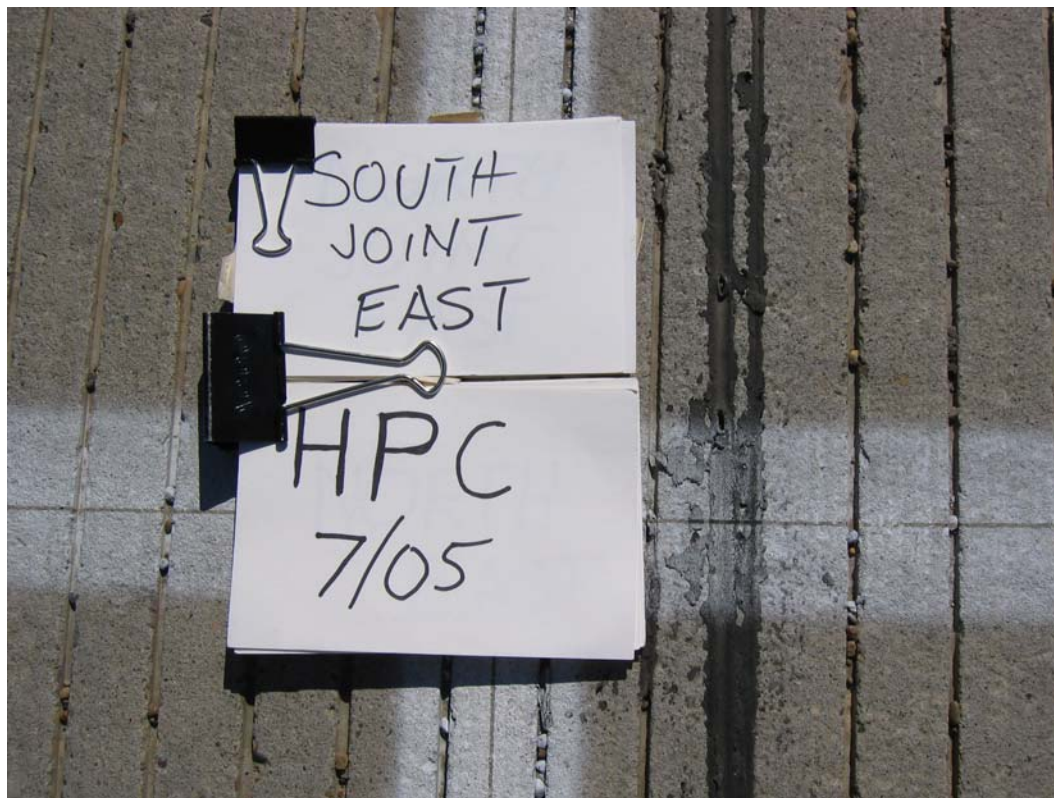**Figure H -26: Full-Depth Transverse Crack at Northern-Most Interior Bent – East HPC Deck**

Figure H -27: Saw Cut at Southern-Most Interior Bent – East HPC Deck

Figure H -28: Top-Surface Cracking at West Side of North Abutment – HPC Deck

Figure H -29: Top-Surface Cracking at East Side of North Abutment – HPC Deck

Figure H -30: Edge Cracking on West Side – HPC Deck

Figure H -31: Hairline Cracking near South Abutment (shown from underside) – HPC Deck

Figure H -32: Paved Approach – Northwest End of HPC Deck

Figure H -33: Paved Approach – Southeast End of HPC Deck